Department of Chemical Engineering

Imperial College London

SW7 2AZ, United Kingdom

Transport Properties of Liquids with Dissolved Gases

Malyanah Binti Mohd Taib

March 2022

A thesis submitted in part fulfilment of the requirements for the degree of
Doctor of Philosophy in Chemical Engineering of Imperial College London
and the Diploma of Imperial College London

Originality Declaration

This is an original work by the author and all of the assistance I received and the sources I used have been properly referenced.

Malyanah Binti Mohd Taib

Dedicated to my family
My late parents, my husband, and my girls.

Acknowledgements

First and foremost, I would like to express my sincere gratitude to my supervisor, Professor J.P. Martin Trusler for his continuous guidance and support during these years. His professionalism and unlimited knowledge provide enormous contributions and without his insightful comments and suggestions, this thesis would not be as it is. Martin has monitored my progress and his enthusiasm for my topic was essential in helping me complete this project. His vast experience has encouraged and inspired me throughout these years. Towards the end of this journey was the hardest for me as the temptation to quit was strong but he was there giving a piece of fatherly advice and I am extremely grateful for that. Martin, I owe you a lot and I know I will never get to pay them back. I wish all the great things in life for you and your family for your kindness and empathy towards all your students. It has been a massive privilege for me to work under your supervision. My special gratitude also goes to my academic mentor, Professor George Jackson for his words of encouragement and guidance at the initial stage of this journey.

Special shoutout to my colleagues from the Thermophysical Group, both past and present, Dr Lorena Dos Santos de Souza, Dr. Emmanuel Efika, Mr. Sultan Al-Habsi, Dr. Benaiah, Dr. Mihaela Stevar, Dr Clauio Calebrese, Dr. Geraldine Torin Ollarves, Dr. Theodor Videnberg and Dr. Yolanda Vincente-Sanchez. Also, to Dr Humera Ansari, Miss Pan Ziqing, Miss Nadine Moustafa and Dr. Zhang Kaiqiang. Thank you for all the help in Lab 424, the long talk about everything, and most importantly thank you for making my life in Imperial a memorable time of my life.

I am indebted to my late parents whom because of them I pursue my PhD. No word can express my appreciations to both of you for all the love and prayers for me. Thank you for raising me to become who I am today and thank you for pushing me beyond my limit. I hope I'm making you both proud.

The biggest thank goes to my husband and my girls, Elviana, Elena and Evaa for their love, patience, sacrifices and understanding throughout this journey. To my girls, I'm sorry for the long working hours, for not being able to put you to sleep for many nights and for all the thing that I had to say no to. I hope this journey inspires and motivates you in a lot of ways. To my husband, I can't thank you enough for being so supportive, always encourage me to do my best and standing by me during the hardest time while I was completing this thesis. Words cannot express how grateful I am to have you by my side. I love you and I pray for Allah to always protect you and reward you Jannah.

Finally, the chapter of my life in Imperial is finally come to an end! The hardest one yet the most precious experience!

Malyanah Binti Mohd Taib
November 2021

Abstract

This study set out to gain a better understanding on the viscosity and diffusion coefficients of hydrocarbons with dissolved CO_2 and CH_4, relevant to enhanced oil recovery and carbon storage. Measurements of the viscosities and diffusion coefficients of the mixtures have been done at high temperature and pressure conditions where carbon storage happens, typically at temperature between (298 and 473) K and pressure up to 100 MPa.

Viscosity measurements were performed using two different types of viscometers where density was measured simultaneously. The viscosity of *m*-xylene + CO_2 were measured using VW-VD apparatus where the wire was tensioned vertically by a sinker while the viscosity of DIDP + CO_2 were measured using VW-VT apparatus where the wire was fixed at both ends horizontally. The viscosity of mixtures of *m*-xylene + CO_2 involved were measured with mole fractions of carbon dioxide between 0 to 0.652 while for DIDP + CO_2 mixtures, the mole fractions of CO_2 studied were x_{CO_2} = 0.207, 0.411, 0.610 and 0.810. The experimental viscosity of the mixtures was correlated using the Tait-Andrade equation and excellent fits were obtained with $\Delta_{AAD} \leq 1.0\%$ for both systems. Surface fits as functions of temperature, pressure and compositions was also done for the *m*-xylene + CO_2 system with a total of 18 parameters for viscosity and 13 parameters for density. All data points fit well with the correlation with Δ_{AAD} = 1.9 % for viscosity and Δ_{AAD} = 0.3 % for density except for density data at x = 0.464 where the values deviate greater than the other mole fractions and noticeably greater than their uncertainty. These correlations allow the interpolation of data with respect to temperature, pressure and composition which enables the comparison with the available experimental data in the literature reported at other conditions.

A simple model for viscosity based on the residual entropy scaling was developed to predict the viscosity of hydrocarbons with dissolved CO_2. This model applied the highly-accurate Helmholtz equations of state to calculate the residual entropy of pure substances and the multi-fluid Helmholtz-energy approximation for the residual entropy of mixtures. For pure substances, decane, *m*-xylene, CO_2, dodecane and octane were chosen based on the availability of both reliable wide-ranging viscosity data and a wide-range Helmholtz equation of state. Each substance collapsed on a single curve when two scaling factors were introduced: (1) a horizontal factor h, which scales the residual molar entropy; and (2) a vertical factor R_η, which scales the reduced viscosity, which revealed the mono-variant relationship over an extended range of temperature and pressure. The universal curve was represented by the third order polynomial function and optimised in a global regression where the deviations of the data from the model for each substance are all within a band of ±10 %. The model was expanded to the octane + dodecane system where linear mixing rule was used to calculate the molar mass, M, and the values of h and R_η . The result shows reasonable agreement with absolute average relative deviation of 2%. To investigate the behaviour of the model to asymmetric mixtures, decane + CO_2 and *m*-xylene + CO_2 mixtures were considered. Results showed that the model systematically underestimates the experimental data by approximately 30% for both systems with *m*-xylene + CO_2 systems showed slightly better results than decane + CO_2 systems. This is a rather encouraging finding considering that only simple mixing rules were used.

Experimental measurement on diffusion coefficient of methane at infinite dilution in methylbenzene and in heptane were done at temperatures ranging from (323 to 398) K and

at pressures from 1 MPa up to approximately 65 MPa. The apparatus used was the Taylor dispersion apparatus (TDA) with overall combined uncertainty of 2.3%. Over the temperature investigated, the diffusion coefficient was found to increase more than 90% for all pressure conditions. To add to that, the diffusion coefficients of methylbenzene were observed to be much lower by not more than 14% than the diffusion coefficient of heptane. The experimental data were fitted using a simple empirical model where the parameters were fitted as linear and quadratic functions of temperature resulting in five parameters per solvent. The Stokes-Einstein model was also used to analyse the experimental data that resulted with just two parameters per solvent. Both approaches represent the data with Δ_{AAD} of around 3.5%. The results from this work provide important insights for future measurements on this type of system.

The experimental data on the diffusion coefficients of CH_4 in methylbenzene and heptane were used to develop an improved model based on the well-established rough-hard sphere model. Numerous experimental data were retrieved from the literature involving several gaseous solutes in hydrocarbon solvents, together with molecular dynamics simulations (MD) for systems of smooth hard spheres in order to establish a general correlation for gaseous solutes in non-polar liquids. The gaseous solutes considered in this work consists of light hydrocarbons, carbon dioxide, nitrogen, and argon and the liquid solvents were all hydrocarbon liquids. To apply this model to a particular system, two parameters are needed: (1) the molar core volume of the solute and solvent; and (2) the roughness factor. Having to have both parameters, the model may be used to predict the tracer diffusion coefficient over wide ranges of temperature and density. The model was found to correlate the experimental data with an average absolute relative deviation of 2.7%.

The results presented in this thesis extends the knowledge of the viscosity and diffusion coefficients of hydrocarbon liquids with dissolved CO_2 at wide range of temperatures and pressures. In addition, it also provides powerful models that can predict the viscosity and diffusion coefficient. The insights gained from this study may be of assistance for future work.

Contents

List of Figures

List of Tables

General Introduction

Project Background

The statistic issued by the International Energy Agency (IEA) report a steady increase in the daily oil demand from 86.4 million barrels in 2010 to almost 100 million barrels in 2020 and, despite a reduction in 2020 due to the global pandemic, further growth is forecast as seen in Figure 1.[1] The EIA also reported that China and India contribute half of the world's growth in the forecast. This is not surprising considering the expansion of China's petrochemical industry and the rising in India's gasoline, jet fuel, and liquid hydrocarbon consumption. It is projected that the consumption growth will outpace supply growth and lead to inventory draw which than lead to more oil production activities to meet the demand.

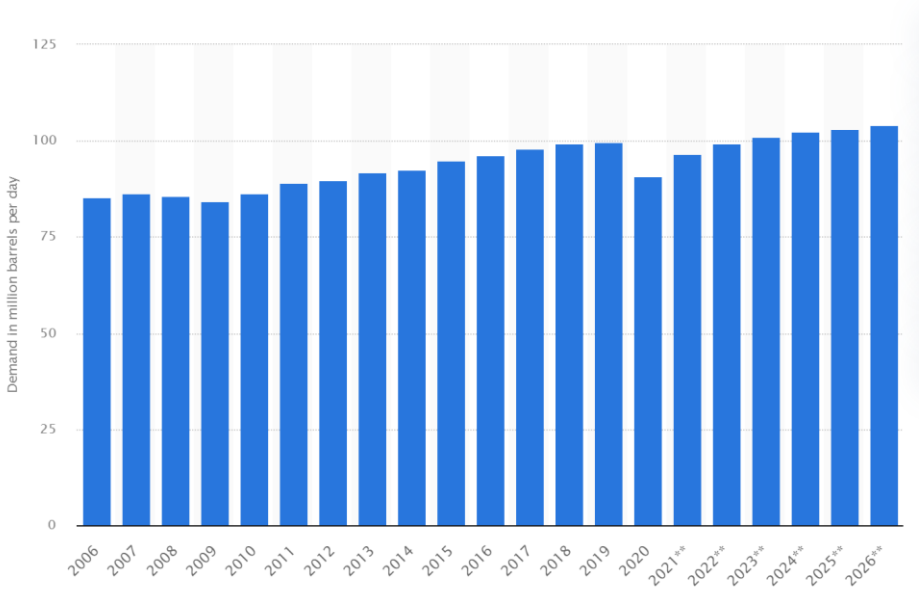

Figure 1 Daily Global Crude Oil Demand 2006-2026. Source: EIA Oil 2021 report[1]

The increase in fossil fuels consumption, however, is not compatible with the climate goal. The Paris climate agreement, which was signed by nearly 200 nations, aims to limit the rise in global average temperature to well below 2°C and nations pursuing efforts to limit the temperature increase to 1.5°C. A report from the Intergovernmental Panel on Climate Change (IPCC) on the impacts of global warming of 1.5˚C showed that at the current warming rate, the global temperatures would reach the 1.5˚C threshold around 2040 (Figure 2).[2] However, deriving from the report's conclusion, the global emissions must fall at least 50 per cent by 2030 to have any chance of limiting the temperature rise to 1.5°C or 2°C.

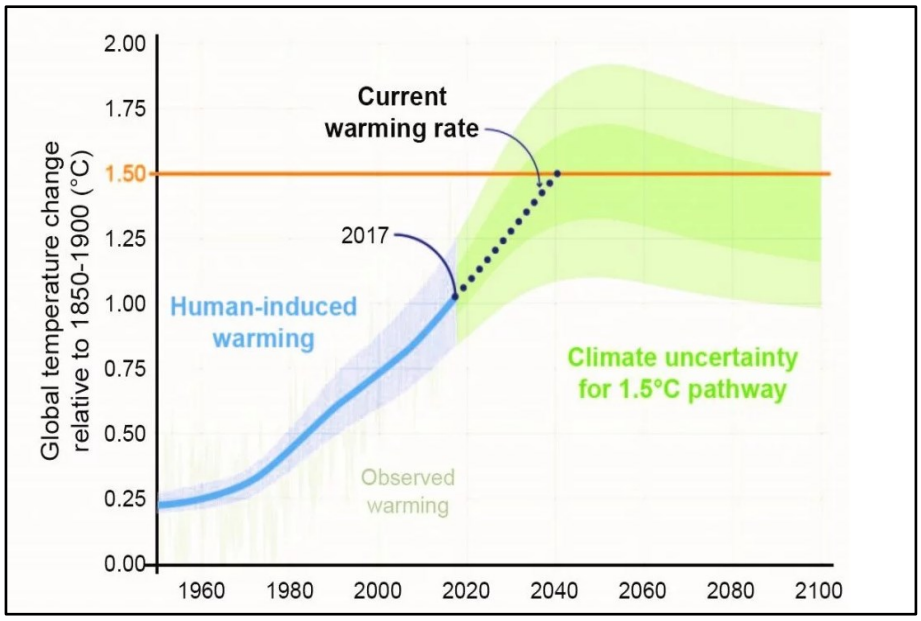

Figure 2 Human-induced warming compared to pre-industrial year (1850-1900). Source: IPCC (2018)[2]

To reach the target in limiting the temperature increase, emission of greenhouse gases (GHG) needs to decline rapidly in all sectors. Greenhouse gases includes carbon dioxide, methane, nitrous oxide and fluorinated-gases (mainly fluorinated alkanes) and are released by many sectors such as buildings, industry, transportation, energy, electricity and heat production, agriculture, forestry and other land use.[3] The breakdown of the global emissions according to sectors are shown in Figure 3. The greenhouse gases trap some of the Earth's outgoing radiative energy, thus retaining heat in the atmosphere and disturb the radiative balance of the Earth. This has affecting various aspect of climate including surface, air and ocean temperatures, precipitation and sea levels.[4]

Reducing global emission of CO_2 will play a major part in controlling global warming due to the fact that it contributes about 75% of the global GHG emissions. Eleven percent of the amount comes from forestry and other land use and the remaining comes from burning fossil fuels and industrial processes. For the energy and industrial sectors, researchers have agreed that a significant decrement on the future of CO_2 emission could be contributed by different low-carbon technologies including carbon capture and storage (CCS).[5-6] In this technology, combustion of fossil fuels can continue to provide the supply, while renewable and various low-carbon technologies are developed.[7] In relation to CCS, one of the important point to be addressed is in the context of industrial decarbonisation. Much of literature on CCS has focused on power generation. This may be relevant in some part of the world such as China. However, in Europe, the situation may be different because the use of renewable energy sources for electricity generation is expanding rapidly. In the UK for example, renewable energy sources have surpassed fossil fuels in generating electricity. Renewables made up 40% of the UK electricity now compared to 24.5% in 2016. Nuclear power, on the other hand, provided slightly less than a fifth while the usage of coal has almost ceased. This means that about three-quarter of the power sectors has been decarbonised.

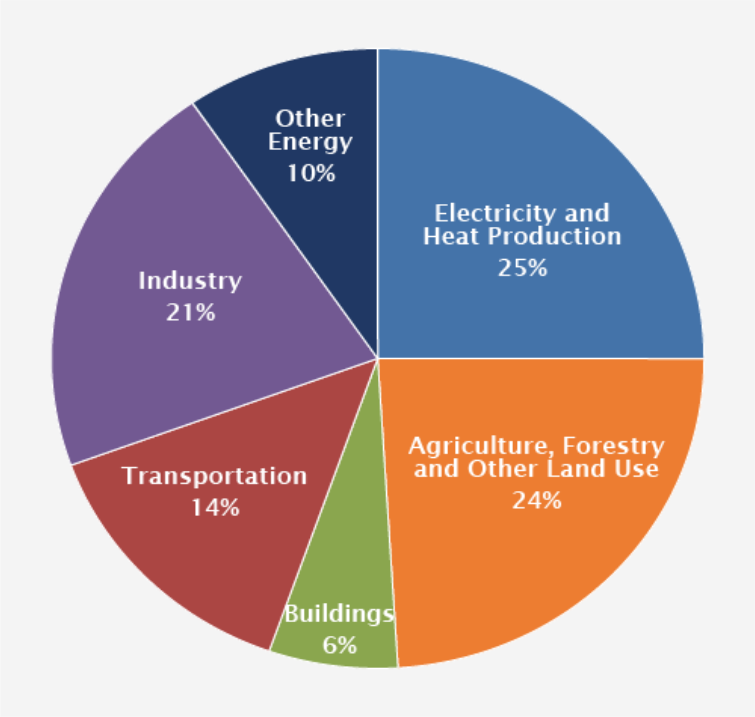

Figure 3 Global greenhouse gas emissions by economic: Source: IPCC (2014)[3]

Nevertheless, for home heating and other industrial processes that release CO_2, little has been done. Thus, the UK government in their effort to explores the potential of other low carbon technologies has supported several technologies to accelerate the development. This includes blue hydrogen technology (H_2 production by reforming natural gas coupled with CCS). In principle, this technology is making use of the H_2 fuel to address some of the emissions in the transport sector, in domestic and commercial heating (such as hot water and space heating) and industrial processes.

In the CCS process, CO_2 that would otherwise be emitted is captured using one of the three main methods: post-combustion, oxyfuel-combustion and pre-combustion including conversion of natural gas to H_2. It is then pressurized to prepare it for transportation via pipeline or by ship for storage. CO_2 storage involves storing CO_2 deep underground in a geological reservoir with a variety of different options including depleted oil and gas fields, enhanced oil or gas recovery (EOR), deep saline formations and other opportunities.[8] During the capture process, CO_2 may be captured together with other impurities and it will be costly to separate the impurities. Co-injection of the impurities with CO_2 for underground storage was also found to be more costly.[9]

Injecting and storing CO_2 into partially depleted oil fields to enhance oil production from reservoirs, while permanently trapping and storing CO_2 is called CO_2-enhanced oil recovery (CO_2-EOR). Figure 4 shows a simplified diagram of EOR. This technology has been successfully applied to improve oil production in conventional and unconventional reservoirs.[10] In this process, CO_2 is injected into the reservoir and allow to mix with the oil and make the oil flow easily, ultimately producing more oil. Some of the CO_2 is stored in the reservoir and some is produced with the oil, separated, and reinjected. The mixture of CO_2-oil that is brought to the surface will undergo a process to separate CO_2 from the oil and recaptured for further

reinjection. This cycle ensures that CO_2 stays in the reservoir. The world's first carbon capture power plant was commenced in 2014 in Canada. The power plant captures 90 percent of the emissions from a 110-megawatt capacity resulting in a 1 million tonnes of CO_2 captured annually from the power station's chimney. On the other hand, Canada's newest CCS project, the Quest Project in Alberta can capture 1 million tonnes per annum of CO_2 to be stored in a deep saline aquifer. In the U.S., the Petra Nova facility in Houston, Texas began its operation in 2017 with a 240-megawatts post-combustion CO_2 capture system. The captured CO_2 was used in enhanced oil recovery in the nearby oil fields. However, this project ceased its operation in 2020 due to COVID-19 pandemic and failed to achieve its carbon sequestration goal by 17% over its first three years of operation. To achieve the climate target set by IPCC, it is important to study the carbon storage requirements. According to the historic CO_2 storage capacity data between 1996 (the year that the first commercial geologic storage project began)[11] and 2020, the annual growth rate calculated is 8.6%. Studies by Zahasky and Krevor[12] has suggested that if the peak injection rates of CO_2 of 40-60 Gt per year can be sustained, it will be sufficient to meet the demand under < 2˚C climate change scenarios.

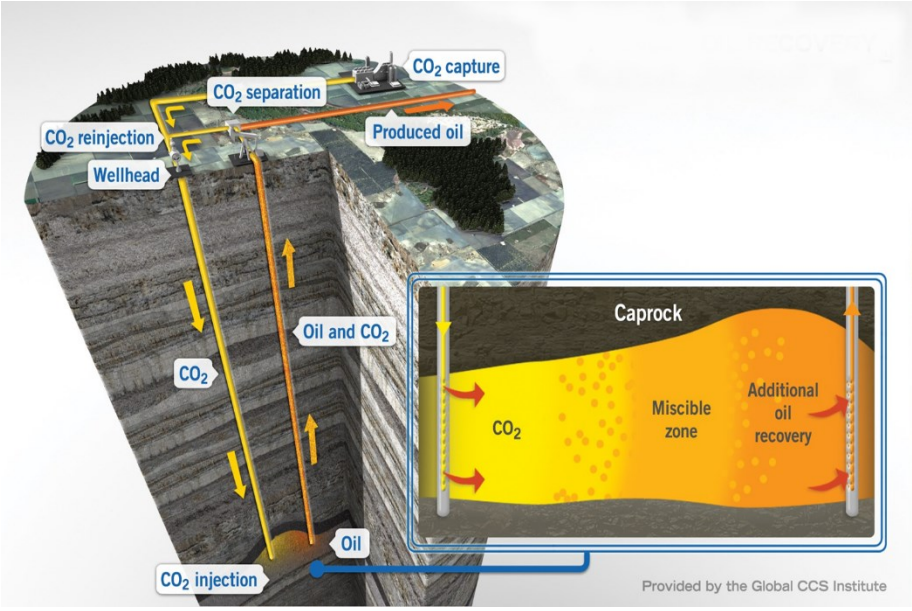

Figure 4 CO_2 for enhanced oil recovery (EOR). Source: Global CCS Institute.

The Importance of Thermophysical Properties

The underlying model may play a key role when detailed analysis of the design and performance of a process is needed. Due to this, an increasing number of study on the thermophysical properties of the reservoir fluids including mixtures containing hydrocarbons and light gases.[7, 13-16] Accurate data on thermodynamic of single phases, transport properties of single phases, as well as interfacial properties and phase equilibria of these mixtures is vitally an important aspect in the design and optimisation of process facilities in EOR and carbon storage.

In this thesis, the topic of interest is investigating and understanding the transport properties relevant to EOR and carbon storage. While the thermodynamic properties determine the feasibility of a process, the transport properties on the other hand are important for the sizing of the equipment.[17] They are fundamentally associated with heat, momentum and mass transfer.[18] Because the topic itself is wide, the study is narrowed to two of the properties, namely viscosities and diffusion coefficients. These two properties are related to one another. For example, in the transportation of CO_2, a laminar flow must be maintained in the pipelines correspond to Reynolds number *Re* approximately below 2100. R_e is inversely proportional to the viscosity but also proportional to the density of the mixture which leads to mass and heat balance equation. This means that additional transport properties including diffusion coefficients will also be needed.

Viscosity is one of the properties that controls the convective flows in the reservoir. It is also important in controlling the rate of injection of fluids into the porous medium as well as the flow of the liquid phase with dissolved gases and the flow of the gases itself. Under certain condition, viscosity is likely to have larger uncertainty as it is very sensitive to changes in temperature, density and composition.[19] Diffusion, on the other hand, is important in controlling interfacial mass transfer rates along with viscosity and some other properties. For instance, in a mixture of oil or brine with dissolved CO_2, the phase equilibria can give us information on the driving force of the dissolution.

Previous research has reported on phase equilibrium of these mixtures, but the information on transport properties such as viscosities and diffusion coefficient scarce. Even when some data are available, the measurements often do not cover a wide range of temperature and pressure especially at conditions where carbon storage happens as seen in Figure 5.

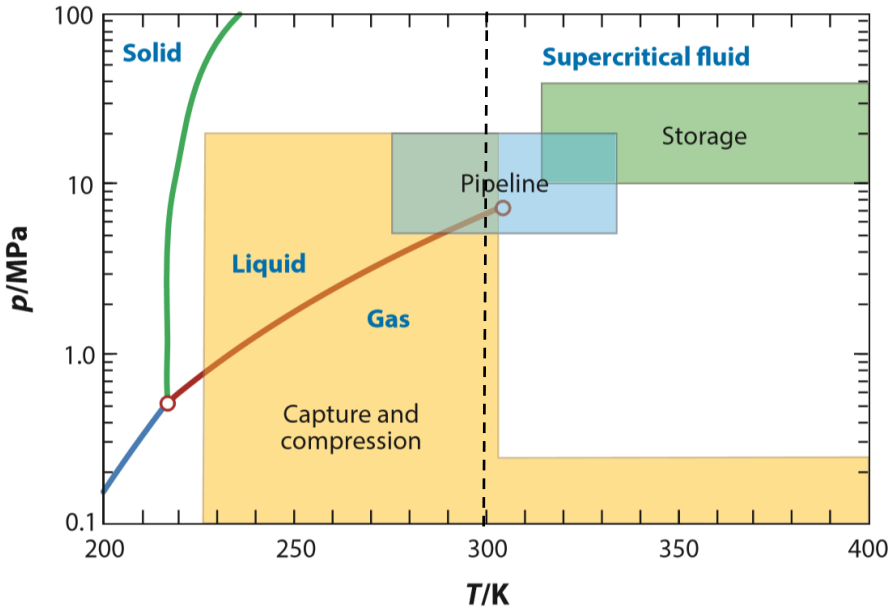

Figure 5 Temperatures and pressures for CCS process drawn on the phase diagram of CO_2.[7] The right side of the dashed line represent temperature and pressure range investigated in this work

General Frameworks

To make experimental measurements on the mixture more meaningful, wide ranges of composition, temperature and pressure are needed. In this study, we choose to focus on temperature between (298 and 473) K and pressure up to 100 MPa as the transportation and storage are mostly occurred within this range. There are potentially many components that may be present in various streams formed during CCS operations, includes CO_2, diluents such as N_2, O_2, CO, Ar and H_2, acid gases, aqueous species such as salt, amines and water, hydrocarbons (as gas, condensates and oils), and other elements such as NO_x and trace elements. In this work, we considered mixtures of 'heavy' hydrocarbons, including aliphatic and aromatic compounds with the light gases CO_2 and CH_4. Viscosity and diffusion coefficient data of such mixtures are important but previously available data are mostly limited to pressure p = 0.1 MPa. A thorough survey on the literature found a large gap especially for mixtures involving aromatic hydrocarbons at high temperature and pressure conditions. A thorough literature survey can be found in chapter 2 and 6 for diffusion coefficient and viscosity, respectively.
The dissolution of CO_2 in hydrocarbons typically causes a reduction in the viscosity of the mixtures. However, most of the references found in the literature investigated low-viscosity systems. Diisodecyl-phthalate (DIDP) in its pure state is a highly viscous hydrocarbon. Therefore, investigating the behaviour of DIDP with dissolved CO_2 could be useful to observe the reduction in the viscosity and to compare its behaviour with a lower viscosity hydrocarbon-CO_2 mixtures. This will be discussed in detail in chapter 9.

Besides experimental work, a theoretical method is another way of obtaining viscosity and diffusion coefficients, especially at conditions that are difficult to access in experimental work. Theoretical models have been developed to successfully predict many thermophysical properties. However, there is presently no well-founded theoretical method for predicting the viscosity and diffusion coefficient of dense fluid mixtures and empirical methods are often unreliable, especially under high-temperature and high-pressure conditions. Several models for predicting viscosity and diffusion coefficient have been proposed. Some approaches offer acceptable results, but others are unsatisfactory especially for mixtures where their molecules are considerably different in size, shape, flexibility, and energetic interactions in the mixture. Molecular simulation is another way of obtaining viscosity from an intermolecular potential model. This method often required large computational efforts, however, in most of the cases, the results obtained are satisfactorily good. An example of a successful molecular simulation can be seen in the work by Zheng et al.[20] where the pressure dependence of the shear viscosity of 2,2,4-trimethylhexane were accurately predicted. In this work, the experimental data obtained were used to validate a prediction model and a universal correlation developed to predict the viscosity and diffusion coefficient, respectively.

Questions and Objectives

The literature data on the viscosity and diffusion-coefficients of hydrocarbons with dissolved gases is very limited especially at high temperature and pressure conditions due to the time-consuming nature of experiments and complex analysis of the data. Subsequently, the knowledge on the effects of dissolved gases in the hydrocarbons is also limited especially for aromatic hydrocarbons. Therefore, this work aims to fill important gaps in the knowledge of

viscosity and diffusion-coefficients of the chosen hydrocarbons with dissolved CO_2 and/or CH_4 over a wide range of temperature and pressure. The work focuses on both aliphatic and aromatic liquid hydrocarbons. The research questions can be expressed as follows:

a) How do the viscosity and diffusion coefficients of mixtures of hydrocarbons with dissolved CO_2 changes when composition, temperature, and pressure change? How do these behaviours relate to the viscosity of the pure hydrocarbon?
b) How can the residual entropy approach be extended to predict the viscosity of mixtures, in particular, hydrocarbon liquids with dissolved CO_2?
c) How can the rough hard-sphere model be extended and validated to correlate the diffusion coefficients of non-polar mixtures?

The research objectives of this study were formulated to answer the questions identified above. The following are the objectives of the study:

a) to provide reliable experimental data on the viscosity and diffusion coefficients of example aliphatic and aromatic liquid hydrocarbons with dissolved CO_2 and/ or CH_4
   This involved experimental measurements using two different apparatus. For viscosity, mixtures involved aromatic hydrocarbons with dissolved CO_2 measured at a temperature ranging from (298 to 423) and at pressures up to 65 MPa and at pressures up to 100 MPa. While for diffusion coefficients, mixtures involved an aliphatic and an aromatic hydrocarbon with CH_4 as the solute. The experimental temperature ranging from (323 to 398) K and pressures up to 65 MPa.
b) to investigate the monovariate relationship between reduced viscosity and residual entropy in binary mixtures of hydrocarbons and hydrocarbons with dissolved CO_2
   The residual entropy model was used to calculate viscosity by incorporating the accurate Helmholtz-energy equations of state for pure fluids.[21] For mixtures, the residual entropy was calculated based on the multi-fluid Helmholtz-energy approximation.[22]
c) to develop an improved predictive model for the viscosity and diffusion coefficients of gaseous solutes in hydrocarbon liquids
   Simple empirical expressions were used to correlate the experimental data collected at any given state point within the temperature and pressure range investigated. A new universal correlation was developed to correlate the diffusion coefficients based on the relationship between reduced diffusion coefficients and reduced molar volume.

Thesis structure

This thesis is divided into three parts. Part 1 which consists of four chapters (chapter 1 to 4) discussed on diffusion coefficient. In chapter 1, theory and basic concept were explained on diffusion coefficient, Taylor dispersion apparatus which was the measurement apparatus in this work, and rough hard sphere theory which was the basis of the model developed in this work. Chapter 2 were mainly on literature review, discussing published work on diffusion coefficients that used Taylor dispersion apparatus to measure the diffusion coefficients of CO_2 and CH_4 in hydrocarbons solvents as well as published modelling work on rough hard sphere and molecular simulations. Chapter 3 are solely on experimental details including operating procedure, data interpretation as well as working equation of Taylor dispersion apparatus. Finally, in chapter 4, experimental results were presented and further discussed.

Part 2 are mainly on viscosity, where chapter 5 and 6 were discussing the theoretical background of the property as well as a thorough review on experimental techniques and

models available in the literature. Chapter 7 explained on the experimental methodology and materials used in the measurements of viscosity. Chapter 8 and chapter 9 presented the experimental results for two systems investigated in this project.
In Part 3 of the thesis, a predictive model, namely the residual entropy model, is discussed. This includes in chapter 10, the theoretical background, concept, calculation equations and the relevancy to use this model in predicting the viscosity of the mixtures containing hydrocarbons and dissolved gases. Results obtained from the modelling work were being discussed in chapter 11. Finally, in chapter 12, several conclusions deduced from all the three parts were discussed and major contributions were listed down. Recommendations for future work were also include in this chapter to complete the thesis.

PART 1 DIFFUSION COEFFICIENTS

CHAPTER 1 THEORY AND CONCEPTS

1.1 Diffusion Coefficient

Study of the diffusion of dissolved gases in liquids has gained interest among researchers due to its importance in mass transfer calculations and correlations.[23] Diffusion, in general, can be defined as a measure of the rate of material transport as a result of the random movement of particles in the presence of a concentration gradient as shown in Figure 1.1. If we consider a container that was divided into two parts, where both parts have the same solute at different concentration, when the partition is taken out, the solute molecules will move from higher concentration to lower concentration. After some time, the concentration will be uniform throughout the container. The phenomenon can also be understood from the concentration profile in Figure 1.1 where it shows the concentration as a function of position before the partition removed, during equilibration and at equilibrium.

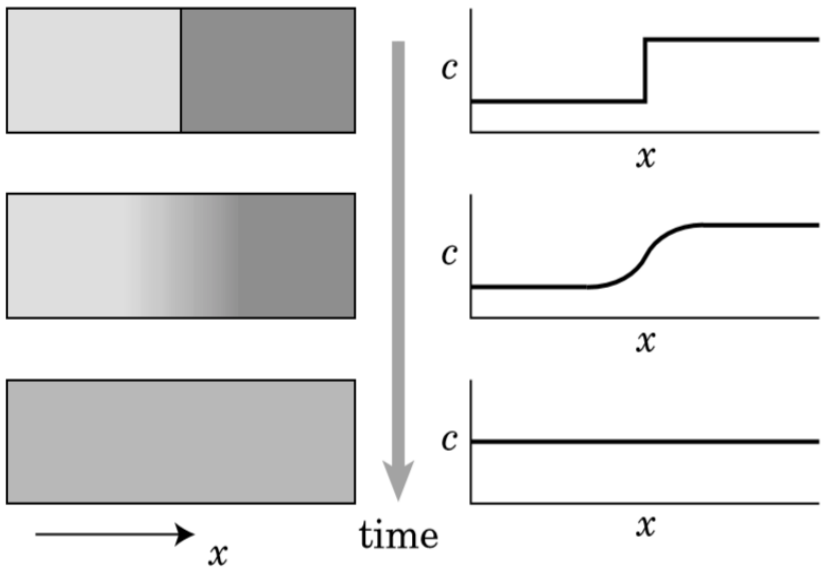

Figure 1.1 Movement of particles of different concentration in a container and the subsequent concentration profile[24]

The diffusion coefficient is a proportionality constant between the diffusion flux and the gradient in the concentration of the diffusing species and is dependent on both temperature and pressure. The most used diffusion coefficient is the Fickian diffusion coefficient, *D* define in Fick's first law which, in one dimension, can be written as

$$J = -D\frac{dc}{dx} \tag{1.1}$$

where *J* is the diffusion flux (moles or mass per unit area per unit time), *c* is the concentration (moles or mass per unit volume), and *x* is distance. The negative sign is necessary to account

for the movement from the high concentration to the low concentration. The other widely used form of diffusion coefficient, primarily used in computational predictions of diffusivity, is the Maxwell Stefan diffusion coefficient, D^{MS}. In Fickian description of diffusion, the concentration gradient is the driving force, while in the MS description, chemical potential is the driving force. In the MS approach, the chemical potential gradient of component *i* is balanced by a friction force

$$-\frac{1}{RT}\nabla\mu_i = \sum_{j=1, j\neq 1}^{n} \frac{x_{j(u_i-u_j)}}{D_{ij}^{MS}} \tag{1.2}$$

Here *R* and *T* are the gas constant and absolute temperature, μ_i is the chemical potential of component *i*, the numerator inside the summation denote the average velocities of component *i* and *j* times the mole fraction of *j* present. The MS diffusion coefficient then describes the magnitude of the friction between *i* and *j*. For binary systems, the Fickian diffusion coefficient can be obtain from the product of the MS diffusion coefficient and the activity coefficient, while for multicomponent systems the matrix of diffusion coefficients usually be interconverted by use of thermodynamic relations based on the components' fugacity coefficients. The diffusion coefficient, also known as the diffusivity, is an important parameter indicative of the diffusion mobility. With the absence of concentration gradient, there is no flux.

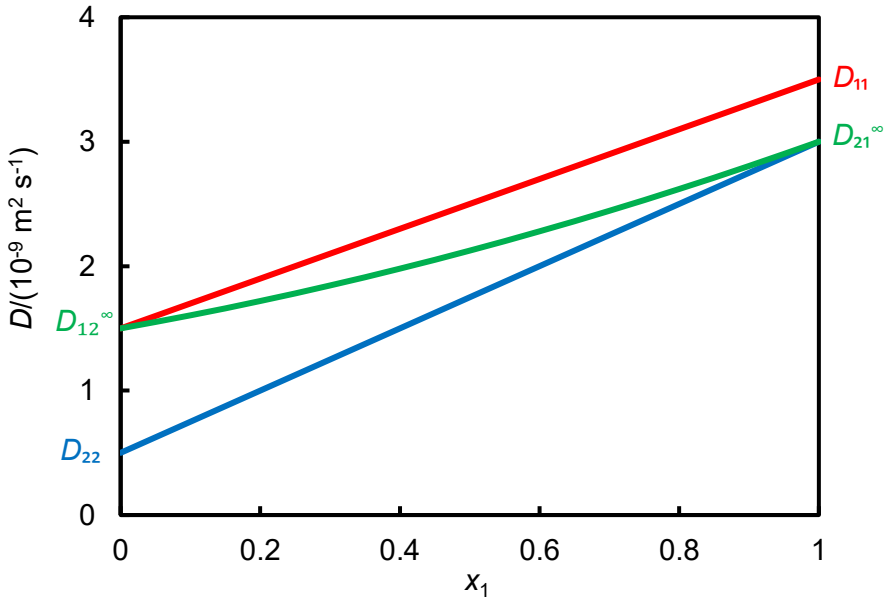

Figure 1.2 Diffusion coefficient of a typical binary system in liquid phase. Blue line: D_1; red line: D_2; green line: D_{12}.

It is important to distinguish between self-diffusion in pure fluids and mutual diffusion in binary mixtures. Self-diffusion in pure fluids or in mixtures at equilibrium describes the random movement of molecules and can be measured by, for example, using a tracer such as an isotopically labelled species. Mutual diffusion in binary mixtures is related to the movement of the two components in a concentration gradient. Mutual diffusion depends on the

thermodynamic behaviour of the components involved. The diffusion coefficients of a typical binary system in the liquid phase can be explained in the diagram shown as Figure 1.2. Here, component 1 is presumably the lighter component as the self-diffusion coefficients are higher than the other component ($D_{11} > D_{22}$). What is measured experimentally in this work is the limits that appear on the left of the graph where the light component (solute) is at infinite dilution in the heavier component (solvent), that is D_{12}^{∞}. D_{22} is the self-diffusion coefficient of the solvent, and its value can be higher or lower the D_{12}^{∞} (in this case, it is lower). D_{11} is the self-diffusion coefficient of the solute component. This diagram is hypothetical because it goes continuously across the mole fraction range, which would not happen for a gas-liquid system due to the phase transition. However, to explain this figure, consider carrying out the experiment at the pressure where there was no phase transition and the components remained liquid throughout. For a given composition, there are three different diffusion coefficients. The blue line is the self-diffusion coefficient of the solvent, the red line is the self-diffusion coefficient of the solute, while the green line is the binary or mutual diffusion coefficient. This general behaviour of the diffusion coefficients has been studied experimentally and rationalised by Anthony and Arthur[25] who measured the tracer diffusion coefficients and mutual diffusion coefficients for the liquid system of *n*-octane and *n*-dodecane as functions of composition.

A wide variety of techniques has been developed in the past to measure diffusion-coefficients. These different techniques can be classified into two groups: direct and indirect methods. Direct methods work by measuring the concentration of the diffusing solute based on the depth of penetration and the diffusivity is estimated by using compositional analysis techniques. However, this method is expensive, time-consuming and most of them are system intrusive. Alternatively, indirect methods measure the changes of the system parameters such as the rate of change of solution volume or movement of the gas-liquid interface, rate of pressure drop in a confined cell, rate of injection from the top to a cell in which the pressure and volume are kept constant, magnetic field characteristics, computed tomography (CT) analysis and dynamic pendant drop analysis. As compared to the direct method, these methods do not need to determine the change in composition.

Some of the common techniques for measuring diffusion coefficient include the pressure decay method, the optical techniques, the Taylor dispersion method and the NMR technique. The pressure decay methods measure the pressure drop in a gas-liquid system as gas dissolves into the liquid and diffuses away from the interface, assuming there is no convection. For example, as shown in Figure 1.3(a), a non-equilibrium gas is brought into contact with oil in a sealed container. The pressure will decrease as a result of the diffusion of gas into the oil. The diffusion-coefficient is calculated from the amount of gas transferred into the oil (based on the level of the liquid in the cell and the pressure drop) until the system reaches equilibrium.

The optical techniques are generally recognized as one of the powerful technique because they enable the simultaneous, real-time analysis of large regions non-invasively.[26] However, they are some drawbacks to this technique. One of it is that the media under investigation must be transparent to radiation and have small physical dimensions. The interferometry technique is one of the well-known optical techniques with Rayleigh and Gouy as the most precise methods.[27] This technique involves a cell with solvent and a diffusing solute. Monochromatic light was made passed through a diffusion boundary within the diffusion cell

to produce the fringe pattern and yield the refractive index at the corresponding cell level. Figure 1.3 (b) shows the diffusion behaviour as a function of the distance.

Figure 1.3 (c) shows the schematic diagram of the Taylor dispersion apparatus. The Taylor Dispersion method employs a steady laminar flow of a solvent pumped through a capillary tube into which a narrow pulse of a mixture of a different composition is injected.[28] The plug containing an excess of solute is injected into the flow and spreads out in the tube under the influence of the parabolic velocity profile characteristic of laminar flow. In the absence of diffusion, the solute particle close to the wall will be stationary while those on the centreline of the flow propagates fastest. However, in the presence of diffusion, the radial concentration gradient stimulated by the parabolic velocity profile is counteracted by mass transport and, after a certain time, the solute pulse will assume a Gaussian distribution where the temporal variance is dependent on both the average flow velocity and the molecular diffusivity. The concentration of the liquid mixture is measured as a function of time at the end of the capillary and the diffusion-coefficients is calculated by fitting the dispersion equation to the experimental data.[29-30] A more detailed description on the principle and working equation for this method will be presented in the next section.

Nuclear Magnetic Resonance (NMR) technique was first used to obtain diffusion coefficients by Stejskal and Tanner[31] in 1965 where the data provide detailed information about the molecular organization and phase structure. Measurements of diffusion commonly employ a spin-echo pulse sequence introduced by Hahn[32] in order to see clearly the effect of the pulse sequences employed. The self-diffusion in a sample is monitored by the application of the magnetic field gradient during the dephasing and rephasing periods. The choice of the pulse sequence to use in the experiment depends on several factors including the relaxation times T1 and T2 of the nuclei under study and the practical problems associated with the application of strong magnetic field gradients. The latter factor usually needs a long waiting time after each applied gradient pulse, thus sets a limit on the time intervals between pulses. Figure 1.3 (d) is a schematic diagram of the NMR technique. A comparison between the common techniques for measuring diffusion coefficients is summarised in Table 1.

Table 1.1 Comparison between the common techniques for measuring diffusion coefficients

Technique	Advantages	Disadvantages
Pressure decay method	simplicity In terms of experimental measurement	not suitable for complex hydrocarbon mixtures
Optical technique	consider the most effective method [33]	Suitable only for transparent fluids. As heavy oil, even when diluted, is opaque,
Taylor Dispersion method	Can be carried out at higher flow rates	experimental difficulties regarding peak shape especially at higher experimental condition
NMR method	Ability to measure values over a wide temperature and pressure range	Limitation to the value measured due to the long interval time

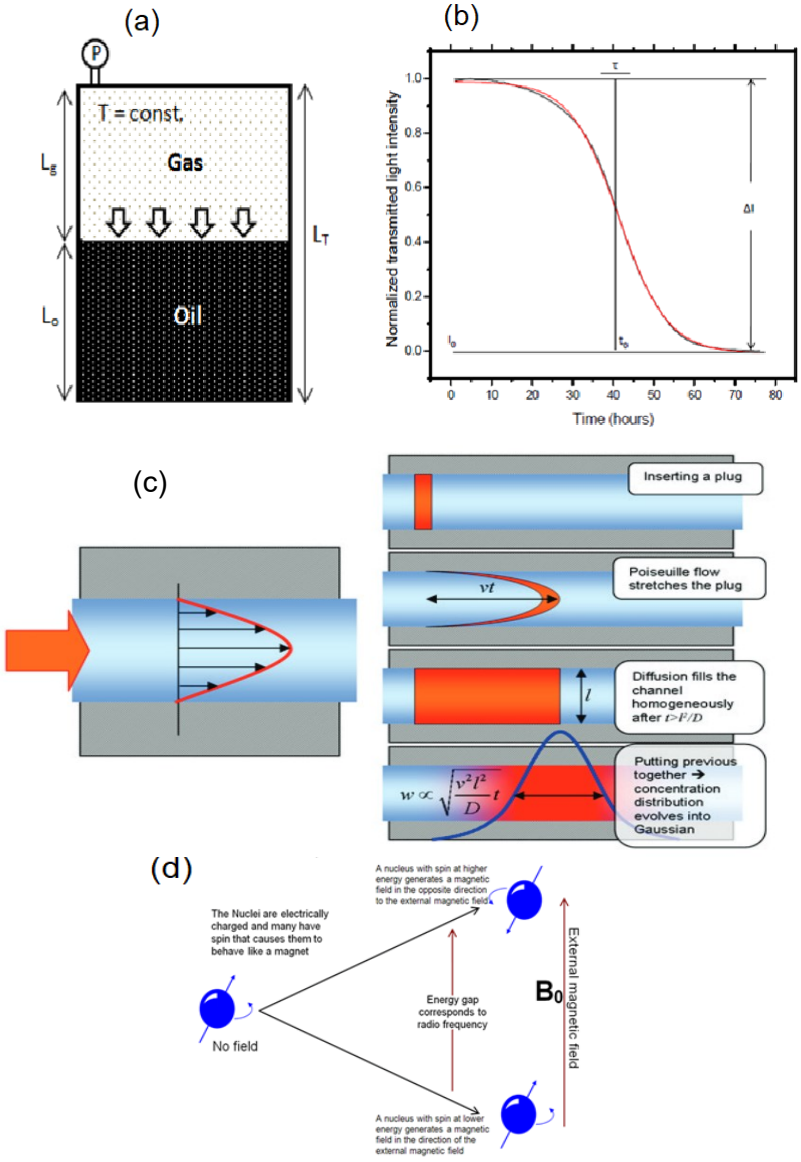

Figure 1.3 Common approaches for diffusion coefficients measurement. (a) Pressure decay method; (b) Optical techniques; (c) Taylor dispersion method; (d) NMR technique.

Having an efficient technique for experimental measurements is important, however, doing measurements at all range of experiment parameters has limitation especially when dealing with the cost of experiment and compatibility of the apparatus used. Hence, developing a suitable model for predicting the property is also essential. The diffusion coefficients for binary mixtures especially the gas-liquid mixtures have been studied widely experimentally and computationally using the hydrodynamic and kinetic theories. Both theories are based on the case in which one of the components is present at infinite dilution, in which case the process can be called tracer diffusion. The hydrodynamic approach is based on the understanding that a diffusing molecule is considered as a particle moving through a continuous solvent medium that creates a resistance to flow, while the kinetic approach treats both the diffusing molecule and the solvent as particles that collide and act to oppose diffusivity.[34]

The Stokes-Einstein equation, which is based on the hydrodynamic theory, has been widely used to correlate diffusion coefficients. In this equation, the diffusion coefficient is proportional in terms of the thermal energy $k_B T$ and inversely proportional to the viscosity of the medium. Consider having a particle moving at a constant velocity v (Figure 1.4). A constant drag force $F = \zeta v$ arises from viscous medium. According to Einstein, the diffusion coefficient of the particle at temperature T is related to the friction coefficient ζ by the following equation:

$$D = \frac{k_B T}{\zeta} \tag{1.3}$$

This equation is called the fluctuation-dissipation theorem due to the fact that diffusion is an a property that is related to friction, a phenomenon of energy dissipation.[24] Stokes showed that the friction coefficient for a spherical particle of radius a is given by

$$\zeta = n_{SE} \pi \eta a \tag{1.4}$$

Where n_{SE} is the Stokes-Einstein number, η is the solvent viscosity and a is the Stokes or hydrodynamic radius. Combining equation (1.3) and (1.4) gives the Stokes-Einstein equation as follows

$$D = \frac{k_B T}{n_{SE} \pi \eta a} \ . \tag{1.5}$$

Based on the equation, the diffusion is faster at a higher temperature, in a less viscous solvent and for a smaller particle. For a non-spherical molecule, the effective hydrodynamic radius can be estimated from experimental data using equation (1.5) where the diffusion coefficient is the value obtained from the experimental measurement. The value of n_{SE} in equations (1.4) and (1.5) is 6 for a no-slip boundary condition around a macroscopic spherical particle moving in a viscous continuum. However, when the model is applied to molecules, the value is changed to 4, corresponding to a slip boundary condition at the surface of a spherical particle.[35]

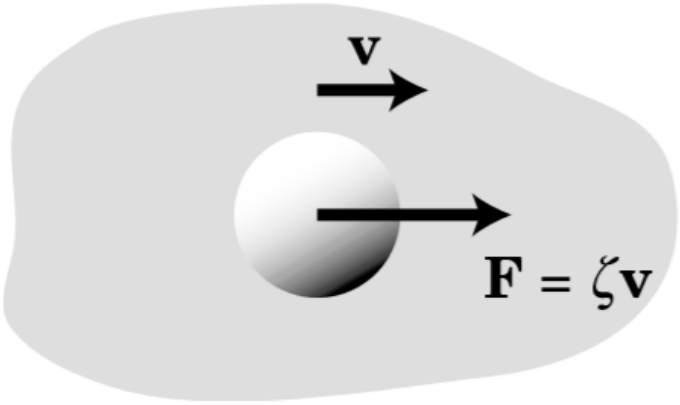

Figure 1.4 Diagram showing a particle moving at a constant velocity v in a viscous liquid pulled by a force F = ζv[24]

The Stokes-Einstein equation has been used to correlate the diffusion coefficients of gaseous solutes in various solvents as a function of temperature at constant pressure. When varying the pressure, the observed behaviour is not captured well by making the hydrodynamic radius a function of temperature alone even when the pressure-dependence of the viscosity is included correctly. However, the hydrodynamic radius corresponding to the measured diffusion coefficient can be expressed in terms of reduced density of the solvent ρ/ρ_c, where ρ_c is the critical density of the solvent. Cadogan et al.[36] have established that with CO_2, the hydrodynamic radius follows a linear correlation with the solvent density except for highly viscous solvents such as squalane.

On the other hand, when it comes to liquefied gases and dense fluids in general, the properties are dominated by repulsive interactions of the nearest neighbour because the molecule are packed closely together. Long range forces are not important to determine the details of the properties. A model that captures repulsive interactive forces is the hard-sphere model which offers a huge simplification of a molecule with just a hard spherical particle. The only sort of collision happened on the molecule is the collision between two molecules or binary collisions. Non-spherical molecules are treated as rough hard-sphere (RHS)[37] and the model is one of the common models that were used in the kinetic theory. The particle in the rough hard-sphere fluid are described as rotating spheres that undergo inelastic collisions upon contact. The particle exchange linear and angular momenta, and energy during a collision. Provided that the structural components of the fluid are unchanged, the rough hard-sphere and the smooth hard-sphere (SHS) are identical. Thus, giving an advantage of studying the effect of the translational-rotational coupling.[38]

For mutual diffusion, the basis of RHS model is taken from the kinetic theory expression for the mutual diffusion coefficient of a dilute binary mixture of the SHS molecules such that

$$\left[nD_{12}\right]_0 = \frac{3}{8\sigma_{12}^2}\sqrt{\frac{k_B T}{2\pi\mu_{12}}} \tag{1.6}$$

where n is the number density, σ_{12} is the arithmetric means of diameter σ_1 of the solute and σ_2 of the solvent, and μ_{12} is the reduced mass.[39] Based on the theory by Enskog et al.[40], for dense fluid, the dilute-gas result should be divided by the value of the unlike pair radial distribution function at contact, $g_{12}(\sigma^{12})$ define by the expression

$$g_{12}\left(\sigma_{12}\right)=\frac{1}{1-\xi}+\frac{3\xi}{\left(1+\sigma_2/\sigma_1\right)\left(1-\xi\right)^2}+\frac{\xi^2}{\left(2\sigma_2/\sigma_1\right)\left(1-\xi\right)^3} \tag{1.7}$$

where $\xi=\pi n\sigma_2^3/6$ is the solvent packing density. The term $g_{12}(\sigma^{12})$ measures how more frequent collisions are in a dense fluid that were predicted by the dilute gas because when the molecule is closely packed together, the collisions frequency is more rapidly than predicted. These values were captured by this term. An additional factor C_{12} should be accounted to the diffusion coefficients of smooth hard sphere as the results of the effect of the molecular collisions. This has led to the following expression for the diffusion coefficient of the smooth hard sphere

$$\left[nD_{12}\right]_{SHS}=\left(\frac{C_{12}}{g_{12}(\sigma_{12})}\right)\left[nD_{12}\right]_0 \tag{1.8}$$

Because the rough hard-sphere fluid is related to the smooth hard sphere fluid by the roughness factor, A_{12}, therefore, the expression for the mutual diffusion coefficient for the rough-hard sphere is given as

$$\left[nD_{12}\right]_{RHS}=\left(\frac{A_{12}C_{12}}{g_{12}(\sigma_{12})}\right)\left[nD_{12}\right]_0 \tag{1.9}$$

The smooth-hard-sphere (SHS) theory[41] has been used to correlate the dimensionless self-diffusion coefficients of pure fluids obtained from molecular simulations as functions of reduced volume V^* where V^* is defined as V/V_0, where V is molar volume and V_0 is the molar core volume. For hard sphere of diameter σ, the molar core volume is given by $N_A\sigma^3/\sqrt{2}$, where N_A is Avagadro's constant. Thus, if we consider the dimensionless self-diffusion coefficient D_{11}^*, it can be computed such that

$$D_{11}^*=\frac{[nD_{11}]}{[nD_{11}]_0}\left(\frac{V}{V_0}\right)^{2/3}=\left(2N_A\right)^{1/3}\frac{8\sqrt{\pi}}{3}\left(\frac{M}{RT}\right)^{1/2}\left(\frac{D_{11}}{V^{1/3}}\right), \tag{1.10}$$

where D_{11} is the self-diffusion coefficient, n is number density, and $[nD_{11}]_0$ is the kinetic-theory expression for the dilute-gas limit of nD_{11}. The relation between the rough hard-sphere and the smooth hard-sphere was extended for real fluids by Li et. al.[42-43] resulting in the following expression

$$D^* = AD^*_{SHS} \tag{1.11}$$

For RHS theory, V_0 is considered as a weak function of temperature. Therefore, if we were to consider the dimensionless self-diffusion coefficient for rough hard sphere theory, equation 1.10 can be written as

$$D^*_{11} = \left(2N_A\right)^{1/3} \frac{8\sqrt{\pi}}{3A_{11}} \left(\frac{M}{RT}\right)^{1/2} \left(\frac{D_{11}}{V^{1/3}}\right), \tag{1.12}$$

where A_{11} is the roughness factor and $0 \leq A_{11} \leq 1$. For mutual diffusion, D^*_{12} can be determined as follows

$$D^*_{12} = \frac{[nD_{12}]}{[nD_{12}]_0} \left(\frac{V}{V_{0,12}}\right)^{2/3} \left(\frac{V_{0,12}}{V_{0,2}}\right)^{2/3} \tag{1.13}$$

Here, $V_{0,2}$ and $V_{0,12}$ are define as follows

$$V_{0,2} = \frac{N_a \sigma_2^3}{\sqrt{2}} \tag{1.14}$$

$$V_{0,12} = \frac{N_a \sigma_{12}^3}{\sqrt{2}} = \frac{\left(V_{0,1}^{1/3} + V_{0,2}^{1/3}\right)^3}{8} \tag{1.15}$$

Thus, by combining the definitions with equation 1.10, the reduced mutual diffusion coefficient at infinite dilution can then be expressed as

$$D^*_{12} = \frac{\left(2N_A\right)^{1/3}}{3V_{0,2}} \left(\frac{2\pi M_{12}}{RT}\right)^{1/2} \left(\frac{V_{0,1}^{1/3} + V_{0,2}^{1/3}}{V^{1/3}}\right)^{2/3} \left(\frac{D_{12}}{A_{12}}\right) \tag{1.16}$$

where M_{12} is the reduced molar mass defined by $M_1M_2/(M_1 + M_2)$ and subscript 1 and 2 is the pure component 1 and 2. The roughness factor can be obtained by fitting the plot of the reduced viscosity against the molar volume in logarithmic scale.[44]

Besides using models such as Stokes-Einstein and RHS, the molecular dynamic (MD) simulation technique is an alternative tool for calculating the diffusion coefficients. One of the earlier works on the MD simulation on the transport properties of the systems containing gases in hydrocarbons was performed by Dysthe and his collaborators to calculate the viscosity,

thermal conductivity and the kinetic diffusion coefficients.[45-46] Several other authors also have performed MD simulation for mixtures containing gases and hydrocarbons.[47-53] Instead of Fick diffusion, this technique calculates the Maxwell-Stefan (MS) diffusivity which is a purely kinetic coefficient. However, a correction to the MS diffusion coefficient called the thermodynamic factor can be estimated to obtain the Fick diffusion coefficient by the following relation

$$D_{12} = D_{12}^{MS} Q \tag{1.17}$$

The value of *Q* can be obtained using different approaches, for example, by means of the group contribution (GC) principle coupled with the PC-SAFT equation of state[52] or by using any thermodynamic model for the mixture. The self-diffusion coefficient of the molecule *i* can finally be calculated through the mean square displacement, according to the Einstein relation

$$D_i = \lim_{t\to\infty} \frac{1}{6t} \langle \left| \vec{r}_i(t) - \vec{r}_i(0) \right|^2 \rangle \tag{1.18}$$

where $\vec{r}_i(t)$ is the center-of-mass vector position of each molecule *i* at time *t* and $\vec{r}_i(0)$ is the position at $t = 0$. Computing diffusion coefficients from MD simulations is important towards developing new correlation model. For example, the results from MD simulation for diffusion in binary hard-sphere mixtures based on the Enskog model can be used to validate and guided in developing a universal function to predict diffusion coefficients.

1.2 Taylor Dispersion Apparatus: Principle and Practice

As discussed in the section before, a wide selection of techniques was developed for the measurement of diffusion coefficients.[54] However, in this section, detail explanations will be discussed on the principle and practise of the Taylor dispersion technique as it was used for all the measurements involved in this study. Figure 1.5 shows the basic diagram of the Taylor dispersion apparatus. The theoretical basis of this method was first given by Taylor and Aris[55-56] while the experimental design criteria were given by Alizadeh et.al.[57] This technique has been proved to be suitable for high-pressure and temperature measurements and have been published for quite a number of publications. [58-61]

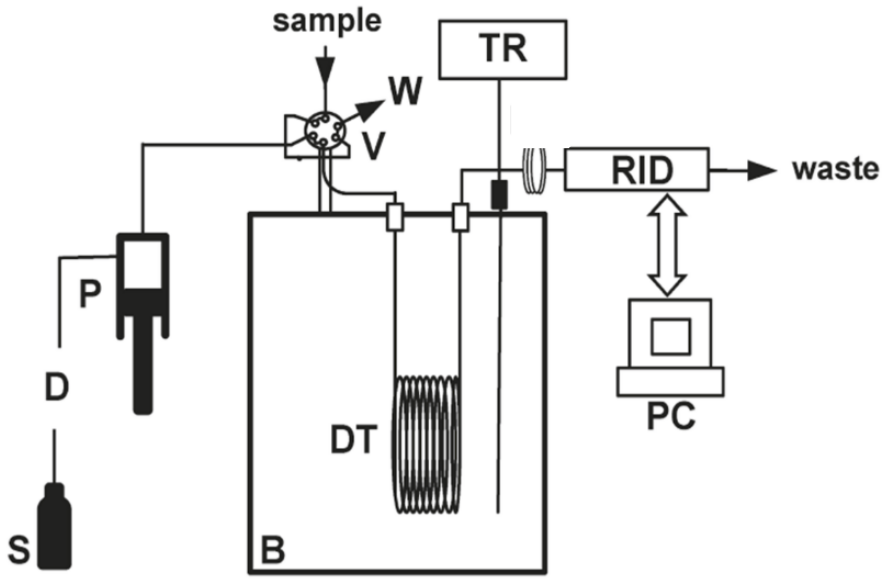

Figure 1.5 Schematic diagram of Taylor dispersion apparatus.[62] S is a reservoir that contain the solvent, D is a vacuum degasser, P is the pump, V is the injection valve, W is the waste, DT is the diffusion tube, B is the oil bath, RID is the refractive index detector, TR is the thermometer readout, and PC is the control computer.

In this method, a pulse contains solute in a solvent is injected in a solvent that flows steadily in a laminar flow through a capillary tube. The pulse disperses after moving in the tube and a normal distribution is assumed due to the effect of diffusion and the laminar velocity profile.[63] Based on Taylor[56], the combination between the flow and the diffusion results in a Gaussian distribution of the solute along the tube where the variance of this distribution can be related to the solute diffusion coefficients.[64] In the theory described by Taylor, the dispersion is assumed to occur in a straight tube, however, the tube used is often coiled to increase its compactness.

The theory developed by Taylor is applicable under certain conditions. These includes laminar flow in the tube and a negligible second flow induced by the coiling effect. To achieve that, we need to ensure, first, a low Reynolds number [*Re*] below 2100, and second, the Dean number [*De*] and the Schmidt number [*Sc*] such that $[De]^2[Sc]$ is less than about 20.[65] Here, [*Re*] = $2R\nu\rho/\eta$, [*Sc*] = $(\eta/\rho D)$ and [*De*] = $R_e(R/R_{coil})^{1/2}$, where R is the column radius, v is the flow speed averaged over the cross-section of the tube, ρ is the solvent density, η is the solvent viscosity D is the diffusion coefficient and R_{coil} is the coil radius. These requirements demand a limitation on the allowable volumetric flow rates.

An example of the concentration profile of a solution corresponding to an injection is shown in Figure 1.6, given by the extended Aris equation:

$$c(t) = \left\{ n / \left(\pi R^2 \sqrt{4\pi K t} \right) \right\} \exp\left[-\left(L - vt \right)^2 / 4Kt \right] \tag{1.19}$$

where n is the amount of solute injected, L is the length of the column, and K is the dispersion coefficient, which is related to the diffusion-coefficients by[55]

However, some practical considerations are needed on the Aris working equation for the analysis of experimental data.[57] Corrections are needed to account for the connecting tubes as well as the method of detection. An analysis on these volumes to the diffusion tubing showed that the effect of tubing sections of radius R_i and length L_i inserted before and after the column has introduce excess dispersion that is equivalent to an additional length of the main column. Therefore, the value of L in equation (1.19) can be given as

$$L = L_c + (D / D_0) \sum_{i=1}^{3} (R_i / R)^4 L_i \tag{1.20}$$

where D is the diffusion-coefficients at the column temperature and D_0 is the diffusion-coefficients at the ambient temperature. Subscript c is for column while subscript i = 1, 2, and 3 are three significant sections of the additional length of the tubing: between the injection valve and the column, between the column and the inlet of the detector and the internal flow path in the detector. To make the corrections smaller, one can consider having a smaller internal radius of the tubing sections or having a longer column.[66]

The concentration profile can be analysed by fitting parameters in an equation to minimise the difference between the experimental points and the analytical solution calculated by equation 1.19. The equation is represented as follows

$$s(t) = a + bt + \alpha c(t) \tag{1.21}$$

where α is the detector sensitivity.

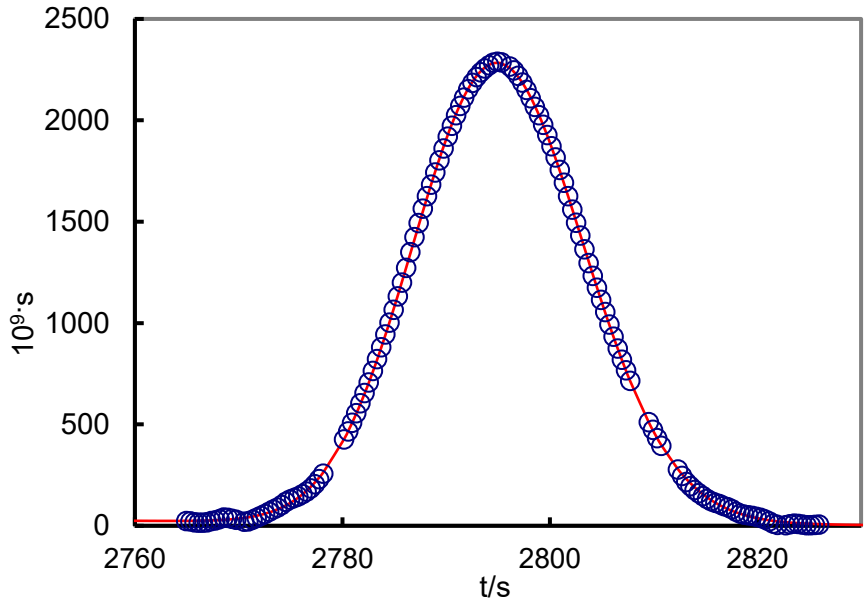

Figure 1.6 Concentration profile. y-axes represent the refractive index, *s* and x-axis represent time, *t* since injection.

1.3 Universal Correlation based on the Rough Hard Sphere Theory

A theoretical model is important to predict properties especially at conditions where the experimental measurements are difficult. The hard sphere model for the transport properties was first proposed by Dymond,[67-68] and has been improved as a predictive tool by Dymond, Assael and their collaborators[69-73]. This theory was originally from the Van der Waals model where the true intermolecular pair potential is replaced by a weak long-range attraction and a rigid-core repulsion.[74] For diffusion coefficient, rough hard sphere (RHS) theory has been used widely to interpret the data.[75] This approach considers the dynamics of the molecular collision between rigid, spherical molecules as a function of liquid densities. It requires the hard core diameter that is temperature dependent resulted from MD calculations and the translational/ rotational coupling factor or the roughness factor.[76] Because this model assume molecule to be treated as spherical bodies and emphasize repulsive interaction at a small intermolecular distance, this model is not suitable for many polar systems due to the strong intermolecular attractive forces.

The rough hard-sphere model described a molecule as a rotating spherical particle that is able to undergo inelastic collisions.[38] The existence of only binary collisions bring about a huge simplification of the theory, built up from the dilute-gas limit transport properties where the theory is known. For hard spherical molecules, we can define a dimensionless reduced viscosity and that is a function only of reduced volume, $V^* = V/V_0$, where V_0 is the molar core volume. For real molecules, we can also define a dimensionless viscosity as a function of V/V_0, where V_0 is a weak function of temperature. Also, for real molecules, there is another parameter that needs to be considered which is the roughness factor, R_η. The value for the roughness factor usually ranges between 0 and 1 due to the effect of reducing the value of self-diffusion of a rough hard-sphere.

If we were to plot the experimental data for viscosity in its dimensionless form against the reduced volume as seen in Figure 1.7, we can observe that by choosing a correct value of V_0 and R_η, all the datapoints will lie on one curve including the computed values for hard spheres. If we adjust the value of R_η it will shift the viscosity in the vertical direction and if we adjust the value of V/V_0, it shifts the data along the horizontal axis. This mean that the model has a universal function of V/V_0 and that it is correlative and not predictive because the value of R_η and V_0 needs to be computed before we can use it to represent the viscosity. The value of R_η and V_0 can be found by fitting the experimental viscosity data.

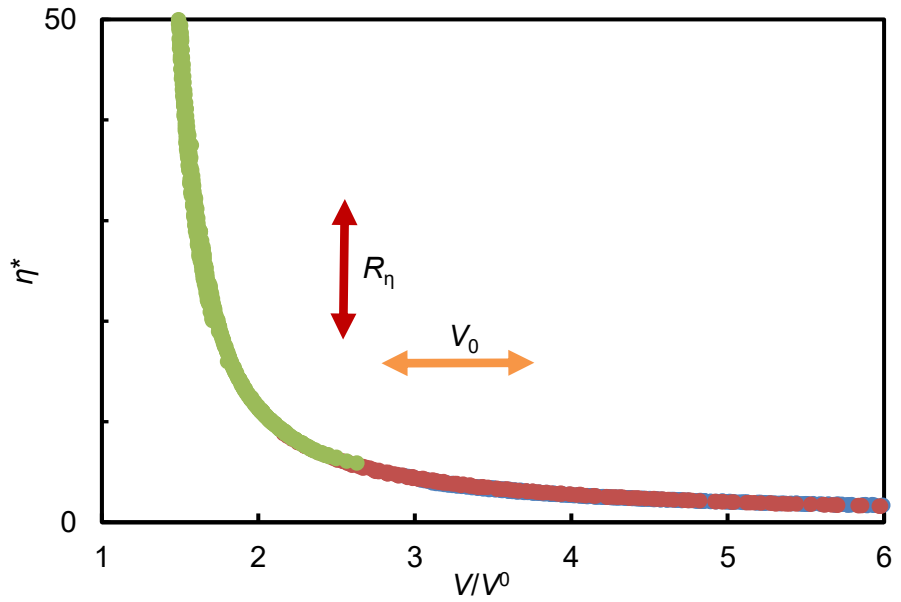

Figure 1.7 Dimensionless viscosity η^* as a function of V/V^0: ● , ethylbenzene; ●, SF_6; ●, N_2

For self-diffusion coefficients of a pure substances, the hard sphere theories apply as well with dimensionless diffusion coefficients incorporates a roughness factor, R_D and the reduced self-diffusion coefficient is as a function of only V/V_0 (the V_0 is the same that were used in the theory with viscosity). For hard sphere theory, as applied to the problem of the mutual diffusion coefficients at inifinite dilution, the dimensionless diffusion coefficients, D_{12}^* can be computed as

$$D_{12}^* = \frac{(2N_A)^{1/3}}{3V_{0,2}} \left(\frac{2\pi M_{12}}{RT}\right)^{1/2} \left(\frac{V_{0,1}^{1/3} + V_{0,2}^{1/3}}{V^{1/3}}\right)^{2/3} \left(\frac{D_{12}}{A_{12}}\right) \tag{1.22}$$

where M_{12} is the reduced molar mass defined by $M_1M_2/(M_1 + M_2)$ and subscript 1 and 2 is the pure component 1 and 2 of solute and solvent, respectively. The equation 23 tells that if we have the experimental value of diffusion coefficients (D_{12}), its dimensionless diffusion coefficients can be found by having its molecular constants (M_{12}, R, T, N_A), the molar core volumes, V_0 for the pure solute ($V_{0,1}$) and solvents ($V_{0,2}$) from the viscosity data, the molar volume (V) from the equation of state and the roughness factor for mutual diffusion coefficients (A_{12}) from fitting the experimental data. The theory also tells us that D_{12}^* is a function of $V/V_{0,2}$ and of the two ratios $V_{0,2}/V_{0,1}$ and M_2/M_1 where $V_{0,i} = N_a\sigma_i^3/\sqrt{2}$ and σ_i is the diameter of molecule of type i. However, based on the molecular-dynamics results [77] for smooth hard-sphere mixtures, D_{12}^* depends not upon $V_{0,2}/V_{0,1}$ and M_2/M_1 separately, but upon the single ratio $M_1V_{0,2}/(M_2V_{0,1})$ which is called the 'asymmetry' ration, χ. This results in the following expression

$$D_{12}^{*} = F_{12}\left(\frac{V}{V_{0,2}}, \frac{M_1 V_{0,2}}{M_2 V_{0,1}}\right) \tag{1.23}$$

where F_{12} is a universal function that needs to be determined. In a study by Cadogan et al.[36] the asymmetry ratio was found to be a fixed value for CO_2 in a family of hydrocarbon solvents. In that case, $F_{12}(V/V_{0,2})$ was represented by a polynomial function such that

$$F_{12}\left(\frac{V}{V_{0,2}}\right) = \sum_{i=0}^{3} a_i \left(\frac{V}{V_{0,2}}\right)^{i}, \tag{1.24}$$

where a_i are the universal constants. The data were able to fit very well except that this function is limited to systems in which $\chi \approx 2.1$, which is the case for CO_2 in typical liquid hydrocarbons. In this work, this theory was extended by considering also CH_4 and other species as solutes in various hydrocarbon liquids. This advances the model towards a universal correlation for the infinite-dilution diffusion coefficient. However, it has only been validated for non-polar solutes in non-polar solvents.

The expressions in equation 1.24 in principle are given by the Enskog theory with corrections determined by the MD studies[78-79] but the experimental data can also be use.[44] The results from the corrected Enskog theory has been used by Assael, Dymond and their collaborators[69-73, 80-81] to determine the universal functions $F(V/V_0)$. In their work, the hard sphere theory has been used to correlate simultaneously the coefficients for viscosity, diffusion coefficients and thermal conductivity for a series of n-alkanes, simple molecular fluids, *n*-alkane mixtures, aromatic hydrocarbon, alcohols as well as refrigerants.

CHAPTER 2 LITERATURE REVIEW

In this chapter, an extensive literature review will be reported on previous work related to diffusion coefficients; it is divided into three sections. First, we will review measurements of diffusion coefficients using Taylor dispersion apparatus specifically. In sections 2.2, we reviewed the literature on the diffusion coefficients of CO_2 and CH_4 in hydrocarbons. Finally, in section 2.3, we will review previous work done to predicts diffusion coefficients using predictions models such as rough hard-sphere and molecular dynamic simulations.

2.1 Measurements using Taylor dispersion apparatus

The Taylor dispersion method has been used widely since decades ago for the measurements of diffusion coefficients. An extensive literature on the method was available, however, a thorough discussion by Alizadeh et al.[57] gives a complete discussion of the method and its application to liquid diffusivity measurements including the corrections from the effect of the finite volume of the injection pulse, the infinite volume of the concentration monitor, the coiling of the tube and the nonuniformity and non-circularity of the cross-section. Until today, measurements using this method is still relevant due to the presence of a fully developed working equation that allows absolute measurements to be made and provide highly accurate experimental data. This method is favourable as it does not need calibration and works well to determine diffusion coefficients either near to infinite dilution, mutual diffusion coefficients in mixtures of liquids as well as self- diffusion coefficients.[82-83]

Since it was introduced for liquids by Pratt and Wakeham[84] and Grushka and Kikta[85], the Taylor dispersion method has been used for the measurements of diffusion coefficients in a wide selection of fluids under various conditions[28, 60, 86-88]. These include measurements in organic mixtures[89] as well as in supercritical fluids.[90-96] Levelt Sangers et al.[96] reported experimental data on diffusion coefficients of benzene and toluene in supercritical CO_2. They have summarized that in order to obtain the diffusion coefficients near-infinite dilution at the general region of the critical density, the measurement needs to be carried out at 20 K or more above the solvent's critical point. Bruno[95] in his work reported measurements of diffusion in supercritical fluid solutions but for an application that is relevant to the design of advanced aircraft and turbine fuels. A correlation was developed by Catchpole and King[94] to estimate both self and binary diffusion coefficients in a range of near-critical solvents. However, it was reported that the correlation is not suitable for estimating binary diffusion coefficients at the binary mixture critical points. Silva and Macedo[93] in their work had evaluated the correlation by Catchpole and King for diffusion coefficients of diethyl ether, diisopropyl ether, and tetrahydrofuran in supercritical CO_2 and obtained a large deviation. They had concluded that one of the reasons for the large deviation is because in this correlation, the temperature (and density) dependence of the hard-sphere diameter has been neglected. More detailed explanation on the effect of small changes in the hard-sphere diameter on the diffusion coefficients has been discussed in their other paper.[97] Other large number of studies on the measurements and predictions of binary diffusion coefficients in the subcritical and supercritical region has been done by Akgerman and his co-workers.[98-101]

The Taylor dispersion method has also been used in measuring multicomponent diffusion coefficients of three-component liquid systems. For example, the ternary multicomponent diffusion coefficients involving mixtures of aqueous salt solution has been reported by

Callendar and Leaist.[102-103] The diffusion coefficients involving aqueous salt solutions have also been measured by several other authors.[104-106] In fact, a vast literature survey has revealed numerous other papers measuring diffusion coefficients of electrolytes involving aqueous potassium chloride (KCl) solutions.[107-149] However, it was restricted to ambient conditions and for dilute solutions. The only data found on diffusion coefficients for KCl in KCl aqueous solutions at elevated pressure was done by Secuianu et al.[66] where the experimental data obtained by Taylor dispersion method were available up to 69 MPa. The Taylor dispersion method has been used widely since decades ago for the measurements of diffusion coefficients. An extensive literature on the method was available, however, a thorough discussion by Alizadeh et al.[57] gives a complete discussion of the method and its application to liquid diffusivity measurements including the corrections from the effect of the finite volume of the injection pulse, the infinite volume of the concentration monitor, the coiling of the tube and the nonuniformity and non-circularity of the cross-section. Until today, measurements using this method is still relevant due to the presence of a fully developed working equation that allows absolute measurements to be made and provides highly accurate experimental data. This method is favourable as it does not need calibration and works well to determine diffusion coefficients either near to infinite dilution, mutual diffusion coefficients in mixtures of liquids as well as self- diffusion coefficients.[82-83]

Table 2.1 Literature for diffusion coefficients of CH_4 and CO_2 in hydrocarbon solvents that were measured by Taylor dispersion method

Solute Gases	Solvent	*T*/K	*p*/MPa	Number of points	Reference
CH_4	Hexane	304 - 435	1.72	6	[150]
		298 - 403	1	4	[151]
	Decane	298 - 433	1	3	[151]
	Tetradecane	298 - 430	1	4	[151]
CO_2	Dodecane	298 - 566	1.45-3.45	9	[61]
	Hexadecane	298 - 566	1.45-3.45	10	[61]
	Toluene	298 - 333	1	5	[152]
		298 - 423	1 to 69	30	[36]
	Hexane	298 - 423	1 to 69	16	[36]
	Heptane	298 - 423	1 to 69	30	[36]
	Octane	298 - 423	1 to 69	30	[36]
	Decane	298 - 423	1 to 69	16	[36]
	Dodecane	298 - 423	1 to 69	15	[36]
	Hexadecane	298 - 423	1 to 69	28	[36]

In recent years, the diffusion of dissolved gases in liquids has gained growing interest among researchers. Some of the studies that have employed the Taylor dispersion method includes the diffusion coefficients of CO_2 in water by Cadogan et al.[62], Ferrell and Himmlebleu[153], Snijder et al.[152] and Frank et al.[154] In their paper, the diffusivity of different other gases in water such as N_2, O_2 and NH_3 have also been measured. In addition to that, Han and Bartels[155] have also reported on diffusion coefficients of O_2 in water. Other systems involving solute gases in liquids include N_2O in aqueous piperazine solution by Hamborg et al.[156] and CO_2 and NH_3 in methanol by Frank et al.[154] The diffusion coefficients of CH_4 in water have also been thoroughly investigated experimentally and mathematically, however none of them has used Taylor dispersion method. Instead, they were using methods such as the capillary cell method, the diaphragm method, the inverted tube method, the modified Barrer method and a simplified method where the capillary tube was used with *in situ* Raman spectroscopy [157-166]. Diffusion coefficients of dissolved gases in hydrocarbon liquids using this method were also available in literature. Table 2.1 summarizes the literature for CH_4 and CO_2 in hydrocarbon solvents that were measured using the Taylor dispersion method. Diffusion coefficients using this method of other gases in hydrocarbons includes dissolved H_2[61], C_3H_6[150], C_2H_6[150] and Argon.[64]

2.2 Previous experimental results

In recent years, the diffusion of dissolved gas solute in liquids have received a growing interest in connection with both geological carbon storage and gas injection for improved oil recovery. In relation to these processes, the most important solute gases are CO_2 and CH4. The diffusion coefficients of these and other gases in liquid solvents have been studied by many researchers, either experimentally or through computational means.

2.2.1 Diffusion coefficients of CO_2 in hydrocarbons

An extensive literature review resulted in a large number of works involving dissolved CO_2 in liquid hydrocarbons. However, many of them have restricted temperature and pressure to ambient condition. This limitation does not represent the carbon storage and enhanced oil recovery as the process involved higher temperature and pressure. Most of the data found were measured at p = 0.1 MPa even though they were measured along with several temperatures. Himmelblau[23] in his review has evaluated and reported experimental results of diffusivities of hydrocarbon gases in liquid hydrocarbons such as methane and ethane in series of alkane up to decane. Guzman and Garrido[167] have determined the diffusion coefficients of CO_2 in twelve alkanes ranging from hexane to heptadecane. However, their measurements were limited at T = 298 K and at pressures varying from 0.1 to 0.7 MPa. Takeuchi et al.[168] and Luthjens et al.[169] reported diffusion coefficients of CO_2 in hexane at T = 298 K and p = 0.1 MPa while Teng et al. [170] used MRI technology to study CO_2 diffusion in decane at T = 297 K and pressures of (2.2 to 4.2) MPa.

Some of the data found however involved a much higher pressure and temperature including the work by Nikkhou et al.[171] who reported the diffusion coefficient of CO_2 in heptane and hexadecane, determined from the swelling of pendant drops at T = (313 to 393) K and pressures up to 8.6 MPa. Additional data for CO_2 in hexadecane have been reported by Du et al.[172] and Hao et al[173] using the Dynamic Pendant Droplet Volume Analysis (DPDVA)

method and the NMR method, respectively. More data were reported for CO_2 diffusion in hydrocarbons: heptane at T = 293 K[174]; dodecane at T = (304 to 566) K[61]; and hexadecane at T = (298 to 564) K.[61, 167, 175] These studies involved pressures of less than 3.5 MPa but the larger range of temperature have initiated the development of predictive theories for diffusion.

The highest pressure measured was done by Pacheco-Roman et al.[176] who used the pressure-decay method to determine the diffusivity of CO_2 in decane and hexadecane at T = (273 to 298) K and at p = 35 MPa. A more recent data at higher pressure up to 69 MPa were found done by Cadogan et al.[36] who measured the diffusion coefficients of dissolved CO_2 in eight liquid hydrocarbons including hexane, heptane, octane, decane, dodecane, hexadecane, squalane and toluene. In his work, the diffusion coefficients were found to be reduced as much as 55% over the range of pressure. The effect of temperature and pressure on diffusion coefficients in this work[36] can be seen illustrated in Figure 2.1 and a summary of the literature for the diffusion coefficients of CO_2 in hydrocarbons is shown in Table 2.2. The diffusion coefficients of CO_2 in a more complicated system have also been measured by several authors. This includes the recent work of Rezk and Foroozesh[177] who studied the diffusivity of CO_2 in crude oil using the pressure decay method at T = 294 K. The diffusivity of CO_2 in crude oil have also been studied by Yang et al [178] and Guo et al.[179]

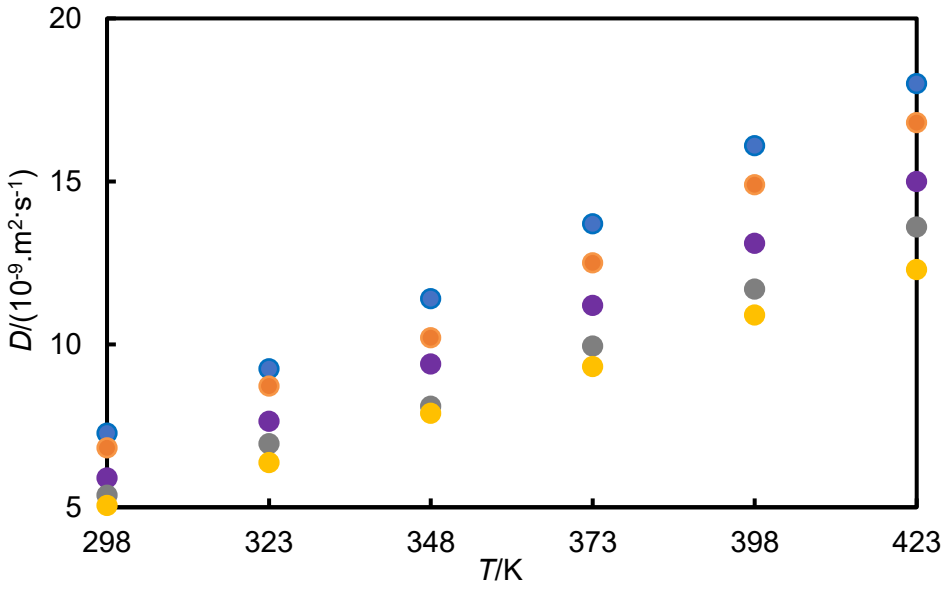

Figure 2.1 Diffusion coefficients D of dissolved CO_2 in heptane as a function of temperature T[36]: □, p = 1 MPa ; □, p = 10 MPa; □, p =30 MPa; □, p = 50 MPa; □, p = 69 MPa.

Table 2.2 Summary of the literature for diffusion coefficients of CO_2 in hydrocarbon solvents

Author	Solvent	*T*/K	*p*/MPa
Guzman and Garrido[167]	C_6H_{14} to $C_{17}H_{36}$	298	0.1
Takeuchi et al.[168]	C_6H_{14}	298	0.1
Luthjens et al.[169]	C_6H_{14}	298	0.1
Teng at al. [170]	$C_{10}H_{22}$	297	2.2 to 4.2
Du et al. [172]	$C_{16}H_{34}$	298 to 353	7 to 19
Nikkhou et al.[171]	C_7H_{16}	313 to 393	0.1 to 8.6
	$C_{16}H_{34}$	313 to 393	0.1 to 8.6
Matthews et al.[61]	$C_{12}H_{26}$	304 to 566	1.4 to 3.4
	$C_{16}H_{34}$	323 to 564	1.4 to 3.4
Hayduk[175]	$C_{16}H_{34}$	298 to 323	0.1
Pacheco-Roman et al.[176]	$C_{10}H_{22}$	273 to 298	35
	$C_{16}H_{34}$	273 to 298	35
Cadogan et al.[36]	C_6H_{14} to $C_{10}H_{22}$		
	C_7H_8	298 to 423	1 to 69
	$C_{30}H_{62}$		

2.2.2 Diffusion coefficients of CH_4 in hydrocarbons

Diffusion coefficients of CH_4 in hydrocarbon have been studied by several researchers. Table 2.3 summarizes the results from the literature survey for methane in hydrocarbon solvents.[150-151, 180-184] Several measurement techniques have been applied including the Taylor dispersion technique, NMR, pressure-time measurements and also chromatographic analysis from a diffusion cell. Helbaek et al.[180] have measured self-diffusion coefficients of CH_4 in hexane, octane and decane at T = 303.2 K and 333.2 K and at p = (30-50) MPa. They have compared the experimental diffusion coefficients data with Sigmund correlation, however it was found not fit because the Sigmund correlation has failed to consider the reduced density maximum for intermediate compositions at constant pressure and temperature and in fact it has assumed that the diffusion coefficients is a unique function of the reduced density. Erkey and Ekgerman[150] in their work reported the infinite diffusion coefficients of CH_4 in octane at T = (304 – 435) K. The diffusion coefficients of CH_4 in octane have also been measured by Killie et al.[182] and Colgate et al.[181] at T = (280.7 - 311.75) K together with nonane and decane at the same temperature and pressure conditions. The diffusivities of CH_4 in octane, decane and tetradecane have been reported by Chen et al.[151] at temperatures from (298 to 403) K. In their work, they have found out that the rough hard-sphere theory predicts well the experimental data especially at the temperature where the ratio of the molar volume to that of the close-packed hard-sphere fluid $V/V_{0,2}$ is less than or equal to 1.5. Only work by Jamialahmadi et al.[184] has managed to measure several points for the diffusion coefficients of CH_4 in dodecane in between T = 318 to 354 K and pressure between 4 to 34 MPa. To summarize, there is a lack of experimental data for CH_4 diffusion in pure liquid hydrocarbons over extended ranges of temperature and pressure. More experimental data are needed to develop a reliable correlation that works well both in low and high temperature and pressure conditions. Other studies on the diffusion of methane in liquid hydrocarbons have focused on heavy crude oils and bitumen.[185-188]

It is worth to mention that the literature reviewed above involved diffusion in liquid form, which is the main interest in this work. However, there is also other literatures available for the diffusion coefficients of hydrocarbon in CH_4 where the whole system is in the gas phase. Typical diffusion values for gas and liquid are 1 x 10^{-5} and 1 x 10^{-9} m^2/s, respectively.[189] These includes the work by Wilhelm and his coworkers[190-191] where binary gaseous diffusion coefficients of CH_4 and some other gases were measured in cyclohexane, methylcyclohexane, benzene and toluene as well as in cyclooctane and *trans*-1,2-dimethyl cyclohexane.

Table 2.3 Summary of the literature for diffusion coefficients of CH_4 in hydrocarbon solvents

Solvent	*T*/K	*p*/MPa	Method*	Number of points	Uncertainty (%)	Ref
Hexane	303.2 - 333.2	30-50	NMR	24	2	[180]
Octane	304-435	1.72	TDA	6	0.8	[150]
	303.2 - 333.2	30-50	NMR	30	2	[180]
	280.7 - 311.75	1.72	CAR	4	0.2	[181]
	298 - 433	1	TDA	4	1	[151]
	301.4 - 373.2	1.72	MZI	4	10	[182]
Nonane	280.7 - 311.75	1.72	CAR	4	0.2	[181]
Decane	280.7 - 311.75	1.72	CAR	4	0.2	[181]
	303 - 423	20 - 60	MZI	9	0.6	[183]
	298 - 433	1	TDA	3	1	[151]
Dodecane	318 - 354	4-34	DC	33	Not specified	[184]
Tetradecane	298 - 433	1	TDA	4	1	[151]

*DC = Diffusion Cell, NMR = Nuclear Magnetic Resonance, TDA = Taylor Dispersion Apparatus, CAR = Cylindrical Acoustic Resonance, MZI = Mach-Zehnder Interferometer.

2.3 Prediction models

Highly accurate experimental data is one of the important parameters in developing a correlation to predict the diffusion coefficients. According to the literature above, most data available were measured at temperature and pressure near the ambient condition. However, available correlations that were developed based on diffusion coefficients at atmospheric conditions cannot be used for higher temperature and pressure conditions.[192] The reason for this is because of the lack of reliable high temperature and pressure experimental data. The Sigmund[193] correlation however did predict better using an extension to the high pressure found in reservoirs a great depths.[194]

2.3.1 Rough hard sphere theory

The rough-hard sphere theory is a well-known theory for predicting transport properties of both pure and binary mixtures. For diffusion coefficient, rough hard-sphere (RHS) theory has been used widely to interpret the data.[75] Erkey and Akgerman Erkey[75] has measured the mutual diffusion coefficients of benzene in carbon tetrachloride and used the RHS theory for the interpretation of the data that they obtained. The theory was found to predicts their data successfully and thus, were used to develop a correlation for prediction of diffusivities in the

sub and supercritical CO_2. The developed correlation managed to fit the data with an average absolute deviation of 7.68%. Akgerman et al.[100] also developed a correlation based on RHS theory for prediction of diffusivities of heavy molecular weights organics such as naphthalene, phenanthrene and hexachlorobenzene in supercritical CO_2. Eaton and Akgerman[101] also have developed a prediction equation based on RHS theory for the determination of infinite dilution molecular diffusion coefficients in supercritical fluids. The correlation predicts the data successfully with an average absolute deviation within 15% over more than 1500 data point.
One of the recent studies on the implementation of RHS model has been carried out by Cadogan et al.[36] In this work, diffusion coefficients are correlated using RHS theory for CO_2 in a series of hydrocarbons and good agreement with the experimental data was found, with an average absolute deviation within 2.5%. In contrast, using the Stokes-Einstein equation, prediction of diffusion coefficients of the same systems resulted in average absolute deviations within 5%. However, the correlation based on the Stokes-Einstein equation for the heaviest species considered, squalane, was unsuccessful based on the high value of average absolute deviation. Nevertheless, the failure has led to the development of a more sophisticated correlation based on an elaboration of the RHS model.[36] In the correlation, the solute was CO_2, and a series of non-polar solvents were investigated. The correlation manages to successfully fit the data for D_{12}* against V* within ±10%. The successful results in Cadogan's work played an important role that encourages the work in this thesis to extend a similar method to a wider range of solutes and solvents. However, to test the theory in a meaningful way, experimental results are needed over wide ranges of temperature and pressure.

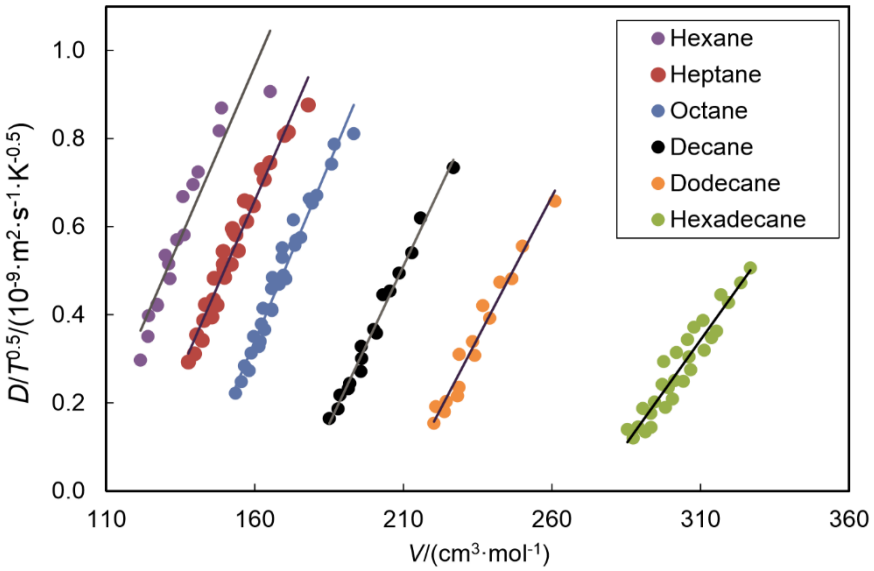

Figure 2.2 Diffusion coefficients D of CO_2 in several hydrocarbons divided by $T^{0.5}$ plotted against solvent molar volume V. Symbols represent experimental data while the solid lines represented the predicted data using RHS theory. [195]

2.3.2. Molecular dynamic simulation

Molecular dynamic simulation (MD) techniques is an alternative tool for calculating diffusion coefficients, especially at conditions that are difficult and unsafe for experimental work. The diffusion coefficients calculated from molecular dynamics are Maxwell-Stefan diffusivities. [196] Several studies by Krishna and his co-workers have used the molecular simulation techniques to calculate self and mutual diffusion coefficients in homogeneous phases[197] as well as in confinement.[198-204] Zabala et al. [52] have computed the diffusion coefficient of systems involving dissolved CO_2 in several hydrocarbons (up to C_{44}) at their bubble pressure and at temperatures varying between (298 and 373) K. Feng et al. [47] also performed molecular simulations to investigate the diffusion coefficients of dilute CO_2 in alkane solvent over a wide density range of solvent, while Higashi et al. [49-50, 53] used molecular simulation to calculate the mutual diffusion coefficient for CO_2 and aromatic hydrocarbons in the critical region. More recent work by Moultos et al.[48] using molecular simulation addressed the diffusion coefficients of CO_2 in hydrocarbons including hexane, decane, hexadecane, cyclohexane and squalane at temperatures up to 423 K and pressures up to 65 MPa. The same group have also simulated the diffusion coefficient of CO_2 in water.[51] In addition to that, Dysthe et al.[45-46] have used the MD and the Green-Kubo formalism to study transport coefficients as a function of composition in mixtures of decane with CH_4, C_2H_6 and CO_2. Diffusion coefficients of mixtures of CH_4/ C_6H_{14} were calculated using MD technique by dos Santos et al.[205] They reported the self-diffusion coefficients of the mixtures in both liquid and supercritical phases and evaluated the finite box size and the choice of the force field on the diffusion coefficients at high pressures. Easteal and Woolf[77], on the other hand, reported the tracer diffusion data through simulation of binary mixtures with solvent/ solute mass ratio (σ_2/σ_1) and size ratio (m_2/m_1) in the range from 0.6 to 10 and 1.2 to 2.0, respectively, and for a specific range of densities. The density of the system was expressed as ration of V/V_0 and varied in steps of 0.1 between 1.5 to 2.0 as shown in Figure 2.3. The MD results from this work were used to determine the universal correlation developed by Cadogan et al.[36]

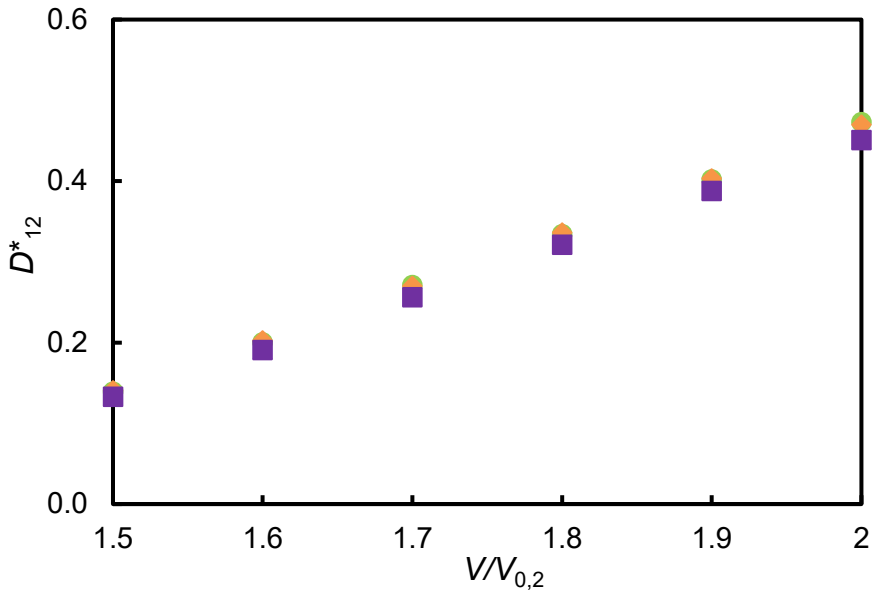

Figure 2.3 Dimensionless tracer diffusion coefficients of SHS systems as a function of the reduced volumes: ●, σ_2/σ_1 = 1.6; ◆, σ_2/σ_1 = 1.8; ■, σ_2/σ_1 = 2.0.[77]

CHAPTER 3 EXPERIMENTAL APPARATUS AND METHOD

As discussed in the chapter before, a wide selection of techniques has been developed for the measurement of diffusion coefficients.[54] However, in this chapter, detail explanations will be discussed on the principle and practise of the Taylor dispersion technique as it was used for all the measurements involved in this study. Description on the operating procedure, data reduction and interpretation will also be carefully explained.

3.1 Taylor Dispersion Apparatus

The measurements of diffusion coefficients for all systems in this thesis were using the Taylor dispersion apparatus as shown in Figure 3.1. This apparatus comprises of four modules, namely: a solvent delivery module that consists of a syringe pump and a degasser, a thermostatic oil bath that housed the diffusion capillary, a solution preparation module where the solvent was being saturated with the gas solute and a differential refractive index detector (RID).

The syringe pump used in this work (Teledyne ISCO, model 100DM, USA) has a capacity of 100 ml and were used to pump the solvent to high pressure and provide a constant flow of solvent through the system. The measurements of diffusion coefficients for both systems involved were made at pressures from atmospheric to a maximum pressure of 65 MPa. To achieve the desired pressure, the syringe pump was first set to a pressure-control mode before changing it to a flow-control mode where a consistent flow rate was set. The measurements of methane in toluene were made at flow rates between (0.028 to 0.117) $ml \cdot min^{-1}$ and the measurements of methane in heptane were made at flow rates between (0.042 to 0.155) $ml \cdot min^{-1}$.

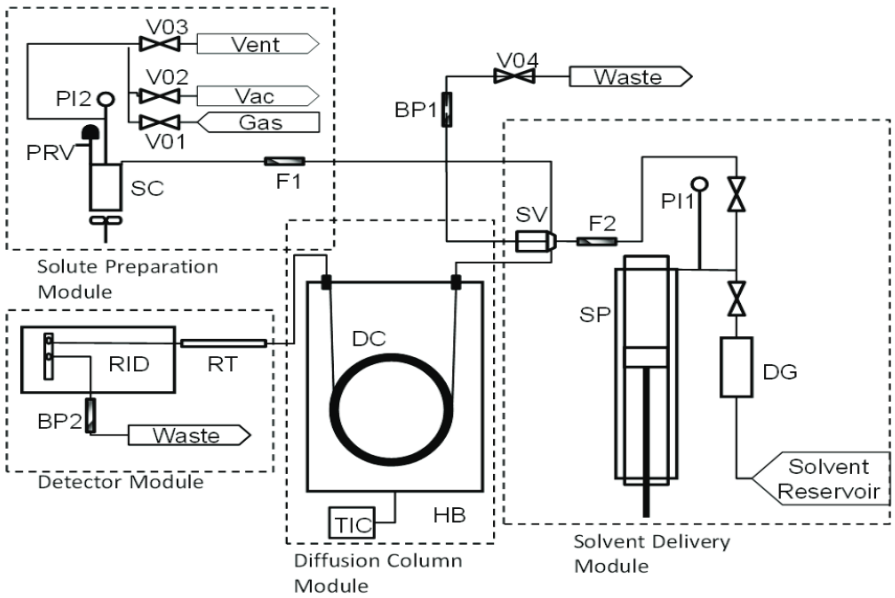

Figure 3.1 Schematic diagram of Taylor dispersion apparatus: DG, vacuum degasser; SP, syringe pump; PI1 and PI2, pressure transducers; F1 and F2, filters; SV, sample valve; DC, diffusion column; HB, thermostatic oil bath; TIC, temperature controller; RT, restriction tube; RID, refractive index detector; BP1 and BP2, back pressure valves; SC, saturation chamber; PRV; proportional relief valve; V01, V02 and V03, gas and vacuum valves; V04; solution outlet valve.

After exiting the pump, the solvent flow passed through a 6-port injection valve (VICI, Cheminert Model C72H – 1696D, Switzerland) and into a coiled diffusion column which housed in a thermostatic oil bath that controls the experimental temperature. The length of the diffusion column, L = 4.518 m, measured with an ordinary tape. The internal radius of the tube, R = 0.5398 mm has been determined by weighing the tube, both empty and after filling with pure water, on an analytical balance with a resolution of 0.1 mg[66]. In the oil bath, the tube was coiled on a drum with a radius of 0.109 m. The temperature of the oil bath was measured with a secondary-standard platinum resistance thermometer (Fluke Hart Scientific, Model 5615, USA) and readout unit (Fluke Hart Scientific, Model 1502A). The thermometer was calibrated before by Cadogan et al.[36, 62] on ITS-90 at the temperature of the triple point of water and compared in a constant temperature bath with a standard platinum resistance thermometer at nominal temperatures of (323, 373, 423 and 473) K. The standard uncertainty of the temperature measurements was reported to be 0.02 K. The pressure was measured with a standard uncertainty of 0.05 MPa by a pressure transducer mounted on the top of the syringe pump. No further calibration has been made prior to starting the measurements.

The RID used in this work (Agilent 1200 series, model G1362A, USA) reads the difference between the refractive index of the sample solute-solvent solution to that of pure solvent and produces a signal that was analysed to obtain the diffusion coefficients. The RID operated at low pressure, typically 0.45 MPa. To control the pressure upstream, a different type of restrictor tubes was inserted in between the column and the RID. The length and diameter of the restrictor tubes were selected depending on the pressure drop required by changing the solvent flow rate. The pressure drop across the restrictor tube can be estimated over a suitable range of flow rates based on the Hagen-Poiseuille equation.[206] The restrictors were PEEK-reinforced-silica tubes with diameters and lengths as detailed in table 3.1 for different target pressure drops.

Table 3.1 Selection of restrictor tube for various range of pressure.

p (MPa)	Restrictor tube
~1	50 µm x 50 mm
~10	25 µm x 100 mm
	25 µm x 150 mm
20 - 40	25µm x 200 mm
> 50	25 µm x 500 mm

The solution preparation module consists of a saturation chamber that was fabricated from titanium. It was used to saturate the solvent with the gas solute at a pressure not more than 0.7 MPa.The chamber had an internal volume of 100 ml and was fitted with a magnetic stirrer bar which aided the dissolution of the gas solute into the solvent. The gas-saturated solution allowed to flow from the chamber through the 5 μL sample loop on the 6-port injection valve, exiting via back-pressure regulator BP1 to the waste bottle via valve V04. The assembly of the equipment in laboratory is shown in Figure 3.2.

Figure 3.2 The setting of Taylor dispersion apparatus in the laboratory

3.2 Operating Procedure

Before starting a measurement, the solvent of choice was initially flushed through the system to the atmosphere to clean the restrictor tube and monitor the flow conditions of the solvent that exit the restrictor tube. The solvent was charged from a solvent reservoir through a filter into an in-line degasser (Knauer, model A5328, Germany) to degas the solvent before entering the syringe pump. The volume of the solvent reservoir was usually 200 ml to ensure the solvent filter were fully submerged in the solvent during the charging. The pump of capacity 103 ml was refilled at regular intervals to ensure sufficient solvent was available for an experimental run. The primary mode of operation used on the pump was the constant flowrate mode since subsequent analysis required the value of the flowrate. However, to obtain the flowrate that corresponded to the desired pressure, the constant pressure mode was initially utilised. The pump adjusted the flow rate to meet the required pressure; this value was then inputted in the constant flowrate mode. The solvent was then moved through the 6-port injection valve, into the diffusion column, the restricted tube, a differential refractive index detector before passing by the backpressure regulator into the waste bottle.

The solution of CH_4 and solvents were prepared in the 100 ml saturation chamber at ambient temperature and pressure of up to 0.7 MPa. The chamber was filled up to approximately 75 % of its maximum volume with the solvent. After a thermal equilibrium and a steady-state flow were established, a series of injection was made. Four to six repeat measurements were made at each temperature and pressure, where the mean and relative standard deviation of the diffusion coefficients were calculated. The time for the system to reach steady state varied depending on the restriction tube used and the system pressure. It usually varied between several hours to three days. The injection time was 5 seconds, with the maximum volume of the plug corresponding to a 7-second injection. It had been previously shown that altering the injection time had no significant effect on the amplitude of the peaks observed and the corresponding measured diffusion coefficients. Prior to starting an injection, the saturated

solution was passed under pressure, through a dip tube in the saturation chamber, into the 5 μL sample loop on the 6-port injection valve, via the back-pressure regulator BP2 to another waste bottle. The experiment was controlled by a program written in Agilent VEE where it logged and collected readings from the RID every 5 s. A master code developed by Cadogan[207] were used allowing the experiment to be run automatically and measurements shown on the Agilent 1200 to be recorded. The program was able to control the solvent flowrate and sample valve actuation and monitored the pressure, RID reading, and the sample valve position as well as other experimental parameters as follows

a) Time delay prior to injections – this was the time lag between the start point for running the programme and the first injection into the system.

b) Time between injections – this was dependent on the flowrate. It was important to allow enough time between injections so that adjacent peaks did not interfere and overlap. A longer time between injection was required for larger flowrates.

c) Purge time – this was the time during which the purge valve opened after each injection had been completed.

d) Injection time – this controlled the volume of solute that was injected into the system.

The main criteria to achieve an optimal conditions for the Taylor Dispersion apparatus is that the flow should be laminar and that secondary flow induced by coiling of the capillary should be negligible.[57, 208] To achieve that, the Reynolds number, [*Re*] and the Schmidt number, [*Sc*] must be kept within the acceptable range so that the product of [*De*]^2[Sc] is less than 20.[65] [*De*] is the Dean number obtained by multiplying [*Re*] with the square root of R/R_{coil}, where R is the column radius and R_{coil} is the coil radius. [*Re*] was given by the relation

$$\left[\mathrm{Re}\right] = \frac{2Rv\rho}{\eta} \tag{3.1}$$

and *Sc* can be calculated from the relation

$$\left[Sc\right] = \frac{\eta}{\rho D} \tag{3.2}$$

where v is the linear flow rate of the solvent averaged over the cross-section of the tube, ρ is the solvent density, η is the solvent viscosity and D is the diffusion coefficient at the column temperature. For the present measurements of CH_4 in methylbenzene and heptane, this criterion was easily followed as the experiment was operated such that $R_e < 8$ and $D_e^2 S_c < 19$.

3.3 Data Interpretation

The Taylor dispersion apparatus used in this work is based upon the dispersion that occurred when a solute plug was injected into a solvent flowing in the laminar regime. Axial dispersion due to the parabolic flow profile of the solvent acted to spread the pulse out longitudinally,

however, radial dispersion acted to keep the pulse combined. The combination of these two competing effects has produced an effective Gaussian distribution for the solute concentration, which was reached upon fully developed flow and was displayed as a Gaussian peak on the Refractive Index Detector.[56]

The RID measured the change in the refractive index corresponded to the difference in concentration between the flowing solute-solvent and the flow of the pure solvent. The signal at the detector $s(t)$ was analysed using the following relationship

$$s(t) = a + bt + \alpha c(t) \tag{3.3}$$

where a and b are the baseline coefficients, t is the time and $c(t)$ is the molar concentration given by following equation (equation 4). α in equation (3) is the detector sensitivity and the value can be either negative or positive depending on how the solute changes the refractive index of the solution. For the cases in this work, analysis showed negative peaks because the dissolved gases reduced the refractive index. Therefore, the refractive index readings had to be multiplied by -1 in order to apply the model. There was also an implicit assumption that the detector sensitivity is linear and so, the relationship between the signal that was measured, and the concentration is dictated by a constant α, which is not a function of concentration itself. As discussed in chapter 1, the concentration profile $c(t)$ is given by the Aris equation such that

$$c(t) = \left\{ n / \left(\pi R^2 \sqrt{4\pi K t} \right) \right\} \exp\left[-\left(L - vt \right)^2 / 4Kt \right] \tag{3.4}$$

where n is the amount of solute injected, L is the length of the column, and K is the dispersion coefficient, which normally related to the diffusion-coefficients by the relation[55]

$$K = D + \left(\frac{R^2 v^2}{48D} \right) \tag{3.5}$$

The value of L in equation 3.4 is given by the relation

$$L = L_c + \left(D / D_0 \right) \sum_{i=1}^{3} \left(R_i / R \right)^4 L_i \tag{3.6}$$

where D is the diffusion-coefficients at the column temperature and D_0 is the diffusion-coefficients at the ambient temperature. Subscript c is for column while subscript i = 1, 2, and 3 are three significant sections of the additional length of the tubing. These additional length from the connecting tubes were added to the main column as it has caused an excess dispersion to the column. Table 3.2 list out the internal radius and length of each of these additional sections. In order to make the corrections smaller, one can consider having a smaller internal radius of these tubing sections or having a longer column.[66] Figure 3.3 shows

an example of the RID signal measured for CH_4 in methylbenzene at T = 373 K and p = 31.37 MPa at flowrate of 0.128 ml/min where the data conform to equation (3) to (5).

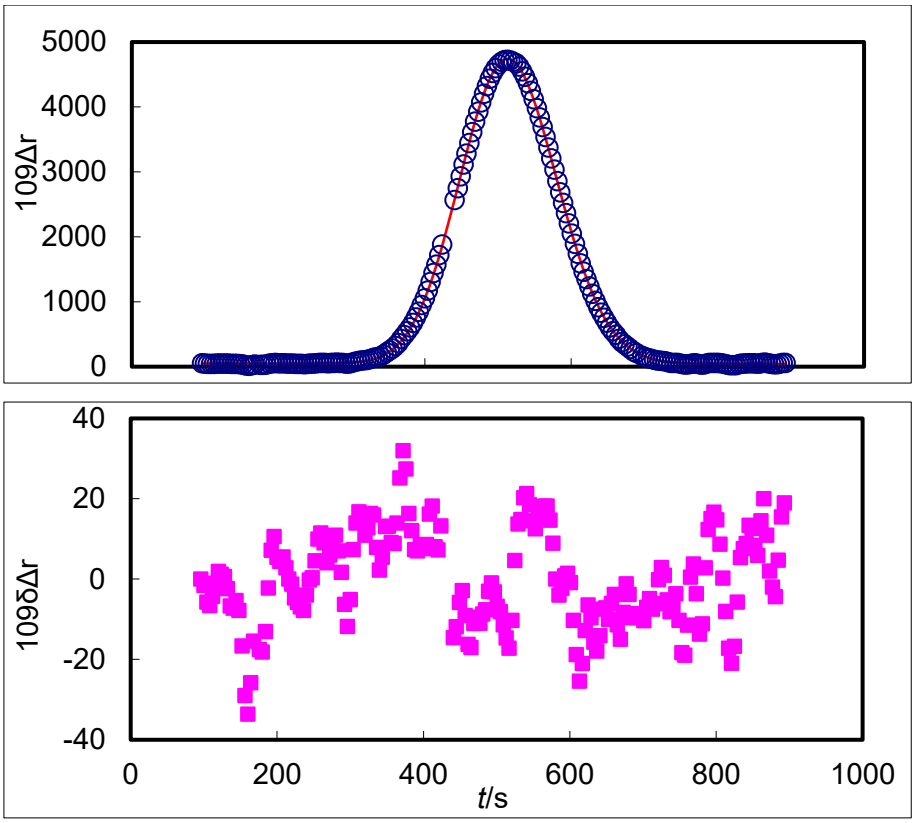

Figure 3.3 Dispersion curve for $s(t)$ for CH_4 in methylbenzene at T = 373 K, p = 31.37 MPa, and a flow rate of 0.128 ml/ min: ○, refractive index signal; ─, Aris model fitted to experimental data. (bottom) Deviation Δs between the experimental data and the model.

Table 3.2 Radius and length of the additional sections.

Sections	R (mm)	L (m)
between the injection valve and the column	0.39	0.3
between the column and the inlet of the detector	0.13	0.6
the internal flow path in the detector	0.22	0.4

The analysis involved fitting parameters into equation 1.3 with the refractive index signal by first approximating the values for the baseline coefficients and the diffusion coefficient. The sum of square differences between the experimental signal and the model equation were calculated and minimized by adjusting the parameters to obtain the actual value of the diffusion coefficient.

CHAPTER 4 RESULTS AND DISCUSSION

This chapter present results and discussion and are divided into three sections. The first section is solely on experimental results obtained and discussions of the behaviour of the diffusion coefficients when temperature and pressure changed. The experimental diffusion coefficients were correlated with the Stokes-Einstein model and is discussed in section 4.2. The experimental results were also used in developing a universal correlation based on the rough-hard-sphere theory and the performance is discussed in section 4.3. The content of this chapter was mainly deduced from two papers that were published earlier. [209-211]

4.1 Experimental results

Experimental results from the measurements of diffusion coefficients D_{12} of methane at effectively infinite dilution in methylbenzene and in heptane are reported. Measurements were made at temperature ranging from (323 to 398) K and at pressure from 1 MPa up to approximately 65 MPa for each temperature using the Taylor dispersion method.

The experimental data for diffusion coefficient of methane in methylbenzene and heptane are illustrated as a function of pressure in Figure 4.1 and Figure 4.2, respectively. As expected, for both systems, the diffusion coefficient was found to increase when the temperature increased and to decrease when the pressure increased. However, the effect of temperature in both systems were found to be more significant as the increment in diffusion coefficient was found to be more than 90% across the temperature range investigated for all pressure conditions. The increasing behaviour in the diffusion coefficient values with the increase in temperature was due to the increase in the internal energy of the particles which then leads to the increase in the kinetic energy. Meanwhile, the decrement in diffusion coefficient between the highest and lowest pressure point was found to be approximately 36% for methylbenzene and 38% for heptane. The decrement of diffusion coefficient value can be well explained by considering the molecular interactions between the solute and solvents. When pressure increases, the molecule in the solvents become more closely packed, resulted to an increase in the solvent viscosity and density. This led to an increase spatial hindrance on the solute and a reduction in translation across the solvent that leads to a reduction in the diffusion coefficients. This finding agrees with other similar work involving diffusion coefficient of light gases in various substances. Cadogan et al. [36 184, 212-214] For instant, Cadogan et al. [36 62, 207] have studied the diffusion coefficient of CO_2 in hydrocarbons, water, and brine solutions over a wide range of temperatures and pressures. In his work, the diffusion coefficients was decrease approximately 35% over the investigated pressure range of (0.1 to 69) MPa, except for squalane, where the decrement was larger with approximately 55%. Riazi[214] in his work has presented the diffusion coefficients of methane-pentane binary system using PVT cell and developed a model to predict the diffusion coefficients at the gas-liquid interface region. In their work, the model has successfully predicted the value of diffusion coefficients to decrease when the pressure increased, and the results yielded the value within ±5% from the reference values. [193, 215-217] In other work, Jamialahmadi et al.[184] has presented the measurement of methane in dodecane using a precision high pressure and temperature diffusion cell apparatus. In their summary, it was stated that the maximum value of diffusion coefficient appeared at a pressure where all gas has dissolved in the liquid phase. They also summarised

that the increase in viscosity and density has led to a decrease in diffusion coefficient when the pressure is increased.

For better observation, the experimental data for methylbenzene and toluene were plotted together as shown in Figure 4.3. In this figure, the diffusion coefficients of heptane were calculated at the same *T* and *P* as of the methylbenzene using a simple correlation that will be discuss later in this section. For each data point, the diffusion coefficients of methylbenzene were observed to be lower than the diffusion coefficient of heptane. However, as the molecular weight of both solvents are not very much differed, the average percentage difference was calculated to be approximately 14% only. This implies that the different in the structure of both solvent (methylbenzene is aromatic and heptane is aliphatic) does not have a large impact in the values of the diffusion coefficient. This statement was supported by the work of Cadogan et al.[36] In his work, the diffusion coefficient showed an increase trend when the carbon number of the alkane decreases due to the decrease in the number of bonds at low carbon number which leads to a lower amount of possible bond rotation.

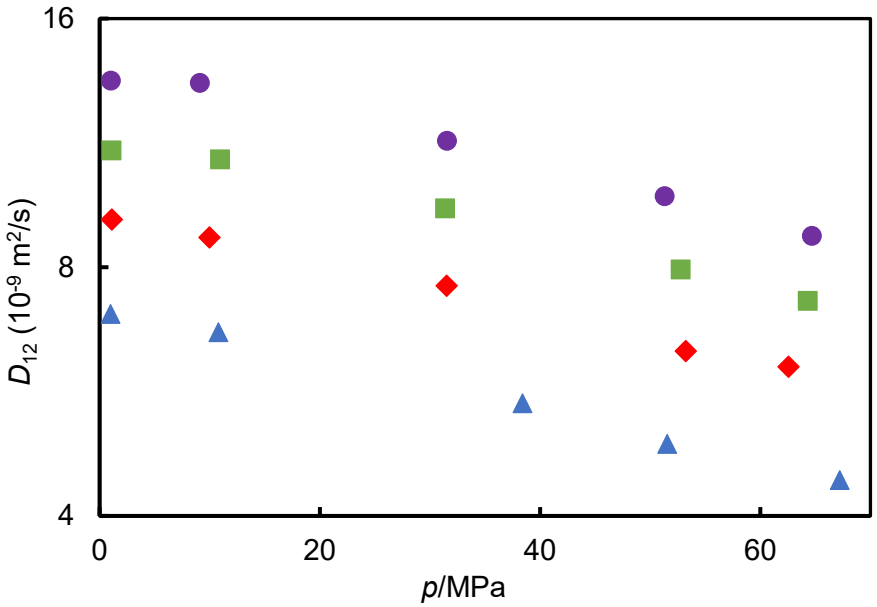

Figure 4.1 Diffusion coefficient D_{12} of methane at infinite dilution in methylbenzene as a function of pressure *p:*▲, *T* = 323 K; ◆, *T* = 348 K; ■, *T* = 373 K; □, *T* = 398 K.

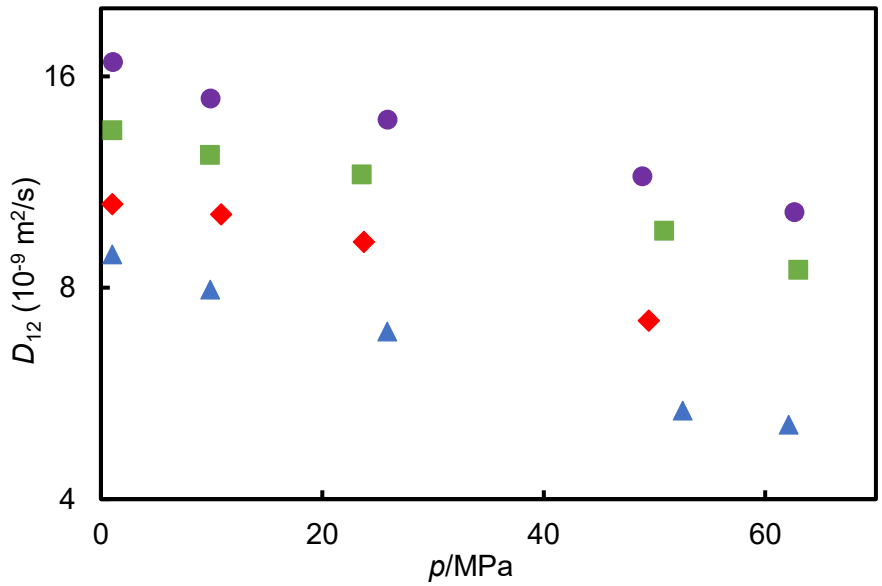

Figure 4.2 Diffusion coefficient D_{12} of methane at infinite dilution in heptane as a function of pressure p: ▲, T = 323 K; ◆, T = 348 K; ■, T = 373 K; □, T = 398 K.

The overall relative standard uncertainty associated with the measurements of the diffusion coefficient can be expressed in the following equation:

$$u_r^2(D) = u_r^2(K) + 4u_r^2(R) + 4u_r^2(v) + \left[\left(\frac{\rho}{D}\right)\left(\frac{\partial D}{\partial p}\right)u_r(p)\right]^2 + \left[\frac{1}{D}\left(\frac{\partial D}{\partial T}u(T)\right)\right]^2 \quad (4.1)$$

where $u_r(X)$ represents the standard relative uncertainty of variable X and $u(X)$ represents the standard uncertainty, K is the dispersion coefficients, R is the radius of the diffusion tube, and v is the axial velocity of the solvent averaged over the cross section of the tube. For the experimental data presented, the following values were considered for the calculation of the overall relative standard uncertainty: $u_r(K)$ = 2.1%, $u_r(R)$ = 0.20%, $u_r(V)$ = 0.50%, and $u_r(p)$ = 0.25%. The partial differential terms contribute to the error from the fluctuations in temperature and pressure over the duration of measurements. However, the values were negligible and therefore the values in the parenthesis were not considered in the calculation. This resulted in the overall relative standard uncertainty u_r(D) = 2.3%. On the other hand, the standard deviations σ_D obtained from repeated injections at each state point are illustrated as a function of temperature in Figure 4.4 and Figure 4.5 for methylbenzene and heptane, respectively. No systematic behaviour was observed in both figures and the data were found to be scattering.

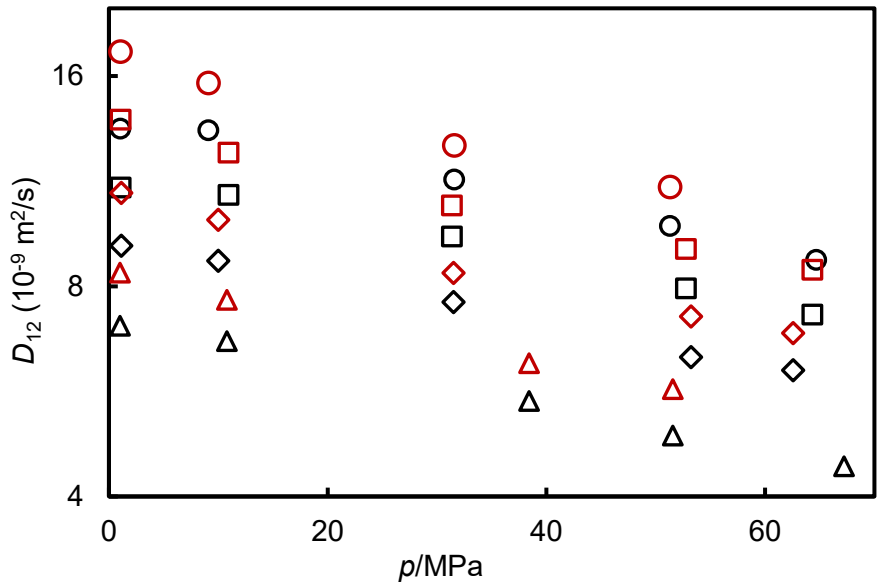

Figure 4.3 Comparison on the diffusion coefficient D_{12} value of methane at infinite dilution in methylbenzene (black symbol) and heptane (red symbol) as a function of pressure p: △, T = 323 K; ◇, T = 348 K; □, T = 373 K; ○, T = 398 K.

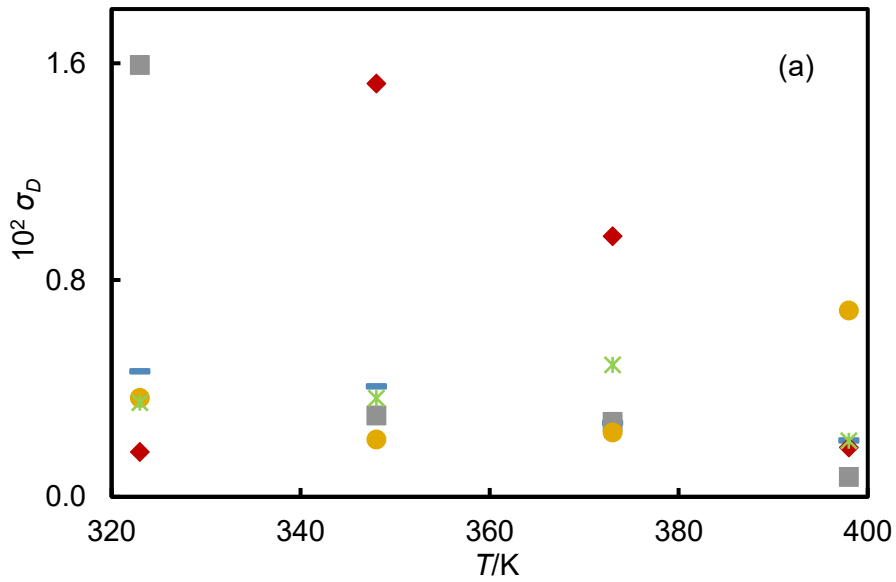

Figure 4.4 Standard deviation of the diffusion coefficient of methane in methylbenzene obtained from repeated injections at each point. —, p = (1 to 1.12) MPa; ◆, p = (9.10 to 10.9) MPa; ■, p= (31.4 to 38.4) MPa; □, p = (51.3 to 53.2) MPa; ✳, p = (62.1 to 67.2) MPa.

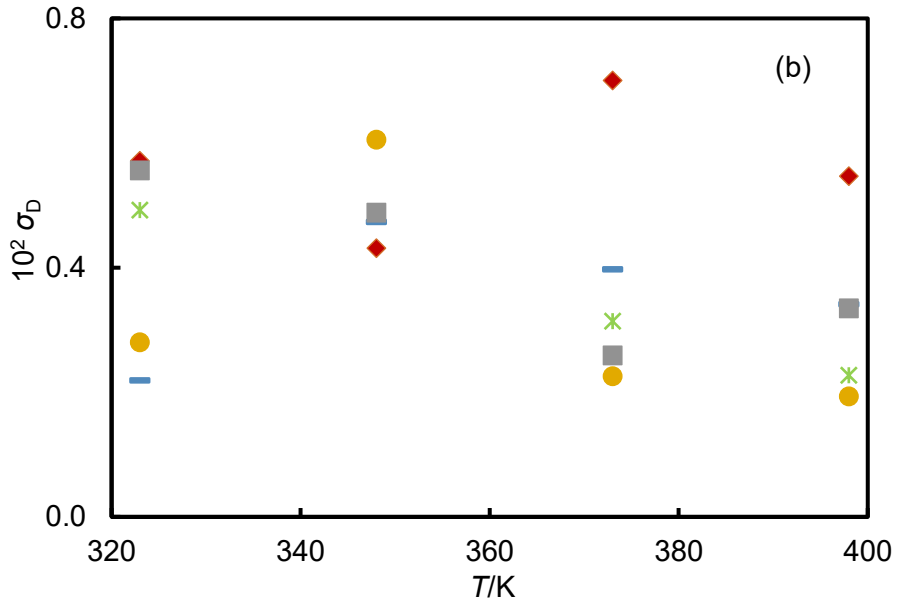

Figure 4.5 Standard deviation of the diffusion coefficient of methane in heptane obtained from repeated injections at each point. —, p = (1.02 to 1.08) MPa; ◆, p = (9.85 to 10.9) MPa; ■, p= (23.6 to 25.9) MPa; □, p = (48.9 to 52.5) MPa; ✳, p = (62.1 to 63.0) MPa.

The experimental data for both systems along each isotherm have been fitted using the following correlation:

$$D_{12} = D_0 \exp\left[-b(p - p_0)\right] \tag{4.2}$$

where D_0 is the diffusion coefficient at p_0 = 0.1 MPa. The parameters D_0 and b determined on each isotherm were listed in appendix 4C and the linear correlations are plotted in Figures 4.6 and 4.7. The parameters D_0 and b were fitted as linear and quadratic functions of temperature, respectively, to develop a surface-fit correlation such that

$$D_0 / \left(10^{-9}\,\mathrm{m^2 \cdot s^{-1}}\right) = d_0 + d_1 (T / K) \tag{4.3}$$

And

$$b / \mathrm{MPa^{-1}} = \sum_{i=0}^{2} b_i \left(T / \mathrm{K}\right)^i \tag{4.4}$$

The parameters for equation 4.3 and 4.4 can be found in appendix 4D and the surface-fit model is also shown along the experimental isotherms as dashed lines in Figures 4.6 and 4.7. The results showed a good representation of the data for both systems with the average

absolute relative deviation (Δ_{AAD}) to be approximately 1.4% and 3.7% for methylbenzene and heptane, respectively and the maximum absolute relative deviation (Δ_{MAD}) to be less than 6% for both systems. The Δ_{AAD} and Δ_{MAD} can calculated using the equation as follows:

$$\Delta_{AAD} = \frac{1}{N}\sum_{i=1}^{N}\left|\frac{D_{12,exp} - D_{12,fit}}{D_{12,exp}}\right| \tag{4.5}$$

and,

$$\Delta_{MAD} = \mathrm{Max}_i\left|\frac{D_{12,exp} - D_{12,fit}}{D_{12,exp}}\right| \tag{4.6}$$

Here, $D_{12,\,exp}$ is an experimental value, $D_{12,\,fit}$ is the value calculated from equation 4. 2 to 4.4 and N is the total number of points. Figure 4.8 compares the values of $D_{0,}$ and b determined in the isotherm fits with equation 4.3 and 4.4. It can be clearly seen that the data for methylbenzene are smoother than the data for heptane. The value of the coefficient b was found to vary between (0.0069 and 0.0093) MPa^{-1} in all the investigated isothermal fits. The optimal value for b was found to be in heptane system with the value of 0.0093 MPa^{-1} corresponding to an average relative reduction in the value of D_{12} of 43% between p = 0.1 MPa and p = 62 MPa. Literature data on diffusion coefficient of CH_4 in either methylbenzene or heptane were not available, however, we found one data point of D_0 for CH_4 in heptane in the work done by Hayduck and Buckley.[218] In their work, they used capillary cell technique to measure diffusion coefficient of methane in normal hexane, heptane, octane, dodecane and hexadecane at T=298K. Using the parameters from equation 4.3 and 4.4, we regressed the data to match the same temperature, and the regressed value was found to be almost 21% smaller than the value reported by Hayduck and Buckley.[218]

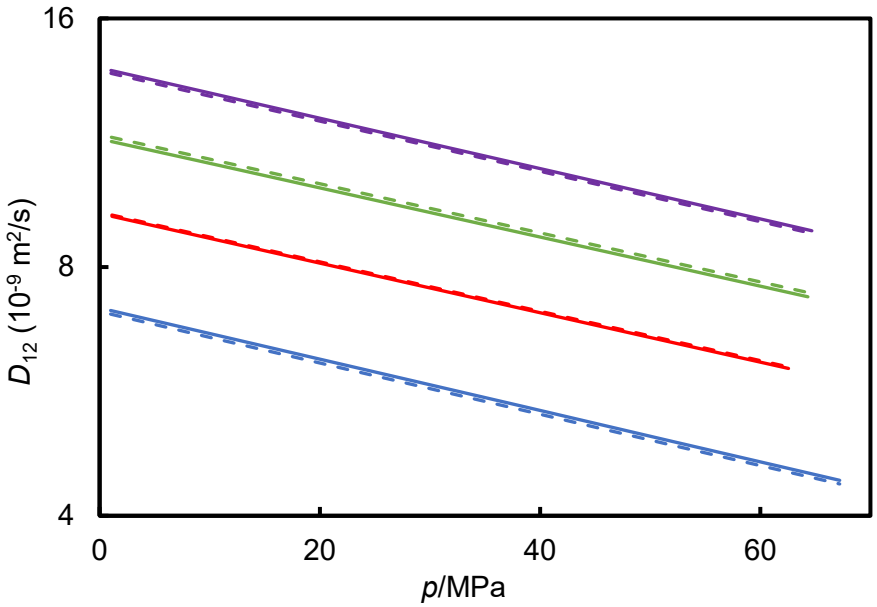

Figure 4.6 Calculated value of diffusion coefficient D_{12} of methane at infinite dilution in methylbenzene as a function of pressure p. Solid lines represent D_{12} calculated from equation 4.2 and dashed lines represent D_{12} calculated from fitting the value of D_0 and b from equation 4.3 and 4.4. Note the semi-logarithmic scale.

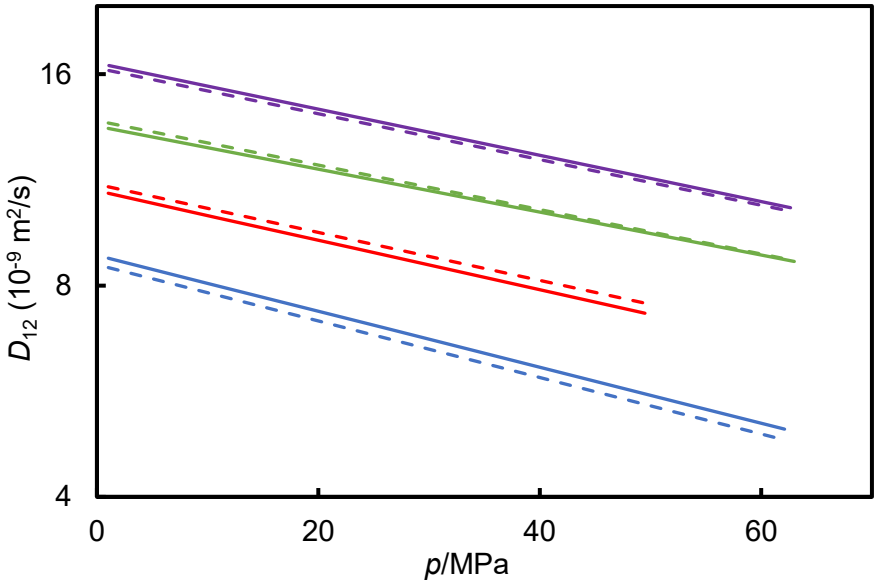

Figure 4.7 Calculated value of diffusion coefficient D12 of methane at infinite dilution in heptane as a function of pressure p. Solid lines represent D12 calculated from equation 4.2 and dashed lines represent D12 calculated from fitting the value of D0 and b from equation 4.3 and 4.4. Note the semi-logarithmic scale.

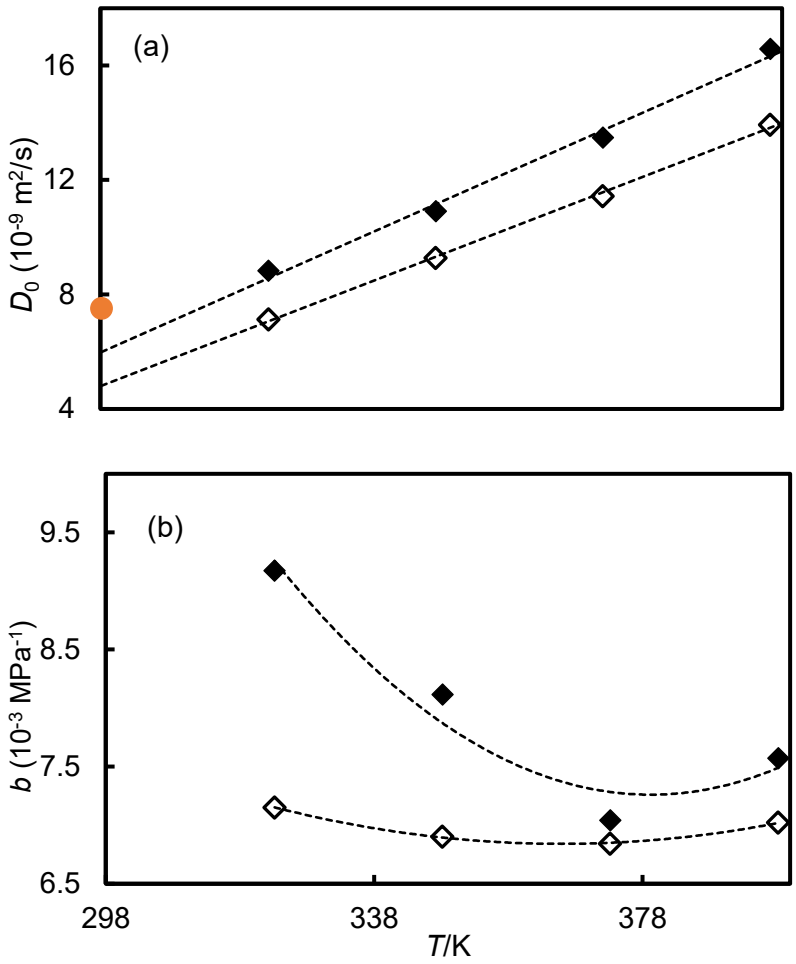

Figure 4.8 Diffusion coefficient D_0 (a) and b (b) as a function of temperature T: ◇, methylbenzene; ◆, heptane; ●, Hayduk and Buckley[218]. Dotted lines in (a) represents linear equation for D_0 and (b) represents quadratic function for b.

4.2 Stokes-Einstein correlation

The diffusion coefficients data were analysed with the Stokes-Einstein (SE) model as such:

$$D_{12} = k_B T / \left(n_{SE} \pi a \eta \right) \tag{4.7}$$

Here k_B is Boltzmann's constant, n_{SE} is the Stokes-Einstein number, taken to be 4, η is the solvent viscosity and a is the hydrodynamic radius of the solute. Derivation of the equation were discussed in chapter 3.

In this work, the values for η and ρ for both solvents were all taken from the REFPROP database. [219] For viscosity of methylbenzene, the values were from the correlations reported by Avgeri et al. [220] while for heptane, the values were from the work by Michailidou et al. [221] The estimated uncertainty for the viscosity of methylbenzene at a 95% confidence level varies depending on the region of temperature and pressure. For the temperature and pressure

investigated in this work, the estimated uncertainty was found to be 0.7%. The estimated uncertainty for heptane at 95% confidence level is 3.5% over the whole range except at the near-critical region. For density, the equation of state developed by Lemmon et al. [21] was used for methylbenzene and that of Tenji et al. [222] was used for heptane.

To calculate *a*, equation 4.7 was rearranged to yield the following equation

$$a = \frac{k_B T}{D_{12} n_{SE} \pi \eta} \tag{4.8}$$

The values of *a* calculated corresponding to a measured diffusion coefficient were calculated for each of data points and were plotted in Figure 4.9 against reduced solvent density ρ/ρ_c, where ρ_c is the critical density of the solvent. Based on the plot, a linear expression relating to the hydrodynamic radius and the reduced solvent density was fitted according to the following equation and the corresponding linear functions are plotted in Figure 4.9 as solid lines.

$$a \,/\, \mathrm{nm} = a_0 + a_1 \left(\rho / \rho_c \right) \tag{4.9}$$

The parameters for equation 4.9 can be found in Appendix 4E. The diffusion coefficients were then calculated using the parameters and the results were compared with the value calculated from the Stokes-Einstein model (equation 4.7). Figure 4.10 shows the deviation between both fits. In both cases, the model fits the experimental data with Δ_{AAD} of about 3.5%. The Δ_{MAD} was found to be 9.4% and 6.2% for methylbenzene and heptane, respectively. When making further analysis, we can observe that in the case of methylbenzene, the Stokes-Einstein model performs slightly worse than the empirical model formed by equation 4.2 to 4.4 while, for heptane, it is the other way around. However, the Stokes-Einstein model requires only two parameters per solvent instead of five.

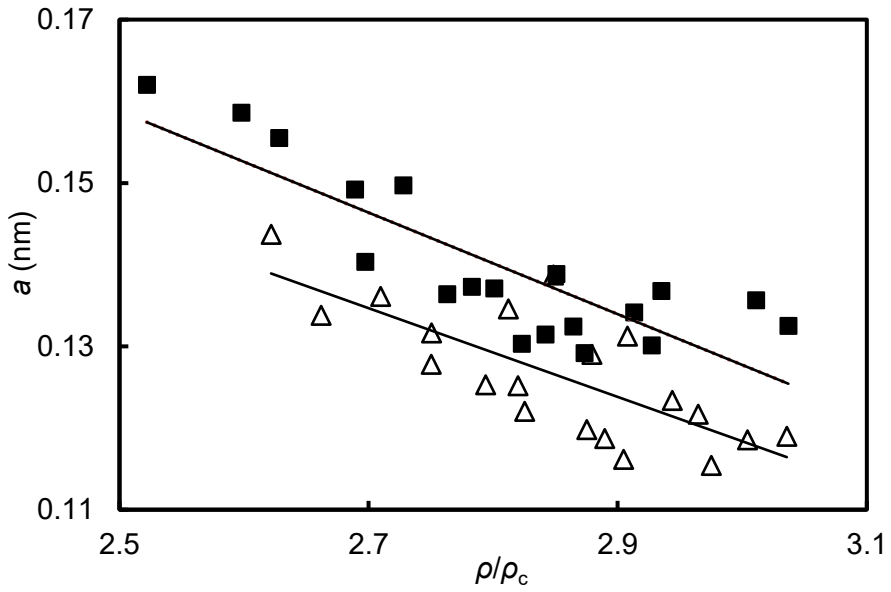

Figure 4.9 Hydrodynamic radius of CH_4, *a*, plotted against ρ/ρ_c for: △, methylbenzene; ■, heptane. The value of *a* was calculated by applying equation 4.8 to each data points. Solid lines represent linear correlation as equation 4.9.

A similar findings were observed in the work by Cadogan et al.[36] where the hydrodynamic radius were also found to exhibit a linear correlation with the solvent density. In their work, they compare the experimental data of diffusion coefficients of CO_2 in *n*-alkanes with the correlation fits using Stokes-Einstein equation with hydrodynamic radius calculated from equation 4.9. It resulted in Δ_{AAD} = 5% and Δ_{MAD} = 19%. However, the same approach was unsuccessful when attempted to a heavier hydrocarbon due to the flexibility of the molecule towards a more complex behaviour of the apparent hydrodynamic radius of the solute.

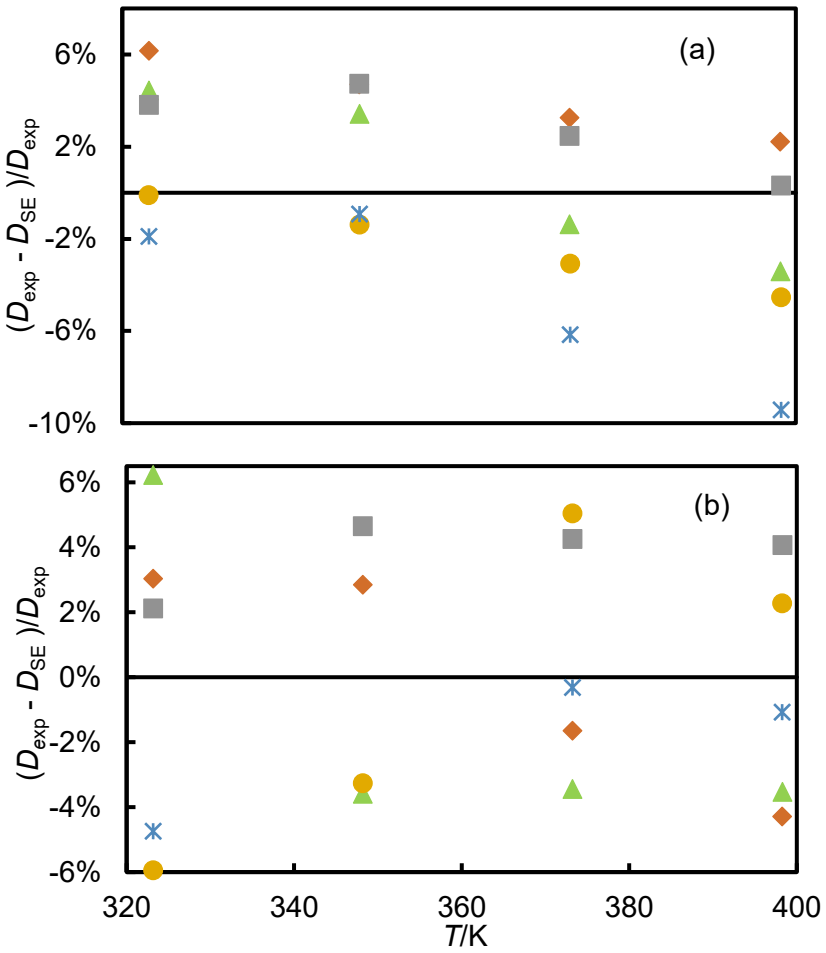

Figure 4.10 Deviation between experimental diffusion coefficient D_{12} and calculated diffusion coefficient from Stokes-Einstein model D_{SE} with hydrodynamic radius a calculated from equation 4.9 for (a) methylbenzene; (b) heptane at various pressures p; ▲, p = (1 to 1.12) MPa; ◆, p = (9.10 to 10.9) MPa; ■, p= (23.5 to 38.5) MPa; □, p = (48.9 to 53.2) MPa; ✳, p = (62.1 to 67.2) MPa.

4.3 Universal correlation based on rough hard sphere theory

In order to apply the extended RHS model, the experimental data of diffusion coefficients measured in this work were not sufficient. Therefore, we retrieved more experimental data from literature involving several gaseous solutes in hydrocarbon solvents that were available in the literature, together with molecular dynamics simulations (MD) for systems of smooth hard spheres. Table 4.1 lists the experimental data from the literature that were involved in the calculations. The MD data anchor the correlation because the roughness factor A_{12} for smooth hard-sphere systems is 1. For this work, data from the work by Easteal and Woolf[77] were used due to the accurate simulation run, relatively high number of data points and realistic value of densities, mass ratio (σ_2/σ_1) and size ratio (m_2/m_1).

Most of the data were measured using the same method that was used in this study which is the Taylor dispersion method. Other methods used were Cylindrical Acoustic Resonance (CAR), Mach- Zehnder Interferometer (MZI) and Capillary Cell (CC). From the table, we can see that most of the measurements were made at low condition with very few data points.

In Figure 4.11, we can see the experimental data of diffusion coefficient of methane in octane at P = 1.7 MPa measured using two different methods by two different literatures. It was calculated that the value obtained by Colgate et al. [220] were slightly higher by 6% than the value obtained by Erkey et al. [150]

Table 4.1 Summary of Experimental Diffusion Coefficients Data from the Literature, where T is temperature, p is pressure, N is number of data points and U_r is expanded relative uncertainty (k = 2).

Solute	Solvent	T/K	p/MPa	N	Method	10^2 Ur	Ref.
CH_4	Hexane	298	0.1-1.0	2	TD	<3	215
	Octane	298-403	0.1	4	TD	1	221
		281-312	1.7	4	CAR	0.2	220
		304-435	1.72	6	TD	1	150
	Nonane	281-312	1.7	4	CAR	0.2	220
	Decane	303-423	20-60	9	MZI	1.4	222
		298-433	0.1	3	TD	1	221
		281-312	1.7	4	CAR	0.2	220
	Dodecane	298	0.1	1	CC	3	215
	Tetradecane	298-430	3-13	4	TD	1	221
	Hexadecane	298	0.1	1	CC	3	215
C_2H_6	Hexane	298	0.1	1	CC	14	176
		303	0.1	1	CC	3	223
	Heptane	303-313	0.1	2	CC	3	223
		298	0.1	1	CC	14	176
	Octane	304-435	1.72	6	TD	1	150
		298	0.1	1	CC	14	176
	Dodecane	298	0.1	1	CC	14	176
C_3H_8	Hexane	298	0.1	1	CC	<5	224
	Heptane	298	0.1	1	CC	<5	224
	Octane	298	0.1	1	CC	<5	224
		335-435	1.72	6	TD	1	225
CO_2	Hexane	298-423	1.2-66	16	TD	2.6	35
	Heptane	298-423	1-68	30	TD	2.6	35
	Octane	298-423	0.9-69	30	TD	2.6	35
	Decane	298-423	1.1-68	16	TD	2.6	35
	Dodecane	298-423	1.3-63	15	TD	2.6	35
	Hexadecane	298-423	1-69	27	TD	2.6	35
	Squalane	298-423	1-67	30	TD	2.6	35
	Methylbenzene	298-423	1-68	30	TD	2.6	35
Ar	Hexane	298	0.3	1	TD	<3	222
	Octane	298-373	0.1	3	TD	1	221
	Decane	298-333	0.1	2	TD	1	221
N_2	Octane	303-399	15	4	MZI	10	183
	Decane	298-422	7.5-15	11	MZI	10	183

Taylor Dispersion (TD), Cylindrical Acoustic Resonance (CAR), Capillary Cell (CC), Mach-Zehnder Interferometer (MZI),

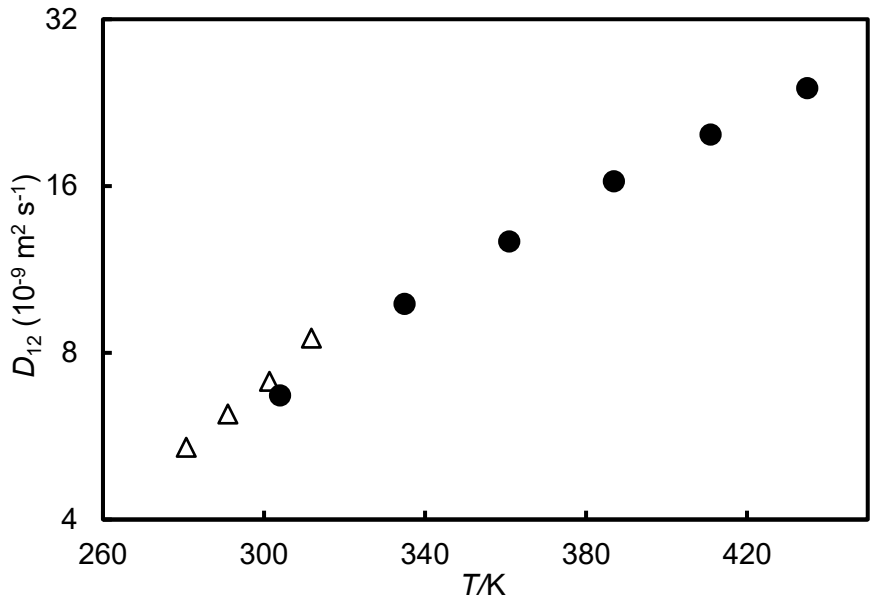

Figure 4.11 Mutual diffusion coefficient D_{12} of methane at infinite dilution in octane at 1.7 MPa as a function of temperature T: Δ, Colgate et al. [220]; ●, Erkey et al. [150]

As described in chapter 1, the RHS theory tells that D_{12}^* are a function of V^* ($V/V_{0,2}$) and upon the asymmetric ratio χ. V_0 is a temperature dependent but have a same value for a given temperature for all transport properties. In this theory, V_0 of the solute and solvents can be taken from the application of rough hard-sphere theory for pure substances. For instance, Assael, Dymond and their collaborators[69-73, 80-81] has used the RHS theory to correlate simultaneously the coefficients for viscosity, diffusion coefficients and thermal conductivity for an impressive number of substances. In this study, the V_0 for solutes and solvents were obtained from the existing correlations published by Assael et al. [226-228] except for hexadecane where the correlation was obtained from Ciotta et al. [229] The summary of the correlations used for all compounds used in this study are listed in Table 4.2. On the other hand, the asymmetric ratio χ can be calculated as follows

$$\chi = M_1 V_{0,2} / M_2 V_{0,1} = \frac{\left(\sigma_2 / \sigma_1\right)^3}{\left(m_2 m_1\right)} \tag{4.12}$$

Based on the MD results, the asymmetric ratio χ for all the gaseous solute involved in this study covers a range from around 0.8 to 3.1. The values are illustrated in Figure 4.12 for five different solutes. Even though the value changes with temperature, the changes are considered small, and the average value was taken. Figure 4.13 shows one example of how the ratio changes for CH_4 in octane and heptane as functions of temperature T.

Following the work by Cadogan et al.[35], the universal function F_{12} were represented by a simple polynomial equation as follows

$$F_{12} = \sum_{i=0}^{3} a_i (V^*)^i \quad . \tag{4.13}$$

where a_i are the universal constants. Therefore, the model required just one system-dependent parameter, A_{12}, and four universal constants a_i, in addition to the molar core volumes of the pure components. In this work, we extended this method to a wider range of non-polar solutions and obtained the dependence of F_{12} on both V^* and χ such that

$$F_{12}(V^*, \chi) = \sum_{i=0}^{3} a_i (V^*)^i + b_0 \chi \tag{4.14}$$

Table 4.3 reports the values of the universal constant while the values of A_{12} for each solutions involved are listed in Table 4.4 together with the values of the average absolute relative deviation (Δ_{AARD}) and the maximum absolute relative deviation (Δ_{MARD}). Entries without values of Δ_{AARD} and Δ_{MARD} are for systems with only a single data point available from which A_{12} was determined. Table 4.4. The parameters in equation 4.14 together with the value of A_{12} for each real-fluid solute-solvent pair were obtained by adjusting the values in a least-squared analysis with an objective function to be minimised was the un-weighted sum of the squares based on the relative deviations of the data from the model.

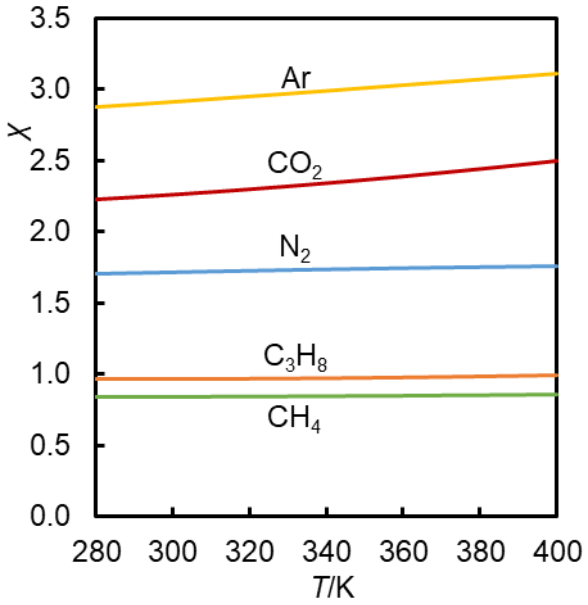

Figure 4.12 Asymmetry ratios χ for five different solutes in octane as functions of temperature T.

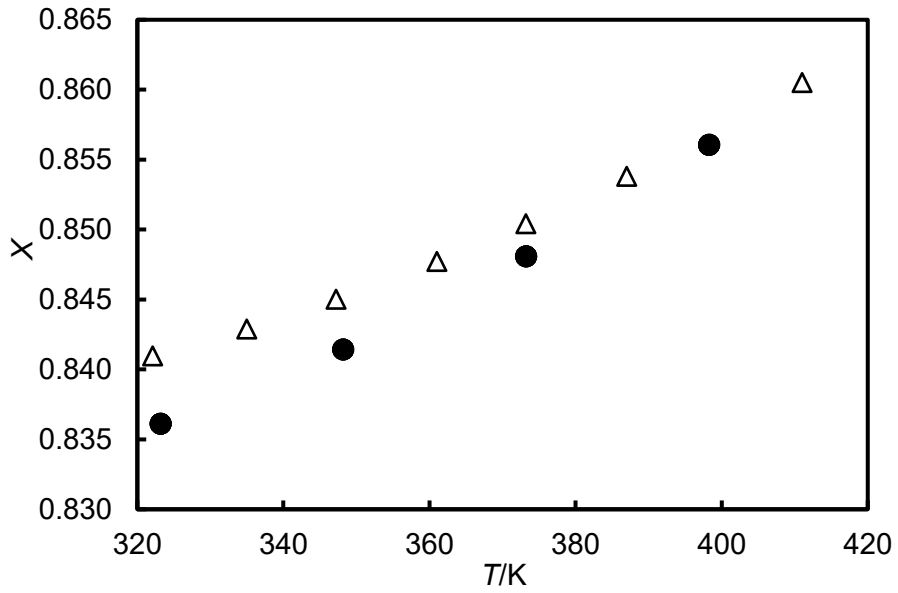

Figure 4.13 Asymmetry ratios χ for CH_4 in octane and heptane as functions of temperature T: Δ, octane; ●, heptane

Table 4.2 Correlations for molar core volume for the solute and solvents involved in this work as functions of temperature, where $\theta = T/\mathrm{K}$ and C = carbon number.

Compound	Correlation for $V_0/(\mathrm{cm}^3\ \mathrm{mol}^{-1})$	Ref.
(C_1 to C_4) alkanes	$45.822 - 6.1867\ \theta^{1/2} + 0.36879\ \theta - 0.007273\ \theta^{3/2} + C\ (2.17871\ \theta^{1/2} - 0.185198\ \theta + 0.00400369\ \theta^{3/2}) + C^2\ (6.95148 - 52.6436\ \theta^{-1/2}) + C_n^3\ (-7.801897 + 42.24493\ \theta^{-1/2} + 0.4476523\ \theta^{1/2} - 0.009573512\ \theta)$	226-227
(C_6 to C_{12}) alkanes	$117.874 + 0.15\ (-1)^C - 0.25275\ \theta + 0.000548\ \theta^2 - 4.246 \times 10^{-7}\ \theta^3 + (C - 6)\ (1.27 - 0.0009\ \theta)\ (13.27 + 0.025\ C)$	226-227
Methylbenzene	$92.929 - 0.10930\ \theta + 0.00012023\ \theta^2$	228
Hexadecane	$276.144 - 0.2384\ \theta + 0.00016983\ \theta^2$	229
Squalene	$631.293 - 0.9545\ \theta + 0.00090351\ \theta^2$	230-231
CO_2	$25.802 - 0.025251\ \theta + 0.000017948\ \theta^2$	230-231
Argon	$7.823 + 12.520 \cdot \exp(-\theta/325.78)$	This work
Nitrogen	$12.545 + 13.298 \cdot \exp(-\theta/171.27)$	This work

Table 4.3 Values of the parameters a_i and b_0 in the universal curve for tracer diffusion coefficients, together with the average absolute relative deviation (Δ_{AAD}) and the maximum absolute relative deviation (Δ_{MAD}) for the fit.

Parameter	**Value**
a_0	1.6874
b_0	0.0341
a_1	-4.0605
a_2	2.8478
a_3	-0.5621
Δ_{AARD}	2.7%
Δ_{MARD}	11.6%

Table 4.4 Roughness factors A_{12} with absolute average relative deviations Δ_{AAD} and maximum absolute relative deviations Δ_{MAD} for the diffusion coefficient

Solute	Solvent	A_{12}	Δ_{AAD} (%)	Δ_{MAD} (%)
CH_4	Hexane	0.771	0.4%	0.4%
	Heptane	0.647	3.2%	6.2%
	Octane	0.765	5.0%	11.6%
	Nonane	0.898	0.2%	5.7%
	Decane	0.779	0.0%	0.0%
	Dodecane	0.731	6.1%	8.7%
	Benzene	1.079		
	Methylbenzene	0.858	2.8%	6.6%
C_2H_6	Hexane	0.732	1.5%	1.5%
	Heptane	0.800	2.2%	3.2%
	Octane	0.792	0.5%	1.4%
	Dodecane	0.749		
C_3H_8	Hexane	0.788		
	Heptane	0.827		
	Octane	0.845	0.4%	0.8%
CO_2	Hexane	0.942	2.2%	8.3%
	Heptane	0.915	3.1%	7.8%
	Octane	0.871	2.3%	6.4%
	Decane	0.788	4.0%	6.3%
	Dodecane	0.750	2.6%	7.6%
	Hexadecane	0.706	3.3%	6.0%
	Squalane	0.514	1.5%	4.0%
	Methylbenzene	1.161	1.9%	6.0%
Ar	Hexane	0.763		
	Octane	0.760	2.0%	2.1%
	Decane	0.653	4.1%	4.3%
N_2	Octane	0.761	4.4%	8.2%
	Decane	0.761	3.8%	7.1%
SHS	SHS	1.000	2.9%	10.2%

Figure 4.14 to 4.18 shows the experimental reduced diffusion coefficient and the values predicted by the universal correlation as a function of reduced molar volume $V/V_{0,2}$. Looking at all the figures, it appears that the deviations tend to be larger at higher values of reduced volume. It is not clear what causes this, but it is expected that the model will break down as one goes to low density because it neglects attractive forces and is expected to be reliable only at high densities. The correlations were also observed to agree well with the molecular dynamics data. Figure 4.19 shows the relative deviations of the experimental diffusion coefficients as a function of the temperature T, reduced volume $V/V_{0,2}$, molar mass ratio M_1/M_2 and asymmetry ratio χ. Average, we can see that most of the data fits well with the correlations with deviations mostly within ±5%. The average absolute relative deviation of the experimental data from the correlation was found to be highest for CH_4-dedocane system with 6.1% and the maximum absolute relative deviation was reported for CH_4-octane with 12%. Although we have covered quite large numbers of systems, this correlation should be restricted to light solute of non-polar solute-solvent systems unless a revised correlation is develop using available experimental data for large molecular solutes in light supercritical solutes and also the molecular simulation data that were excluded from the present analysis (those with $\sigma_1/\sigma_2 > 1$ and/or $M_1/M_2 > 1$).

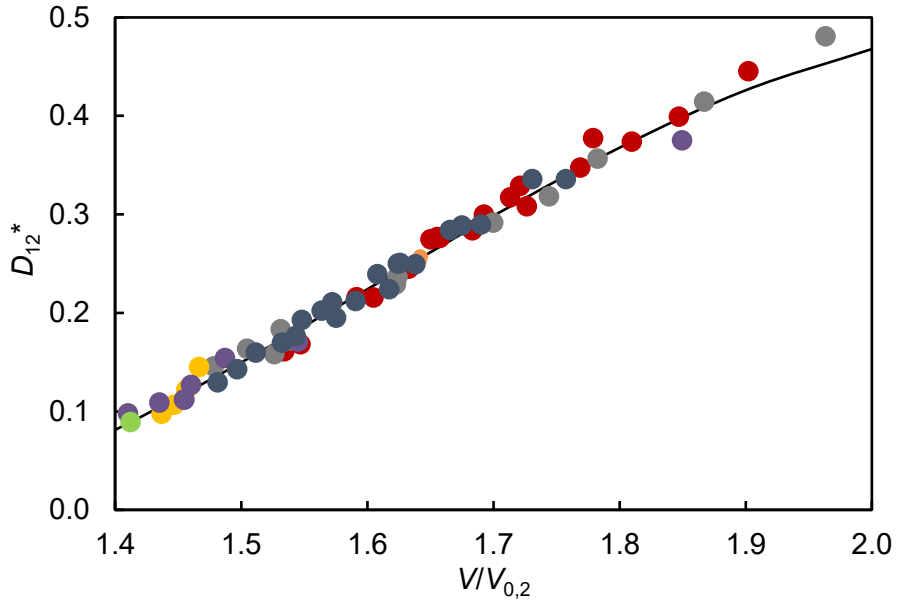

Figure 4.14 Calculated reduced mutual diffusion coefficients D_{12}^* of CH_4 in liquid hydrocarbons solvents as a function of reduced molar volume $V/V_{0,2}$: ●, hexane; ●, heptane; ●, octane; ●, nonane; ●, decane; ● methylbenzene; ●, dodecane; —, RHS theory plotted for a value of χ = 0.86.

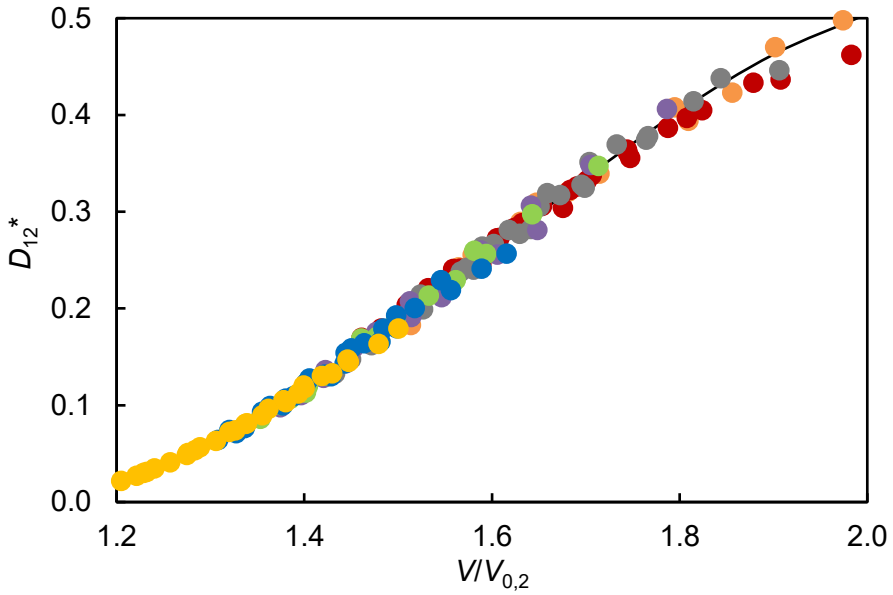

Figure 4.15 Calculated reduced mutual diffusion coefficients D_{12}^* of CO_2 in liquid hydrocarbons solvents as a function of reduced molar volume $V/V_{0,2}$: ●, hexane; ●, heptane; ●, octane; ●, decane; ● methylbenzene; ●, dodecane; ●, hexadecane; ●, squalane; —, RHS theory plotted for a value of χ = 2.1

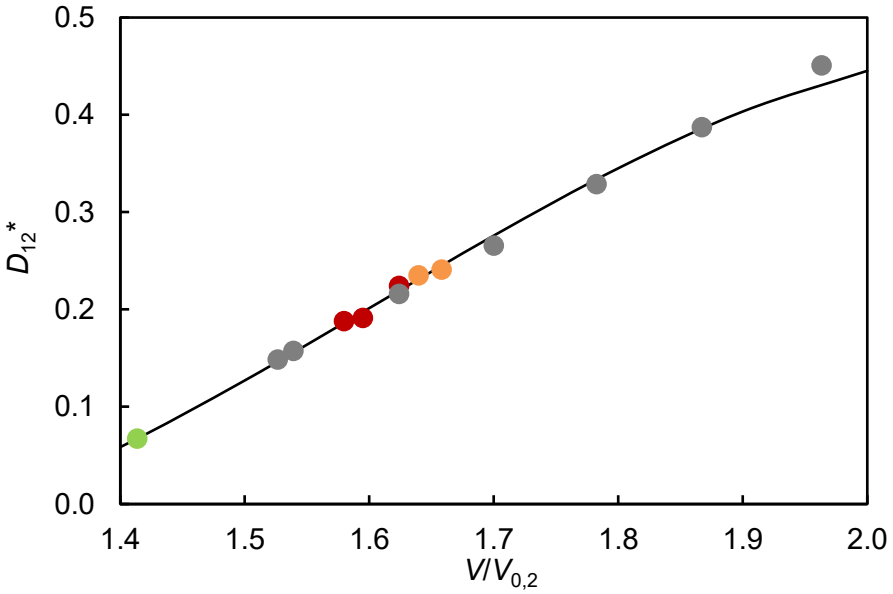

Figure 4.16 Calculated reduced mutual diffusion coefficients D_{12}^* of C_2H_6 in liquid hydrocarbons solvents as a function of reduced molar volume $V/V_{0,2}$: ●, hexane; ●, heptane; ●, octane; ●, dodecane; —, RHS theory plotted for a value of χ = 0.97

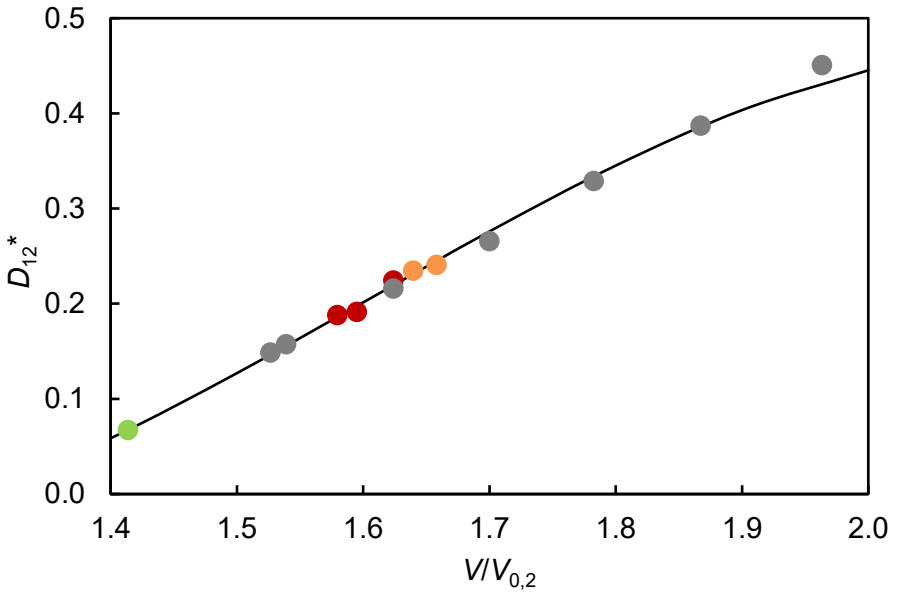

Figure 4.17 Calculated reduced mutual diffusion coefficients D_{12}^* of C_3H_8 in liquid hydrocarbons solvents as a function of reduced molar volume $V/V_{0,2}$: ●, hexane; ●, heptane; ●, octane; —, RHS theory plotted for a value of χ = 0.98

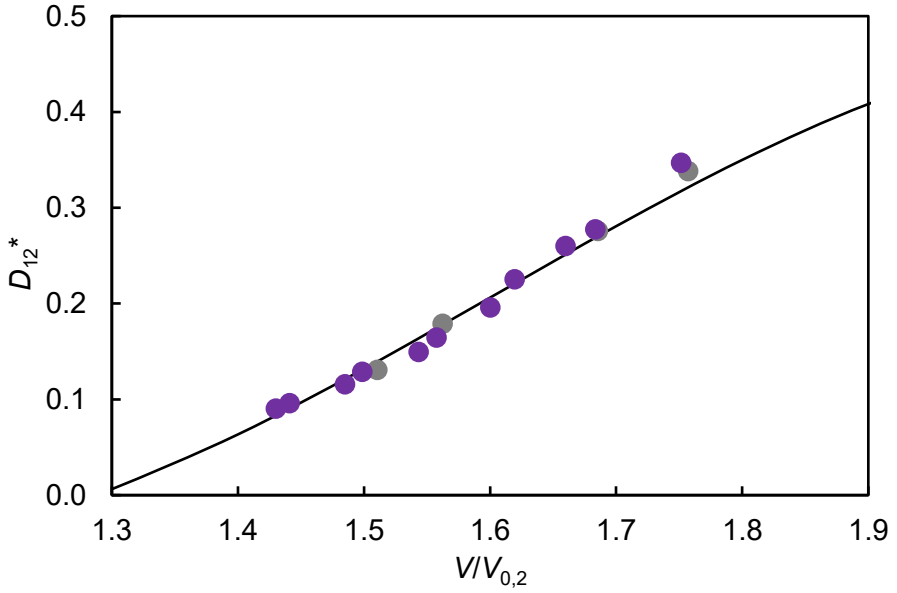

Figure 4.18 Calculated reduced mutual diffusion coefficients D_{12}^* of N_2 in liquid hydrocarbons solvents as a function of reduced molar volume $V/V_{0,2}$: ●, octane; ●, decane; —, RHS theory plotted for a value of χ = 0.84

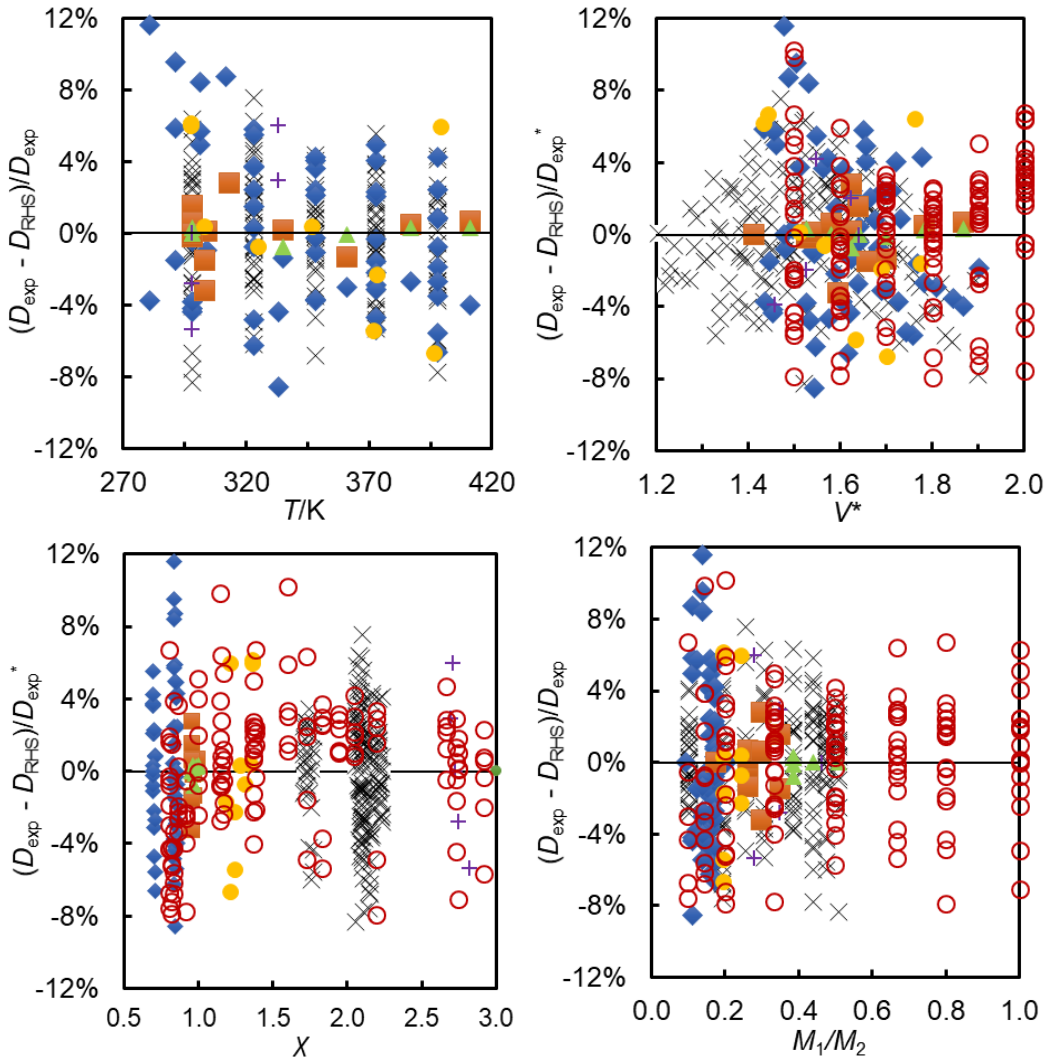

Figure 4.19 Deviation between the experimental values and the calculated values from the RHS model as functions of temperature T, reduced volume $V/V_{0,2}$, molar mass ratio M_1/M_2 and asymmetry ratio χ, where 1 denotes solute and 2 denotes solvent. Symbols indicate solutes: ×, CO_2; ◆, CH_4; ■, C_2H_6; ▲, C_3H_8; ●, N_2; +, Ar; ○, smooth hard sphere

These are interesting findings considering that, before this study, there was already available experimental data for many hydrocarbons diffusing in supercritical CO_2 (typically measured in a TDA with supercritical CO_2 as the mobile phase) but only very limited amounts of data with hydrocarbons as the solvent. For example, commonly studied systems are those in which CO_2, ethane or ethylene act as the solvent and a heavier hydrocarbon as the solute. However, in the present study, what has been measured is the opposite. CO_2 or CH_4 becomes the diffusing species while a liquid hydrocarbon solvent is the mobile phase. Experimental data on this condition are rather scarce especially when involving methane as the diffusing solute.

Some limitations need to be noted regarding the present study. This model is restricted to cases where the light component is present at high dilution. The inverse cases, for example the diffusion of trace amounts of heavy hydrocarbon in supercritical CO_2, where the solute is heavy and the solvent is light, might not conform to the present version of the model. The model was also only tested for non-polar solute-solvent systems. Other systems, for example involving polar solutes or solvents, is not within the scope of this model. Nevertheless, the findings of this study have open path to future work relevant to the area discuss above.

PART 2 VISCOSITY

CHAPTER 5 THEORETICAL BACKGROUND

This chapter introduces the macroscopic definition of viscosity, theoretical approaches to predicting it and the major techniques for measuring viscosity experimentally, focusing on techniques and methods that were available and suitable for liquid and gas mixtures for high pressure and high temperature conditions. In addition, a comprehensive literature review of the existing predictive models for viscosity is presented, focusing mainly on mixtures of hydrocarbon liquids with light gases.

5.1 Introduction to Viscosity

Transport properties such as diffusion coefficients, viscosity and the thermal conductivity are of great scientific importance and are associated with the transport of mass, momentum, and energy, respectively. Viscosity in general can be defined as a measure of resistance when a fluid is forced to flow. It can also be known as the thickness or internal friction of the fluid to flow. The viscosity reflects the underlying microscopic interactions between the molecules of the materials and is relevant to both liquid and gaseous states of matter. Fluids for which the rate of deformation is proportional to the shear stress τ (so-called Newtonian fluids), the shear stress can be expressed by the linear relationship

$$\tau = \eta \frac{du}{dy} . \tag{5.1}$$

In this equation, η is the coefficient of viscosity or dynamic viscosity of the fluid and (du/dy) is the gradient of fluid velocity at the same time in the material. The viscosity depends on the thermodynamic state of the fluids and were determined by two variables, either (T, p) or (T, ρ) and should include composition dependence when mixtures are involve.[223] The quantity defined in the above equation is called dynamic viscosity or absolute viscosity. On the other hand, kinematic viscosity which is basically a measure of the resistive flow of a fluid under the influence of gravity and is defined as the ratio of the dynamic viscosity of the fluid to the fluid density at the same temperature and same pressure conditions. As there is a strong relationship between viscosity and density, measuring viscosity will usually involve also measuring density.

In general, measuring viscosity and density are very crucial in the study of any process involving fluid mechanics and transport phenomena.[224] The knowledge of viscosity and density over wide range of temperature, pressure and composition is required in the design and optimisation of many process in oil, chemical and biotechnology industries. The importance of viscosity can be seen in the determination of Reynold's number which is the key value in determining the fluid flow and heat transfer phenomenon. It can also be found in the Navier-Stokes equations that describe the three-dimensional motion of viscous fluid substances that is consistent with the principles of mass and momentum conservation. In refrigeration engineering, the knowledge of viscosity, particularly in the liquid phase and the ratio of liquid to vapor viscosity are essential for the fluid flow behaviours, convection characteristics and

two-phase heat transfer and pressure drop.[225] In some specific oil and gas processes such as enhanced oil recovery (EOR) and carbon capture and storage (CCS), viscosity is key to process optimisation with respect to many aspects including economy, operability and safety. These processes cannot be compromised with high uncertainties as large errors will give great influence in each of the aspects mentioned. A study by Hernandez et al. [226] on the sensitivity of reservoir simulation to uncertainties in viscosities concludes that the results of reservoir simulations were very much sensitive to the fluid viscosity. Each percentage point of deviation in viscosity leads to a deviation in the predicted cumulative oil production as high as 7%. To add to that, knowledge of the brine viscosity is important to determine the pressure generated at the bottom of a brine injection well. It is also as important as the brine density in evaluating the volumetric flow rate of a downhole pump in a production well.[227]

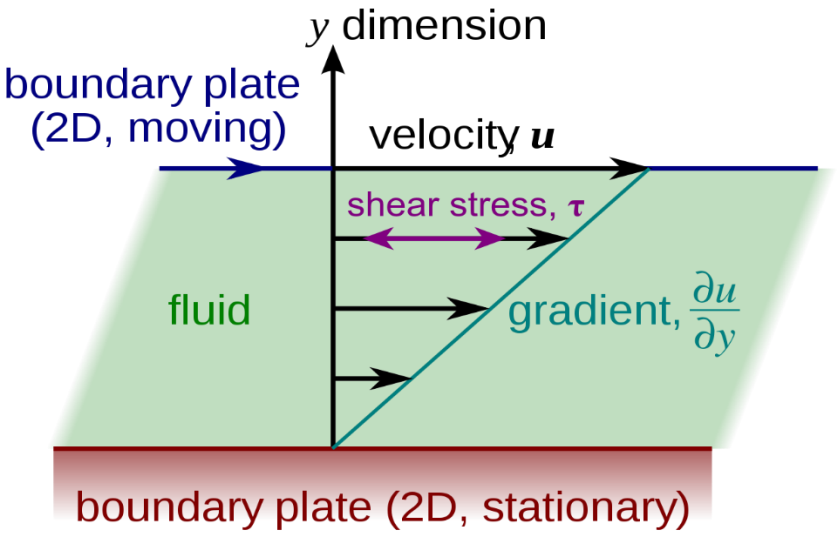

Figure 5.1 Schematic diagram showing a simple shearing flow (Couette configuration) using two infinite flat plates to define the viscosity.

5.2 Review of experimental techniques

According to equation 1, viscosity can be obtained measuring the shear stress in a one-dimensional steady-state flow with a velocity gradient. However, it is worth to mention that most of the practical viscometers do not have linear velocity gradients or uniform shear stress. To overcome this, the shear stress was measured at one location but the rate of strain is not known at the same location.[223] Hence, the measurement of viscosity should be based on the determination of some important effect of the stresses amenable to precise measurement in a known flow field.

A viscometer is an instrument used to measure viscosity. It is different from a rheometer which is used to measure the rheology and flow properties as well as fluid's internal flow resistance. A viscometer measures over a limited range of shear rate, usually with good accuracy, and is generally applicable only to fluids that follow Newton's law of viscosity. However, rheometers can be used to measure viscosity over a wide range of share rates and can measure both Newtonian and non-Newtonian fluids. Table 5.1 lists some differences between rheometers

and viscometers. In this study, we preferred to use viscometers as we were measuring Newtonian fluids and seek high accuracy results. They are several types of viscometers that were developed in the past to suit the wide ranges of viscosity. Some examples are the capillary viscometer, falling body viscometer, rotational viscometer and vibrational viscometer as shown in Figure 5.2.

Table 5.1 Comparison between rheometer and viscometer.

Comparison	Rheometer	Viscometer
Description	It can measure rheological properties, fluid's internal flow resistance and flow properties of liquids	It can only measures viscosity of liquids.
Functionality	It is used for those fluids which cannot be defined by a single value of viscosity and needs more parameters to be set and measured.	It is used to measure those fluids which can be defined by a single value of viscosity
Shear rate range	It measures viscosity over a wide shear rate range.	It measures viscosity over a limited shear rate range.
Capability	It can work as a viscometer	It cannot work as a Rheometer.
Measurement	It can measure the properties of fluids under any condition (Newtonian or Non-Newtonian fluids)	It can only measure the viscosity of the fluid under certain conditions (Newtonian fluids)

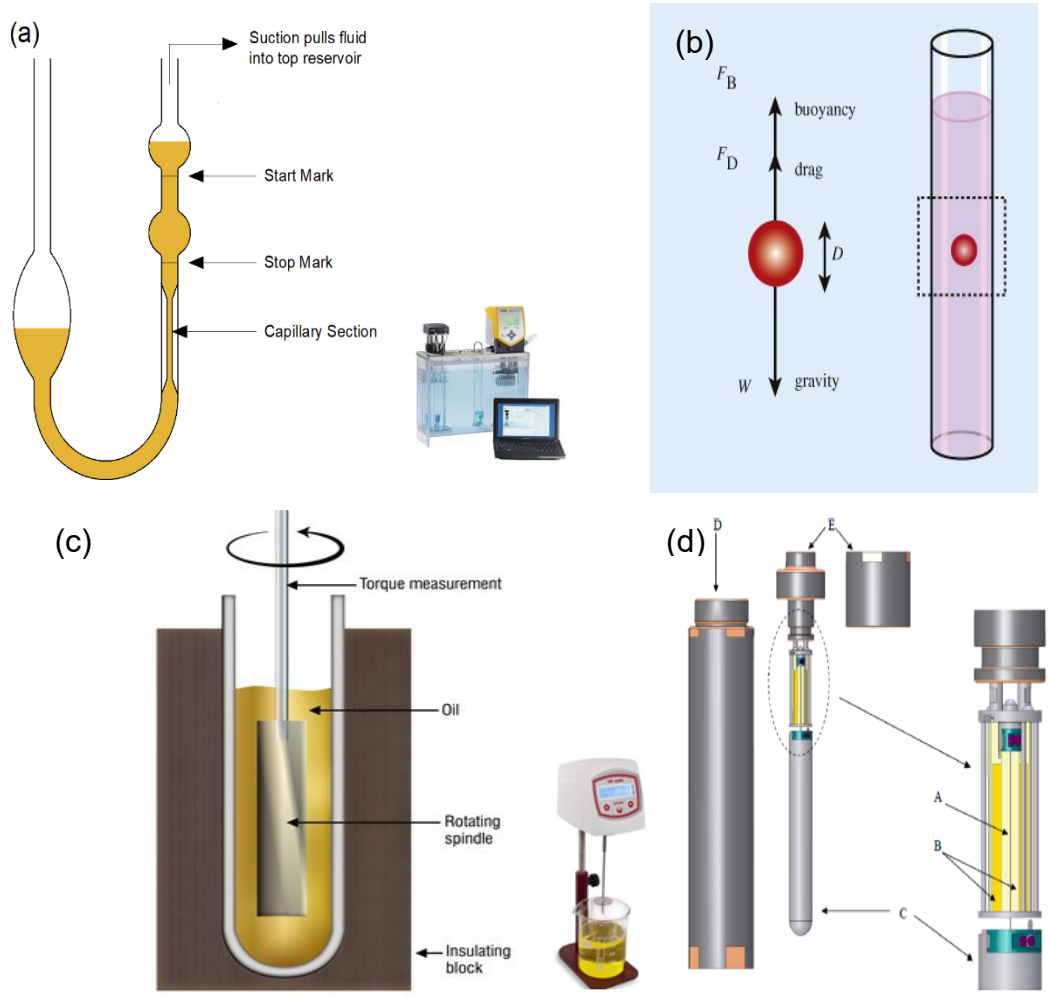

Figure 5.2 Experimental techniques for viscosity measurement. (a) capillary viscometer[228]; (b) falling body[229]; (c) rotational[228]; (d) vibrating wire[13]

Capillary viscometers are one of the most extensively used types, especially for liquids, due to their simple method and operation. Capillary viscometers were used to determine the standard reference viscosity of water at 20 °C for establishment of viscosity standards within the International Organization for Standard (ISO), the American Society for Testing and Materials (ASTM), the Japanese Industrial Standards (JIS) and the Deutsche Institut für Normung (DIN).[230] The capillary viscometer uses a specific capillary tube, and the viscosity is determine based on the times it takes for the fluid to pass through a certain length of the tube as shown in figure 5.2(a). Some of the many capillary tubes available including Ubbelohde, Cannon- Fenske and Ostwald. Capillary viscometers are based on the following working equation:[231]

$$\eta = \frac{\pi r^4 \Delta p}{8Q(L+nr)} - \frac{mpQ}{8\pi(L+nr)}. \tag{5.2}$$

In this equation, r is the radius of the capillary, Δp is the pressure drop across the capillary tube, Q is the volumetric flowrate, L is the length of the capillary tube, n is the end-correction

factor, m is the kinetic-energy correction factor and ρ is the fluid density. To use this equation, a few assumptions need to be satisfied including steady flow, no slip at the wall, flow parallel to the axis of the capillary, constant temperature, and a straight capillary tube of uniform cross-section. However, some of these assumptions can be relaxed by calibration with a fluid with known viscosity. A difficulty may be encountered when using the capillary tube as the tube is hard to clean and no single tube is suitable for all ranges of viscosity. This means that several capillary tubes might be needed to measure viscosity of a fluid at a wide range of temperatures. Capillary viscometers are most suitable for measuring the viscosity of liquids at ambient pressure conditions. However, it can also be used to measure the viscosity of gases and liquids at high temperature and high pressure (HTHP) conditions. For instance, Kashifi et al. [232] used capillary viscometers to measure the viscosity of binary and multicomponent hydrocarbon fluids at pressure between 35 to 138 MPa and temperature up to 473 K. Maitland and Smith [233] performed viscosity measurements for binary gas mixtures at temperatures up to 1600 K while Guevara et al. [234] measured the viscosity of several gases including hydrogen, helium, argon and nitrogen at temperatures up to 2000 K. Trappeniers et al. [235] used capillary viscometer to measure the viscosity of neon at temperature 298 K and 348 K and pressure up to 100 MPa by using a high-pressure gas capillary viscometer. On the other hand, Nagashima et al.[236] measured the viscosity of water and heavy water in the liquid and vapor phase at temperatures in the range between 323 – 773 K and pressures up to 80 MPa using a closed-circuit capillary viscometer. Rivkin et al.[237] also used a similar apparatus to measure the viscosity in the critical region of water while Ejima et al.[238] employed the capillary viscometer to measure the viscosity of molten salts at temperatures up to 1200 K.

The falling sphere viscometer uses a sphere of known density, dropped in the fluid of interest and the viscosity is calculated based on the time taken for the sphere to fall freely to a certain point. This technique is achieved with the help of a uniform gravitational force. While it is small and portable, its usage is limited to translucent Newtonian fluids. It is usually applicable to the measurement of the viscosity of highly viscous liquids. A more general class of falling-body viscometers use a solid of revolution, such as a cylinder with a hemispherical cap, falling within a fluid-filled tube. This viscometer is used in a relative mode of operation using a calibration of the instrument with standards liquids.[231] The working equation for a falling cylinder of length L_S and radius r_1, falling in a tube of radius r_2, is given as follows

$$\eta = t\frac{\left(1-\rho/\rho_s\right)}{A} \tag{5.3}$$

where

$$A = \frac{2\pi L_s L_T}{mg\left\{\ln\left(r_2/r_1\right)-\left[\left(r_2^2-r_1^2\right)/\left(r_2^2+r_1^2\right)\right]\right\}} \tag{5.4}$$

Here, ρ is the density of the fluid, ρ_S and m are the density and mass of the falling body, respectively. To use this equation, the fluid is assumed to be laminar and steady and that there is no slip between the surface of the cylinder. It is also important to assumed that the cylinder

falls along the axis of the tube even though it is impractical. To overcome this problem, an alternative device has been successfully designed by Isdale[239], Irving[240], and Glen[241] where a self-centring sinker was used. Some measurements of viscosity involving hydrocarbons have been performed at high pressure with only 2-3 % uncertainty recorded. Other work that employed the falling-body viscometers at HTHP conditions were the work by Dymond et al.[242] who reported on the viscosity of toluene and n-hexane mixtures at temperatures from (298.15 to 373.15) K at pressures up to 500 MPa.

The rolling ball viscometer are like the falling body viscometers in its principle and design. The difference between these two viscometers is the position of the cylindrical vessel containing the sample. Instead of vertically positioned, the sample vessel is inclined at certain angle and measurement is made by noting the time taken for a spherical ball to roll down between two points along the slanted plane. The fundamental of the general viscosity equation was developed by Hubbard and Brown[243] and Lewis[244] where they treated the calibration coefficient of the viscometers to be independent of the inclination angle. The rolling ball viscometer has been used for measurement of the viscosity of hydrocarbon liquids saturated with gases by Sage.[245] Nishibata and Izuchi[246] has made an improvement to the viscometer to allow simultaneous measurement of the density by assembling a potentiometric displacement meter. The viscometer has an uncertainty not better than 3% due to the difficulties in determining the diameter of the tube and the ball, the exact rolling time and the angle of inclination of the tube

The rotational viscometer measures the torque required to turn an object in the fluid at a controlled speed. This technique uses a cylindrical container with radius r, that is filled with the fluid of interest and the rate of rotation of a solid body (usually cylindrical shape) in the fluid is measured. The rotational viscometer can be relatively expensive and the size of it is often large and not portable. However, this type of viscometer can measure viscosities of opaque, settling, and Newtonian fluids. Because it does not use the gravitational force to function, their instruments are based on the fluid's internal shear stress. The shear stress can be constant for an extended period, thus, making this viscometer one of the preferred instruments in measuring the rheological properties of fluids. The cone and plate rotational viscometer have been widely used using the working equation as follows

$$\eta = \frac{3\theta_0 T}{2\pi r^3 \omega} \tag{5.5}$$

Here, T is the torque and ω is the angular velocity, r is the radius of the cone base and θ_0 is the cone base angle. Equation (5.5) is applicable to smaller cone angles typically $\theta_0 < 3$, where the shear rate is considered constant for a constant value of ω. For a larger values of the angle, equation (5.5) should consider the radii of the inner and outer cylinders such that

$$\eta = \frac{T}{4\pi l \omega}\left(\frac{1}{r_i^2} - \frac{1}{r_0^2}\right) \tag{5.6}$$

Where *l* is the length of the cylinders. However, using these two equations did not produce high accuracy of viscosity data and need to consider some correction factors. More detail explanation on this matter was discussed by Walters[247] and Cheng.[248]

Vibrating-wire viscometer is a simple form of vibrating viscometer which consists of a thin wire of radius *R* with known density ρ_s, subject to a tension and clamped to be stationary at either end. The vibrating element will transverse oscillation (due to the passage current that pass through a magnetic field), and its frequency as well as the width of the resonance peak will determine the density and viscosity of the surrounding fluid, respectively. The main advantage of this viscometer is that the sample volume required for the measurements are quite small, thus making measurements at extremely high pressure much easier. To use these techniques, some parameters in the working equation needs to determine by calibration of the device in vacuum condition and in known-viscosity fluid. Though the determination of parameters may be complex, data that is generated from the vibrating wire viscometer is one of the most reliable compared with data that is generated from the other methods. It is not surprising that this method has been widely used to measure viscosity of pure and mixtures especially when HTHP conditions are involved. The uncertainty of the viscosity measurements using this viscometer can be better than ±0.5% especially when operated in relative manner.[231] Measurements of viscosity using the vibrating wire viscometers usually recorded uncertainty of not more than 2%. Some of the work includes the measurements of hydrocarbons liquid and gas mixtures relevant to EOR and CCS.[13, 16, 249-256] Other work that were using the vibrating viscometer was the work by Assael and his co-workers. In their work, they measure liquid hydrocarbons such as hexane and heptane at temperatures up to 348 K and pressures of up to 250 MPa.[257-258] The viscosity of liquid di-isodecyl phthalate (DIDP) were also measured using the vibrating viscometer by Peleties and Trusler at temperatures between (298.15 and 373.15) K and pressures up to 140 MPa, with an uncertainty of 2%.[259] More applications of vibrating-wire viscometers employed at high temperature and pressure conditions can be found in work by Wakeham and his co-workers.[231] In this work, vibrating wire techniques were being used in all of the viscosity measurements. Therefore, a more detail description of the method is available in chapter 7. A comprehensive summary between various methods for the measurement of viscosity is shown in Table 5.2.

5.3 Predictive Models for Viscosity

Theory is generally a conclusion that is proven scientifically and supported by evidence, usually from results of experiments. Experimental data can be considered as the primary source of data for many thermophysical properties and are one of the best methods of evaluation that provide reliable data. However, especially at extreme conditions, doing experiments is not only expensive and time-consuming, but may be practically impossible. Meanwhile, a model is a representation to explain theory and simplify a complex theory for better understanding. Models can be useful in understanding complex phenomenon, however, in some cases, the key assumptions embedded in the models need to be properly determined. Models may have theoretical contents, but they are not the first principles theory themselves. The best way to encounter the problems from all of the route are by combining measured data from reliable experiments with predictive models that have been validated and can provide accurate and reliable values.[252] Numerical molecular simulations are an alternative route that

can provide a valuable insight into the behaviour of the viscosity as it can reduce the calculation-time after being simplified.

Table 5.2 Comparison between several experimental techniques for measuring viscosities.

Technique	Advantages	Disadvantages
Capillary tube	-Measure precise viscosities for many diverse fluids -Small and portable -Can use a wide variety of capillary tubes on the same viscometer	-No single tube is suitable for all viscosities -Basic models can only be used for translucent fluids -Difficult to clean the capillary tubes
Rotational	-Can measure viscosities of opaque, settling, or non-Newtonian fluids -Useful for characterizing shear-thinning and time-dependent behavior -Speed of the rotating part easily adjusted	-Can be relatively expensive -Often large and not portable
Falling body	-Easy operation	-Limited to Newtonian fluids
Vibrational	-Small sample volume -Most suitable for high pressure measurements	-Needs to determine some parameters before measurement. -Not suitable for measuring the viscosity of a fluid whose flow behavior is not known

Models for predicting viscosity can be divided into three categories which are theoretical, semi-theoretical, and simple empirical correlations. Theoretical model are fundamental theories based on kinetic theory whereby the viscosity is expressed in terms of intermolecular potential functions. It is restricted to dilute gases only at wide range of temperature and pressure. It is based on some assumptions that need to be determined properly for the model to predict closely and correctly. Semi- theoretical or semi- empirical, as the name represent, uses part of experimental results and part of assumptions and approximations. It contains adjustable parameters which can be determined from fitting the model to the experimental values or using empirical correlations. The viscosity predicted using semi- theoretical method are usually as a function of temperature and density, hence, the equation of state to predict density is also needed. On the other hand, empirical models are simple correlations that are based on experimental observations and relate directly with parameters such as pressure and temperature as well as density. There are some accurate theoretical and correlation models for predicting viscosity of dilute gases, unfortunately, for dense liquid there is no viable first principals' route to calculate the viscosity even when all interactions between the molecules are known. Thus, there is no simple theoretical method available for predicting liquid viscosities. The models that are available in the literature are mostly semi-empirical or empirical. For single components, several models for predicting the viscosity for dilute and dense gas and liquid states are available in the literature. While for mixtures, the viscosity is

usually determined from the viscosities of the pure components by employing appropriate mixing rules. Table 5.3 listed summary of the theories and models available.

Table 5.3 Summary on theories and models available for predicting viscosities.

Theory/ Model	**References**
Free Volume Theory (FVT)	260-264
Friction Theory	265-269
Residual entropy model	270-282
Dymond and Assael (DA) model	70, 249, 283-286
Hard sphere model (HS)	13, 16, 283, 287-289
The Vesovic-Wakeham (VW) scheme	255, 290-291

Based on Table 5.3 there are a wide variety of theories and models that were used to describe viscosity. Kinetic theory is the natural choice for the development of the theoretical model. Models that use kinetic theory were based on a rigorous theory of fluid behaviour that relate the observable macroscopic properties of a system to the microscopic properties of the individual molecules and their interaction potential. It uses molecular description as a starting point to develop the model. Temperature and pressure are common parameters used to specify quantities for viscosity, but a more significant parameters are temperature and density as shown in equation below.

$$\eta\left(\rho_n, T\right) = \eta^0\left(T\right) + \Delta\eta\left(\rho_n, T\right) + \Delta\eta_c\left(\rho_n, T\right) \tag{5.7}$$

Here, ρ_n is the molar density, T is the absolute temperature, η_0 is the dilute gas viscosity, $\Delta\eta$ is the excess viscosity and $\Delta\eta_c$ is the critical enhancement to viscosity.

For dilute gases based on the kinetic theory, the simplest models have assumed that the molecules behave as identical non-interacting hard sphere with diameter, σ and mass, m that were moving along the free path and collides with each other given that

$$\left\langle c\right\rangle = \left(\frac{8kT}{\pi m}\right)^{1/2} \tag{5.8}$$

Here, *k* is the Boltzmann's constant and *T* is the temperature. A simple kinetic theory can be used provided that the molecules of a pure component are in continuous random motion, exerting no force on each other and treated as identical hard spheres that only consider binary collisions. The dilute gas viscosity can then be described as

$$\eta = \frac{5}{16}\left(\frac{mkT}{\pi}\right)^{1/2}\frac{1}{\sigma^2} \tag{5.9}$$

However, if the molecules repel or attract each other rigorously, the expression for the viscosity apply the Chapman-Enskog theory, in which the Boltzmann transport equation was solved rigorously. For this case, the viscosity can be expressed as follows:

$$\eta_0 = \frac{5}{16}\left(\frac{mkT}{\pi}\right)^{1/2}\frac{f_n}{\sigma^2\Omega^*} \tag{5.10}$$

Here, Ω* is a dimensionless collision integral, typically estimated from the Lennard-Jones potential.[292-293] It is worth to mention that the viscosity of a dilute gas (where pressure are relatively low) is a function of temperature only and does not depend on the density of the gas, hence it is defined as the viscosity at zero density (η_0). Another way to estimate dilute gas viscosity is through empirical correlations such as described by Monnery et al.[294] and Poling et al.[295] and the simplest empirical equations is Yaws's correlation [296] such that

$$\eta_0 = A + BT + CT^2 + DT^3 \tag{5.11}$$

Where A, B, C, and D are fluid-specific fitting parameters. Yaws in his book provides values of the fitting parameters for many substances including hydrocarbons and non-hydrocarbons.

For dilute gas mixtures, the viscosities can be calculated using several mixing rules, such as described by Wilke[297] and Herning and Zipperer.[298] For liquids and high pressure supercritical fluids, the η_0 is negligibly small and can be neglected. However, it is an important parameter as a scaling factor for many models.

The models used for predicting and correlating viscosities of dense fluids (liquids, high-pressure gases, and high-pressure supercritical fluids) can be summarised in Figure 5.3.

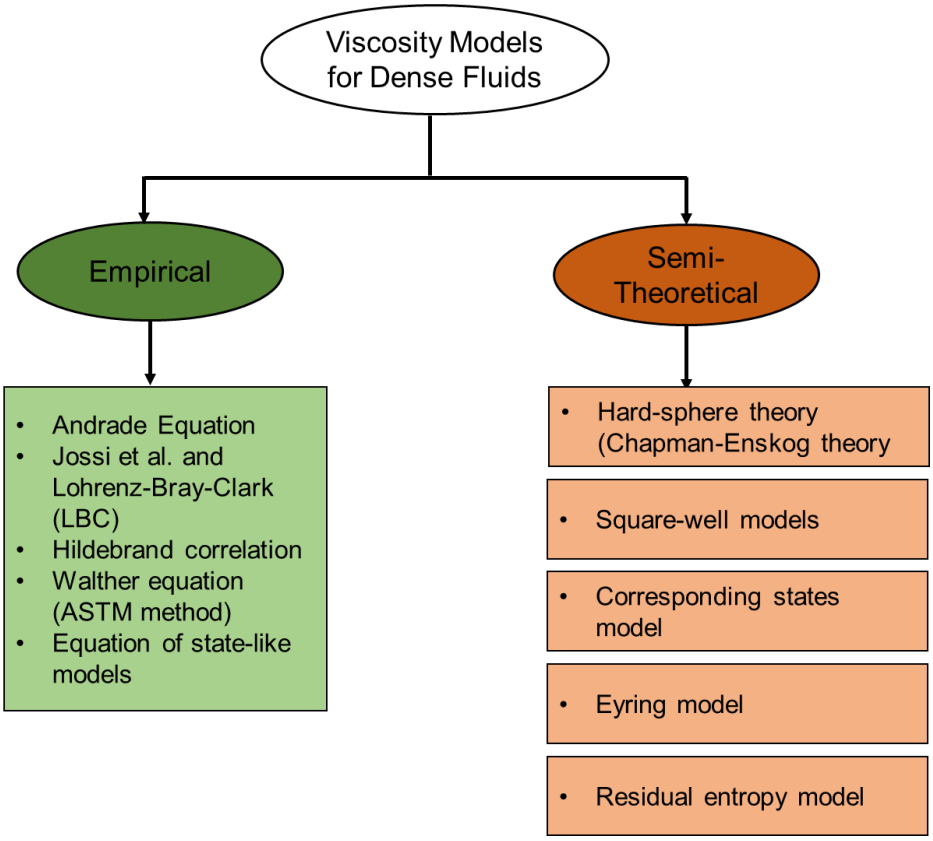

Figure 5.3 Summary of dense-fluids viscosity models

For the empirical models, the De Guzman-Andrade equations popularly known also as the Andrade equation is one of the most common equations for calculating the viscosity as function of temperature. The original equation of this models is shown below

$$\ln\eta = A + \frac{B}{T} \tag{5.12}$$

This model requires viscosity data to determine the parameter A and B. However, there were many drawbacks from this model including its failure to capture the slight curvature of the relationship between lnη and 1/T for associated liquids and hydrocarbon mixtures of higher viscosity[299] as well as the effect of pressure on viscosity.[300] The Lohrentz-Bray-Clarke (LBC) method is widely used for petroleum systems[301] because it is simple and fast. In the LBC method, the reduced excess viscosity is expressed as a function of reduced density for reservoir oils and gases in what amounts to a corresponding-states treatment. However, an important thing to note is that the results with the LBC method are sensitive to values of the density since the correlation is a sixteenth-degree polynomial in the reduced density. In the Hildebrand correlation, fluidity of non-associating liquids, $\Phi = 1/\eta$, is proportional to the ratio of free volume (V-V_0) to the volume V, where V_0 is the volume at which fluidity goes to zero. There were seven parameters involved in this equation, including critical volume, critical temperature, critical pressure, freezing point, molar volume at the freezing point, molecular mass, and acentric factor.[302] The Walther equation have only two empirical constant involved which can be determined from the experimental viscosity data. This equation is the simple

correlations that were used for crude oils and is recommended by ASTM as the standard of the relationship between viscosity and temperature. However, this equation does not have a theoretical basis and it becomes meaningless when the viscosity approaches the value 0.3.

In semi-theoretical model, the hard-sphere theory (Chapman-Ekskog theory) is among the most-used theory to predict viscosity. In this theory, one important assumption of hard spheres is that the forces between the molecules on collisions are impulsive, meaning that the collision time is approaches to zero.[303] In this model, the viscosity was predicted based on the expression given as

$$\frac{\eta}{\eta_0} = \left[\frac{1}{g(\sigma)} + \frac{0.8b}{V_m} + 0.761 g(\sigma) \left(\frac{b}{V_m} \right)^2 \right] \tag{5.13}$$

where $g(\sigma)$ is the radial distribution function at contact for spheres diameter σ which can be determine from equation of state, V_m is the molar volume, and b is the volume occupied by the hard spheres molecules which equal to $2\pi N_A \sigma^3/3$. The Enskog theory needs modification when used to predict the viscosity of real fluids. This were concluded in the work by Alder et al.[304] where a significant deviations occurred in the dense fluid region between results from the Enskog's theory and molecular dynamic calculations for a hard-sphere. To overcome the problem, Chandler[37] proposed a rough-hard-sphere (RHS) theory that take into accounts the translational and rotational motions of molecules for systems of rough hard spheres. This results in the relationship between RHS and smooth-hard-sphere (SHS) such that

$$\eta_{RHS} = A\eta_{SHS} \tag{5.14}$$

where A is a weakly temperature dependent, coupling parameter.

For the mixtures, the schemes provide by Dymond and Assael (DA) model [70, 283-286] has proved to have a significantly improved method for the correlation, and accurate prediction (±6%) of dense fluid transport coefficient data. The hard sphere model captures the interaction between molecules and play a major role in determining the structure and properties of most fluids and colloidal systems [305]. The method considering the attractive forces of real molecule and the experimental data were considered as a smooth hard-sphere and being compared with predicted values from the Enskog theory. In Dymond and Assael method, the term dimensionless viscosity η^* is a universal function of V_m/V_0 (V_0 is the molar volume for close packed spheres of diameter σ) and independent of temperature. This method was able to predict the viscosity of many pure liquids and liquid mixtures in a homologous series such as the alkanes mixtures at a very high pressure (up to 500 MPa). However, this method is restricted to reduced volumes in the range of $1.5 \leq V_r \leq 5$ and outside this region, the scheme breaks down and presents large deviations with respect to experimental data at high reduced densities[283]. To overcome this matter, Caudwell et. al. [254-255] and Ciotta[306] proposed to use the excess reduced viscosity that allow the model to behave relatively at low densities region while offering improved prediction accuracy at high-density regions[283]

$$\Delta\eta^* = \frac{16}{5}(2N_A)^{1/3}\left(\frac{\pi}{MRT}\right)^{1/2} V_m^{2/3}\frac{\eta-\eta_0}{R_\eta} \tag{5.15}$$

where, $\Delta\eta^*$ is the reduced residual viscosity and $(\eta - \eta_0)$ is the residual viscosity. The following correlation of log10($\Delta\eta^*$ + 1) as a function of $1/V_r$ resulted in the following expression

$$\log_{10}\left(\Delta\eta^* + 1\right) = \sum_{i=1}^{7} a_i \left(1/V_r\right)^i \tag{5.16}$$

The proposed extended hard-sphere theory was able to correlate or predict the viscosity of different fluid families including linear alkanes, refrigerants, aromatic hydrocarbons, and alcohols within ±5 % for most of the thermodynamic states. The theory can also be used to predict the viscosity of a mixture of *N* components by applying mixing rules for R_η and V_0 with the best mixing rules are those with linear mole fraction.

Vesovic-Wakeham (VW) method[307-308] is also another approach to predict the viscosity of liquid mixtures, that were based on the kinetic theory of hard-sphere fluids that is modified to fit for the behaviour of real gases. In the original VW method, the value of the radial distribution function at contact was adjusted at each state point such that the model matched the viscosities of the pure species that made up the mixture of interest. The later work by Wijn et al.[290] has determined the adjustable parameter by implementing a number of thermodynamically consistent mixing rules using the statistical associating fluid theory (SAFT). The VW and DA models can provide a good prediction of the viscosity of dense fluid mixtures but both approaches require fitting to the transport properties of the pure components. More works based on the hard-sphere theory includes the work by Assael et al.[70], Sun and Teja[285], and Riesco and Vesovic [291].

The square well model, derived from Boltzmann's equation was the simplest potential model that accounts for repulsion and attraction to predict viscosity of hard sphere dense fluids of molecules interacting with the square-well potential.[309] It was extended to binary mixtures by McLaughlin and Davis[310] but it turned out to be very complex for engineering application. The extended model has then been modified to overcome the problems by Du and Guo and Monnery et al., however both works only reported at low pressure conditions. One alternative intermolecular potential to the square-well approach is the the Lennard-Jones potential. It realistically describes the interactions between simple molecules but needs some simplifications due to the difficulty in obtaining analytic expression for the viscosity. Galliero et. al.[311-312] predicts the viscosity of Lennard-Jones fluids based on molecular dynamics (MD) simulations where, for simple fluids such as methane, ethane, propane, argon, nitrogen, oxygen and carbon dioxide, the molecular parameters were deduced from the experimental critical temperature and volume. The model predicted within 15%, having a lower viscosity value particularly at low temperatures due to the lack of electrostatic contributions.

Corresponding states models used the basic principles that a reduced property of a fluid is equal to that of a reference fluid at the same reduced conditions. For viscosity, this means that the two fluids will have the same reduced viscosity at the same reduced temperature and pressure. Some of corresponding-states treatments have been developed, including the TRAPP model of Ely and Hanley[313], the models of Pedersen and Fredenslund[314-315], Teja and

Rice[316], and Aasberg-Petersen et al.[317] Although useful, these methods employ empirical functions to account for density dependence and involve uncertain mixture of critical parameters.

The Eyring model or the absolute reaction rate theory was another semi-theoretical model to predict the viscosity of dense fluids. It was first developed to describe the rates of chemical reaction.[318-319] However, it can also been used to viscous flow where the molecules are activated to pass through a potential energy barrier and move to a vacant site nearby. The model represents simple techniques, however, the value of molar free energy of activation that were required in the equation were difficult to obtain making it hard to use especially on the petroleum industry.

Other works on predicting viscosities of dense fluids include Free- Volume Theory (FVT) and the Friction Theory which capable of predicting viscosity at low pressure as well as at high pressure and temperature conditions. The FVT model requires density data from the equation of state as an input while the Friction theory needed the values for the repulsive and attractive pressure. Burgess et al.[320] in his work used different kind of EoS including the perturbed-chain statistical associating fluid theory (PC-SAFT), the HTHP-volume-translated (VT) Peng−Robinson EoS, and the HTHP-volume-translated-Soave−Redlich−Kwong EoS (HTHP-VT-PR and HTHP-VT-SRK) at pressures from ambient to 533 K and pressures from 6.9 to 276 MPa. They have found out that the parameters for each of the models differ significantly when using different EoS. The FVT model and the Friction model is similar in such a way that these models are focusing on robust extrapolations and predictions. The works by LLovell et. al. [264, 321-322] has coupled the FVT with the soft-SAFT equation to extend the capabilities of the equation. The equation performs very well in all cases with average absolute deviation (AAD) ranging between 0.44% to 3.61% in a wide range of temperature and pressure, including predictions along the critical isotherm. On the other hand, Quinones et al. (2000)[268] has obtained quite a good result using the Friction Theory with AAD very close to, or even within, the experimental uncertainty. They also tried to predict some simple mixture viscosities based on pure component correlations and obtained good results, mostly within experimental uncertainty.[266, 268]

The excess entropy scaling or the residual entropy model is originally proposed by Rosenfeld[323] has been developed for semi quantitative relationship between structure, entropy, and mobility in a wide range of fluids. It states that the complex temperature and density dependence of the reduced viscosity and the reduced self-diffusion coefficient can be collapsed into a mono-variant function of the residual entropy. The residual entropy is defined for specified temperature T and molar density ρ as follows:

$$S^{\mathrm{r}}(T,\rho) = S(T,\rho) - S^{\mathrm{id}}(T,\rho) \tag{5.17}$$

where $S(T, \rho)$ is the molar entropy and $S^{\mathrm{id}}(T, \rho)$ is the molar entropy of the hypothetical ideal gas at the same temperature and molar density. The entropy scaling approach is a hypothesis and is not based on an exact theory; therefore, it cannot be derived from first principles. According to the original model proposed by Rosenfeld,[323] the reduced viscosity η^* was defined in terms of the thermal velocity $(k_B T/m)^{1/2}$ and the number density n as follows:

$$\eta^* = \frac{\eta n^{-2/3}}{\left(mk_B T\right)^{1/2}}, \tag{5.18}$$

where m is the mass of one molecule and k_B is Boltzmann's constant. The underlying physics, and the associated concept of isomorphic invariance, has been discussed by Dyre[324] who also reviewed molecular simulation results that exemplify the working of the approach. Other works that used molecular dynamics simulations and tested the residual-entropy scaling relationship for the diffusivity and viscosity includes Dzugutov[325-328] and Goel et. al.[329]. Loetgering-Lin and Gross presented a group contribution method for the correlation and prediction of pure-component viscosities[330], diffusion coefficients[331] and thermal conductivity[332-334] involving nonpolar, polar, and self-associating components. They used the PCP-SAFT equation of state for the residual entropy and represented the reduced viscosity by a summation over functional groups involving three parameters per group. Loetgering-Lin et al. also applied an entropy-scaling model, based on their earlier work on pure substances,[330] to mixtures of real fluids.[335] Nevertheless, the mixtures considered were mainly of similar molecules. Entropy scaling based on the PC-SAFT equation has also been used to predict the viscosity by Fouad and Vega[336-337] and Rokni et al. [338] A modified entropy-scaling approach for viscosity was proposed by Bell and Laesecke[280, 282] wherein a dimensionless residual entropy per unit volume was used as the scaling variable and a reference fluid was used to establish the functional dependence of reduced viscosity upon that variable. The method was applied with some success over the whole fluid region to a family of ten refrigerant fluids, methanol, and water by introducing an appropriate density scaling. Literature reports pertaining to the viscosity-entropy relation of mixtures are limited and restricted to mixtures of similar components.[335, 339-340] Delage-Santacreu et al.[340] explored the application of entropy scaling to the viscosity of model fluids, including mixtures that interact according to the Mie potential. A simple logarithmic mixing rule was used to estimate the viscosity of mixtures from pure component values. More recent studies on the residual entropy model by Taib and Trusler[272] shows the application of highly accurate Helmholtz equations of state for the calculation of residual entropy and the subsequent correlation of reduced viscosity for pure substances. A scaling factors were introduced to reduce the data to a universal function. To apply the method to mixtures, they applied the multi-fluid Helmholtz-energy approximation and simple combining rules for the scaling factors. Other recent works on residual entropy model were discussed here.[271, 277]

All of the models discussed in this section are certainly not perfect, however, some offer reasonable and more accurate and reliable than other. To conclude on the models and theories discussed on dense-fluids viscosity models, it can be said that most of them are suitable and can predict very well the pure substances and mixtures involving the hydrocarbons. However, what interest the most are models or theories that can predict well the system that are of interest in this thesis which are hydrocarbons and light gases mixtures. Therefore, based on our judgements, residual entropy model offers promising results, hence, detailed discussions on the residual entropy model will be discussed in Part 3. To summarize, detail comparison between semi-theoretical models available for dense fluids is listed in Table 5.4.

Table 5.4 Detail comparison on the semi-theoretical models available for predicting viscosities.

Theory/ Model	Input	Strength	Limitations
Dymond and Assael (DA) model	-Roughness factor -molar volume for close packed spheres, V_0 at atmospheric pressure	Can predict viscosity of liquid mixtures in a homologous series up to 500 MPa	-restricted to reduced volumes in the range of $1.5 \leq V_r \leq 5$ -highly sensitive to density
Vesovic-Wakeham (VW) method	- Viscosity of pure species - two correction factors which account for the increased collision frequency and the excluded volume of hard spheres observed in a dense fluid	-the radial distribution function was treated as an adjustable parameter that can be obtained from the viscosities of pure species -can be applied to mixtures of either spherical or chain molecules	Not suitable for highly asymmetric mixtures
Extended hard sphere	- residual viscosity - viscosity in the dilute-gas region	- can predict wide range of viscosity (dilute to dense region) - has the correct zero-density limit -covered much wider range of V_r than the DA model	Not suitable for asymmetric mixtures
Corresponding states models	viscosity and density of the reference fluid (methane), the critical properties, acentric factor, and molar mass of the liquid of interest	works well for straight nonpolar hydrocarbons	- fails to accurately predict the viscosity of branched hydrocarbons, cyclic hydrocarbons, and polar fluids
Friction Theory	- require highly accurate equations of state	Do not require the density as an input	
Free-volume theory	- needs three material-specific constants - hard core volume	FVT parameters fitted to viscosity data over a limited temperature range can be used at higher temperatures allowing for reasonable extrapolated viscosity predictions	- the need for experimental viscosity data for fitting the adjustable parameters -needs to try and error the mixing rules for mixtures application
Residual entropy model	- established EoS for entropy - Molar core volume - scaling factor for pure substances	- complex (T,ρ) dependence can be collapsed into mono-variant function of the residual entropy - can be applied to pure, mixtures of homologous series and gas- liquids non-polar mixtures	Apply to components that have the EoS to calculate the entropy

CHAPTER 6 LITERATURE REVIEW

This chapter provides a comprehensive literature review of the available experimental viscosity data. In section 6.1, the focus is mainly on the viscosity of mixtures of hydrocarbons with light gases, including carbon dioxide, methane, and some other gases such as nitrogen, propane, and argon. In section 6.2, the focus of the review is on the viscosity of diisodecyl-phthalate (DIDP) with dissolved CO_2. The review presented in this chapter aims to highlight the gaps in the database for the viscosity of these mixtures, which provided the basis for the selection of the systems to be measured in this research and to point out for future study.

6.1 Viscosity Measurement of Hydrocarbons and light gases

A thorough review on the available experimental data for binary mixtures of hydrocarbons with dissolved gases is presented in this section to identify the gaps and inconsistencies in previous work, as well as to avoid repeated measurements at the same experimental conditions. Viscosity measurements of hydrocarbons mixtures with dissolved light gases have been carried out over the past several decades; however, the data are quite limited and only available at certain temperature and pressure conditions. Figure 6.1 shows the statistical analysis of available viscosity data of methane + hydrocarbons and CO_2 + hydrocarbons plotted against the published year. The focus of the present research is mainly on the mixtures of methane or carbon dioxide with liquids hydrocarbons, however, other gases such as nitrogen and propane have also been studied as solutes but will not be discuss in this work. Based on figure 1, the viscosity of dissolved CH_4 in hydrocarbons has gained momentum only between 1960 to 1990s before it became stagnated. Despite the increase attention on CO_2 in regards with the climate change and reduction of CO_2 emissions through processes such as carbon capture and storage (CCS), the number of available experimental data of CO_2 mixtures with hydrocarbon is still very limited. It was not until the late 1980s that the experimental viscosity of dissolved CO_2 in hydrocarbons gained much attention.

Table 6.1 Experimental viscosity data of hydrocarbons and light gases mixtures at temperatures *T* and Pressures *p*

Fluids	*T*/K	*p*/MPa	No pts.	Ref.	*T*/K	*p*/ MPa	No pts.	Ref.
	CH_4 + hydrocarbons				CO_2 + hydrocarbons			
Methane	---	---	---	---	311 to 455	35 to 172	49	[341]
	---	---	---	---	229 to 348	1 to 32	120	[342]
	---	---	---	---	289 to 473	0.1	---	[343]
	---	---	---	---	273 and 303	0.1 to 2.53	---	[344]
	---	---	---	---	298	---	14	[345]
Ethane	100 to 300	1.5 to 35	321	[346]	298 to 468	0.1	---	[347]
	298 to 468	0.1	15	[348]	210 to 320	0.1 to 30	158	[349]
	253 to 473	0.1 to 2	251	[350]	---	---	---	---

Propane	298 to 468	0.1	15	[348]	298 to 468	0.1	---	[347]
	311 to 411	0.1 to 55	279	[351]	---	---	---	---
	153 to 311	0.1 to 35	158	[352]	---	---	---	---
	311	0.1 to 40		[353]	---	---	---	---
	203 to 424	2 to 31	57	[354]	---	---	---	---
	200 to 423	10 to 31	26	[355]	---	---	---	---
	280 to 328	1.5 to 6.5	14	[356]	---	---	---	---
Butane	293 to 303	0.1 to 2.53	41	[344]	298 to 468	0.1	---	[347]
	298 to 468	0.1	20	[348]	---	---	---	---
	278 to 478	0.1 to 36	132	[357]	---	---	---	---
	311 to 511	0.7 to 69	18	[358]	---	---	---	---
	200 to 423	2 to 30	58	[359]	---	---	---	---
Pentane	373	---	---	[360]	---	---	---	---
Hexane	256	0.6 to 8.2	---	[361]	298 to 328	0.1 to 11	25	[362]
	373	---	---	[360]	---	---	---	---
Heptane	185 to 373	1 to 11.8	---	[363]	---	---	---	---
	373	---	---	[360]	---	---	---	---
	323 to 473	0.1 to 140	---	[232]	---	---	---	---
Octane	290 to 430	---	---	[364]	---	---	---	---
	373	---	---	[360]	---	---	---	---
Decane	256	0.6 to 8.2	---	[361]	311 to 344	7	4	[365]
	290 to 430	---	---	[364]	310 to 403	7 to 30	73	[366]
	303 to 393	10 to 75	100	[224]	298 to 328	0.1 to 11	27	[362]
	311 to 444	0.1 to 69	---	[367]	323	1 to 6	6	[368]
	298 to 373	20 to 140	65	[369]	373	0.1.to 6	6	[370]
	293 to 373	0.1 to 140	295	[371]	---	---	---	---
	311	0.1 to 40	---	[353]	---	---	---	---
	274 and 373	0.1 to 140	---	[372]	---	---	---	---
	303 and 313	0.1 to 80	15	[373]	---	---	---	---
	293 to 423	0.1 to 40	---	[374]	---	---	---	---
	323 to 473	0.1 to 140	37	[232]	---	---	---	---
Tetradecane	298 to 448	0.1 to 10	24	[375]	298 to 328	0.1 to 11	29	[362]
	---	---	---	---	323	1 to 6	6	[368]
	---	---	---	---	373	0.1.to 6	6	[370]

Hexadecane	298 to 473	1 to 100	71	[13]	298 to 473	1 to 120	102	[13]
Octadecane	323 to 448	0.1 to 10	24	[376]	323	0.9 to 5.9	6	[370]
Squalane	---	---	---	---	303 to 448	1 to 170	120	[16, 377]
	---	---	---	---	293 to 353	10 to 20	72	[378]
***m*-xylene**	---	---	---	---	298 to 423	0.1 to 100	112	[379]
Methylbenzene	293 to 373	140 MPa	280	[380-381]	---	---	---	---

According to the literature study carried by Thol and Richter, the viscosity of methane mixtures with hydrocarbons have been investigated experimentally at least to the extent that a systematic investigation is possible.[382] As seen in Table 6.1, there is a larger volume of published literature on the viscosity of dissolved CH_4 in hydrocarbons than for the viscosity of dissolved CO_2 in hydrocarbons. At least one dataset was found for the mixtures of CH_4 with hydrocarbons from C_2 up to C_{18}. Also found in the literature were the mixtures of CH_4 with toluene at quite a wide range of temperature and pressure. Among all hydrocarbons, mixtures with decane are the most studied with experimental covering pressure from atmospheric up to 140 MPa and temperatures up to 473 K. From Table 6.1, it can also be seen that the measurements of dissolved CO_2 in hydrocarbons do not cover such wide temperature and pressure ranges. Most of the measurements were made at atmospheric pressure and some higher pressure of not more than 30 MPa except for the mixtures of CO_2 with hexadecane and squalane where the measuring pressure were up to 120 MPa. Also, what is obviously seen in the table is that most of the mixtures with either CO_2 or CH_4 are with aliphatic hydrocarbons. Thus far, the only aromatic mixtures investigated were one in the present work, the mixture of CO_2 with 1,2-dimethybenzene (*m*-xylene),[379] and also the mixtures of CH_4 with toluene studied by Baylaucq et al.[381] This review has demonstrated the shortcomings of the experimental viscosity data for the mixtures of CH_4 and CO_2 with aromatics hydrocarbons.

Some of the experimental apparatus used in the measurements includes the oscillating disk apparatus and the rolling ball viscometer, but the most used apparatus was the vibrating wire viscometer. However, all these techniques yield uncertainties of between 2 and 3%. Analysis of the experimental results of the mixtures has shown that the dissolution of the gases in the liquid hydrocarbons has resulted in a significant reduction of viscosity. However, it should be noted that most of the literature for mixtures of the gases with simple hydrocarbons relate to hydrocarbons that themselves have relatively low viscosity. Whereas the situation where CO_2 could be used to enhance oil recovery could be one in which the initial hydrocarbon viscosity is high. Therefore, to get a better understanding, viscosity measurement needs to be done in a more “highly-viscous” mixtures. For example, the viscosity measurement of CO_2-saturated toluene-crude oil mixtures by Hu et al.,[383-384] at T = 298.15 K and pressures up to 22 MPa address such as situation. In their results, they observed an exponential reduction in the viscosity values of the diluted crude oils with increasing pressure in the liquid-vapour coexistence region. Even though no composition data were provided, their results indicate a much stronger decrease in viscosity value than in the CO_2/CH_4 + hydrocarbon system.

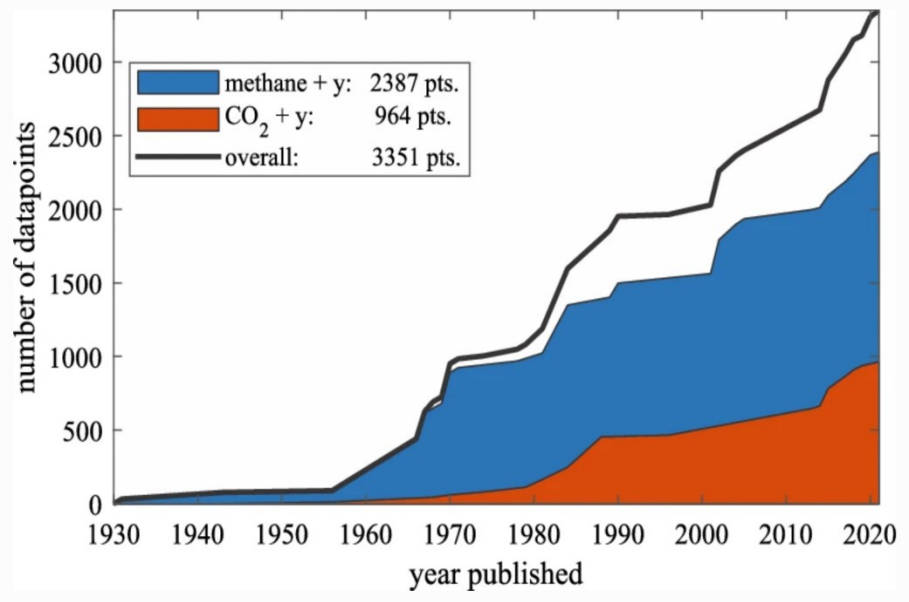

Figure 6.1 Statistical analysis on available experimental data for viscosity of methane + hydrocarbons and CO_2 + hydrocarbons plotted against the published year [382]

6.2 Viscosity Measurement of Di-isodecyl-phthalate (DIDP)

Pure DIDP is a highly viscous hydrocarbon that its value is at least 50 times higher than the viscosity of a simple hydrocarbon such as heptane or decane. As mentioned earlier in the previous chapter, DIDP was proposed as an industrial standard reference fluids for the calibration of viscometers that measures the viscosity in the range between (50 to 125) mPa.s at temperatures near 298.15 K.[385-389] Due to that, a considerable amount of literature has been published on the thermodynamic properties as well as transport properties of pure DIDP. These studies were summarized in Table 6.2. By far, most of the properties were only available at atmospheric pressure except for the work by Peleties et al.[390] Their work has provided the experimental values of speed of sound and density of DIDP at temperature from (273 to 423) K and pressure from atmospheric pressure up to 140 MPa. They also manged to successfully developed an equation of state from the experimental density value.

To investigate the viscosity behaviour of dissolved CO_2 in the condition where CO_2 could possibly be used to enhance oil recovery, the behaviour of DIDP with dissolved CO_2 could be useful since there was a lack of data of the effect of CO_2 on highly viscous hydrocarbons. Essentially, the viscosity of binary mixtures of DIDP and CO_2 could be used to observe the reduction in the viscosity in comparison with the viscosity of CO_2 in low viscosity hydrocarbon. However, to date, no viscosity data of DIDP with dissolved CO_2 can be found in the literature. The data from this work could be beneficial in developing a model to predict viscosity for the mixtures of DIDP and CO_2. In addition to that, to establish a prediction model for viscosity, it is usually necessary to identify the density of the fluid in sufficiently wide ranges of temperature and pressure. In view of all that has been mentioned so far, there is strong evidence that there is a need for the establishment of viscosity and density of DIDP and CO_2 mixtures at wide temperature and pressure conditions.

Table 6.2 Thermodynamic and transport properties available for pure DIDP at temperatures *T* and Pressures *p*

Properties	*T*/K	*p*/ MPa	No pts.	Ref.
Speed of sound	273 to 423	1 to 140	79	[390]
Isobaric specific heat capacity	293 to 423	0.1	7	[390]
Density	273 to 423	0.1 to 140	48	[390]
	283 to 313	0.1	8	[386]
Surface tension	288 to 308		5	[388]
Viscosity	288 to 308	0.1	5	[387]
	283 to 313	0.1	8	[386]
	273 to 373	0.1 to 400	112	[385]

CHAPTER 7 EXPERIMENTAL METHODOLOGY AND APPARATUS

In this work, two different types of viscometers were used, namely a vibrating-wire viscometer-densimeter (VW-VD), in which the wire was tensioned by a sinker, and a combined vibrating-wire vibrating-tube (VW-VT) apparatus in which the wire was fixed at both ends. The viscosity of *m*-xylene + CO_2 were measured using VW-VD apparatus while the viscosity of diisodecyl-phthalate (DIDP) + CO_2 were measured using VW-VT apparatus. The VW-VT instrument incorporated a vibrating-tube densimeter to permit simultaneous measurement of the density. The measurement procedures including fluid preparation, cleaning and validation, for both instruments have been described separately in section 7.1 and 7.2. In section 7.3, we provide the working equation for both type of vibrating wires used. Finally, in section 7.4, we described the experimental fluids used, including their stated purities, their sources and any further purification undertaken.

7.1 Vibrating-Wire Viscometer-Densimeter (VW-VD) Apparatus

7.1.1 Experimental Apparatus

The VW-VD that is available in the laboratory can measure viscosity and density for temperature up to 473 K and pressure up to 200 MPa. It has been used previously to measure the viscosity of a variety of systems over a wide range of temperature and pressure including the viscosity of mixtures of hydrocarbons and CO_2.[13, 16, 249, 255, 306, 377] The VW-VD consist of a gold-plated tungsten wire (Lumma Metall AB, Sweden) with a nominal diameter of 100 μm and a nominal length of 65 mm, clamped at the top and tensioned by an aluminium sinker with a nominal mass of 0.4 kg attached at the bottom. Figure 7.1 is a schematic illustration of the wire and sinker in the vibrating wire cell. Tungsten was chosen as the wire material because of its high tensile strength, young's modulus and density, whereas aluminium was chosen as the sinker material for better sensitivity to buoyant forces when immersed in the fluid, therefore, permitting accurate density measurement of the fluid surrounding the sinker. The tungsten wire was located between the poles of a permanent magnet assembly with a magnetic field strength of about 0.3 T at T = 298.15 K. The vibrating-wire and magnet assembly were housed within a pressure vessel which in turn was enclosed within an aluminium-block thermostat, the temperature of which was regulated by means of a three-zone electric heating system with temperature sensors, electric cartridge heaters and PID controllers. This system controlled the process temperature to ±0.02 K with uniformity within 0.1 K. The temperature of the cell was measured using a platinum resistance thermometer inserted into a hole bored in the cap of the pressure vessel.

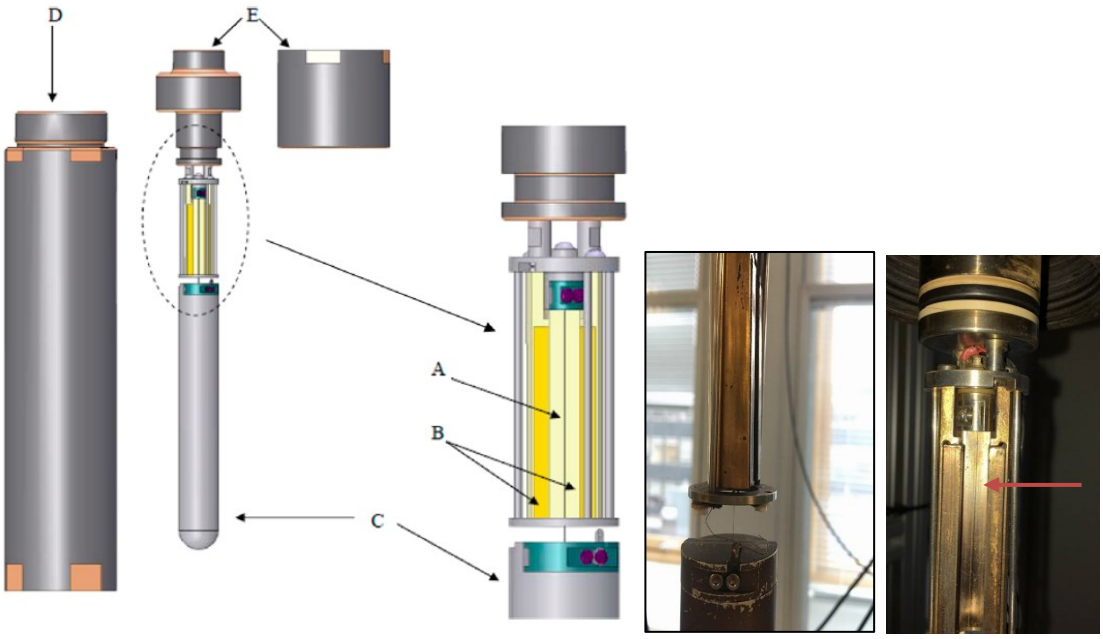

Figure 7.1 Schematic illustration of the vibrating wire and the sinker in the cell: A, tungsten wire; B, magnet; C, sinker; D, pressure vessel; E, pressure vessel plug and cap. [306]

The whole system consists of three major units, namely, the fluid handling system, the accumulator, and the pressure cell as shown in Figure 7.2. These three units were connected to form a closed loop using 1/4" stainless steel tubing with 2.4 mm internal diameter. It was designed to operate with mixtures containing dissolved gases; such mixtures were prepared *in-situ* and a circulation pump was used to mix the fluids at high pressure. The fluid handling unit permitted the following operations: filling, draining, flushing and evacuation, pressurization (using syringe pump E-1) and homogenisation (using circulation pump E-2). The fluid handling unit contained a screw injector (Sitec – 2000 bar), a pressure gauge, a pressure transducer (Stellar Technology Inc., model GT1600 series) and a magnetic circulating pump. The entire unit was temperature-controlled by means of a PID controller, thermocouple sensor and two 150 W finned-strip heaters by Watlow. The circulation pump was built in house to the design developed by Peleties et al.[391] Safety devices such as a thermal cut-out switch and a bursting disk (SD) were also installed to prevent over temperature exposures of the pressure transducer. The thermal cut-out switch and the bursting disk were set at 323 K and 240 MPa, respectively.

The accumulator (vessel E-3) with a capacity of 100 mL was used to hold a reservoir of homogeneous fluid mixture at an intermediate pressure of up to 28 MPa. The accumulator contained a gas-pressurised bladder so that its internal volume could adjust to accommodate the test fluid. This reservoir was used during pressure adjustments when the amount of fluid to be injected or withdrawn exceeded the single-stroke capacity of the syringe pump. The accumulator was placed in a separate thermally insulated box together with several valves (V7 - V9) and a bursting disk set at 33 MPa and a thermal switch unit set at 323 K to prevent the accumulator being exposed to over-pressure and/or over-temperature conditions respectively. Valve V9 is a high-pressure bypass line, inserted to cut off the accumulator from the system and to enable one if necessary to circulate the fluid at the maximum rated pressure

of the system (200 MPa) while V7 and V8 were three-way valves used to isolate the accumulator from the main system.

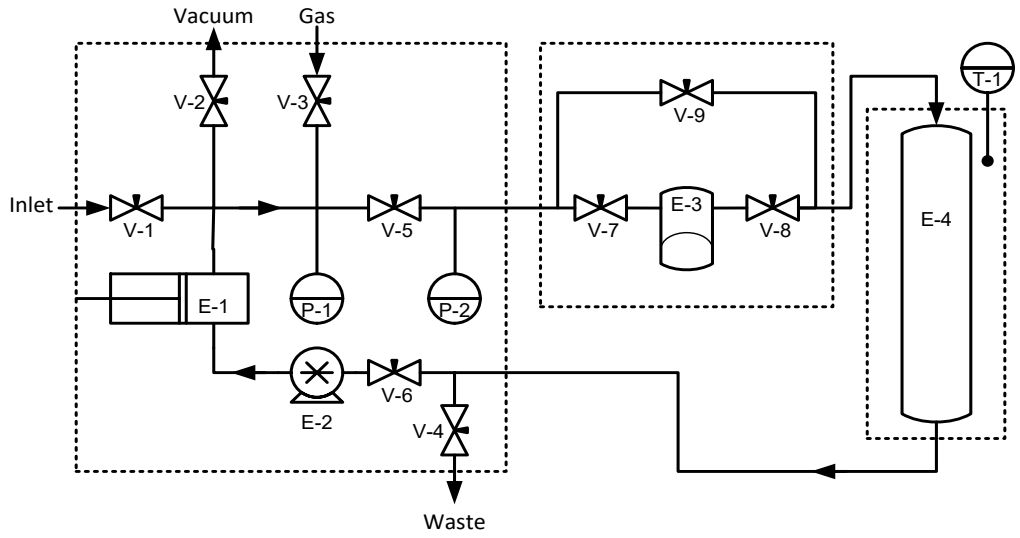

Figure 7.2 Fluid handling system: V-1, fluid inlet valve; V-2, vacuum valve; V-3, purge gas inlet valve; V-4, drain valve; V-5, V-6, V-7, V-8, isolation valves; V-9, bypass valve; E-1, pressure generator (manual syringe injector); E-2, magnetic circulation pump; E-3, accumulator vessel; E-4, pressure cell; P-1, pressure gauge; P-2, pressure transducer.

The pressure cell that housed the vibrating-wire and the magnet assembly is a high-strength stainless steel vessel that can operate up to 200 MPa and 473 K. The cell was placed inside an aluminium block, where ten 110 W cartridge heaters is embedded in three different zones (top, middle, and bottom) to control the process temperature within ±0.02 K and uniformity within 0.1 K. The overall temperature of the cell is being measured using a platinum resistance thermometer inserted from the top of the pressure vessel cap. The aluminium block was than fitted inside a thermal insulation box that guaranteed a satisfactory insulation of the cell in the range (up to 473) K and served as a support for an electronic lift designed to manoeuvre the vessel during assembling. The view of the exterior setup is shown in Figure 7.3.

Figure 7.3 View of the pressure vessel, aluminium jacket, thermal insulation box and electrical lift system.

7.1.2 Operating procedures

Prior to starting measurement, the system was flushed thoroughly with hexane and nitrogen before being dried under vacuum for several hours. Hexane was chosen as the solvent as it is effective in removing hydrocarbon residues and its high volatility makes it easy to remove by gas flushing and evacuation. While the system was still under vacuum, freshly dried, and degassed *m*-xylene was admitted to the evacuated system from a sample bottle via valve V-1. The amount of *m*-xylene injected was determined by weighing the sample bottle before and after this operation (liquid in the connecting tube was allowed to drain back to the bottle before weighing). Additional weighing operations were used to verify that an insignificant amount of *m*-xylene remained in the connecting tube; the mass change of the tube before and after transfer was not more than 1 mg. Furthermore, any *m*-xylene remaining in the inlet port of the fluid system was pushed into the system by the subsequent transfer of CO_2. Figure 7.4 shows the filling setup for *m*-xylene from the reservoir into the system through valve V1.

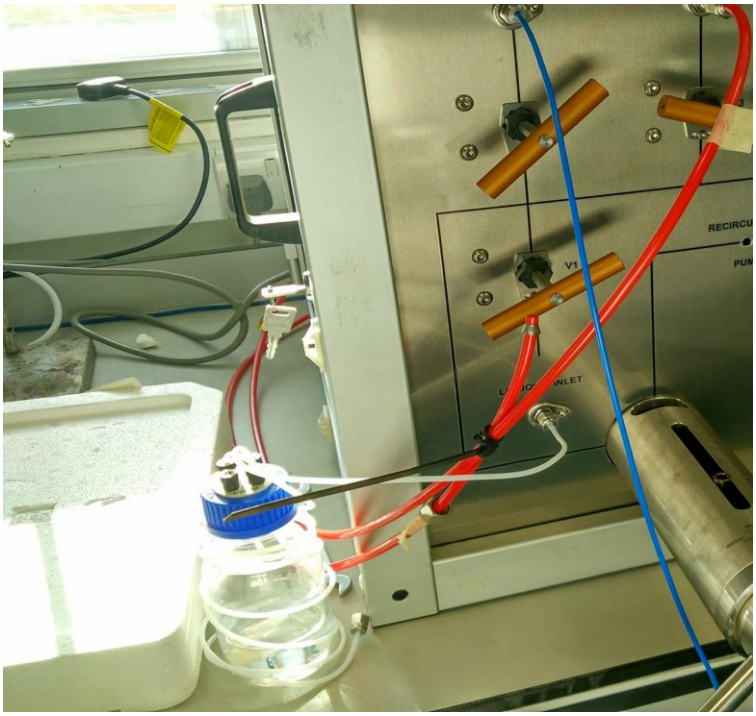

Figure 7.4 Filling *m*-xylene from the reservoir into the system

Meanwhile, CO_2 was transferred from the supply cylinder into a previously evacuated 250 ml high-pressure weighing cylinder (with a maximum working pressure of 35 MPa). To ensure that an adequate amount of CO_2 was available for transfer into the system, the weighing cylinder was partially filled with liquefied CO_2. To do this, the lower part of the weighing cylinder was immersed in a solid CO_2-ethanol cryogenic bath at -78˚C (195.15 K) until thermal equilibrium was achieved. CO_2 gas was then allowed to flow from the supply cylinder into the weighing cylinder at a pressure of 10 bar. Since the upper half of the cylinder was not chilled, it remained close to ambient temperatures. As a result, only bottom half of the cylinder was sufficiently cool for liquefaction to occur, whereas CO_2 in the upper part of the cylinder remained in gaseous form. From the phase diagram of CO_2, the liquefaction occurred at a temperature of close to -40 ˚C at filling pressure of 10 bar. The flow of gas into the cylinder diminished when half of the cylinder was filled with liquid and no further condensation was possible above the liquid surface. The weighing cylinder was then disconnected from the supply and allowed to warm up to ambient temperature before weighing. Finally, the weighing cylinder was connected to V1 and CO_2 was allowed to flow into the system. The process was able to raise the internal pressure of the weighing cylinder between 50 to 60 bar, high enough for CO_2 to flows into the system (the system was at atmospheric conditions after filling *m*-xylene) and sufficient to transfer the amount of desired CO_2 into the system. The total amount of CO_2 added into the system was calculated by measuring the mass of the weighing cylinder before and after the injection. The mixture composition was then calculated from the masses of the two components and their respective molar masses.

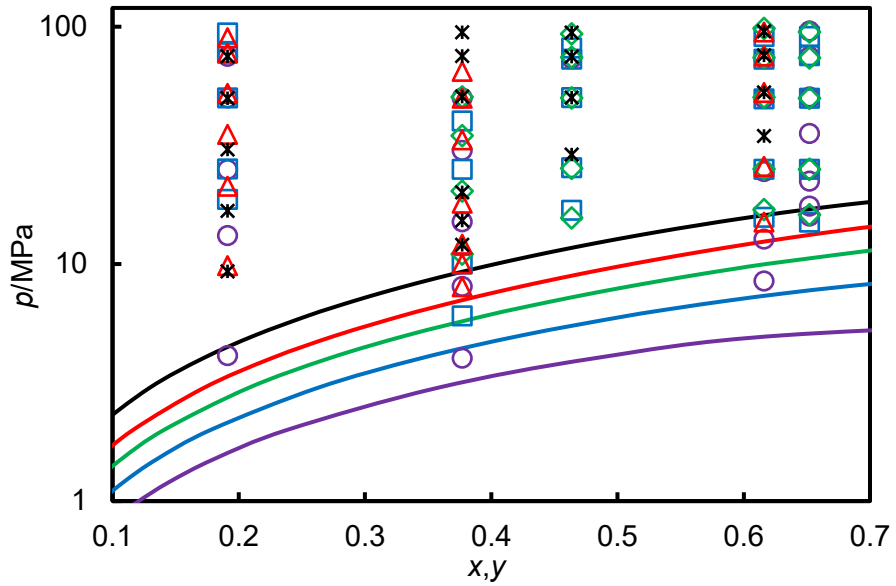

Figure 7.5 Pressure-composition diagram for (m-xylene + CO_2) showing the distribution of experimental data points at each temperature: ○, T = 298 K; □, T = 323 K; ◇, T = 348 K; △, T = 373 K; ∗, T = 423 K. Lines show bubble curves calculated with the Predictive Peng Robinson equation of state at the same temperatures (denoted by colour). Note the logarithmic scale for pressure.

The measurement campaign was designed to address homogeneous liquid states only. Therefore, the experimental states investigated were always at pressures above the mixture bubble pressure at given temperature and composition. To guide the experiments, bubble curves for (*m*-xylene + CO_2) were calculated from the Predictive Peng-Robinson equation of state[392] at each temperature. Figure 7.5 shows the calculated bubble curves and the location of the experimental data points on a pressure-composition graph. All of the experimental data points fall above the corresponding bubble curve and are therefore located in the homogeneous liquid. In addition to that, the circulation pump was also run for 12 hours at a pressure above the calculated bubble pressure to ensure total homogenization. An initial check measurement of viscosity and density was made at the starting temperature and pressure, after which mixing was continued for a further 2 hours. A second check measurement was then made as a test of the homogenisation of the mixture. The first and second check measurements always agreed to within 1% and 0.1% for viscosity and density, respectively. Following the measurements at a given composition, either additional CO_2 was added to increase the mole fraction, or the system was emptied, and a new mixture was formed from scratch. Figure 7.6 shows the filling of CO_2 into the weighing cylinder and the system.

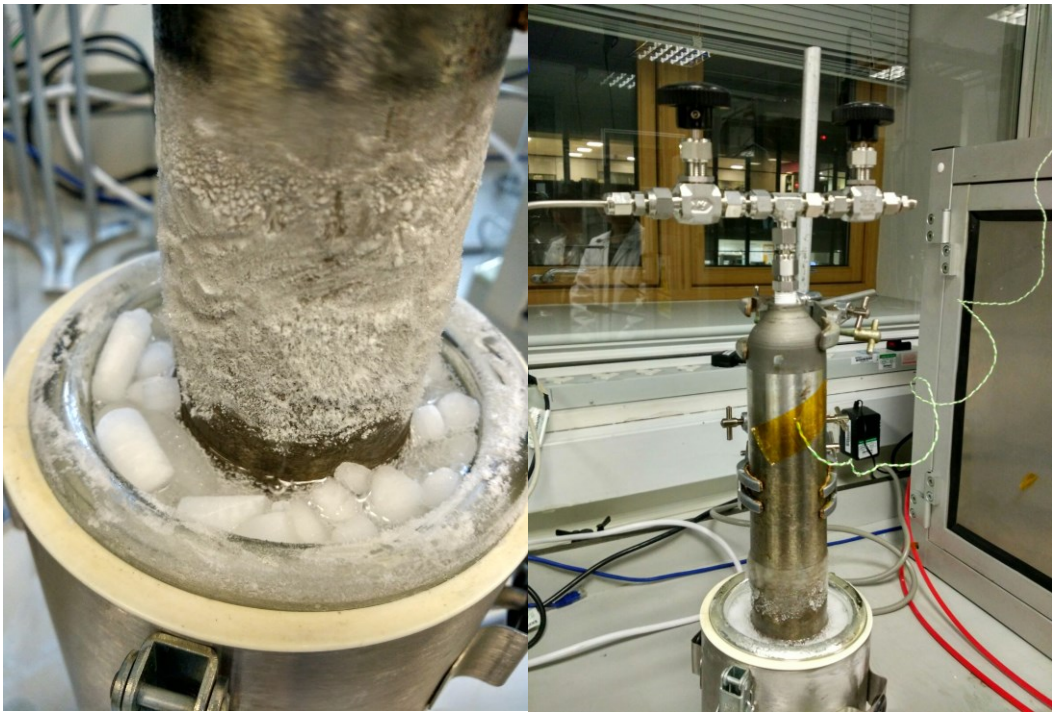

Figure 7.6 Filling CO_2 into the weighing cylinder and the system

The viscosity and density of (*m*-xylene + CO_2) were measured at temperatures between (298 to 423) K, pressure up to 100 MPa and at mole fractions of CO_2 (x_{CO_2}) of 0.191, 0.377, 0.464, 0.616 and 0.652. For validation purposes, some measurements were also made on pure *m*-xylene. Using the methodology detailed by Mohammed et al.,[13] the combined expanded relative uncertainties for viscosity and density were estimated to be 2% and 0.2%, respectively at a coverage factor of 2. Figure 7.7 compares the new results for pure *m*-xylene with data from the literature[393-397] together with the viscosity correlation and equation of state as implemented in the REFPROP software (version 10.0).[398] For viscosity, our data agree with the correlation of Cao *et al*.,[399] to within ±0.7% and also show good agreement with previous experimental studies. In the case of density, our measurements agree with the equation of state of Zhou *et al*.,[384] to within ±0.1%. These comparisons successfully validate the measurement system.

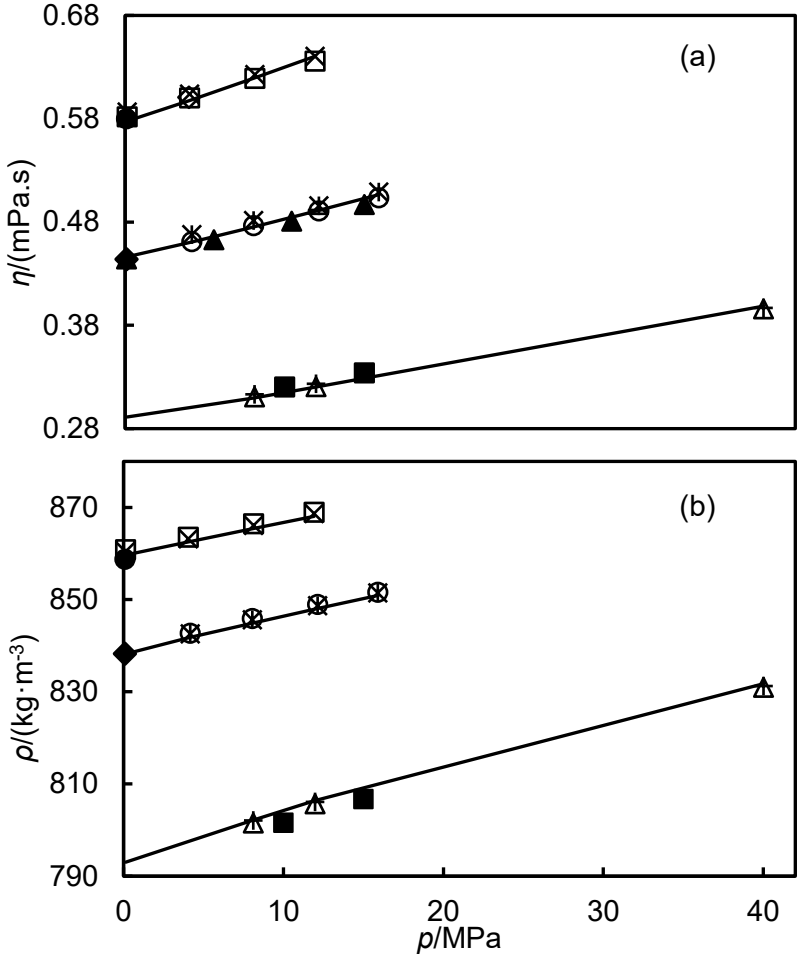

Figure 7.7 (a) Viscosity η and (b) density ρ of *m*-xylene. This work: □, T = 298 K; ○, T = 323 K; △, T = 373 K. Caudwell *et al*.[249]: ×, T = 298 K, ∗, T = 323 K; +, T = 373 K. Yang *et al*.[397]: ◆, T = 323 K. Assael *et al*.[393]: ▲, T = 323 K. Meng *et al*.[396]: ■, T = 373 K. Kashiwagi and Makita *et al*.[395]: ◇, T = 298 K; -, T = 323 K. Et-Tahir *et al*.[394]: ●, T = 298 K. Solid lines represents values calculated from the correlation of Cao *et al*.,[399] for viscosity and the equation of state of Zhou *et al*.[384] for density.

7.2 Vibrating-Wire Vibrating-Tube (VW-VT) Apparatus

The viscosity of diisodecyl-phthalate (DIDP) + CO_2 were measured using VW-VT apparatus. The VW-VT that is available in the laboratory can measure viscosity and density for temperature between (274.15 to 448.15) K and pressure up to 100 MPa. Figure 7.8 is a schematic diagram of the VW-VT apparatus.[400] Unlike the VW-VD apparatus, the wire employed in this apparatus was a horizontally orientated and clamped at both ends under tension. The wire was a centerless-ground tungsten cylinder of free length 52 mm and diameter 0.1 mm (Metal Cutting Corp., New Jersey, USA). The permanent magnet, in this case located outside the pressure vessel, provided a magnetic field of approximately 0.38 T at the midpoint between the poles at T = 298.15 K. During assembly, the viscometer cell was put in the vertical orientation, the wire was secured at the top clamp, and tensioned by attaching a mass of approximately 0.5 kg to its lower ends. The wire was then left in this condition for a period of typically 24 h before the lower end clamp was tightened and the

excess wire protruding from each end cut off. The end clamps on the sensor were provided with screw terminals for the attachment of the electrical lead wires. Figure 7.9 shows the illustration of the vibrating-wire sensor.[259] The vibrating U-tube densimeter used in this work was a commercial instrument from Anton Paar (model DMA HP) that can be operated at pressures up to 138 MPa and temperatures from (263.15 to 473.15) K. It was equipped with internal heat exchanger that were used with circulating oil bath to control its temperature. The outer surface of the densimeter was covered with silicone-rubber sponge and the whole assembly was enclosed within an aluminium box.

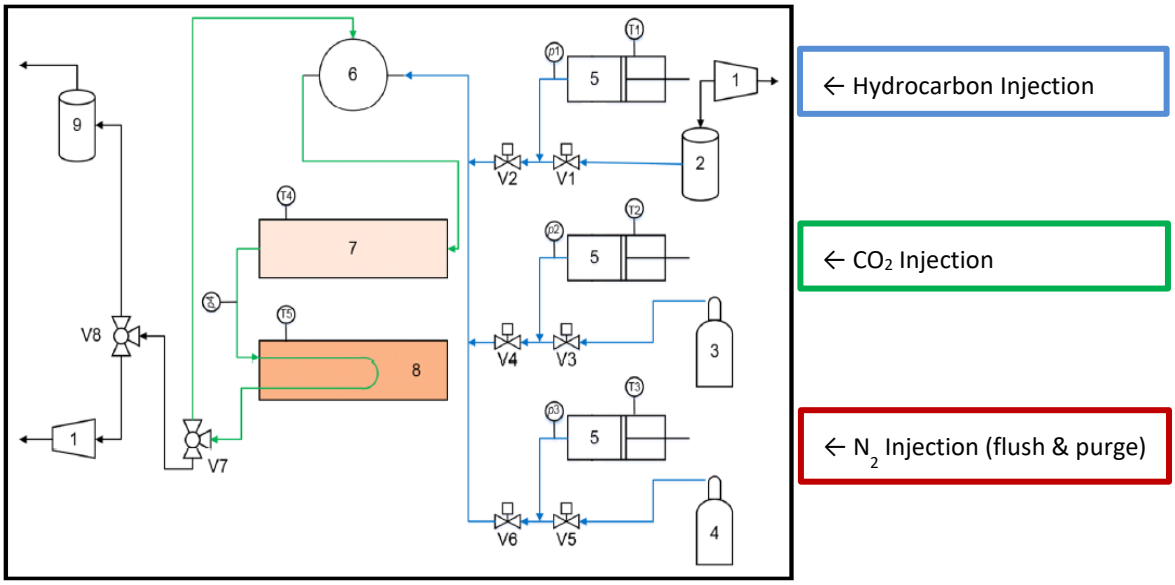

Figure 7.8 Schematic diagram of the VW-VT apparatus: (1) vacuum pumps, (2) sample bottle (3) CO_2 gas cylinder, (4) N_2 gas cylinder, (5) QUIZIX pumps, (6) circulating pump, (7) VW viscometer, (8) VT densimeter, (9) waste bottle.

Some of the key components of the system, apart from the vibrating wire viscometer and the U-tube densimeter, include the high-pressure syringe pump for injecting the fluids, the circulation pump to homogenize the mixtures and the pressure vessel that encases the viscometer. Three injecting pumps (QUIZIX pump) were available to inject fluids into the apparatus and to control the pressure of the system. These pumps were interfaced with a computer equipped with a software application (Quizix PumpWorks, version 7.02) that was able to monitor the displaced volume of the fluid. The amount of fluid injected inside the system were then calculated based on that volume recorded. One vacuum pump allowed the liquid to be degassed before entering the system. Two chillers were used in the system: one to control the temperature of the densimeter and viscometer and the other to control the temperature in the QUIZIX pumps. The viscometer and densimeter were connected in a loop (green line in Figure 7.8) with a circulation pump that permitted *in situ* homogenization of the mixtures and circulation of solvents during cleaning of the apparatus. The circulation pump is a pneumatically operated reciprocating pump and was the best possible option for a good mixing of fluids circulating in closed-circuit high-pressure.[253, 391] The pressure cell that housed the vibrating viscometer has a maximum working pressure of 100 MPa at T = 473 K. It was

classified as “thick-walled” because the ratio between the outer and inner diameter of the vessel was found to be greater than 1.2.

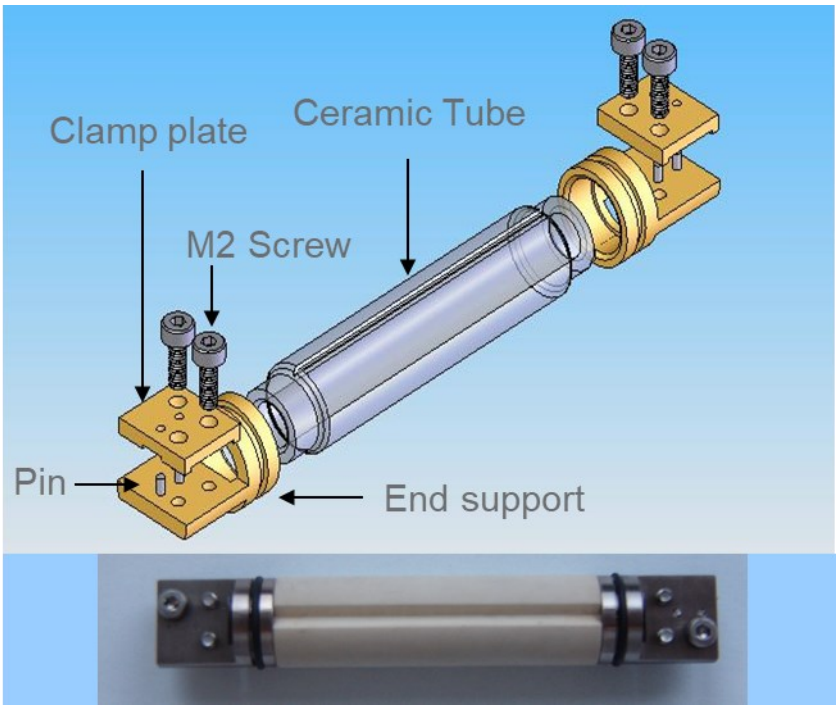

Figure 7.9 The vibrating-wire sensor

7.2.1 Operating Procedures

Before starting any measurement campaign, the apparatus was carefully cleaned with appropriate liquid solvents. In this work, a combination of two solvents was used for cleaning, namely, toluene and hexane. The two solvents were chosen because the heavy hydrocarbon and aromatic components are more solubilized in toluene, while for a lighter compound, the solubility was higher in hexane. During the cleaning process, one of the syringe pumps was used for the fluid injection while the circulation pump was used to flush the entire loop and discharge the solvents to the waste line. Some measurements were carried out simultaneously during the cleaning process. The measured density values were compared with the values calculated from the equation of state for hexane[401] and toluene[21] while the viscosity results were compared with calculated viscosity from the correlation equations developed by Michailidou et al.[402] and Avgeri et al.[220] for hexane and toluene, respectively. Figure 7.10 shows the relative deviation plot against pressure of measurements at ambient temperature. The results of the measurements were found to agree within ± 0.3 % for density and ± 3 % for viscosity for both heptane and toluene. After these measurements, the system was flushed with nitrogen several times at a pressure of about 0.5 MPa to discharge any remaining solvent to the waste line before increasing the temperature of the system at a temperature high enough for the evaporation to occur. The system was then evacuated for about twelve hours using the vacuum pump.

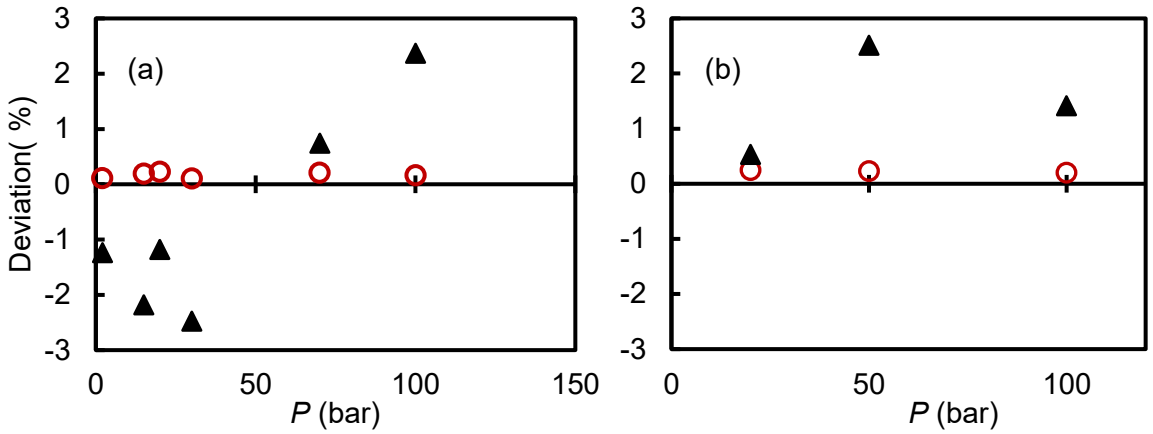

Figure 7.10 Relative deviations $\Delta x/x = (x - x_{calc})/x$ where x are the properties measured and x_{calc} were values calculated from reference as a function of pressure: (a) hexane; (b) toluene at ambient temperature: ▲= η; ○= ρ

Measurement of pure DIDP were carried out before starting the measurements campaign for the mixtures. The pure DIDP was first dried and degassed to eliminate possible traces of water and dissolved air before being injected into the system. Figure 7.11 shows the relative deviation between the experimental measurements and the correlation developed by Peleties[259, 390] as a function of pressure at several temperatures. The results were found to agree within ± 0.5 % for density and ± 2 % viscosity.

The preparation of mixtures was done by filling gaseous CO_2 into the system through valves V3 and V4 (in Figure 7.9) to an initial filling pressure of between 0.5 MPa and 3 MPa. The amount of CO_2 was computed based on the volume obtained and by using the density value calculated from the equation of state of Span and Wagner[403]. For mixtures, dried and degassed DIDP were injected using one of the QUIZIX pumps that was set at T = 298 K using a chiller. Several strokes of the pump were required to fill the system until the system reached a desired pressure with known density calculated from the correlation of Peleties and Trusler.[259] The amount of liquid injected were calculated from the initial and final value of pressure and volume from the QUIZIX pump. The circulation pump was activated for several hours to homogenize the mixtures. The system was then allowed to rest at least an hour before taking a measurement to stabilize the system. All the measurements were carried out along an isotherm by increasing the pressure, before heating up to the next temperature.

The viscosity and density of (DIDP + CO_2) were measured in single phase liquid mixtures at temperatures between (298 to 373) K, pressure up to 80 MPa and at mole fractions of CO_2 (xCO_2) of 0.207, 0.411, 0.610 and 0.810. During the measurements, it was important to maintain a single homogenous liquid mixture. Therefore, all measurements were done at pressures above the bubble curve of the mixtures.

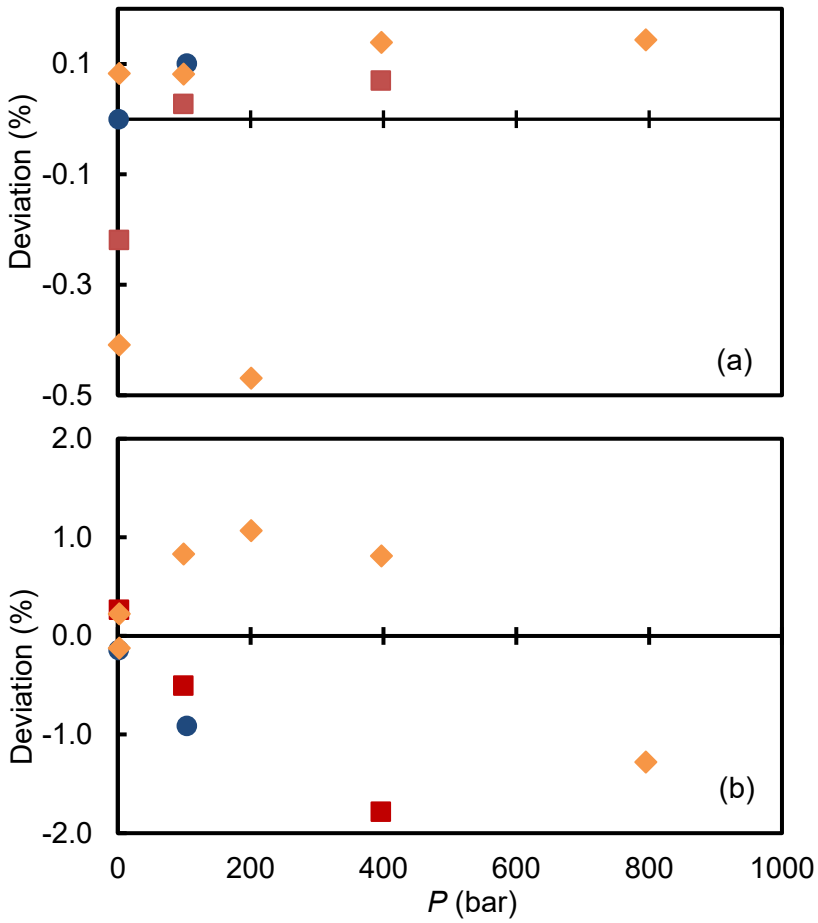

Figure 7.11 Relative deviations $\Delta x/x = (x - x_{calc})/x$ where x are the properties measured and x_{calc} were values calculated from reference[259, 390] as a function of pressure for pure DIDP: (a) ρ; (b) η, at various temperatures: ●, T = 313 K; ■, T = 343 K; ◆, T = 473 K.

7.3 The Working Equation

The electric circuit shown in Figure 7.12 can be used to describe the theory for the vibrating wire viscometer. The lock-in amplifier provided a constant voltage which was converted into a constant current by using the fixed resistor R_s (1.4 KΩ) that was connected in series with the vibrating wire. The wire is positioned between two magnets of opposite poles. Due to the presence of a magnetic field perpendicular to the wire, the flow of current in the wire produced a sinusoidal force which acts on the wire to drive its transverse oscillation. The electromotive force generated across the wire can be expressed as a function of its frequency of vibration. The vibration of the wire induces a voltage proportional to the velocity of the wire in addition to that arising from the passage of the current through the electrical impedance presented by the stationary wire. The voltage developed across the vibrating wire was detected by means of a lock-in amplifier which was connected to a computer via GPIB interface.

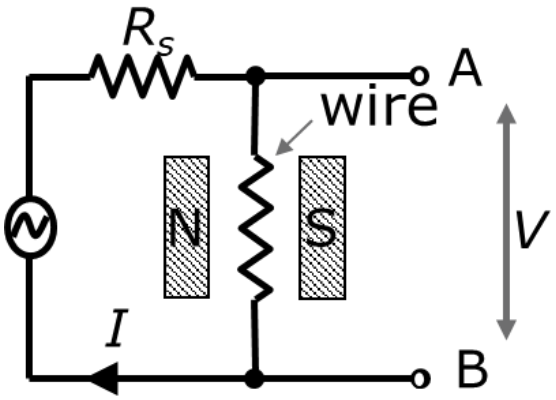

Figure 7.12 Electric circuit representing the vibrating wire viscometer

The width of the resonance curve is affected by the viscosity of the fluid, while the resonance frequency of this mode of oscillation is sensitive to the density of the surrounding fluid. Figure 7.13 illustrates a typical resonance frequency curve obtained in liquid hydrocarbon and air at ambient conditions. The width of the resonance curve for the liquid hydrocarbon is much wider than that obtained in air since liquid hydrocarbon has higher viscosity than the air.

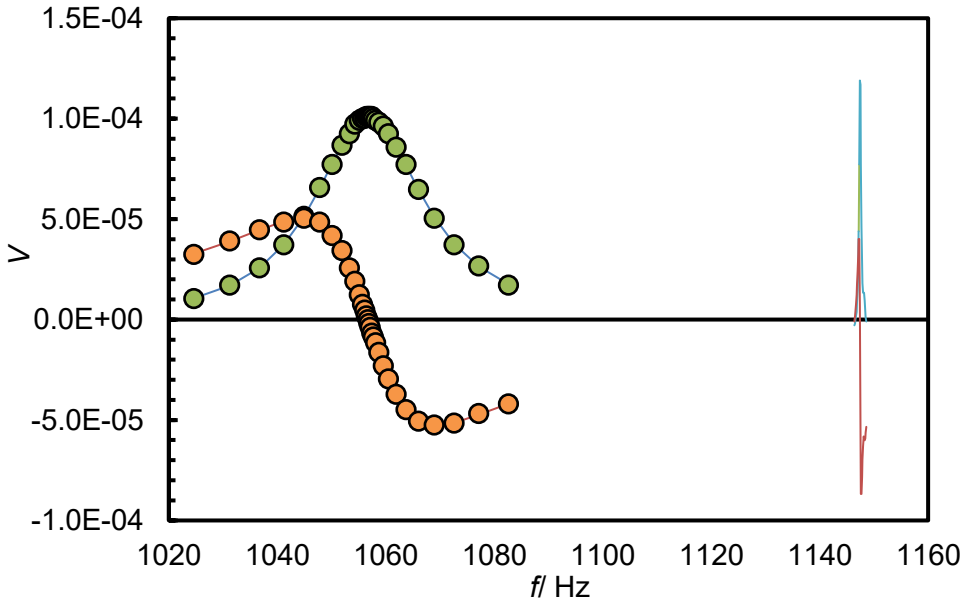

Figure 7.13 Resonance frequency curve obtained in liquid hydrocarbon and ambient air. Orange symbols denote the real parts of the experimental data and, green symbols represent the imaginary part of the experimental data. Lines represent the model.

The vibrating wire used in the measurements of viscosities were using two different configurations. The VW-VD is using a wire that was tensioned by a sinker, and the VW-VT is using a wire that was clamped at both ends. The working equation for both viscometers are detailed in the following sub-sections.

7.3.1 Vibrating Wire Clamped at Both Ends

The lines in Figure 7.13 represent the voltage calculated from the working equation such that

$$V = \frac{\Lambda f i}{f_0^2 - f^2\left(1+\beta\right) + f^2\left(\beta' + 2\Delta_0\right)i} + a + ib + icf \tag{7.1}$$

The voltage V in the equation can be expressed as the sum of two terms: the first, $V_1(f)$, arises from the electrical impedance of the stationary wire; while the second, $V_2(f)$ is an induced voltage due to the motion of the wire. The first term, $V_1(f)$ can be express empirically by a complex function as follows

$$V_1\left(f\right) = a + ib + icf \tag{7.2}$$

where a, b and c are real constant. Meanwhile, the second term, $V_2(f)$ can be express as

$$V_2\left(f\right) = \frac{\Lambda f i}{f_0^2 - f^2\left(1+\beta\right) + \left(\beta' + 2\Delta_0\right)i} \tag{7.3}$$

Equation (7.1) was measured in the fluid of interest as a function of the driving frequency, f in the neighbourhood of f_0, which is the wire resonance frequency in vacuum. The parameters in equation 7.1 are define as follows: Λ is the amplitude, a, b, and c are real constants and, β and β' are the mass and viscous damping parameters that are related to the densities of both the wire and the fluid according to the following dimensionless expressions

$$\beta = k\frac{\rho}{\rho_s}, \text{ and } \beta' = k'\frac{\rho}{\rho_s}, \tag{7.4}$$

where ρ and ρ_s are the density of fluids and wire, respectively. k and k' are the kelvin functions of Ω which is a function of viscosity such that

$$\Omega = \frac{2\pi f \rho R^2}{\eta} \tag{7.5}$$

Δ_0 is the logarithm decrement of the wire in vacuum inferred from the measurement carried out in nitrogen at ambient pressure and temperature via the following relation

$$\Delta_0 = \left(\Delta_0^{'} - \frac{1}{2}\beta^{'} \right) \tag{7.6}$$

where Δ_0' is the measured decrement of the wire in nitrogen and β' is the damping parameter for nitrogen. The values of density and viscosity of nitrogen at measurement conditions T, P were calculated from the equation of state by Span et al.[404] and Lemmon and Jacobsen[405], respectively. The wire radius R was taken from calibration with toluene.

The density from the vibrating u-tube densimeter in the VW-VT apparatus were obtained from the measurement of the period of oscillation of the vibrating-tube densimeter, τ , by means of the following physical model

$$\rho = \frac{\left(\rho_M / S_{00}\right)}{\left(1 + \alpha_V t + \beta_V p\right)} \left[\left(\frac{\tau}{\tau_{00}\left(1 + \varepsilon_{\tau 1} t + \varepsilon_{\tau 2} t^2\right)} \right)^2 \left(1 + \beta_\tau p\right) - 1 \right] \tag{7.7}$$

where ρ_M is the density of the tube material, t is the Celsius temperature and p is the pressure. The seven parameters S_{00}, τ_{00}, α_v, β_v, $\varepsilon_{\tau 1}$, $\varepsilon_{\tau 1}$ and β_τ was determined according to the calibration method in vacuum and with water by minimizing the sum of squared differences between the experimental densities and the calculated values from the IAPWS-95 equation of state.[406] The vacuum calibration measurements were performed at temperatures from (274.66 to 448.19) K and the calibration in deionized water were made in the temperature range from (298.15 to 448.24) K at pressures from (1 to 100) MPa.

7.3.2 Vibrating Wire Tensioned by a Sinker

The standard working equation for the vibrating wire as described in equation (7.1) to equation (7.6) is applied to this type of vibrating wire as well. However, the term f_0 in equation (7.1) is the hypothetical resonance frequency for condition where the wire is in vacuum and the sinker is immersed in the fluid as described in a physical model by Ciotta et al.[407]

$$f_0 = \frac{1}{2L} \left[A \sqrt{\frac{(m - \rho V) g}{\rho_w \pi R^2}} + \sqrt{\frac{E R^2}{\rho_w L^2}} + \left(1 + \frac{\pi^2}{8}\right) \sqrt{\frac{E^2 \pi R^6}{(m - \rho V) g \rho_w L^4}} \right] \tag{7.8}$$

m and V are the mass and volume of the sinker, A is an empirical parameter in the model, g is the gravitational acceleration, ρ_w, R, L and E are the density, radius, length, and the young's modulus of the wire material, respectively. Some of the parameters were measured and some were quantified through calibration before the measurement started. The radius of the wire obtained through measurement in pure octane using known value of viscosity and density from the reference[401, 408] The length of the assembled wire was measured with an internal calliper (Kroeplin, model H260) calibrated against a 70 mm i.d. setting ring with measuring range of 60 – 80 mm. The mass and volume of the sinker were determined by hydrostatic

weighing using a precision electronic balance by Mettler Toledo (model PR5003) with a standard uncertainty of 5 mg. Table 7.1 shows the mass of the sinker measured using the balance in ambient air l_a and in water l_w.

Table 7.1 Mass of the sinker measured in ambient air l_a and in water l_w

	T_a / ºC	l_a / g	l_w / g
1	21.4	399.59	140.842
2	21.4	399.59	140.840
3	21.4	399.59	140.840
Average	**21.4**	**399.59**	**140.841**

The mass shown in Table 7.1 were then corrected for air buoyancy effects using the equation below.

$$m_c \,/\, \mathrm{g} = \left[\frac{1-(\rho_a \,/\, \rho_c)}{1-(\rho_a \,/\, \rho)}\right] \times l_a \,/\, \mathrm{g} \tag{7.9}$$

where m_c is the corrected weight of the sinker in g, ρ is the density of the material, ρ_c is the conventional body density, given as 8000 kg/m^3. The density of air ρ_a were calculated such that

$$\rho_a \,/\, \left(kg.m^{-3}\right) = \frac{0.348444\left(p_a \,/\, hPa\right) - 100h_a\left[0.00252\left(T_a \,/^{o} C\right) - 0.020582\right]}{273.15 + \left(T_a \,/^{o} C\right)} \tag{7.10}$$

where p_a is the ambient pressure, h_a is the relative atmospheric humidity, and T_a is the ambient temperature. On the other hand, the volume of the sinker V_s was measured as

$$V_s = \frac{m_c}{\rho_s} \tag{7.11}$$

m_c were calculated using equation 7.9 and ρ_s, which is the true density of the sinker were calculated such that

$$\rho_s \,/\, (kg.m^{-3}) = \left[l_a \,/\, l_w.\left(\rho_w - \rho_a\right) / (kg.m^{-3})\right] + \rho_a \,/\, (kg.m^{-3}) \tag{7.12}$$

where l_a is the weight of the sinker in ambient air; l_w is the weight of the sinker in water; ρ_w is the density of water at the operating temperature and ρ_a is the density of air at the operating

(ambient) temperature. Table 7.2 shows the summary of all the properties measured and calculated for the sinker in the VW-VD apparatus.

Table 7.2 Measured and calculated properties of the sinker

T_a / °C	21.4
p_a / kPa	101.33
RH / %	39.3
t_w / °C	22.89
ρ_a / kg.m^{-3}	1.1943
m_c / kg	0.399703
ρ_s / kg.m^{-3}	2829.05
V_s / m^3	0.000141

7.4 Materials

The chemicals used in this work is summarised in this Table 7.3. Carbon dioxide supplied by BOC with a mole fraction purity higher than 0.99995 and were used as supplied. All liquid hydrocarbon components were supplied by Sigma Aldrich (UK). The specified purity for 1,3-dimethylbenzene, octane, toluene, hexane and DIDP were 0.998, 0.996, 0.99, 0.99, and 0.998 respectively. The purity of the liquid solvents were determined by the supplier by gas chromatography and no further purification was attempted. Before use, *m*-xylene and octane and DIDP was dried over 4 Å molecular sieves supplied by Sigma-Aldrich and degassed under vacuum. The saturated molecular sieves were regenerated by heating to 473.15 K using a Thermo-oven before and after use. Degassing under vacuum was done as follows: Transfer solvent in a glass bottle with a close-fitting screw cap and a dip tube through which sample could be drawn. Connect the vacuum pump via another tube through the screw cap. The end of the tube should be above the liquid level in the reservoir. Turn on vacuum and keep the reservoir under stirring for approximately 10 minutes. DIDP was also dried at least one hour in a rotating evaporator to eliminate possible traces of water. All mixtures were prepared *in-*situ prior to starting a measurement campaign.

Table 7.3 Description of Chemicals where w denotes mass fraction and x denotes mole fraction

Chemical Name	CAS Number	Supplier	Purity as supplied	Additional Purification
m-xylene	108-38-3	Sigma-Aldrich	w = 0.998	Dried and degassed
Octane	111-65-9	Sigma-Aldrich	w = 0.996	Dried and degassed
Carbon dioxide	124-38-9	BOC	$x \geq 0.99995$	None
DIDP	26761-40-0	Merck	w = 0.998	Dried and degassed
Toluene	108-88-3	Sigma-Aldrich	w = 0.99	None
Hexane	110-54-3	Sigma-Aldrich	w = 0.99	None

CHAPTER 8 VISCOSITY OF *M*-XYLENE WITH DISSOLVED CO_2

This chapter presents the experimental results for mixtures of 1,3-dimethylbenzene (*m*-xylene) and carbon dioxide.[1] The viscosity and density measurements were carried out simultaneously using the vibrating-wire viscometer-densimeter (VW-VD) at temperatures ranging from (298 to 423) K and at pressures up to 100 MPa. The combined expanded relative uncertainties for viscosity and density were estimated to be 2% and 0.2%, respectively at a coverage factor of 2. The subsequent sections present the results for each of the systems investigated. The Tait-Andrade and Tait equations have been used to correlate the experimental data for viscosity and density, respectively, at each composition. In this chapter, a correlation for the viscosity and density surfaces as functions of temperature, pressure and mole fraction were also discussed. This chapter provides new experimental data that can be used in the development and validation of predictive models for the thermophysical properties of asymmetric mixtures at high temperature and pressure conditions. The results discussed in this chapter have been published and therefore contain some of the figures and tables similar to the paper. [379]

8.1 Experimental Results and discussions

Before working on the mixtures, some measurements were made on pure *m*-xylene and the results are given in Table 8.1. The results have been compared with the existing literature listed in Table 8.2 and the analysis of comparison have been discussed in chapter 7. The experimental data from this work were found to fit well with the data from Caudwell et al.,[249] with difference below 2% and 0.4% for viscosity and density, respectively. Additionally, the new data are also in agreement with the viscosity correlation of Cao et al.,[399] to within ±0.7% while, for the case of density, the measurements agree with the equation of state (EoS) of Zhou et al.,[384] to within ±0.1%. However, experimental data for the viscosity and density of (*m*-xylene + CO_2) systems are not available in the literature.

The viscosity and density of (*m*-xylene + CO_2) were measured at mole fractions of CO_2 of 0.191, 0.377, 0.464, 0.616 and 0.652. The viscosity and density of each composition were measured simultaneously along isotherms at nominal temperatures of (298.15, 323.22, 348. 31, 373.26, and 423.31) K at pressures up to 100 MPa. The results are given in Appendix 8A to 8E and, as examples, the viscosity and molar density as functions of mole fractions of CO_2 at fixed *T* are shown in Figure 8.1 and Figure 8.2, respectively. As expected, the viscosity and density of the mixtures was found to increase with increasing pressure and decrease with increasing temperature. Looking at the figures, it is also apparent that the dissolution of CO_2 into *m*-xylene resulted in a large reduction in viscosity. However, the relative effect of the dissolution on density is not as dramatic. Experimental density data were found to differ less than 6% from the density of pure *m*-xylene. Another point to point out from figure 8.1 and 8.2 is the results for x_{CO_2}= 0.616 which are slightly off trend due to the possibility of experimental error during the measurement for this mixture.

[1] The experimental measurements on two of the mixtures were carried out in collaboration with two undergraduate students.

409. Wong, C. K.; Qiu, F. *Experimental Measurement of viscosity of the binary mixture of m-Xylene and CO2*; Report, Imperial College London London, UK, 2017.

Table 8.1 Experimental Viscosity η and Density ρ of pure *m*-xylene

p/MPa	η/(μPa·s)	ρ/(kg·m^{-3})	p/MPa	η/(μPa·s)	ρ/(kg·m^{-3})
	T = 298.42 K			T = 372.70 K	
0.132	581.69	860.83	8.127	310.86	801.56
4.047	600.06	863.60	11.972	320.59	805.72
8.137	619.12	866.52	40.022	395.99	830.99
11.912	635.75	868.99	80.022	501.82	857.64
	T = 323.08 K				
4.182	461.01	842.74			
8.052	476.58	845.91			
12.147	490.70	848.98			
15.897	503.52	851.65			

Expanded uncertainties are $U(T)$ = 0.20 K, $U(p)$ = 0.04 MPa, $U(x)$ = 0.0015, $U(\rho)$ = 0.002ρ and $U(\eta)$ = 0.02η with a coverage factor k of 2.

Table 8.2 Available experimental data for viscosity η and density ρ of pure *m*-xylene

Reference	property	T/K	p/Mpa
Caudwell et al. [249]	ρ, η	298.15 to 473.15	0.1 to 200
Yang et al. [397]	ρ	323.2	0.1
Assael et al. [393]	η	323	0.1 to 15
Meng et al. [396]	ρ, η	373	10 and 15
Kashiwagi and Makita[395]	η	298.15 and 323.15	4 to 12.1
Et-Tahir et al. [394]	ρ, η	298.15	0.1 to 100

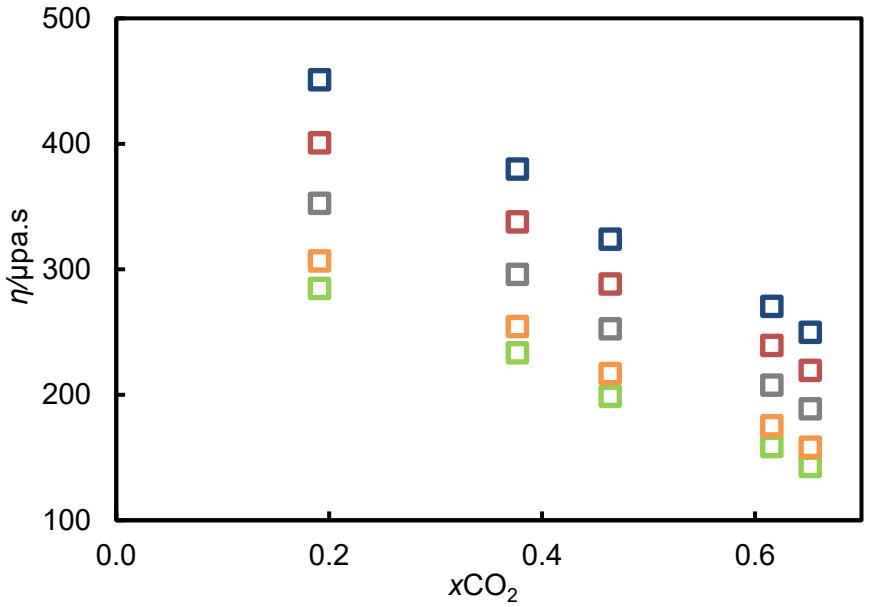

Figure 8.1 Experimental viscosity η as a function of mole fraction of CO_2 at T = 373 K: □, p = 10 MPa; □, p = 20 MPa; □, p = 40 MPa; □, p = 60 MPa; □, p = 80 MPa.

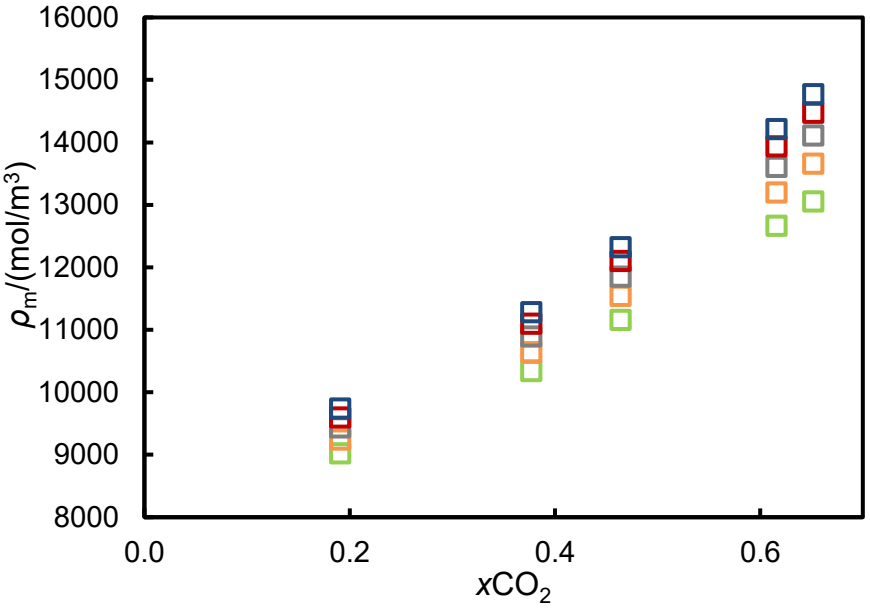

Figure 8.2 Experimental molar density ρ_m as a function of mole fraction of CO_2 at T = 323 K: □, p = 1 MPa; □, p = 25 MPa; □, p = 50 MPa; □, p = 75 MPa; □, p = 100 MPa

8.2 Correlations

The experimental viscosity data for each individual mixture composition were correlated using Tait-Andrade equation,[410] expressed as follows:

$$\eta = A_\eta \exp\left(\frac{B_\eta}{T + C_\eta}\right)\left(\frac{p + E}{p_0 + E}\right)^D \tag{8.1}$$

where A_η, B_η and C_η are adjustable parameters, p_0 = 0.1 MPa, and D and E are functions of temperature represented by the following equations

$$D = \sum_{i=0}^{2} d_i \left(T / T_0\right)^{-i} \tag{8.2}$$

$$E\,/\,\mathrm{MPa} = \sum_{i=0}^{2} e_i \left(T / T_0\right)^{i} \tag{8.3}$$

Similarly, the experimental density data were correlated using the widely known modified Tait equation[411] expressed as

$$\rho = \rho_0 \left[1 - C \log_{10} \left(\frac{p + B}{p_0 + B} \right) \right]^{-1} \tag{8.4}$$

where C is a constant, ρ_0 is the density at $p = p_0$ as a function of temperature and B is a temperature-dependent parameter:

$$\rho_0 / \left(\mathrm{kg \cdot m^{-3}} \right) = \sum_{i=0}^{2} a_i \left(T / \mathrm{K} \right)^i \tag{8.5}$$

$$B / \mathrm{MPa} = \sum_{i=0}^{2} b_i \left(T / T_0 \right)^i \tag{8.6}$$

The parameters in equations (8.1) and (8.4) were obtained by a nonlinear optimization that minimized the sum of the squared relative residuals. The quality of the fit was assessed in terms of the absolute average relative deviation (Δ_{AAD}) and maximum absolute relative deviation (Δ_{MAD}) that were defined by

$$\Delta_{AAD} = \frac{1}{N} \sum_{i=1}^{N} \left| \frac{X_i - X_{i,\mathrm{fit}}}{X_i} \right| \tag{8.7}$$

$$\Delta_{MAD} = \mathrm{Max}_i \left| \frac{X_i - X_{\mathrm{i,fit}}}{X_i} \right| \tag{8.8}$$

Here, N is the total number of point, X_i is the experimental datum and $X_{\mathrm{i,fit}}$ is the value calculated from the correlation applied at the same state point. The parameters obtained, together with Δ_{AAD} and Δ_{MAD}, are given in Tables 8.3 and 8.4 for viscosity and density, respectively.

Figures 8.3 and 8.4 compare the experimental data with the correlations developed for each composition and show an absence of systematic deviations for either viscosity or density. These results suggest that both correlations fitted well the present experimental data, with an absolute average relative deviation of less than 0.7% for viscosity and 0.1% for density, for all investigated composition. Figures 8.5 and 8.6, which show the corresponding deviation plots from equations (8.1) and (8.4), further illustrate the effectiveness of the Tait-Andrade and Tait equations in correlating the results on individual isopleths. Figures 8.3 and 8.4 also shows that at each composition, both the viscosity and density data show an increasing trend when increasing pressure as expected.

Table 8.3 Fitting Parameters for Viscosity Correlation and Statistical Parameters

coefficient	x = 0.191	x = 0.377	x = 0.464	x = 0.616	x = 0.652
d_0	1.4110	1.1394	1.0966	1.1031	0.9896
d_1	1.057E-04	6.080E-05	3.860E-05	2.003E-05	1.490E-05
d_2	0.3427	-0.2444	-0.2640	-0.4219	-0.1750
e_0	-4.344E-03	-1.488E-03	-1.196E-03	6.854E-04	1.137E-03
e_1	401.20	182.96	165.15	125.39	144.08
e_2	-186.981	-77.523	-70.115	-52.392	-62.959
A_η	7.5370	5.7242	7.0537	4.7467	5.0971
B_η	1677.7	1770.3	1498.6	1584.7	1548.9
C_η	99.060	115.806	89.175	93.463	100.800
$10^2\,\Delta_{AAD}$	0.7	0.5	0.4	0.6	0.6
$10^2\,\Delta_{MAD}$	1.9	1.9	0.9	1.6	1.5

Table 8.4 Fitting Parameters for Density Correlation and Statistical Parameters

coefficient	x = 0.191	x = 0.377	x = 0.464	x = 0.616	x = 0.652
a_0	1.022E+03	1.108E+03	9.266E+02	9.901E+02	8.117E+02
a_1	-3.602E+01	-1.177E+02	2.497E+02	2.219E+02	5.620E+02
a_2	-9.257E+01	-8.144E+01	-2.576E+02	-2.821E+02	-4.443E+02
b_0	3.176E+02	4.266E+02	3.888E+02	4.433E+02	2.066E+02
b_1	-2.603E+02	-4.495E+02	-4.116E+02	-5.238E+02	-1.434E+02
b_2	4.932E+01	1.219E+02	1.086E+02	1.562E+02	3.841E-01
C	0.21	0.21	0.21	0.21	0.21
$10^2\,\Delta_{AAD}$	0.09	0.07	0.10	0.03	0.05
$10^2\,\Delta_{MAD}$	0.31	0.22	0.16	0.09	0.08

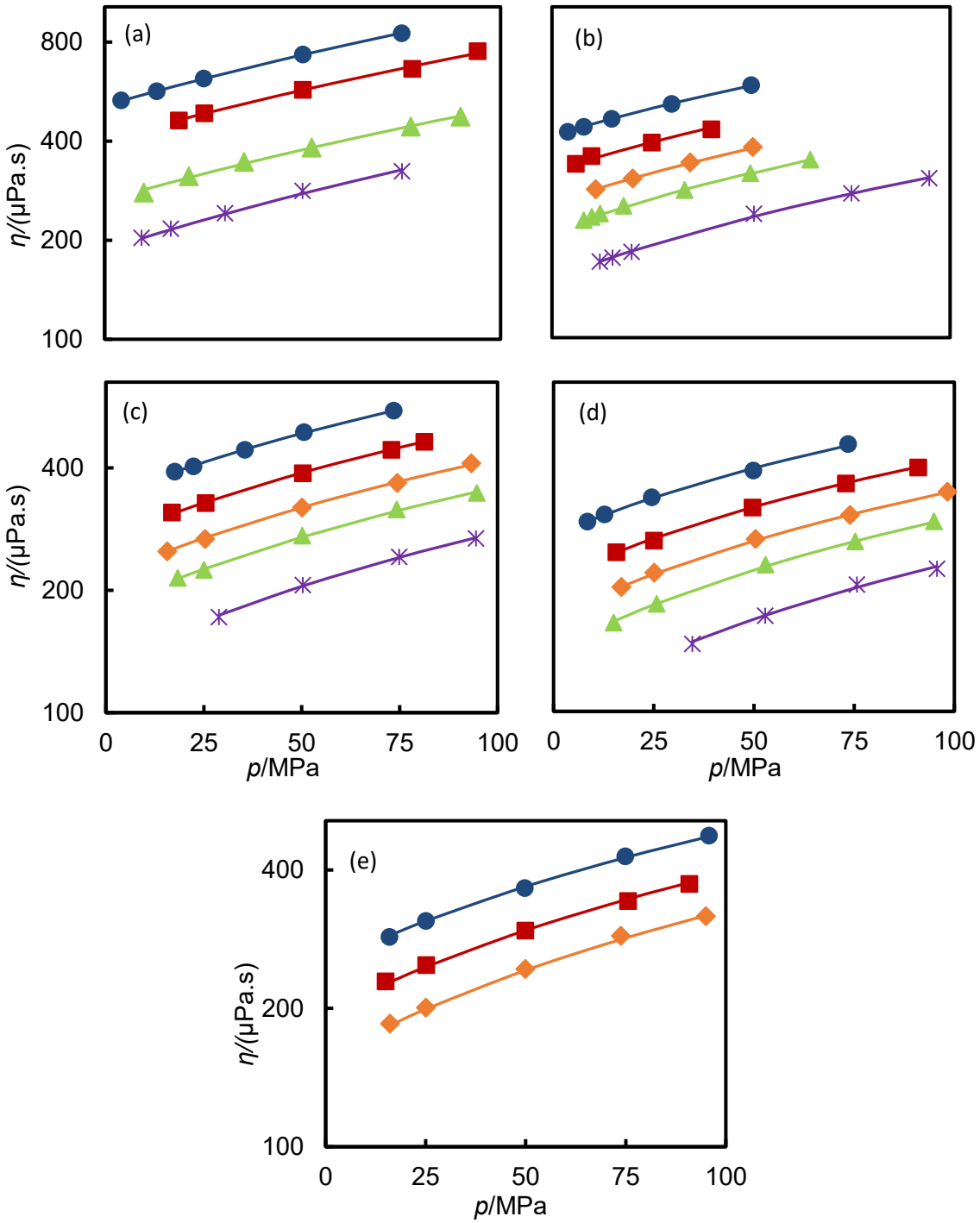

Figure 8.3 Experimental viscosity η as a function of pressure for (a) x = 0.191; (b) x = 0.377; (c) x = 0.464; (d) x = 0.616; and (e) x = 0.652, at various temperatures: ●, T = 298 K; ■, T = 323 K; ◆, T = 348 K; ▲, T = 373 K; ✳, T = 423 K. Solid lines represent equation 8.1.

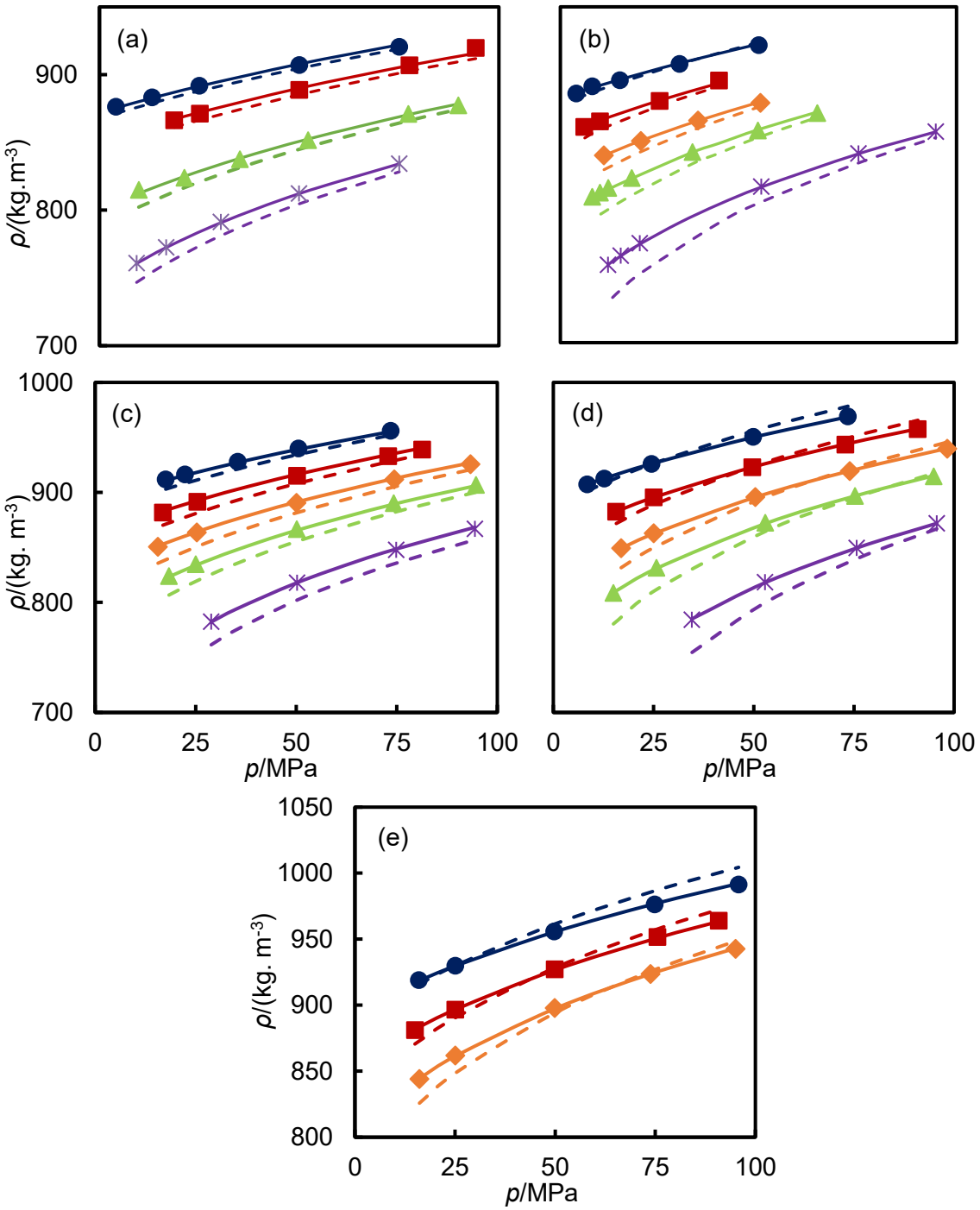

Figure 8.4 Experimental density ρ as a function of pressure for (a) x = 0.191; (b) x = 0.377; (c) x = 0.464; (d) x = 0.616; and (e) x = 0.652, at various temperatures: ●, T = 298 K; ■, T = 323 K; ◆, T = 348 K; ▲, T = 373 K; ✳, T = 423 K. Solid lines represent equation 8.4 and dashed lines represent data calculated from REFPROP.[398]

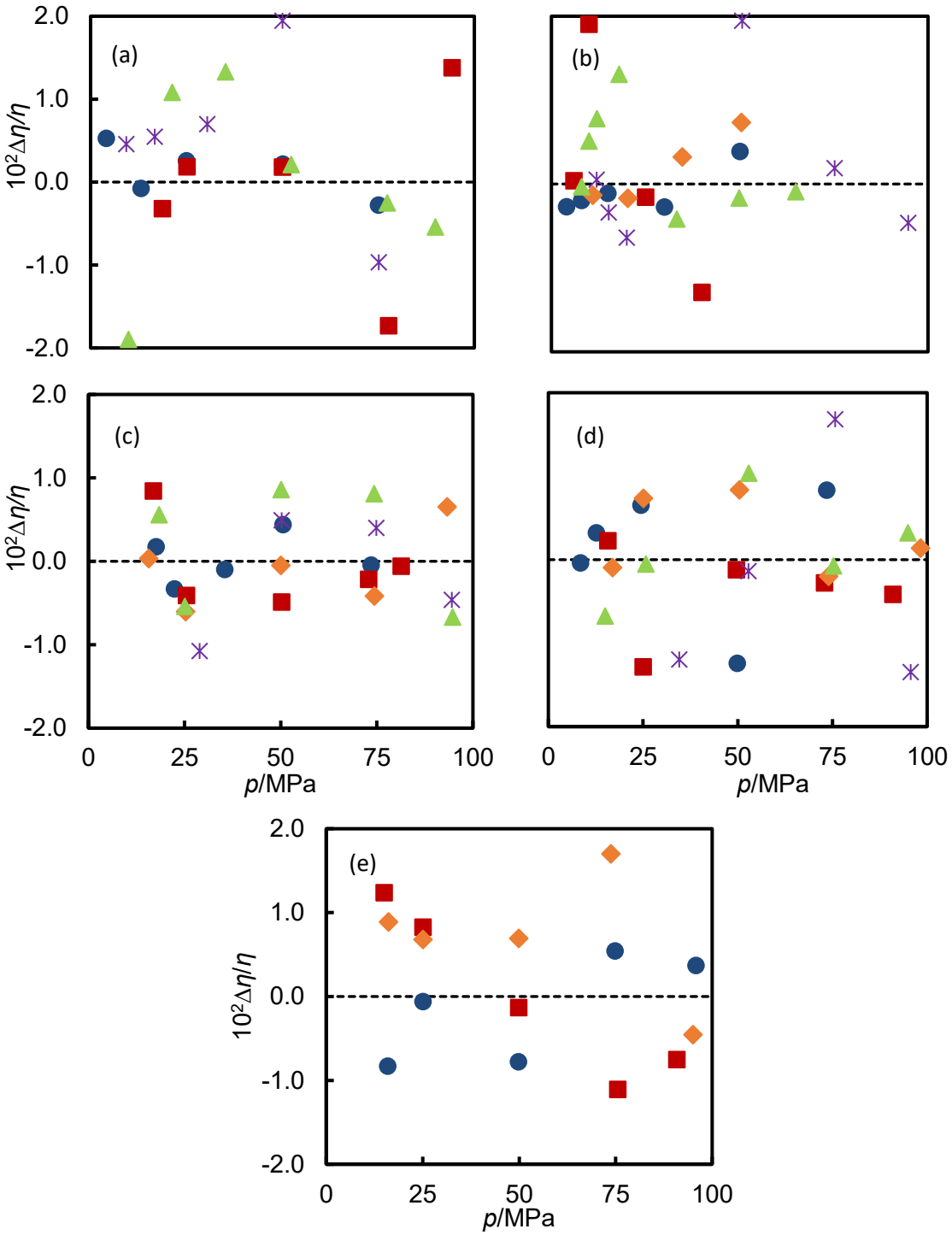

Figure 8.5 Relative deviations $\Delta\eta/\eta = (\eta - \eta_{fit})/\eta$ between experimental viscosities η and values η_{fit} calculated from equation (8.1) as a function of pressure: (a) x = 0.191; (b) x = 0.377; (c) x = 0.464; (d) x = 0.616; and (e) x = 0.652, at various temperatures: ●, T = 298 K; ■, T = 323 K; ◆, T = 348 K; ▲, T = 373 K; ✳, T = 423 K. Dashed lines represent the origin.

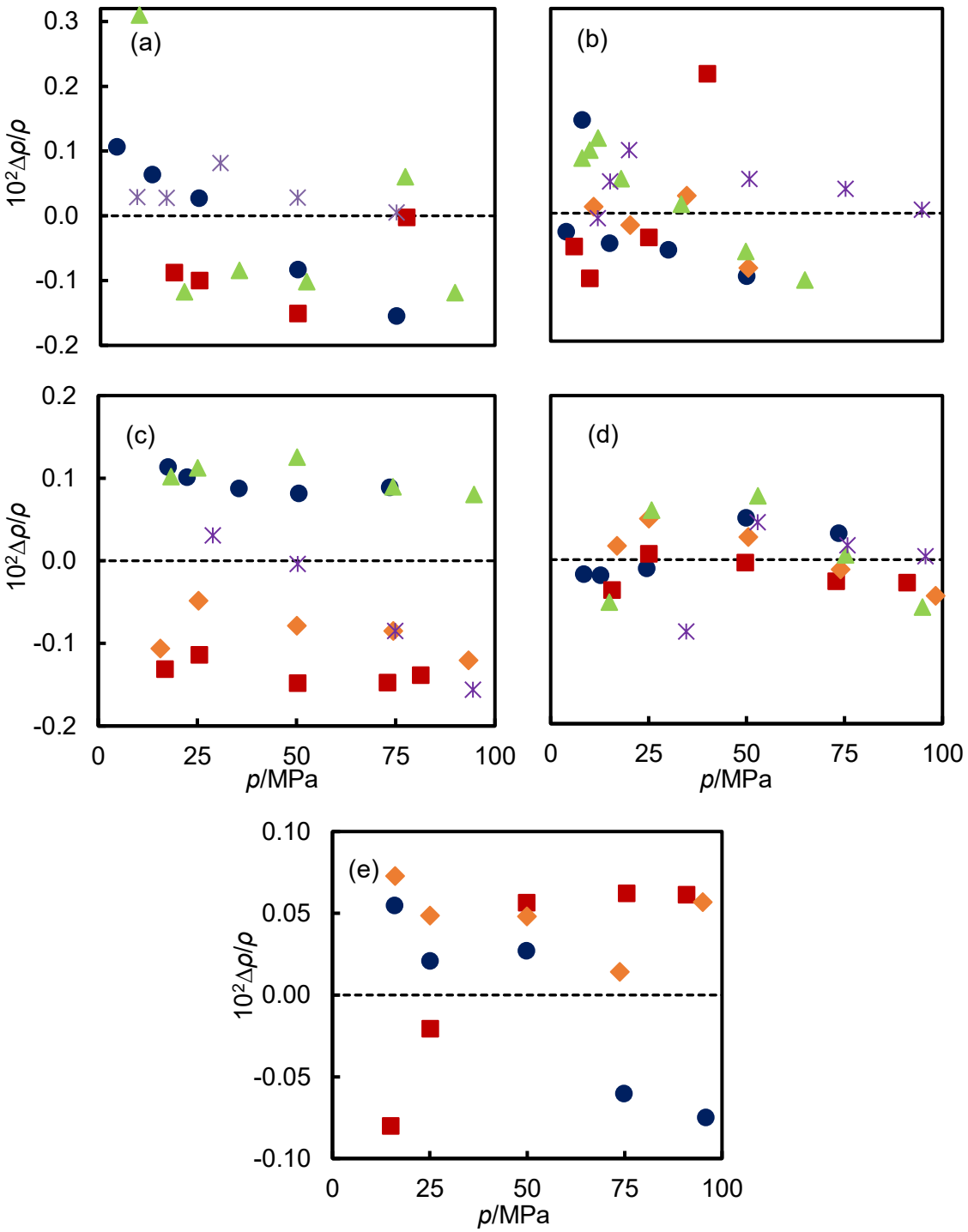

Figure 8.6 Relative deviations $\Delta\rho/\rho = (\rho - \rho_{fit})/\rho$ between experimental densities ρ and values ρ_{fit} calculated from equation (8.4) as a function of pressure: (a) x = 0.191; (b) x = 0.377; (c) x = 0.464; (d) x = 0.616; and (e) x = 0.652, at various temperatures: ●, T = 298 K; ■, T = 323 K; ◆, T = 348 K; ▲, T = 373 K; ✳, T = 423 K. Dashed lines represent the origin.

8.3 Surface Fits

The experimental viscosity and density were also used to developed surface fits in which all parameters in the Tait-Andrade and Tait equations (except *C* from equation 8.4) are expressed as linear functions of mole fraction. This resulted in following equations

$$\left.\begin{aligned} A_\eta &= A_{\eta,0} + A_{\eta,1}x \\ B_\eta &= B_{\eta,0} + B_{\eta,1}x \\ C_\eta &= C_{\eta,0} + C_{\eta,1}x \end{aligned}\right\} \tag{8.9}$$

$$D = \sum_{i=0}^{2}\left(d_{i,0} + d_{i,1}x\right)\left(T/T_0\right)^{-i} \tag{8.10}$$

$$E/\mathrm{MPa} = \sum_{i=0}^{2}\left(e_{i,0} + e_{i,1}x\right)\left(T/T_0\right)^{i} \tag{8.11}$$

$$\rho_0/\left(\mathrm{kg\cdot m^{-3}}\right) = \sum_{i=0}^{2}\left(a_{i,0} + a_{i,1}x\right)\left(T/\mathrm{K}\right)^{i} \tag{8.12}$$

$$B/\mathrm{MPa} = \sum_{i=0}^{2}\left(b_{i,0} + b_{i,1}x\right)\left(T/T_0\right)^{i} \tag{8.13}$$

A total of 18 parameters were deduced for viscosity and 13 parameters for density which were regressed against the experimental data. The parameters obtained are given in Tables 8.5 and 8.6. For viscosity, we have Δ_{AAD} = 1.9 % and Δ_{MAD} = 6.0 % while, for density, Δ_{AAD} = 0.3 % and Δ_{MAD} = 2.1 %. Figure 8.7 illustrates the quality of the fit at a representative temperature of *T* = 323.15 K. Here, the experimental data, interpolated to round values of pressure, are plotted together with isobars calculated from the surface fit equations. Generally good agreement can be observed, although the density data at *x* = 0.464 deviate by an average of 0.7%, which is substantially greater than their uncertainty. Figure 8.7 (a) also illustrates the quite rapid reduction in viscosity observed upon dissolution of CO_2 under conditions of constant temperature and pressure. A reduction of approximately 50% is observed between the viscosity of pure *m*-xylene[399] and that of the mixture with *x* = 0.6. The magnitude of the reduction can be compared with other CO_2-hydrocarbon systems. For example, Ciotta et al.[16] studied the system CO_2 + 2,6,10,15,19,23-hexamethyltetracosane (squalane). Their data also show an approximately linear dependence of viscosity on CO_2 mole fraction at constant temperature and pressure but with a somewhat greater slope. In particular, at *T* = 348.15 K and *p* = 50 MPa, the viscosity reduces by about 70% between *x* = 0 and *x* = 0.6. Hu et al.,[383-384] measured viscosities of CO_2-saturated toluene-crude oil mixtures at *T* = 298.15 K and

pressures up to 22 MPa. They observed that the viscosity of the diluted crude oils reduced exponentially with increasing pressure in the liquid-vapour coexistence region. Even though no composition data were provided, their results indicate a much stronger decrease in viscosity than we observed in the present relatively-low-viscosity system.

Table 8.5 Fitting Parameters for Viscosity Surface Fit

coefficient	parameter	coefficient	parameter
$d_{0,0}$	1.2679	$e_{2,0}$	758.10
$d_{0,1}$	3.7697	$e_{2,1}$	-1141.00
$d_{1,0}$	-6.3558	$A_{\eta,0}$	7.5163
$d_{1,1}$	0.0000	$A_{\eta,1}$	-7.5025
$d_{2,0}$	9.4307	$B_{\eta,0}$	1724.10
$d_{2,1}$	-9.7033	$B_{\eta,1}$	630.17
$e_{0,0}$	2582.4	$C_{\eta,0}$	96.331
$e_{0,1}$	-3992.2	$C_{\eta,1}$	121.040
$e_{1,0}$	-2766.3		
$e_{1,1}$	4297.0		

Table 8.6 Fitting Parameters for Density Surface Fit

coefficient	parameter	coefficient	parameter
$a_{0,0}$	1036.39	$b_{0,0}$	436.504
$a_{0,1}$	613.078	$b_{0,1}$	-199.885
$a_{1,0}$	-93.280	$b_{1,0}$	-432.317
$a_{1,1}$	-739.762	$b_{1,1}$	134.239
$a_{2,0}$	-62.640	$b_{2,0}$	111.517
$a_{2,1}$	212.658	$b_{2,1}$	-13.408
		C	0.2100

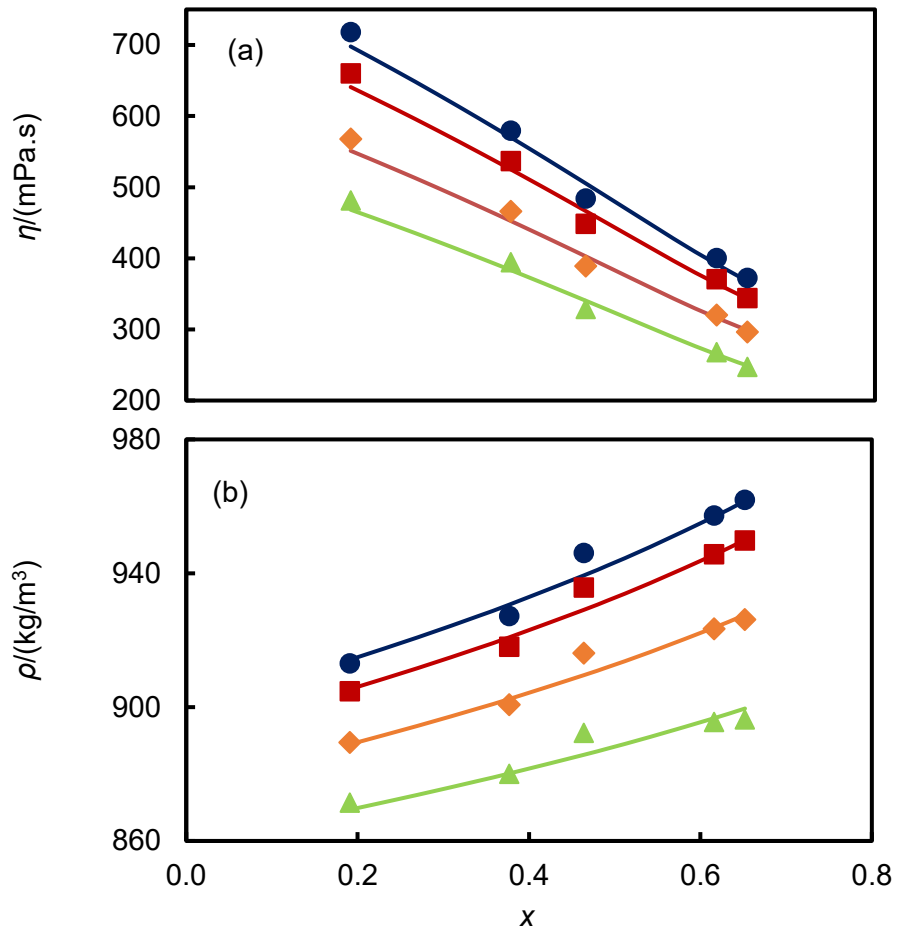

Figure 8.7 (a) viscosity η and (b) density ρ at T = 323.15 K as a function of composition for various pressures: ▲, p = 25 MPa; ◆, p = 50 MPa; ■, p = 75 MPa; ●, p = 90 MPa. Solid lines represent values from the surface fit equations: Equations (8.1), (8.9), (8.10) and (8.11) for viscosity and Equations (8.4), (8.12) and (8.13) for density.

All correlations discussed in this chapter provide a convenient means of interpolation; however, extrapolation is not recommended. Taken together, the viscosity data obtained in this work will be especially useful in testing and parameterising models. The density data show that the model in the current version of REFPROP is somewhat inaccurate. Therefore, the present data were used to optimise the binary interaction parameters between *m*-xylene and CO_2. Discussion on the optimisation of the binary interaction parameters for this mixture is discuss in chapter 10. The general trend seen in the present work and in other CO_2-hydrocarbon systems[16, 383] is that dissolution of CO_2 in the liquid hydrocarbon brings about a rapid reduction in viscosity. The next chapter, therefore, moves on to discuss the viscosity of CO_2 mixtures with hydrocarbon of higher initial viscosity than *m*-xylene.

CHAPTER 9 VISCOSITY OF DIISODECYL-PHTHALATE WITH DISSOLVED CO_2

This chapter provides a comprehensive data set of viscosity and density of diisodecyl-phthalate (DIDP) and carbon dioxide mixtures.[2] The measurements were carried out using the combined vibrating-wire vibrating-tube (VW-VT). The measurement temperatures were at (313.15, 343.15 and 373.15) K at pressures ≤ 80 MPa but always above the bubble pressure. The results for viscosity and density were correlated using the Tait-Andrade and Tait equations, respectively. The results presented in this chapter provide important insights into the reduction of the viscosity of highly viscous hydrocarbons upon dissolution of CO_2.

9.1 Experimental Results and discussion

The measurements of pure DIDP were carried out prior to starting the measurements on the mixtures. The results presented in Table 9.1, are compared with the values calculated from the viscosity correlation and the equation of state (EoS) of Peleties[259, 390] who reported an uncertainty not worse than 2% and 0.025% in viscosity and density, respectively. The experimental viscosity and density of pure DIDP measured in this work were found to deviate within the combined uncertainties of the experimental data and the correlations from Peleties[259, 390] with ± 2 % and ± 0.2 % for viscosity and density, respectively. The results are plotted in Figure 9.1 and 9.2.

Table 9.1 Experimental Viscosity η and Density ρ of pure DIDP

p/MPa	η/mPa·s)	ρ/(kg·m^{-3})	p/MPa	η/(mPa·s)	ρ/(kg·m^{-3})
	T =313.1 K			T = 372.53 K	
0.138	37.444	952.35	0.218	5.031	910.82
10.429	46.463	959.58	0.255	5.113	906.75
	T = 342.70 K		9.934	5.942	918.88
0.172	11.444	929.32	20.078	6.842	920.89
9.868	13.493	938.37	39.689	9.118	939.53
39.602	22.178	956.81	79.500	15.001	960.97

The mixtures of (DIDP + CO_2) were prepared *in-situ* at mole fractions of CO_2 (x_{CO_2}) of 0.207, 0.411, 0.610 and 0.810. The results are given in Appendix 9A to 9D. As expected, the viscosity and density of the mixtures were found to increase with increasing pressure and decrease with increasing temperature. In line with expectations, it was also found that the viscosity increased with increasing density when the temperature and mole fraction of CO_2 were kept constant, as illustrates in Figure 9.3. Meanwhile, Figure 9.4 presents the viscosity and density

[2] Some of the experimental measurements described in this chapter were carried out in collaboration with an undergraduate student.

412. Fesard, A. *Viscosity and Density of liquid Diisodecyl-phthalate with dissolved CO2 at Temperatures between 313 and 373K and Pressures up to 800 bar*; Report, Imperial College London: London, UK, 2018.

as a function of CO_2 mole fraction. The viscosity was found to be decreasing rapidly with increasing mole fraction of CO_2. The maximum difference between the viscosity of pure DIDP and the viscosity of the mixtures was found to be at the lowest temperature and highest pressures of each mixture. For density, we can see a gradual increase when the mole fraction of CO_2 is increasing, and this continues through to $X_{CO2} = 1$ for higher pressures. However, for lower pressures, rapid changes were seen for pure CO_2 because the density of pure CO_2 is lower as it is a supercritical fluid with gas-like behaviour at low pressures. The viscosity and density of pure CO_2 was calculated from the viscosity correlation[413] and equation of state.[403]

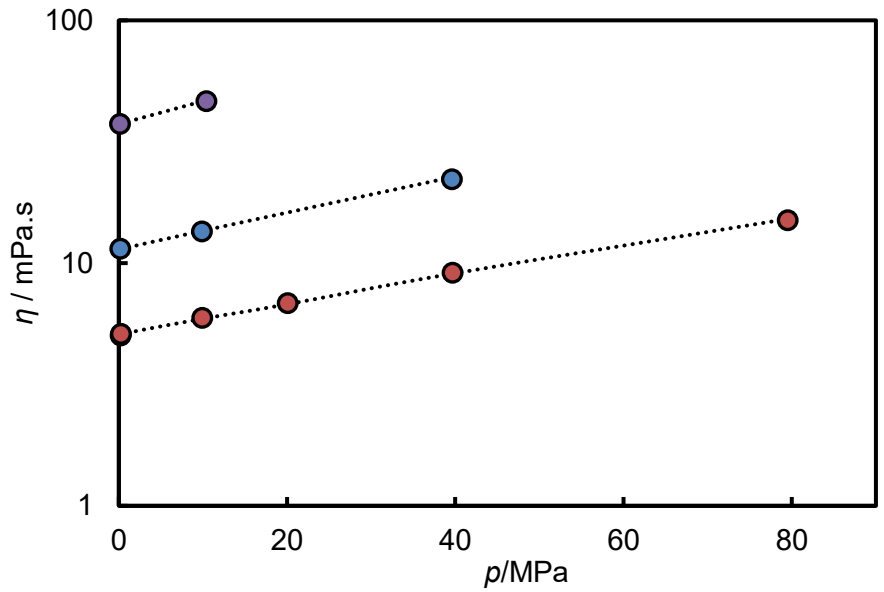

Figure 9.1 Experimental viscosity η as a function of pressure p for pure DIDP: ●, T = 313 K; ●, T = 343 K; ●, T = 373 K. Dotted lines represent values calculated from the work by Peleties[259]

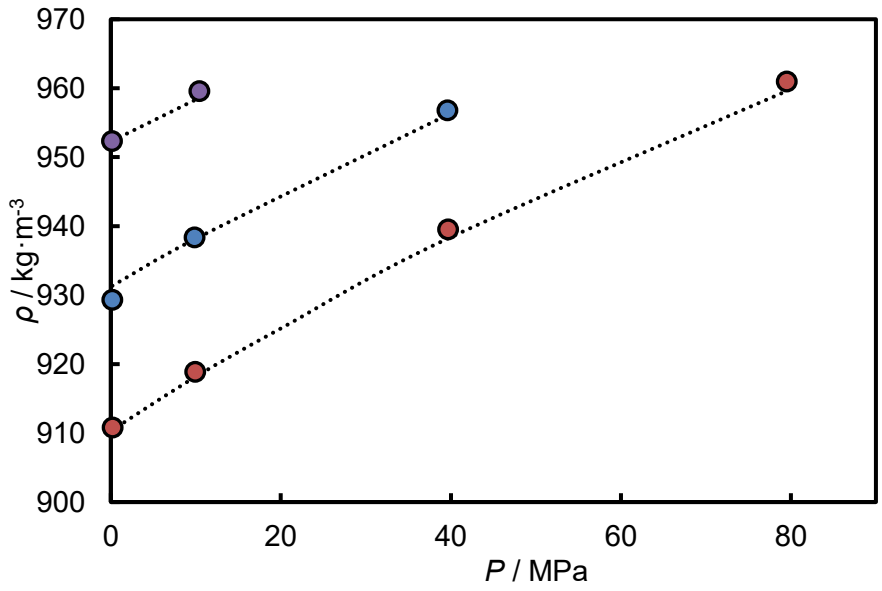

Figure 9.2 Experimental density ρ as a function of pressure P for pure DIDP: ●, T = 313 K; ●, T = 343 K; ●, T = 373 K. Dotted lines represent values calculated from the work by Peleties[390]

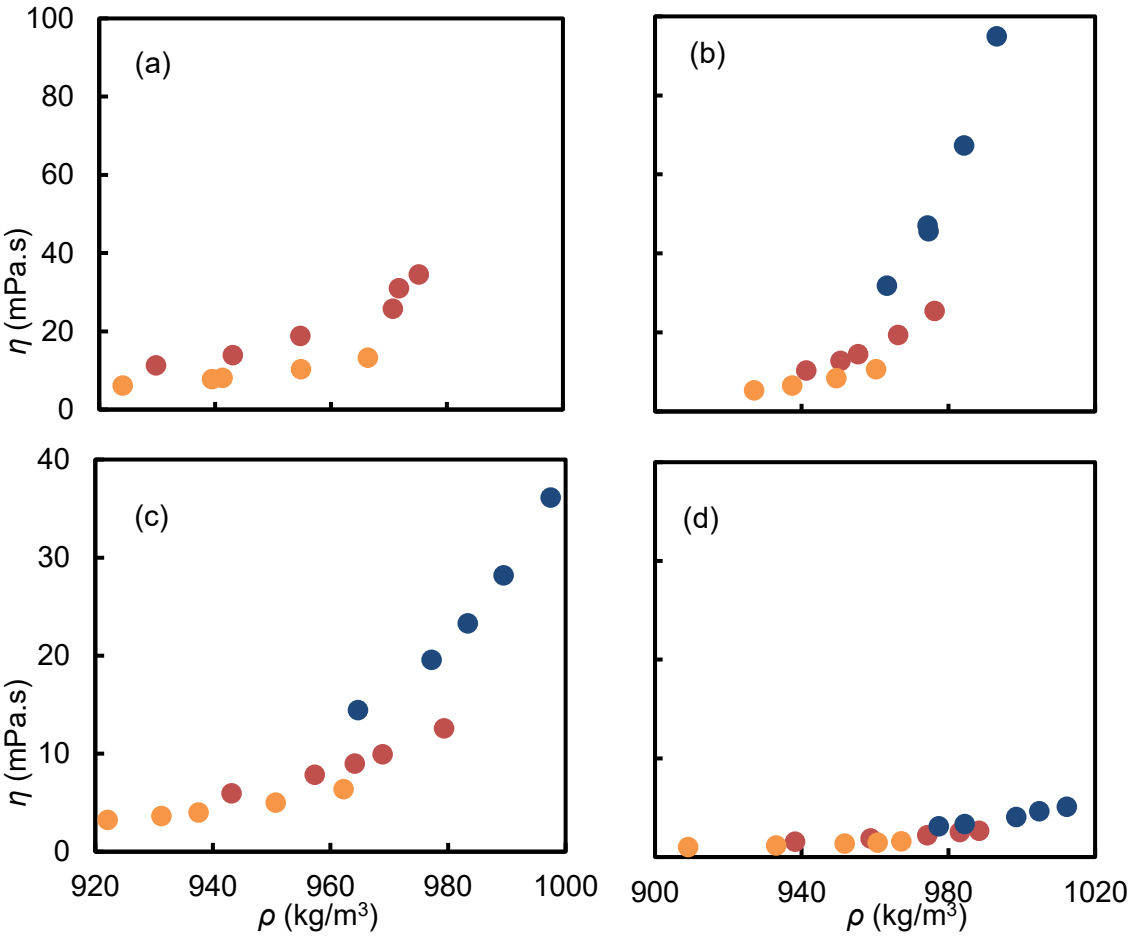

Figure 9.3 Experimental viscosity η as a function of density ρ for (a) x = 0.207; (b) x = 0.411; (c) x = 0.610 and (d) x = 0.810, at various temperatures: ●, T = 313 K; ●, T = 343 K; ●, T = 373 K.

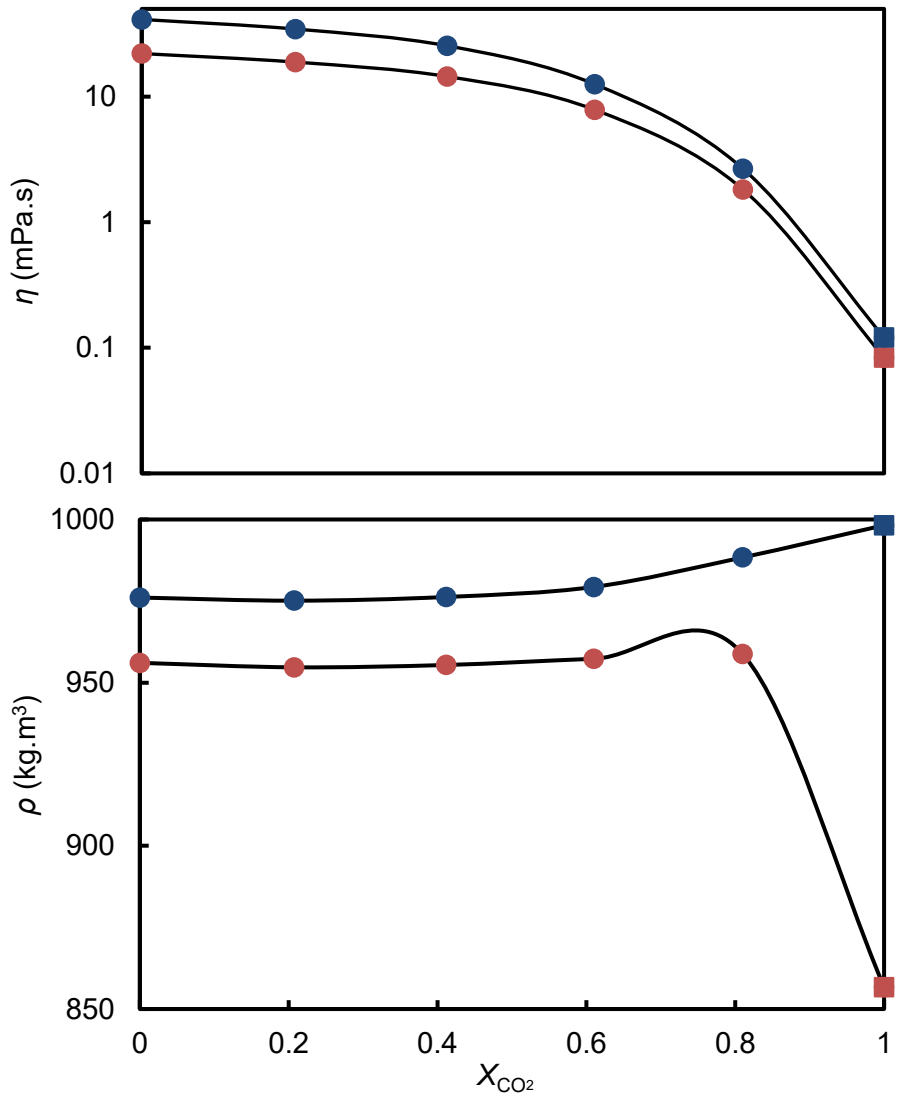

Figure 9.4 Experimental viscosity η and density ρ as a function of CO_2 compositions at nominal temperature T = 343K: ●, P = 80 MPa and ●, P = 40 MPa. The viscosity and density of pure CO_2 was calculated from the viscosity correlation[413] and equation of state.[403]

9.2 Correlations

The Tait-Andrade[410] equation was used to correlate the viscosity, whereas for density, the Tait[411] equation was employed to provide useful correlations of the experimental results for all mixtures involved. The correlations were applied to the individual compositions by expressing viscosity and density as a function of temperature and pressure as equation 8.1 and 8.4 in chapter 8. The parameters in equations (8.1) and (8.4) were determined by a nonlinear optimization that minimized the sum of the squared relative residuals. The quality of the fit was assessed in terms of the absolute average relative deviation (Δ_{AAD}) and maximum absolute relative deviation (Δ_{MAD}) that were already been defined in equation (8.7) and (8.8) in chapter 8. The parameters obtained, together with Δ_{AAD} and Δ_{MAD}, are given in Tables 9.2 and 9.3 for viscosity and density, respectively.

Figures 9.5 and 9.6 compare the experimental data with the correlations developed for each mixture while Figure 9.7 and 9.8 shows the corresponding deviation plots deduced from equation 9.7. As seen in both figures, the results proved that both correlations fitted well the present experimental data, with an absolute average relative deviation of less than 1.0% for viscosity and 0.1% for density, and maximum absolute relative deviation of 2.2% and 0.2% for viscosity and density, respectively.

Table 9.2 Fitting Parameters for Viscosity Correlation and Statistical Parameters

coefficient	X_{CO2} = 0.201	X_{CO2} = 0.411	X_{CO2} = 0.610	X_{CO2} = 0.810
d_0	1.4523	0.8456	5.4264	7.5441
d_1	12.5802	35.3655	86.8161	45.6643
d_2	0.0202	0.0206	0.0243	0.0242
e_0	7.4074	0.0050	0.0200	0.0200
e_1	704.84	1341.62	2988.41	3860.83
e_2	-116.52	143.12	1361.91	3.66
A_η	4.63E-03	1.20E-01	1.68E-01	2.80E-02
B_η	1952.14	615.44	490.90	946.54
C_η	-88.97	-195.63	-194.46	-96.17
Δ_{AAD}	0.7	0.7	0.8	0.9
Δ_{MAD}	1.9	2.2	1.6	2.2

Table 9.3 Fitting Parameters for Density Correlation and Statistical Parameters

coefficient	X_{CO2} = 0.207	X_{CO2} = 0.411	X_{CO2} = 0.610	X_{CO2} = 0.810
a_0	1.301E+03	1.229E+03	1.162E+03	1.234E+03
a_1	-3.981E+02	-2.745E+02	-1.528E+02	-2.113E+02
a_2	7.906E+01	2.846E+01	-2.698E+01	-3.427E+01
b_0	1.314E+04	5.381E+02	4.990E+02	2.004E+02
b_1	-1.975E+04	-5.127E+02	-4.736E+02	-1.038E+02
b_2	7.454E+03	1.357E+02	1.215E+02	-7.350E+00
C	0.20	0.20	0.20	0.20
Δ_{AAD}	0.08	0.02	0.04	0.05
Δ_{MAD}	0.22	0.06	0.07	0.21

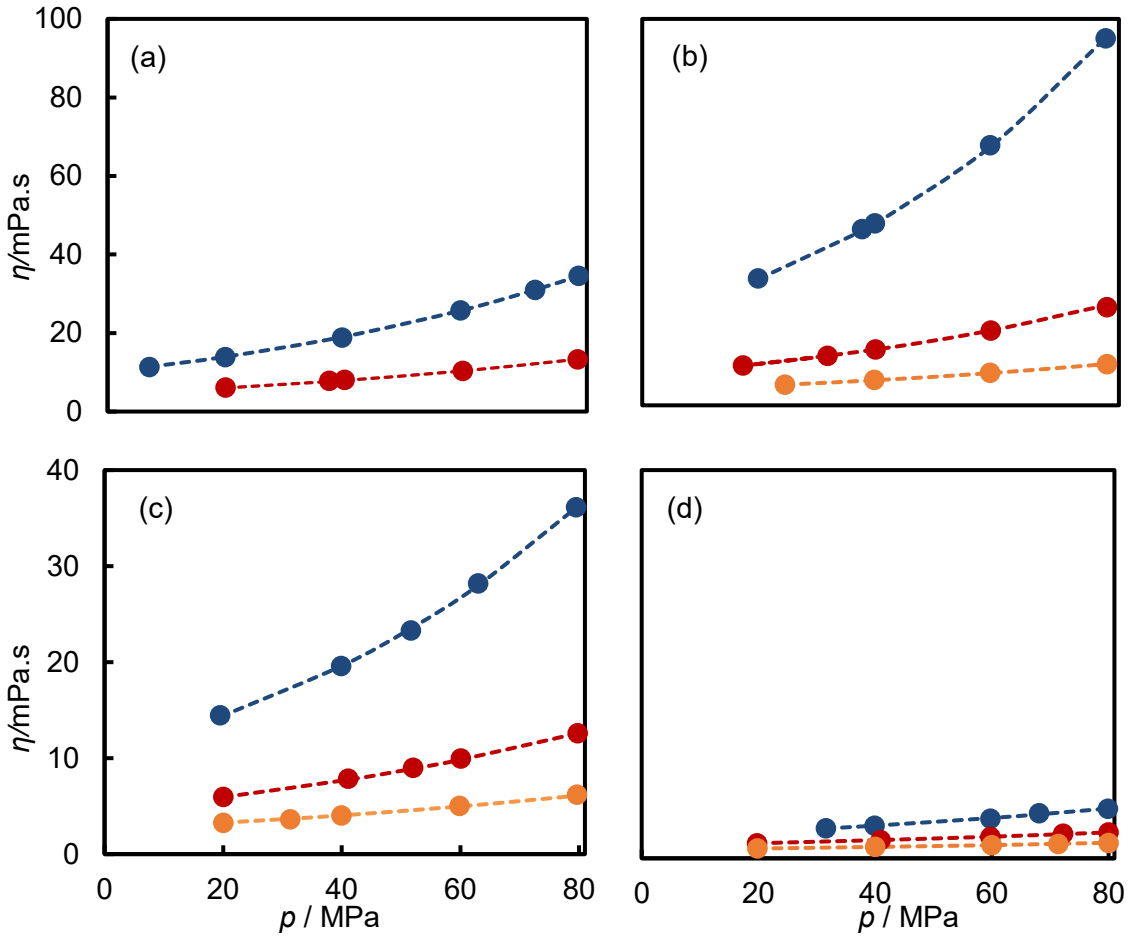

Figure 9.5 Experimental viscosity η as a function of pressure for (a) x = 0.207; (b) x = 0.411; (c) x = 0.610 and (d) x = 0.810, at various temperatures: ●, T = 313 K; ●, T = 343 K; ●, T = 373 K. Solid lines represent equation 8.1.

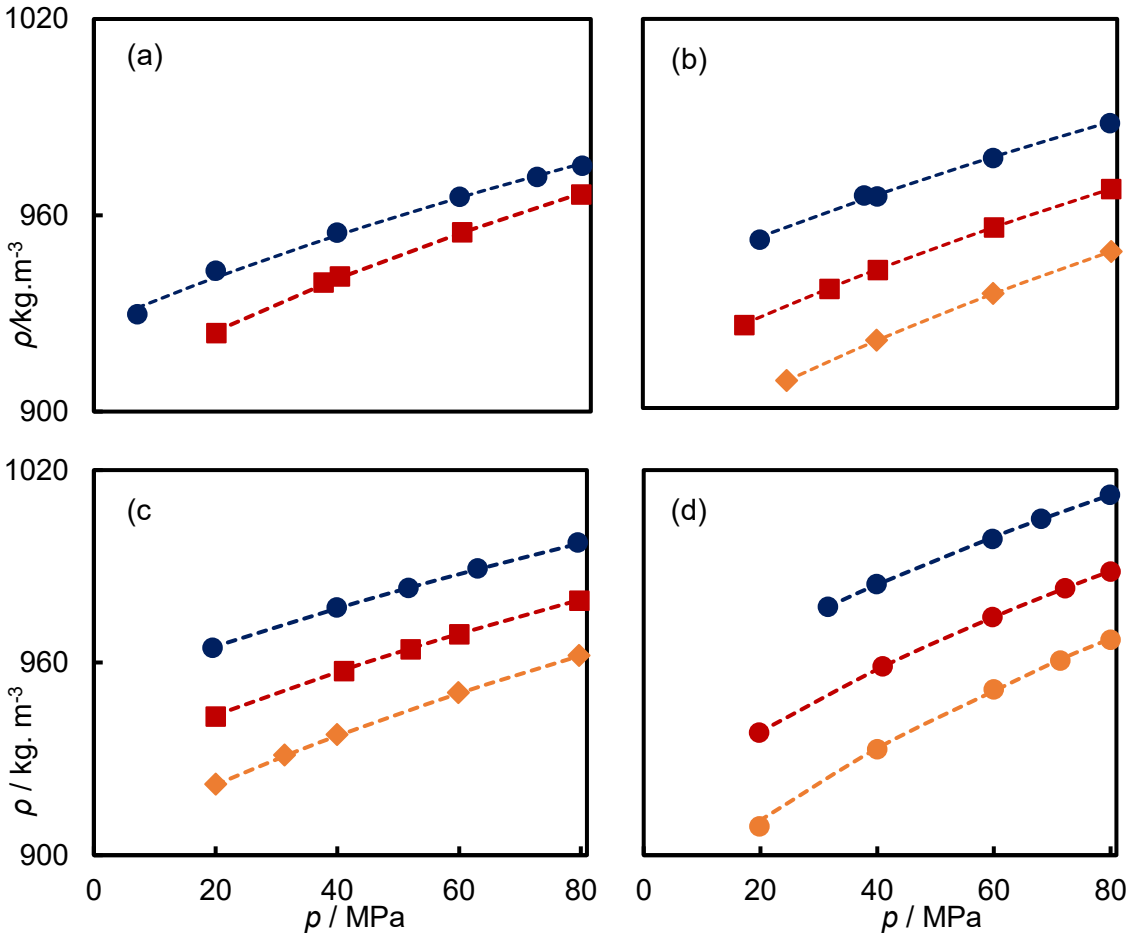

Figure 9.6 Experimental density ρ as a function of pressure for (a) x = 0.207; (b) x = 0.411; (c) x = 0.610; and (d) x = 0.810, at various temperatures: ●, T = 313 K; ●, T = 343 K; ●, T = 373 K. Solid lines represent equation 8.4.

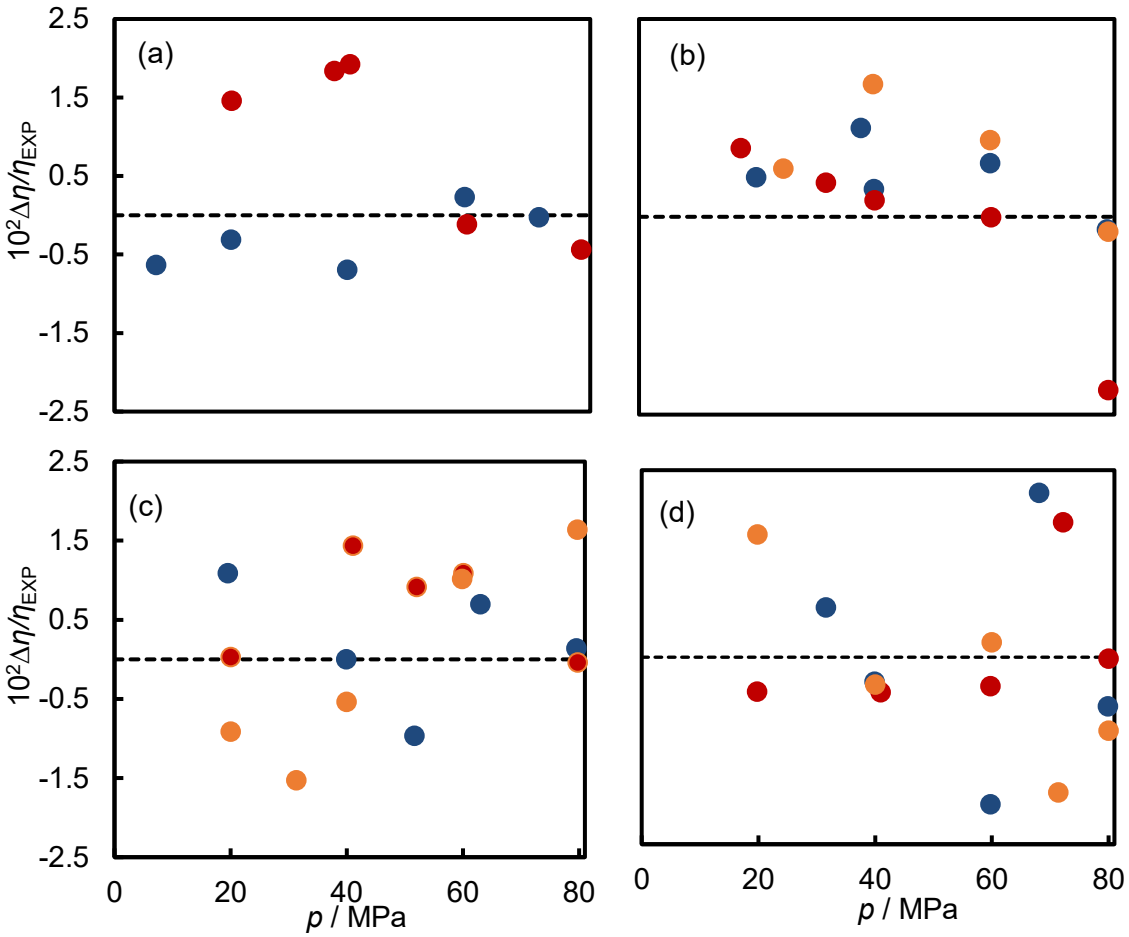

Figure 9.7 Relative deviations $\Delta\eta/\eta = (\eta - \eta_{fit})/\eta$ between experimental viscosities η and values η_{fit} calculated from equation (8.1) as a function of pressure: ●, T = 313 K; ●, T = 343 K; ●, T = 373 K.

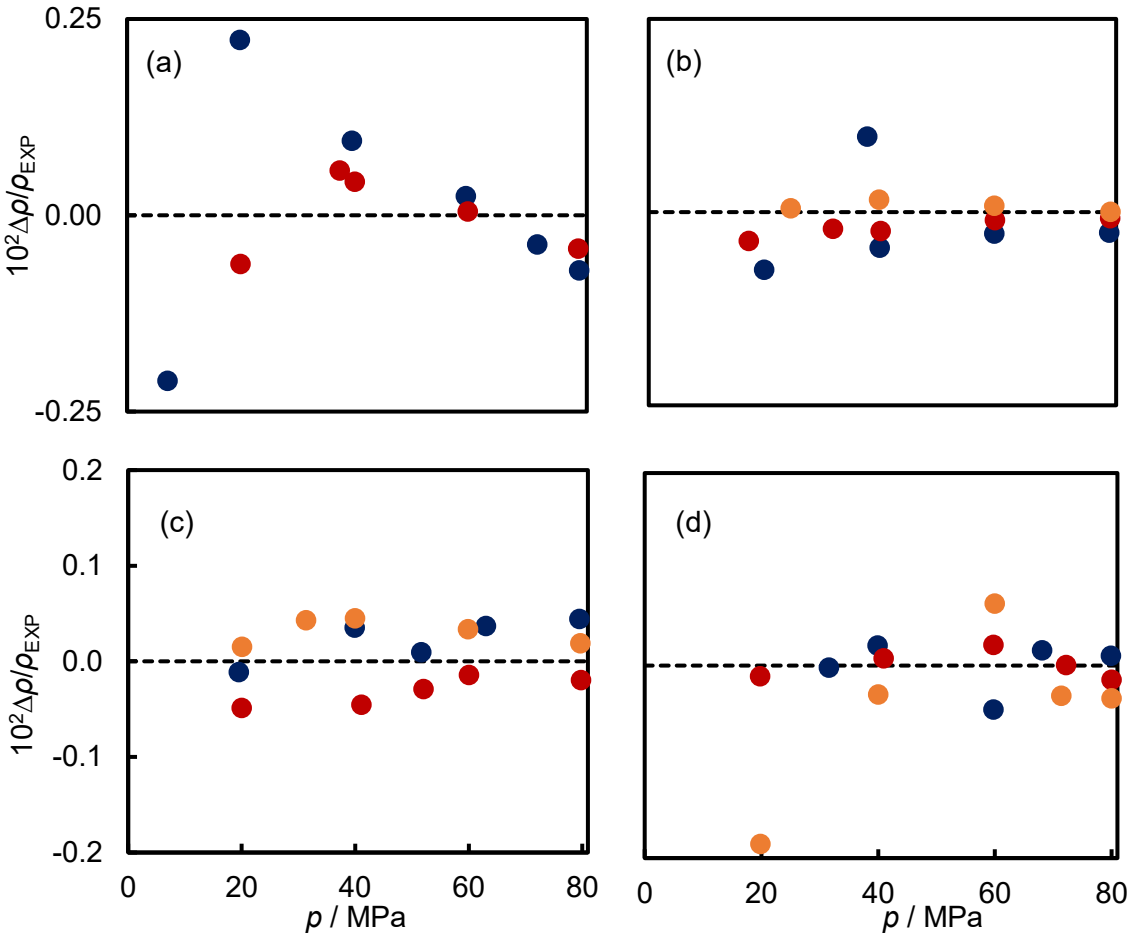

Figure 9.8 Relative deviations $\Delta\rho/\rho = (\rho - \rho_{fit})/\rho$ between experimental densities ρ and values ρ_{fit} calculated from equation (8.4) as a function of pressure: ●, T = 313 K; ●, T = 343 K; ●, T = 373 K

These findings provide an important insight into the behaviour of the highly viscous hydrocarbon when added with CO_2. The pure DIDP is approximately 50 times more viscous than the lighter hydrocarbon like as *m*-xylene. When added with CO_2, both systems show a rapid reduction in viscosity. However, it was found that the reduction in the viscosity of DIDP + CO_2 system were more significant than the viscosity reduction in *m*-xylene + CO_2 system. This is not surprising as the viscosity of pure DIDP is 300 times higher than the viscosity of pure CO_2. The present study raises the possibility of predicting the viscosity of the mixtures of (DIDP + CO_2) using the residual entropy model. However, the thermodynamics of this system is not sufficiently well developed. Future studies on the thermodynamics of this mixtures are therefore recommended. The residual entropy model will be discuss in the coming chapters.

PART 3 RESIDUAL ENTROPY MODEL

CHAPTER 10 RESEARCH BACKGROUND

In this chapter, a residual entropy model is discussed.[3] This include the concept and theory of the model in section 10.1 and the definition of reduced viscosity and reduced residual entropy that was used in this work in section 10.2 and 10.3, respectively. Following this section, the application of the model to different transport properties is presented in section 10.4.

10.1 Concept and Theory

The residual entropy model was originally introduced in the work by Rosenfeld[323] in 1977. Generally, the model stated that the temperature and density dependence of the reduced transport properties approximately exhibit a linear function of the residual entropy when scaled with appropriate reference value. In 1999, Rosenfeld extended the work by proposing the model to dilute gases regime. [414] The residual entropy was defined for specified temperature T and molar density ρ such that

$$S^{\mathrm{r}}\left(T,\rho\right)=S\left(T,\rho\right)-S^{\mathrm{id}}(T,\rho) \tag{10.1}$$

where $S\,(T,\rho)$ is the molar entropy and $S^{\mathrm{id}}(T,\rho)$ is the molar entropy of the hypothetical ideal gas at the same temperature and molar density. This approach is a hypothesis and is not based on an exact theory; therefore, it cannot be derived from first principles. S^{r} behaves like full entropy S where the values increase with the increase in temperature, but the values are always negative. The residual entropy approaches zero when the temperature tends to infinity at fixed density due to the system approaching ideal-gas behaviour. In the Rosenfeld residual entropy model, reduced units are used. For example, number density defines the length unit l_0, the temperature defines the energy unit e_0, and the number density and thermal velocity define the time unit t_0. These units can be defined as [323, 415-416]

$$l_0=n^{-1/3},\ e_0=k_BT,\ t_0=n^{-1/3}\sqrt{m/k_BT} \tag{10.2}$$

[3] The content of this part is based on the published paper.

272. Taib, M. B. M.; Trusler, J. P. M., Residual entropy model for predicting the viscosities of dense fluid mixtures. *The Journal of Chemical Physics* **2020,** *152* (16), 164104.

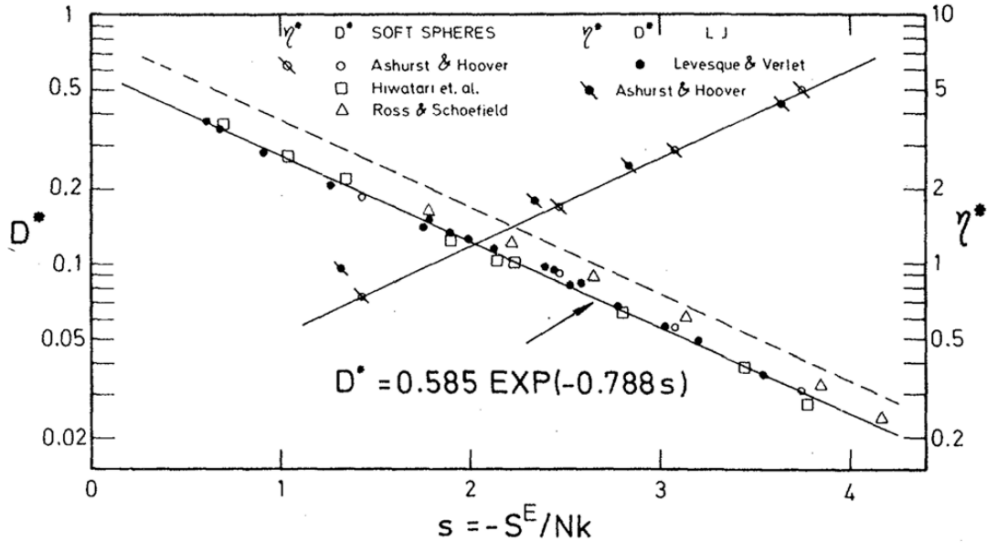

Figure 10.1 Simulation data for the reduced diffusion coefficient and the reduced viscosity as a function of residual entropy. Data are shown for the standard Lennard-Jones (LJ) liquid and the purely repulsive "soft-sphere" inverse-power-law pair potential $v(r) \propto r^{-12}$. Figure reproduced from Rosenfeld's findings. [323]

Figure 10.1 is reproduced from the work by Rosenfeld's where the *x*-axis represents the negative of residual entropy per particle and the y-axis represent the reduced viscosity η^* and reduced diffusion coefficient D^*. Rosenfeld discovered that the two properties are approximately exponential functions of the excess entropy. This relation has led to the development of the residual entropy model as we shall see in the coming sections.

10.2 Reduced Viscosity

According to the original model proposed by Rosenfeld,[323] the dimensionless viscosity η^* was defined in terms of the thermal velocity $(k_BT/m)^{1/2}$ and the number density n as follows:

$$\eta^* = \frac{\eta n^{-2/3}}{\left(mk_BT\right)^{1/2}}, \tag{10.3}$$

where m is the mass of one molecule and k_B is Boltzmann's constant. The choice of reducing function is justified by noting that dimension of viscosity in terms of mass m, length L and time t are $m{\cdot}L^{-1}{\cdot}t^{-1}$, which match those of $n^{2/3}(mk_BT)^{1/2}$. This definition of reduced viscosity is illustrated in Fig. 10.2 (a), where we plot data for pentane in the following ranges of temperature T and pressure p: $200 \le T/\mathrm{K} \le 550$ K and $0.1 \le p/\mathrm{MPa} \le 50$. These data were taken from a correlation[417] of experimental data that has an estimated expanded relative uncertainty ($k = 2$) of 4 %. It can be seen that $\log(\eta^*)$ is a very-nearly linear function of residual molar entropy in the dense-fluid region. However, in the low-density region ($-S^r/R \le 1.0$), $\log(\eta^*)$ is divergent. To counter this issue, Novak[281, 339, 418-419] proposed an alternative definition of reduced viscosity,

$$\eta^* = \eta/\eta_0 \,, \tag{10.4}$$

in which η_0 is the zero-density viscosity of the fluid. For pure substances, Novak obtained η_0 from the Chapman-Enskog formula:

$$\eta_0 = \frac{5\sqrt{mk_BT/\pi}}{16\sigma^2\Omega^{*(2,2)}}, \tag{10.5}$$

where σ is the characteristic molecular diameter and $\Omega^{*(2,2)}$ is a dimensionless collision integral, typically estimated from the Lennard-Jones potential.[292-293] Fig. 10.2 (b) illustrates this definition of reduced viscosity, again for the case of pentane, and shows that the $\log(\eta^*)$ goes smoothly to zero as $S^r/R \rightarrow 0$. In his work,[281] Novak showed that a small amount of data was sufficient to obtain a correlation that could then be applied to determine the viscosity in the entire fluid region.

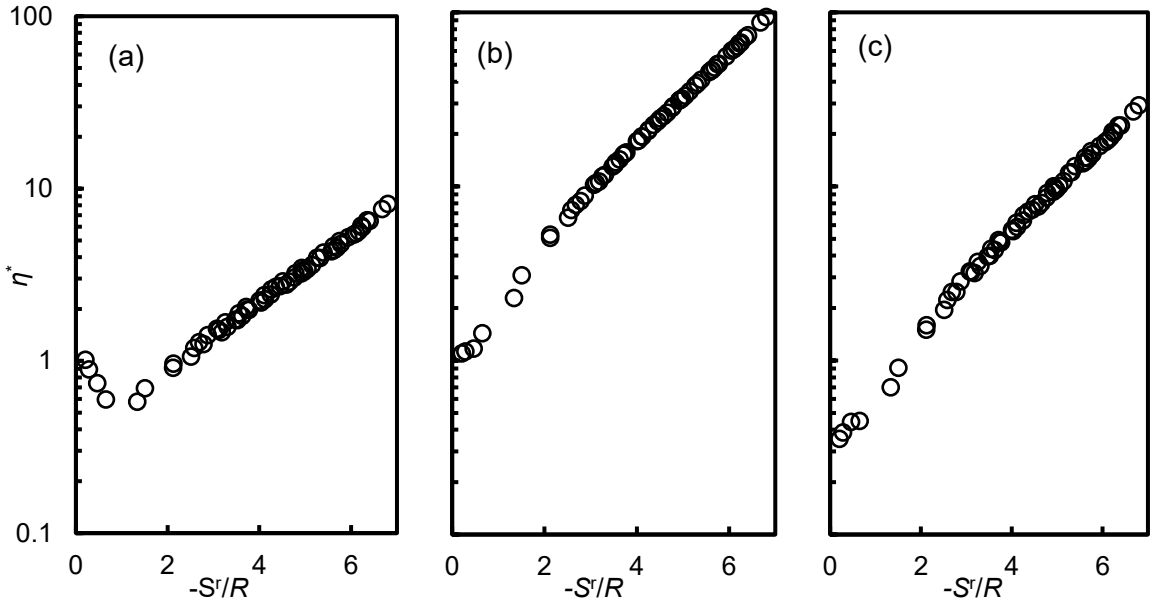

Figure 10.2 Reduced viscosity η^* and residual entropy (S^r/R) for n-pentane: (a) based on Rosenfeld [323]; (b) based on Novak [418] ; (c) based on Bell [282]

Bell [282] proposed another approach to eliminate the divergence of the reduced viscosity in the zero-density limit. Based on the theory of Rosenfeld,[414] according to which the transport properties should be proportional to the residual entropy raised to the power of -2/3 in the dilute gas, the reduced viscosity of Eq. (10.4) was multiply by $(-S^r/R)^{2/3}$ to give the following definition:

$$\eta^* = \frac{\eta n^{-2/3}}{\left(mk_B T\right)^{1/2}}\left(-\frac{S^r}{R}\right)^{2/3} = \frac{\eta \rho^{-2/3} N_A^{1/3}}{\left(MRT\right)^{1/2}}\left(-\frac{S^r}{R}\right)^{2/3} \tag{10.6}$$

Here, ρ is molar density, M is the molar mass, T is temperature, R is the gas constant and N_A is Avagadro's constant. Fig. 10.2 (c) shows that this definition also yields an approximately mono-variant relationship. In a subsequent paper by Bell et al., [420] the same approach was applied to analyse the viscosity, thermal conductivity and self-diffusion coefficients of Lennard-Jones 12-6 fluids. Further discussion of the behaviour of the scaled viscosity in the limit of zero-density for different types of molecules can be found in Bell et al.[278] Other alternatives have also been proposed to eliminate the divergence at low densities however, despite success in eliminating the divergence, these somewhat compromise the mono-variant scaling in the compressed liquid region.[280-281, 330, 335, 339, 418-419] It is worth to mention that in this work, we adopt Bell's definition of reduced viscosity and our model was then developed without making any assumption about the form of interaction between molecules.[420]

10.3 Reduced Entropy

Fundamental equations of state, expressed in terms of the Helmholtz energy, have been developed for many fluids.[21] In these formulations, the dimensionless Helmholtz energy of a pure component is separated into ideal-gas and residual parts:

$$\alpha\left(T,\rho\right) = \alpha^{\mathrm{id}}\left(T,\rho\right) + \alpha^{\mathrm{r}}\left(T,\rho\right) \tag{10.7}$$

where $\alpha = A/RT$ and A is molar Helmholtz energy. The residual molar entropy is then given by,

$$S^{\mathrm{r}} / R = \tau\left(\partial\alpha^{\mathrm{r}}/\partial\tau\right)_{\delta} - \alpha^{\mathrm{r}} \tag{10.8}$$

where τ and δ are the inverse reduced temperature and the reduced density, respectively, defined as follows:

$$\tau = T_{\mathrm{r}}/T \tag{10.9}$$

And

$$\delta = \rho/\rho_{\mathrm{r}}\ . \tag{10.10}$$

For pure fluids, the reducing temperature T_r and reducing density ρ_r are the critical temperature T_c and critical density ρ_c, respectively.

For a mixture, the basic structure of equation (10.7) is retained. The ideal-gas part is given exactly by

$$\alpha^{\mathrm{id}} = \alpha^{\mathrm{id}}\left(T,\rho,x\right) = \sum_{i=1}^{N} x_i \alpha_i^{\mathrm{id}}\left(T,\rho\right) + \sum_{i=1}^{N} x_i \ln x_i \,, \tag{10.11}$$

where N is the number of components and x_i is the mole fraction of component i. The residual part is generally approximated as follows:

$$\alpha^{\mathrm{r}}(\tau,\delta,\mathbf{x}) = \sum_{i=1}^{N} x_i \alpha_i^{\mathrm{r}}(\tau,\delta) + \Delta\alpha^{\mathrm{r}}(\tau,\delta,\mathbf{x}) \,, \tag{10.12}$$

where $\boldsymbol{x}$ is the vector of mole fractions. The first term in Eq. (10.12) represents a corresponding-states approximation while the second term, $\Delta\alpha^{\mathrm{r}}$, is a departure function that can be used to improve the representation of the properties of specific mixtures. For the mixtures considered in this work, no binary-specific departure functions have been developed and $\Delta\alpha^{\mathrm{r}} = 0$.

The inverse reduced temperature and reduced density of the mixture are given as before by Eqs (10.9) and (10.10) but the reducing parameters are now functions of composition as follows:

$$T_{\mathrm{r}}(\mathbf{x}) = \sum_{i=1}^{N} x_i^2 T_{\mathrm{c},i} + \sum_{i=1}^{N-1}\sum_{j=i+1}^{N} 2x_i x_j \beta_{T,ij}\gamma_{T,ij} \frac{x_i + x_j}{\beta_{T,ij}^2 x_i + x_j} \left(T_{\mathrm{c},i} T_{\mathrm{c},j}\right)^{0.5} \tag{10.13}$$

and

$$\frac{1}{\rho_{\mathrm{r}}(\mathbf{x})} = \sum_{i=1}^{N} x_i^2 \frac{1}{\rho_{\mathrm{c},i}} + \sum_{i=1}^{N-1}\sum_{j=i+1}^{N} 2x_i x_j \beta_{\upsilon,ij}\gamma_{\upsilon,ij} \frac{x_i + x_j}{\beta_{\upsilon,ij}^2 x_i + x_j} \frac{1}{8}\left(\frac{1}{\rho_{\mathrm{c},i}^{1/3}} + \frac{1}{\rho_{\mathrm{c},j}^{1/3}}\right)^3 \tag{10.14}$$

Here, $T_{\mathrm{c},i}$ and $\rho_{\mathrm{c},i}$ are the critical temperature and density of component i and $\beta_{T,ij}$, $\beta_{v,ij}$, $\gamma_{T,ij}$ and $\gamma_{v,ij}$ are a set of adjustable binary parameters. Note that, while $\gamma_{T,ij} = \gamma_{T,ji}$ and $\gamma_{v,ij} = \gamma_{v,ji}$, $\beta_{T,ij} = 1/\beta_{T,ji}$ and $\beta_{v,ij} = 1/\beta_{v,ji}$. A more details explanation on this method can be found in the original work of Lemmon,[421] and in connection with the GERG-2004[422] and GERG-2008[423] equations of state.

In the published version of the results, we used the values of the binary parameters β_T, β_V, γ_T and γ_V from the REFPROP database. However, in a subsequent analysis the binary parameters for CO_2 + *m*-xylene were optimised using the experimental densities presented in Part 2 of the thesis together with other available thermodynamics data for the mixture including

the gas solubility and VLE data.[424-430] The binary parameters used for each of the mixtures involved in this work are given in Table 10.1.

Table 10.1 Mixing parameters for mixtures involved in this work

Mixtures	octane (1) + dodecane (2) [398]	CO_2 (1) + *m*-xylene (2)	CO_2 (1) + decane (2) [423]
β_T	0.99884	0.99327	1.02003
β_v	1.00000	1.08117	1.00015
γ_T	1.02500	1.08254	1.14551
γ_V	1.00000	1.10781	1.18339

10.4 Applications of Residual Entropy Models

The residual entropy model has not been receiving much attention even 20 years after Rosenfeld's first findings of the model. In recent year however, there has been extensive research focusing on the application of residual entropy model in transport properties especially viscosity, diffusion coefficient and thermal conductivity. For instance, Dzugutov[325] used molecular dynamics simulations to demonstrate that the self-diffusion coefficient of monatomic fluids, reduced to dimensionless form, was a *universal* function of the residual molar entropy only. In non-monoatomic fluids, it has been established that entropy scaling also applies but that the dimensionless transport properties do not follow exactly the same universal relation; instead, they exhibit a substance-specific but mono-variant dependence upon residual entropy.[326-328] Goel et. al.[329], also using molecular dynamics simulations, tested the residual-entropy scaling relationship for the diffusivity and viscosity of Lennard-Jones chain fluids, restricted to short chains that do not show significant entanglement. He concluded that the residual-entropy scaling associated with the transport properties shows a simple but strong dependence on chain length. It has been confirmed in other simulation work that this mono-variant dependence applies to more complex substances such as the n-alkanes[274, 431-432] and hard dumbbell-shaped particle.[327] The analysis has also been applied to the experimental data for water.[326, 433-434] Loetgering-Lin and Gross[330] presented a group contribution method for the correlation and prediction of pure-component viscosities involving nonpolar, polar, and self-associating components. They used the PCP-SAFT equation of state for the residual entropy and represented the reduced viscosity by a summation over functional groups involving three parameters per group. A similar approach was used by the same group to predict self-diffusion coefficients[331] of pure substances using the group contribution method. They showed that the transport properties of these systems could be predicted well even in the absence of a large experimental database. In his recent work, Gross[435] has proposed a modified Stokes-Einstein equation based on residual entropy approach and introduce a universal function model for predicting molecular self-diffusion coefficients.

A modified entropy-model approach for viscosity has been proposed by Bell and Laesecke[280] where a dimensionless residual entropy per unit volume was used as the scaling variable and a reference fluid was used to establish the functional dependence of reduced viscosity upon

that variable. The method was applied successfully over the whole fluid region to a family of ten refrigerant fluids. More recently, Bell[282] investigated the relationship between reduced viscosity and residual entropy for molecular fluids including argon, methane, CO_2, SF_6, refrigerant R134a, refrigerant R125, methanol and water by introducing an appropriate density scaling. It was concluded that the liquid viscosity of a dense fluid could be predicted within about 20% by using a universal scaling approach along with scaling parameters. Bell also applied the model fluids by incorporating the accurate Helmholtz-energy equations of state[420] and subsequently working on pure hydrocarbons. [436-437] Recently, the same group expand their work to the mixtures of refrigerants including natural refrigerants.[438]

Literature reports pertaining to the viscosity-entropy relation of mixtures are limited and restricted to mixtures of similar components.[335, 339-340] Novak[339] studied the viscosity of the methane-ethane system and came to a conclusion that a new entity-based scaled viscosity model correlated well the pure components and their corresponding mixtures to a single semi-logarithmic function. Delage-Santacreu et al.[340] explored the application of entropy scaling to the viscosity of model fluids, including mixtures that interact according to the Mie potential. A simple logarithmic mixing rule was used to estimate the viscosity of mixtures from pure component values. Loetgering-Lin et al. applied an entropy-scaling model, based on their earlier work on pure substances,[330] to mixtures of real fluids.[335] In their paper, they considered almost 140 pure substances and 566 mixtures of various complexity and used molecular dynamic simulations and PCP- SAFT to develop a mixture model for viscosity and residual entropy, respectively. Nevertheless, the mixtures considered were mainly of similar molecules. Fouad and Vega[336-337] applied a similar approach to the viscosities of hydroflourocarbon and hydroflouroolefin refrigerants and their mixtures. Entropy scaling based on the PC-SAFT equation has also been used to predict the viscosity of hydrocarbon mixtures and diesel fuels at several extreme conditions by Rokni et al. [338] In their work, two calculated or measured properties were used as the inputs and, in comparison with experimental data, average mean absolute percent deviations of 12.2% for hydrocarbon mixtures and 21.4% for diesel fuels. In recent years, the Helmholtz-energy mixture equations of state has been used in conjunction with viscosities calculation. Mairhofer[439] has been able to covers 21 components of the GERG-2008 while Yang et al.[438] used the plus-scaled reduced residual viscosity similar to the work by Bell. [440]

Increasing interest in using the residual entropy model to thermal conductivity of a few real fluids can also be seen recently.[277, 333-334, 420, 441-442] In comparison with viscosity and diffusion coefficient, predicting thermal conductivity from residual entropy model may encounter some challenges. One of it is the critical enhancement that rises from the long-range density fluctuation that occur in a fluid near its critical point.[442] Most of the work does not consider the critical enhancement except for the work by Yang et al. [442] Hopp et al.[441] used the PC-SAFT equation of state to calculate the residual entropy for the real pure hydrocarbons. They proposed a new expression for the reference thermal conductivity and the expression for the ideal gas limit. Hopp et al.[334] also consider the effect of intramolecular degree of freedom using the Chapman-Cowling approximation. A similar work is also seen in the work by Fouad[277] where the PC-SAFT was used by incorporating the Chapman-Cowling and Mason and Saxena mixing rule for predicting the thermal coefficient of refrigerant mixtures containing hydrocarbons, hydrofluorocarbons, hydrofluoroolefins, and CO_2. A more recent work by Yang et al.[442] applied the residual entropy model to pure refrigerants, including natural refrigerants,

hydrofluoroolefins, hydrochlorofluoroolefins, perfluorocarbons, hydrofluorocarbons, chlorofluorocarbons, and hydrochlorofluorocarbons and their mixtures. In their work, four fitted parameters and a fluid-specific scaling factor were used in the development of the correlation functions between the dimensionless residual thermal conductivity and the dimensionless residual entropy. All the work discussed above on the application of residual entropy to predict diffusion coefficient, viscosity and thermal conductivity are summarized in Table 10.2.

In this thesis, we have investigated the monovariate relationship between reduced viscosity and residual entropy in pure fluids and in binary mixtures of hydrocarbons and hydrocarbons with dissolved carbon dioxide.[272] For pure hydrocarbons, the residual entropy were calculated using the application of highly-accurate Helmholtz equations of state while for mixtures, we apply the multi-fluid Helmholtz-energy approximation and simple combining rules for the scaling factors. Detailed discussions are available in the next chapter.

Table 10.2 Previous published work on predicting transport properties using residual entropy model.

Properties	Substances	References
Diffusion coefficient	Lennard-Jones chain fluids	Dzugutov[325]
	Lennard-Jones chain fluids	Goel et. al.[329]
	alkane	Galliero and Boned[274, 431]
	alkane	Gerek and Elliott [432]
	water	[326, 433-434]
	Pure fluids and mixtures	Gross [331, 435]
Viscosity	Lennard-Jones chain fluids	Goel et. al.[329]
	Pure fluids and mixtures	Loetgering-Lin and Gross[330, 335]
	refrigerants	Bell and Laesecke[280]
	argon, methane, CO_2, SF_6, refrigerants	Bell[282]
	pure alkanes and refrigerants mixtures	Bell [420, 438, 440, 443]
	Methane-ethane	Novak[339]
	refrigerants mixtures	Fouad and Vega[336-337]
	Hydrocarbon mixtures	Rokni et al. [338]
	Mixtures of Mie n-6 fluids	Delage-Santacreu et al.[340]
Thermal conductivity	Pure hydrocarbons	Hopp et al.[334, 441]
	refrigerants mixtures	Fouad[277]
	refrigerants	Yang et al.[442]

CHAPTER 11 RESIDUAL ENTROPY MODEL FOR BINARY MIXTURES OF HYDROCARBONS WITH DISSOLVED CO_2

In this study, we first explore the application of highly-accurate Helmholtz equations of state for the calculation of residual entropy and the subsequent correlation of reduced viscosity for pure substances. We introduce scaling factors to reduce the data to a universal function. We then apply the method to mixtures based on the multi-fluid Helmholtz-energy approximation for the mixture residual entropy and simple combining rules for the scaling factors. In our work, the compounds of interest are aliphatic and aromatic hydrocarbons and their mixtures with CO_2. We have tested these methods in comparison with experimental mixture viscosities in the temperature range from (200 to 500) K and at pressures up to 200 MPa.

11.1 Pure fluids

In this work, five pure components were studied: decane, 1,3-dimethylbenzene (*m*-xylene), CO_2, dodecane and octane. The viscosity data for CO_2 was taken from a precise correlation having an estimated expanded relative uncertainty (k = 2) of approximately 3 %[444] as well as experimental data from Iwasaki and Takahashi[445]. The viscosity data of octane, decane, dodecane and *m*-xylene were original experimental data published [249, 251, 254-255] with estimated relative uncertainties of 2 %. These data span temperatures from (298 to 473) K and pressures from (0.1 to 200) MPa. Additional experimental data were added for from several previous works: octane[446], decane[447-448], dodecane[449] and *m*-xylene[393-394]. The criterion for selecting the hydrocarbons were based upon the availability of both reliable wide-ranging viscosity data and a wide-range Helmholtz equation of state.

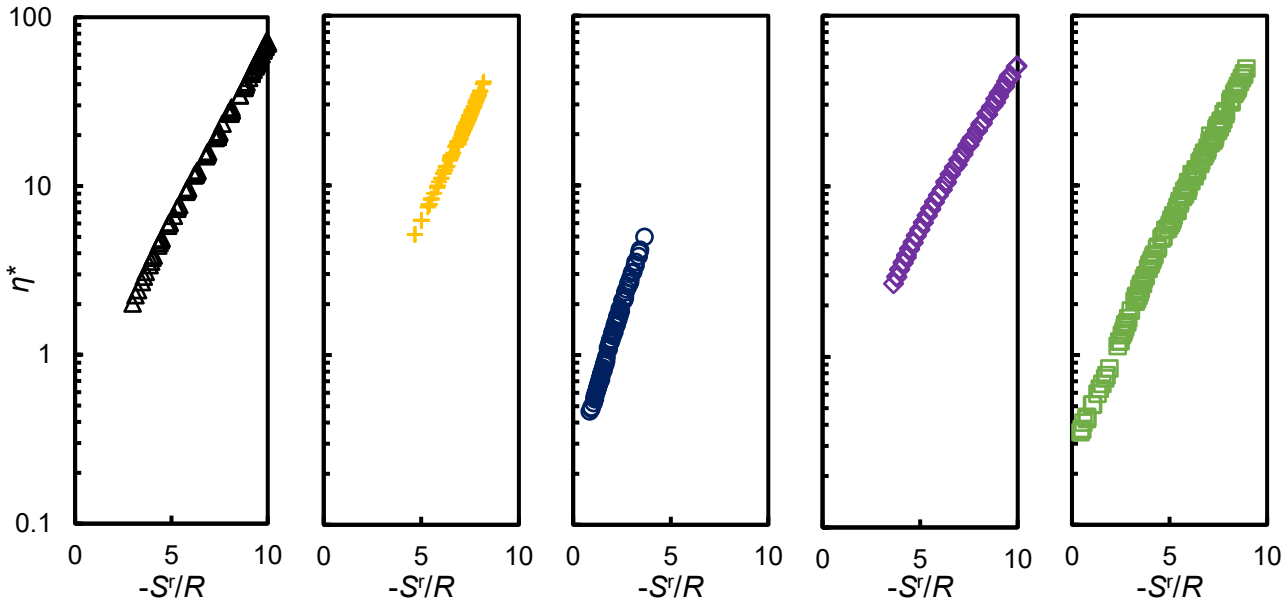

Figure 11.1 Reduced viscosity η* and residual molar entropy (Sr/R) for pure fluids: △,decane; +, *m*-xylene; ○, CO_2; ◇, dodecane; □, octane.

For each substance, reduced viscosities were calculated from Equation 10.6 while the residual molar entropy was calculated from the relevant Helmholtz equation of state[22] via equation 10.7. Figure 11.1 shows the reduced viscosities of the pure components plotted against residual molar entropy. To a good approximation, the data for each substance fall approximately on a single curve, demonstrating the expected mono-variant relationship over an extended range of temperature and pressure. On the semi-logarithmic scale of the plot, these mono-variant relationships happen to be nearly linear but different from one substance to the next.

Table 11.1 Scaling parameters for each substance

Substance	h	R_η
decane	1.000	1.000
m-xylene	0.8309	0.6792
CO_2	0.6370	0.5483
dodecane	1.0901	1.1037
octane	0.9045	0.8681

In order to reduce all of the data to a single universal curve, we introduce two scale factors: a horizontal factor h, which scales the residual molar entropy, and a vertical factor R_η, which scales the reduced viscosity. The latter is incorporated into our definition of η^* as follows:

$$\eta^* = \frac{\eta \rho^{-2/3} N_A^{1/3}}{R_\eta \left(MRT\right)^{1/2}} \left(-\frac{S^r}{R}\right)^{2/3} . \tag{11.1}$$

Since the data for decane span the widest range of residual molar entropy, we selected this substance as a reference fluid to which we assigned the scaling factors h = 1 and R_η = 1. However, this choice is arbitrary. The universal correlation (which is slightly non-linear on a semi-log scale) was then represented by the polynomial function

$$\ln \eta^* = \sum_{i=0}^{3} c_i \left[-S^r/(hR)\right]^i . \tag{11.2}$$

The parameters c_i, together with the values of h and R_η, for each substance other than decane were optimised in a global regression that minimised the following objective function:

$$\Theta = \frac{1}{N} \sum_{i=1}^{N} \left(\frac{\eta_{i,\mathrm{exp}} - \eta_{i,\mathrm{fit}}}{\eta_{i,\mathrm{exp}}} \right)^2 \tag{11.3}$$

where $\eta_{i,\mathrm{exp}}$ is an experimental datum and $\eta_{i,\mathrm{fit}}$ is the value calculated from Eq. (11.2) with the best-fit parameters. The scaling factors so determined for each substance are given in Table

11.1 while the coefficients c_i are given in Table 11.2 together with the absolute average relative deviation Δ_{AAD} and the maximum absolute relative deviation Δ_{MAD} for all data. These metrics are defined by

$$\Delta_{\mathrm{AAD}} = \sum_i \left| \frac{\eta_{i,\mathrm{exp}} - \eta_{i,\mathrm{fit}}}{\eta_{i,\mathrm{exp}}} \right| \tag{11.4}$$

and

$$\Delta_{\mathrm{MAD}} = \mathrm{Max} \left| \frac{\eta_{i,\mathrm{exp}} - \eta_{i,\mathrm{fit}}}{\eta_{i,\mathrm{exp}}} \right|. \tag{11.5}$$

Figures 11.2 shows the scaled experimental data in comparison with the universal function and illustrates the generally excellent mono-variant representation. The deviations of the data from the model, shown for each substance separately in Figure 11.3, are all within a band of ±10 %. With this finding, we concluded that, by an appropriate scaling, the experimental data for each component can be collapsed onto a single curve relating reduced viscosity to residual molar entropy.

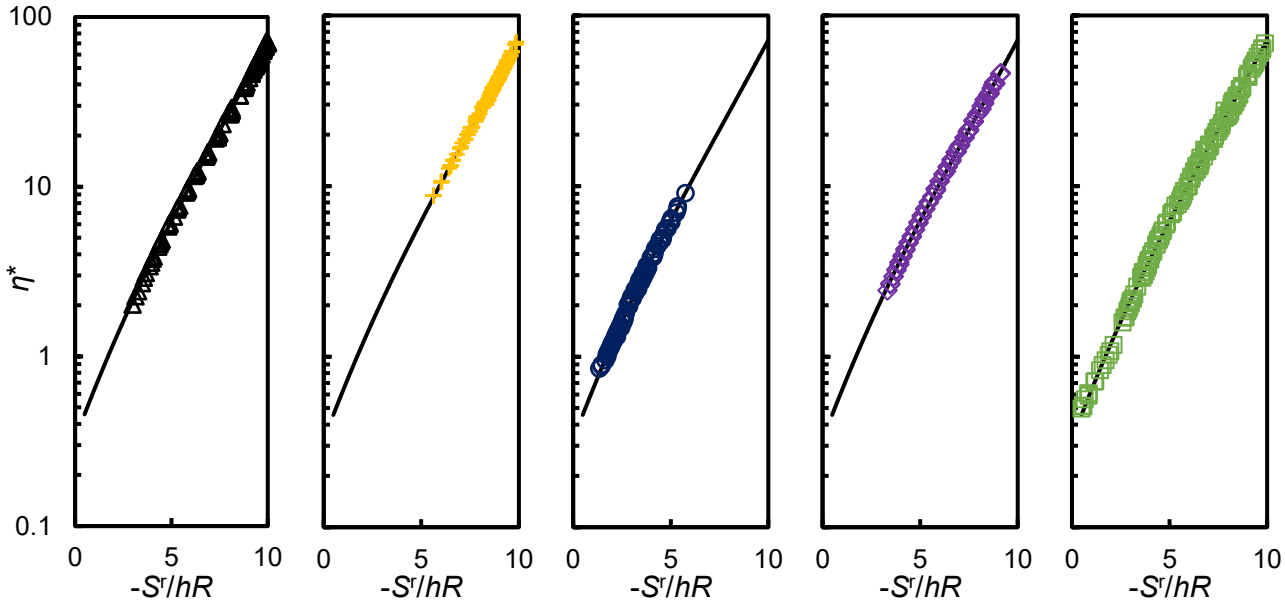

Figure 11.2 Scaled reduced viscosity η^* against scaled residual entropy (S^r/hR) for each pure substance: △, decane; +, *m*-xylene; ○, CO_2;◇, dodecane; □, octane. The solid line represents Eq. 11.2.

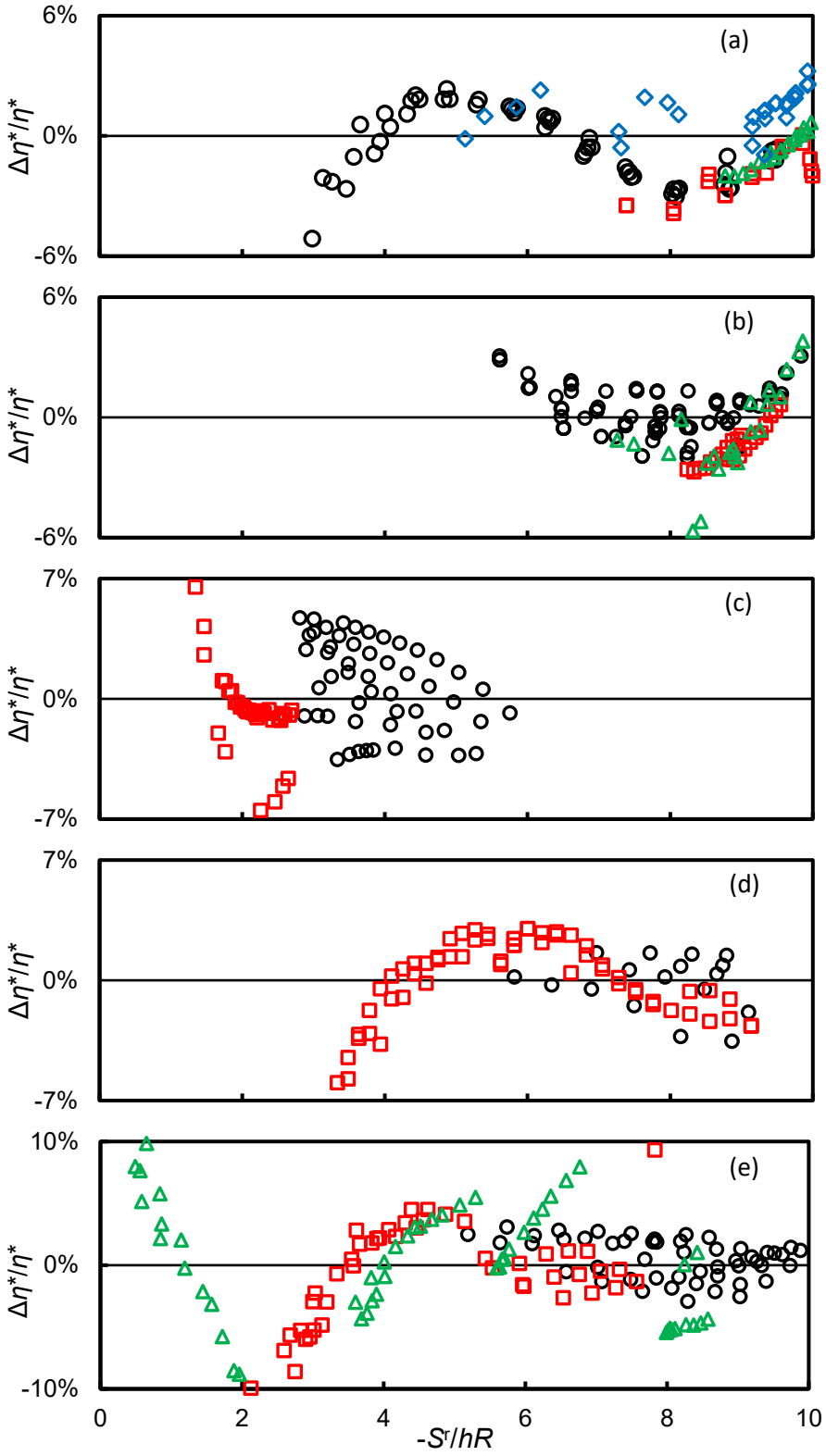

Figure 11.3 Relative deviations $\Delta\eta^*/\eta^*$ of the scaled reduced viscosity from the values estimated from equation (12.3) for each component: (a) decane: O, Liu et al.[251]; □, Caudwell et al.[249]; △, Assael et al.[447]; ◇, Carmichael et al.[448] (b) *m*-xylene: O, Caudwell et al.[249]; □, Assael et al.[393]; △, Et-tahir et al.[394] (c) CO_2: O, Fenghour et al.[444] ; □, Iwasaki and Takahashi[445] (d) dodecane: O, Caudwell et al.[254-255]; □, Yang et al.[449] (e) octane: O, Caudwell et al.[249]; □, Badalyan and Rodchenko[446]; △, Stephen and Heckelberger.[450]

Table 11.2 Coefficients of equation 11.2 and statistical parameters for the universal correlation

i	c_i
0	-1.12478
1	0.70260
2	-0.02813
3	1.1865 x 10^{-3}
Δ_{AAD}	1.9%
Δ_{MAD}	9.9%

11.2 Application to Mixtures

In order to apply the model to mixtures, one simply needs a means of determining the molar mass M in Eq. (12.2) and the scaling factors h_{mix} and $R_{\eta,mix}$ that apply. These can of course be fitted to experimental data but, to obtain a predictive model, we postulate the simplest possible mixing rules as follows:

$$M_{\text{mix}} = \sum_i x_i M_i \tag{11.6}$$

$$h_{\text{mix}} = \sum_i x_i h_i \tag{11.7}$$

$$R_{\eta,\text{mix}} = \sum_i x_i R_{\eta,i} \tag{11.8}$$

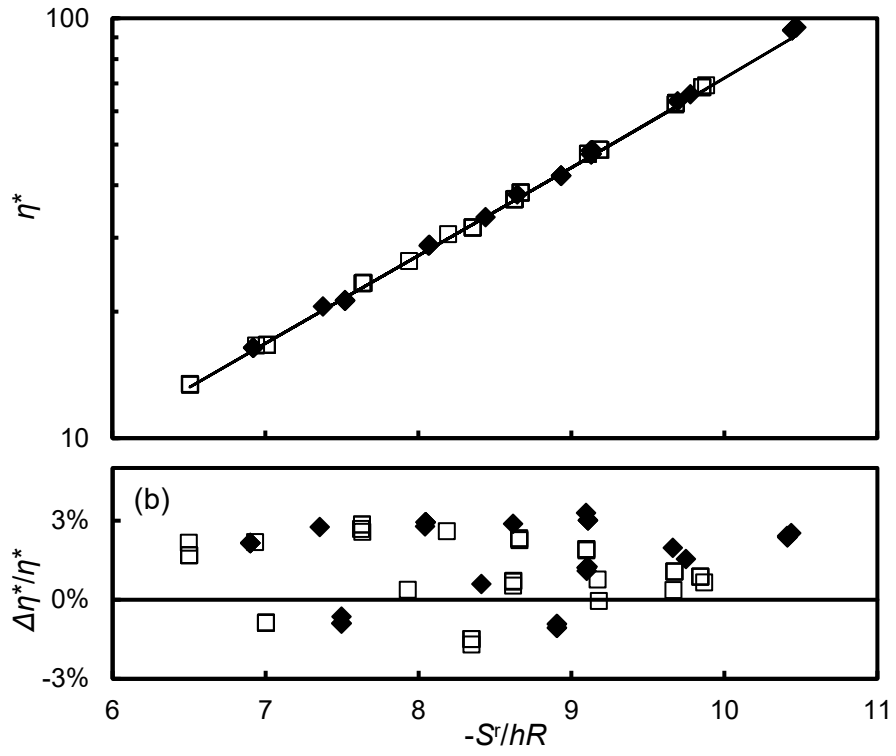

Figure 11.4 Scaled reduced viscosity η^* (a) and relative deviations $\Delta\eta^*/\eta^*$ (b) for octane (1) + dodecane (2) system as a function of scaled residual entropy: □, x_1 = 0.743; ◆, x_1 = 0.434.

An initial test of this postulate is provided by a comparison with data for a mixture of two hydrocarbons having similar characteristic. Due to the availability of wide-ranging and precise experimental data at more than one mixture composition, the (octane + dodecane) system was chosen for this test.[254] Figure 11.4 compares the experimental data with the model and shows reasonable agreement with absolute average relative deviation of 2%.

A more severe test of the approach is provided by data for asymmetric mixtures, for example hydrocarbon liquids with dissolved CO_2. Two such mixtures are considered here, namely (CO_2 + decane) and (CO_2 + *m*-xylene). The experimental viscosity data for the (CO_2 + decane) system were those of Cullick et al.[366] while those for the (CO_2 + *m*-xylene) system were our experimental data presented in Part 2. All data considered fall in the homogeneous liquid region. To test the accurate of the equation-of-state model, we compare in Figure 11.5 the measured density values with those predicted by the model. The values for the relative differences $\Delta\rho/\rho$, where $\Delta\rho = \rho$(experimental) – ρ(predicted) was found to be within $|\Delta\rho/\rho| \leq$ 4%. Figures 11.6 and 11.7 compare the viscosity data for these two systems with the model. Clearly, the deviations are larger in these cases, particularly for (CO_2 + decane) where a few points deviate by more than 30%. The three most discrepant points relate to the highest composition of CO_2 at a temperature of 403 K. It is also observed that the model systematically underestimates the experimental data for both systems.

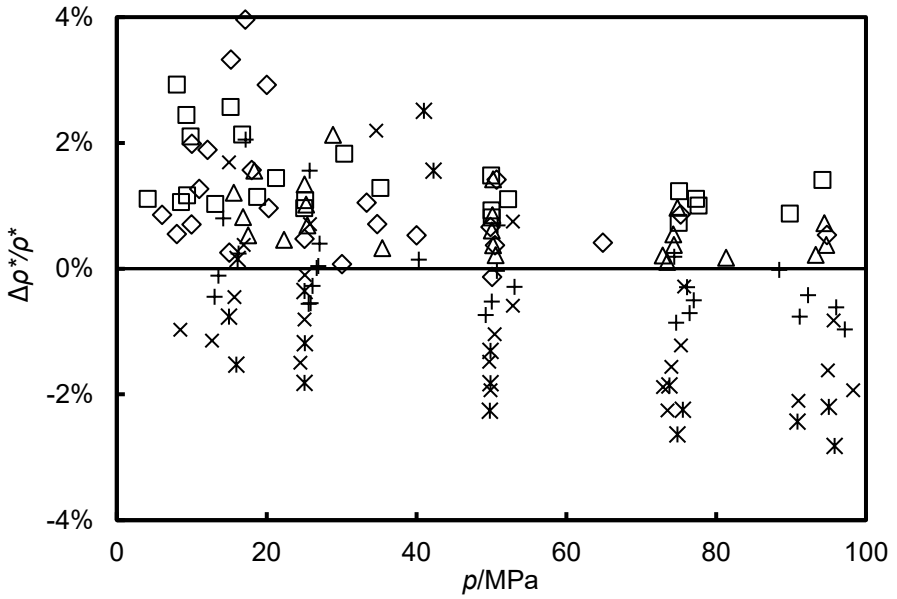

Figure 11.5 Density deviation as a function of pressure for CO_2 (1) + *m*-xylene (2).

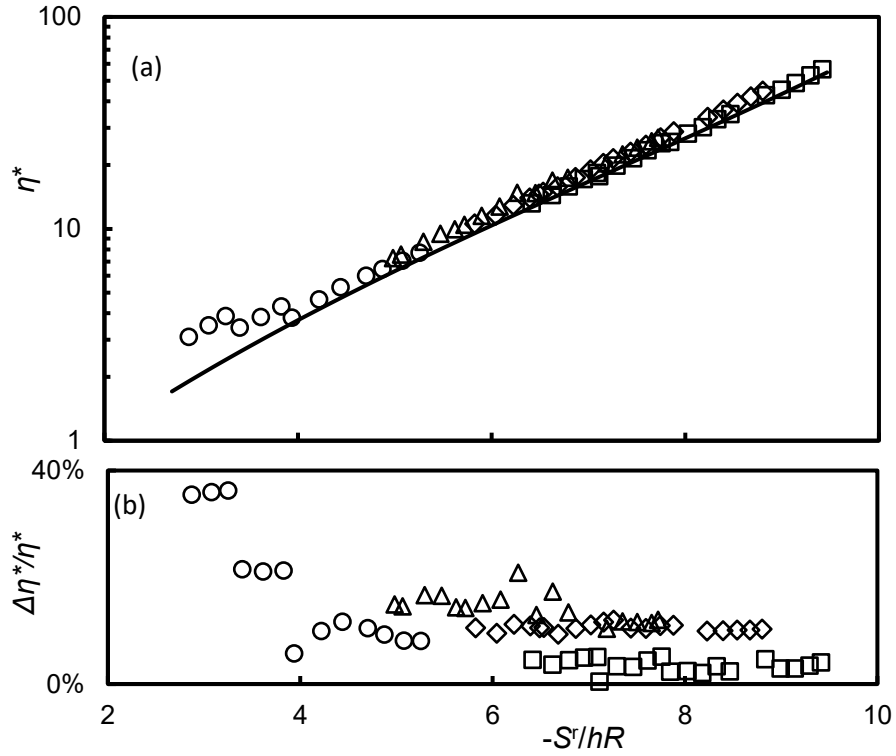

Figure 11.6 Scaled reduced viscosity η^* (a) and relative deviations $\Delta\eta^*/\eta^*$ (b) for CO_2 (1) + decane (2): □, x_1 = 0.15; ◇, x_1 = 0.30; r, x_1 = 0.51; ○, x_1 = 0.85. Solid line in (a) represents the predicted values.

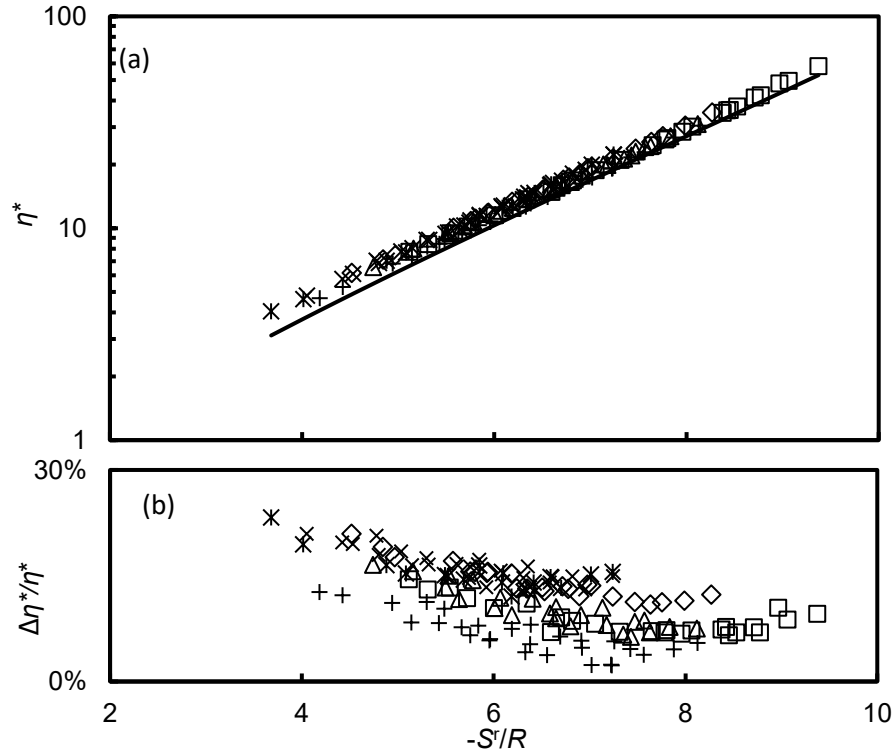

Figure 11.7 Scaled reduced viscosity η^* (a) and relative deviations $\Delta\eta^*/\eta^*$ (b) for CO_2 (1) + *m*-xylene (2): □, x_1 = 0.19; ◇, x_1 = 0.38; △, x_1 = 0.46; + , x_1 = 0.51; ×, x_1 = 0.62; ∗, x_1 = 0.65. Solid line in (a) represents the predicted values.

11.3 Discussion

The method proposed in this work has the potential to be a universal model, at least for the class of non-polar and non-associating fluids consider in this paper. The approach is contingent upon the availability of an accurate method for calculating the residual molar entropy of pure fluids and mixtures. The use of multi-parameter Helmholtz-energy models limits the approach to the 100 or so pure substances for which such models have so far been developed and to mixtures of these for which the binary parameters β_T, β_V, γ_T and γ_V, and any necessary binary-specific departure functions, have been adequately determined. Of course, other equation of state models, such as SAFT approaches,[335] could be used but the multi-parameter Helmholtz-energy models are preferred.

The scaling used to map the reduced viscosity onto a universal curve is somewhat similar to that in the hard-sphere theory of Dymond and Assael (DA) wherein a scaled reduced viscosity is represented as a universal function of a reduced molar volume. However, whereas the reducing molar volume in the DA theory is a function of temperature, the scaling factors in the present method are constants for a given substance. This means that only a limited amount of viscosity data is required to determine the scaling parameters. The performance of the present method appears to be excellent for pure substances and competitive with correlation models that involve many more parameters. When applied to mixtures, larger deviations are observed and it is not clear if these reflect inaccuracies in the prediction of the mixture residual entropy, limitations of the simple linear mixing rules used for the scaling factors, or both. Nevertheless, we consider the results encouraging and worthy of further investigation.

Referring to Fig. 11.2, one can observe that data points at $-S^r/R < 2$ are included. These points are located near the critical point or in the supercritical region and, in Figure 11.3, they show greater and somewhat systematic deviations from the correlation. If one considers only those points at $-S^r/R \geq 2$ then a better fit can be obtained with an AAD of 1.5% and MAD of 7.8%.

A simple mixing expression was adopted to the molar mass of the mixture appearing in Equation (11.1). As discussed by Galliero et al.,[451] several other rational possibilities exist including: (1) a quadratic model

$$M_{\text{mix}}^{1/2} = \sum_i \sum_i x_i x_j M_{ij}^{1/2} , \tag{11.9}$$

in which M_{ij} is the reduced molar mass ($1/M_{ij} = 1/M_i + 1/M_j$); (2) a linear square-root model

$$M_{\text{mix}}^{1/2} = \sum_i x_i M_i^{1/2} , \tag{11.10}$$

and (3) a log-linear square-root model

$$\ln M_{\text{mix}}^{1/2} = \sum_i x_i \ln M_i^{1/2} . \tag{11.11}$$

To test the effect of these different assumptions, an additional calculation has been made with each of these alternative definitions for M_{mix} and, in Table 11.3, the results were being compared in terms of the AAD and MAD statistics. However, these different rules do not offer any improvement, being either the same or slightly worse than the results obtained with Equation (11.6) for M_{mix}.

Table 11.3 Summary of the AADs and MADs for several mixing rule equations referred from Galliero et al.[451]

Mixture	Equation (11.6)		Equation (11.9)		Equation (11.10)		Equation (11.11)	
	AAD	MAD	AAD	MAD	AAD	MAD	AAD	MAD
octane + dodecane	2%	4%	2%	4%	2%	4%	2%	4%
decane + CO_2	11%	36%	16%	41%	13%	38%	15%	40%
m-xylene + CO_2	12%	23%	17%	32%	14%	29%	16%	31%

Based on the results presented, the residual entropy approach was able to correlate the viscosity of CO_2 and several hydrocarbon liquids over wide ranges of temperature and pressure with average absolute relative deviations of less than 2 % and maximum absolute relative deviations of less than 10 % for all components investigated. Applying the method to mixtures yield a larger deviation that appear to increase with the molecular asymmetry of the system. Nevertheless, the findings are considered successful when compares with other methods for predicting the viscosity of such systems and could initiate more future research.

CHAPTER 12 CONCLUSIONS AND RECOMMENDATIONS FOR FUTURE WORK

12.1 Conclusions

The following conclusions can be drawn from the present study:

1. The Tait-Andrade and Tait equations which are usually applied to systems at fixed compositions, can be successfully extended as functions of composition even for asymmetric systems like *m*-xylene + CO_2. The surface fits developed have been tested for mole fraction of CO_2 up to 0.652.
2. Looking at the viscosity results, what is most compelling is the effect of CO_2 dissolution on the viscosity of the mixtures. For both systems, adding CO_2 has resulted in a large reduction in the viscosity of the mixtures. However, it was found that the relative reduction in viscosity for the *m*-xylene + CO_2 system is not as much as the viscosity reduction that was obtained in the DIDP + CO_2 system. This interesting result might be explained by the fact that at its pure state, the viscosity of *m*-xylene is not very high compared to the viscosity of pure DIDP. The viscosity of DIDP is approximately 50 times higher than the viscosity of *m*-xylene and almost 300 times higher than the viscosity of pure CO_2 whereas the viscosity of *m*-xylene is only 6 times higher than the CO_2 viscosity. Returning to the questions posed at the beginning of this thesis, it is now possible to state that hydrocarbons with higher initial viscosity led to a more significant reduction in the viscosity when adding CO_2 compared to hydrocarbons with a relatively lower initial viscosity. These results are in accord with the findings of Ciotta *et al.*[16] and Ruien *et al.*,[452] who studied the system of squalane + CO_2 and CO_2-saturated methylbenzene-crude oil mixtures, respectively. The study has contributed to a better understanding of the behaviour of the viscosity of highly viscous hydrocarbons+CO_2 mixtures.
3. The results of the modelling work on the viscosity of mixtures showed that using the highly accurate multi-fluid Helmholtz energy approximation and a simple mixing rule, the model works well within a certain envelope. For mixtures of similar molecules, the model shows reasonable agreement with absolute average relative deviation of 2%. While for asymmetric mixtures that were tested, it was not worse that 30% with average relative deviation of approximately 13%. This is a rather encouraging finding considering that only simple mixing rules were used.
4. The diffusion coefficient of CH_4 in heptane and in methylbenzene does not differ very much. However, by comparing aliphatic and aromatic hydrocarbon with the same carbon number, it was observed that the diffusion coefficient was lower by about 14% in the aromatic.
5. Based on the experimental results of diffusion coefficients, it was found that a correlation of logarithm of diffusion coefficient is a linear function of pressure along isotherms. Also, based on the experimental results, the Stokes Einstein model provides a good correlation, provided that the hydrodynamic radius of the solute is represented as a linear function with the solvent density.

6. The rough hard sphere has been extended in a way that provides a powerful correlation for the diffusion coefficients of light solutes in heavier solvents at infinite diffusion. The correlated model can be used for predictions on the basis of single experimental datum in order to determine the roughness factor. The model proved to provide good correlation where deviations were mostly within ±5%.

12.2 Contributions

The research provides an extensive study of transport properties of hydrocarbons and hydrocarbons with the addition of CO_2/CH_4. Accurate experimental data were measured at wide range of temperature, pressure, and composition to fill in the existing gaps in the literature and provide a fundamental basis to understanding the behaviour of hydrocarbon mixtures that are relevant to CCS. These experimental data are providing information in developing improved models especially for asymmetric mixtures. The present study makes several noteworthy contributions including:

1. A large set of experimental viscosity and diffusion coefficients for hydrocarbons with dissolved CO_2/ CH_4 which have never been reported in the literature. These data not only provided a large contribution to literature, but also served as a basis for understanding the behaviour of the hydrocarbons when mixed with CO_2. The experimental data were also used to develop the residual entropy model for viscosity and the universal model for diffusion coefficients where it fits well with the models. The experimental results in this work can potentially be used as literature reference in comparison with future studies. These will be of great importance in improving the current reference equations of state developed for each component. The density data of DIDP + CO_2 mixtures can be used in developing a thermodynamic model for the system in order to apply the residual entropy model in predicting the viscosity of the mixtures.
2. Successful models that can predict viscosity and diffusion coefficients of the asymmetric mixtures with acceptable agreement with the experimental results. These models make it possible to correlate the viscosity and diffusion coefficients with minimum requirements.
3. Several papers were published that provides valuable insights on the measurements and models for predicting viscosity and diffusion coefficient. These papers are listed below:
    a) Diffusion coefficients of methane in methylbenzene and heptane at temperatures between 323 K and 398 K at pressures up to 65 MPa. International Journal of Thermophysics, Volume 41, Issue 8, 2020[210]
    b) Viscosity and density of 1,3-dimethylbenzene + carbon dioxide at temperatures from 298 to 423 K and at pressures up to 100 MPa. Journal of Chemical Engineering Data, Volume 65, 2020[379]
    c) Residual entropy model for predicting the viscosities of dense fluid mixtures, The Journal of Chemical Physics, Volume 152, Issue 16, 2020[272]

d) Modelling the diffusion coefficients of dilute gaseous solutes in hydrocarbon liquids. International Journal of Thermophysics, Volume 42, 2021[209]

12.3 Recommendation for future work

As a result of these investigations, suggestions were identified for future research. For the prediction of viscosity in this work, the correlation function was developed based on the non-polar and non-associating fluids only. Recent work by Yang et al.[438] on the other hand presented the model for mixtures of refrigerants while Rokni et al.[338] works on hydrocarbon mixtures and diesel fuels. The model would be a fruitful area for further work considering wider systems including polar fluids, more asymmetric systems as well as crude oil mixtures. A greater focus on using different types of mixing rules could produce interesting findings especially when predicting viscosity of asymmetric mixtures. In this work, preliminary results showed not much difference on three of the simplest mixing rules as discussed by Galliero et al.,[451] However, several other rational possibilities exist and might become another possible area of future research. Another important future work that is worth to explore is applying the residual entropy model to predict the viscosity of DIDP + CO_2 mixtures. However, before we could do that, a thermodynamic model needs to be established to calculate the residual molar entropy of the mixtures. Therefore, important thermodynamic properties such as density needs to be measured as well as VLE and solubility data for such mixtures. In addition to that, one can explore any other predictive models that might be use that address the issue.

For diffusion coefficient, measurement of diffusion coefficients of CH_4 in other hydrocarbons would be of future interest as available experimental data are still scarce. The availability of more diffusion coefficient data would be beneficial as the application of the universal model to a new compound requires at least one experimental value of the tracer diffusion coefficient besides sufficient pure-component data to determine $V_0(T)$. To add to that, further investigation on the roughness factor reveals a clear trend with carbon number for CO_2 as the solute. The smooth trend for CO_2-alkane systems suggests that the diffusion coefficients for CO_2 in other alkanes could be predicted. Further studies should be undertaken to prove this statement and new measurements over extended ranges of temperature and pressure would be helpful. However, for other solutes such as C_2H_6, no clear trend was seen. This would be caused by the lack of data for the system where the light solute is C_2H_6. What is available in the literature were restricted to C_2H_6 with octane, hexane, and heptane as the solvents with less than 10 data points. Therefore, further investigation on the relation between roughness factor and carbon number for each of the solutes would be of great efforts. Although the model has been developed for liquid hydrocarbons with inorganic and light hydrocarbon solutes, the model is expected to apply to other non-polar solute-solvent systems. The present study lays the groundwork for future research into other non-polar solvents. As mentioned in the earlier section, the correlation was restricted to light solutes of non-polar solute-solvent systems only. It is recommended to revise and extend the correlation to the case where large molecular solutes diffuse in light supercritical solvents and the molecular simulation data that were excluded from the present analysis ($\sigma_1/\sigma_2 > 1$ and/or $M_1/M_2 > 1$). When the correlation has successfully be extended to the case where the solvent is light, modelling can be done across the entire composition range. For example, if we have a mixture with certain composition and the diffusion coefficient of the two components are needed in their equimolar mixture. The

work could open the path to a model that would work over the entire composition range for binary system.

Overall, with all the findings discussed in the earlier parts and the scientific conclusions that arose from it, it can be said that the objective of this work which was to advance the science in transport properties particularly in asymmetric mixtures have been successfully achieved. The present study lays the groundwork for future research into investigating other transport properties such as thermal conductivity and apply such models to predict the experimental data.

References

1. Sönnichsen, N. *IEA Oil 2021 report*; International Energy Agency: **2021**.
2. Allen, M. R.; O.P. Dube; W. Solecki; F. Aragón-Durand; W. Cramer; S. Humphreys; M. Kainuma; J. Kala; N. Mahowald; Y. Mulugetta; R. Perez; M. Wairiu, a.; K. Zickfeld, Framing and Context. In:. *Global Warming of 1.5°C. An IPCC Special Report on the impacts of global warming of 1.5°C above pre-industrial levels and related global greenhouse gas emission pathways, in the context of strengthening the global response to the threat of climate change, sustainable development, and efforts to eradicate poverty* **2018,** *[Masson-Delmotte, V., P. Zhai, H.-O. Pörtner, D. Roberts, J. Skea, P.R. Shukla, A. Pirani, W. Moufouma-Okia, C. Péan, R. Pidcock, S. Connors, J.B.R. Matthews, Y. Chen, X. Zhou, M.I. Gomis, E. Lonnoy, T. Maycock, M. Tignor, and T. Waterfield (eds.)]. In Press.*
3. IPCC, Contribution of Working Group III to the Fifth Assessment Report of the Intergovernmental Panel on Climate Change [Edenhofer, O., R. Pichs-Madruga, Y. Sokona, E. Farahani, S. Kadner, K. Seyboth, A. Adler, I. Baum, S. Brunner, P. Eickemeier, B. Kriemann, J. Savolainen, S. Schlömer, C. von Stechow, T. Zwickel and J.C. Minx (eds.)]. *Cambridge University Press, Cambridge, United Kingdom and New York, NY, USA.* **2014**.
4. Agency, U. S. E. P., Report on the Environment: Greenhouse Gases.
5. Pires, J. C. M.; Martins, F. G.; Alvim-Ferraz, M. C. M.; Simões, M., Recent developments on carbon capture and storage: An overview. *Chemical Engineering Research and Design* **2011,** *89* (9), 1446-1460.
6. Tapia, J. F. D.; Lee, J.-Y.; Ooi, R. E. H.; Foo, D. C. Y.; Tan, R. R., Planning and scheduling of CO2 capture, utilization and storage (CCUS) operations as a strip packing problem. *Process Safety and Environmental Protection* **2016,** *104*, 358-372.
7. Trusler, J. P. M., Thermophysical Properties and Phase Behavior of Fluids for Application in Carbon Capture and Storage Processes. *Annual Review of Chemical and Biomolecular Engineering* **2017,** *8* (1), 381-402.
8. Hannis, S.; Lu, J.; Chadwick, A.; Hovorka, S.; Kirk, K.; Romanak, K.; Pearce, J., CO2 Storage in Depleted or Depleting Oil and Gas Fields: What can We Learn from Existing Projects? *Energy Procedia* **2017,** *114*, 5680-5690.
9. Wang, J.; Ryan, D.; Anthony, E. J.; Wildgust, N.; Aiken, T., Effects of impurities on CO2 transport, injection and storage. *Energy Procedia* **2011,** *4*, 3071-3078.
10. Faltinson, J. E.; Gunter, B., Net CO2 Stored in North American EOR Projects. *J. Can. Pet. Tech.* **2011,** *50* (Preprint), 55-60.
11. Benson, S. M.; Bennaceur, K.; Cook, P.; Davison, J.; de Coninck, H.; Farhat, K.; Ramirez, A.; Simbeck, D.; Surles, T.; Verma, P.; Wright, I.; Ahearne, J., Carbon Capture and Storage. In *Global Energy Assessment: Toward a Sustainable Future*, Global Energy Assessment Writing, T., Ed. Cambridge University Press: Cambridge, 2012; pp 993-1068.
12. Zahasky, C.; Krevor, S., Global geologic carbon storage requirements of climate change mitigation scenarios. *Energy Environ. Sci.* **2020,** *13* (6), 1561-1567.
13. Mohammed, M.; Ciotta, F.; Trusler, J. P. M., Viscosities and Densities of Binary Mixtures of Hexadecane with Dissolved Methane or Carbon Dioxide at Temperatures from (298 to 473) K and at Pressures up to 120 MPa. *J. Chem. Eng. Data* **2017,** *62* (1), 422-439.
14. Bui, M.; Adjiman, C. S.; Bardow, A.; Anthony, E. J.; Boston, A.; Brown, S.; Fennell, P. S.; Fuss, S.; Galindo, A.; Hackett, L. A.; Hallett, J. P.; Herzog, H. J.; Jackson, G.; Kemper, J.; Krevor, S.; Maitland, G. C.; Matuszewski, M.; Metcalfe, I. S.; Petit, C.; Puxty, G.; Reimer, J.; Reiner, D. M.; Rubin, E. S.; Scott, S. A.; Shah, N.; Smit, B.; Trusler, J. P. M.; Webley, P.; Wilcox, J.; Mac Dowell, N., Carbon capture and storage (CCS): the way forward. *Energy Environ. Sci.* **2018,** *11* (5), 1062-1176.
15. Sanchez-Vicente, Y.; Tay, W. J.; Al Ghafri, S. Z.; Trusler, J. P. M., Thermodynamics of carbon dioxide-hydrocarbon systems. *Appl. Energy* **2018,** *220*, 629-642.
16. Ciotta, F.; Maitland, G.; Smietana, M.; Trusler, J. P. M.; Vesovic, V., Viscosity and Density of Carbon Dioxide + 2,6,10,15,19,23-Hexamethyltetracosane (Squalane). *J. Chem. Eng. Data* **2009,** *54* (9), 2436-2443.
17. Hendriks, E.; Kontogeorgis, G. M.; Dohrn, R.; de Hemptinne, J.-C.; Economou, I. G.; Žilnik, L. F.; Vesovic, V., Industrial Requirements for Thermodynamics and Transport Properties. *Ind. Eng. Chem. Res.* **2010,** *49* (22), 11131-11141.

18. Li, H.; Wilhelmsen, Ø.; Lv, Y.; Wang, W.; Yan, J., Viscosities, thermal conductivities and diffusion coefficients of CO2 mixtures: Review of experimental data and theoretical models. *Int.J. Greenhouse Gas Control* **2011,** *5* (5), 1119-1139.
19. Assael, M. J.; Goodwin, A. R. H.; Vesovic, V.; Wakeham, W. A., Experimental thermodynamics series, vol. IX. Advances in Transport Properties. *The Royal Society of Chemistry, Cambridge* **2014**.
20. Zheng, L.; Trusler, J. P. M.; Bresme, F.; Müller, E. A., Predicting the pressure dependence of the viscosity of 2,2,4-trimethylhexane using the SAFT coarse-grained force field. *Fluid Phase Equilib.* **2019,** *496*, 1-6.
21. Lemmon, E. W.; Span, R., Short Fundamental Equations of State for 20 Industrial Fluids. *J. Chem. Eng. Data* **2006,** *51* (3), 785-850.
22. Lemmon, E. W.; Tillner-Roth, R., A Helmholtz energy equation of state for calculating the thermodynamic properties of fluid mixtures. *Fluid Phase Equilib.* **1999,** *165* (1), 1-21.
23. Himmelblau, D. M., Diffusion of Dissolved Gases in Liquids. *Chem. Rev.* **1964,** *64* (5), 527-550.
24. Teraoka, I., *Polymer Solutions: An Introduction to Physical Properties*. Wiley-Interscience: New York, NY, 2002.
25. Geet, A. L. V.; Adamson, A. W., Diffusion in Liquid Hydrocarbon Mixtures. *J. Phys. Chem.* **1964,** *68* (2), 238-246.
26. Ambrosini, D.; Paoletti, D.; Rashidnia, N., Overview of diffusion measurements by optical techniques. *Optics and Lasers in Engineering* **2008,** *46* (12), 852-864.
27. D.G. Miller; Albright, J. G., Optical methods. In *Measurement of the Transport Properties of Fluids*, Blackwell Scientific Publication, Oxford: 1991; pp 272-294.
28. Van de Ven-Lucassen, I. M. J. J.; Kieviet, F. G.; Kerkhof, P. J. A. M., Fast and Convenient Implementation of the Taylor Dispersion Method. *J. Chem. Eng. Data* **1995,** *40* (2), 407-411.
29. Taylor, G. I., Dispersion of soluble matter in solvent flowing slowly through a tube. *Proceedings of the Royal Society of London. Series A. Mathematical and Physical Sciences* **1953,** *219* (1137), 186-203.
30. Aris, R.; Taylor, G. I., On the dispersion of a solute in a fluid flowing through a tube. *Proceedings of the Royal Society of London. Series A. Mathematical and Physical Sciences* **1956,** *235* (1200), 67-77.
31. Gerek, Z. N.; Elliott, J. R., Self-Diffusivity Estimation by Molecular Dynamics. *Ind. Eng. Chem. Res.* **2010,** *49*, 3411.
32. Hahn, E. L., Spin Echoes. *Phys. Rev.* **1950,** *80* (4), 580-594.
33. Miller, D. G., The History of Interferometry for Measuring Diffusion Coefficients. *J. Solution Chem.* **2014,** *43* (1), 6-25.
34. Cadogan, S. P.; Trusler, J. P. M. Diffusion of CO_2 in Fluids Relevant to Carbon Capture, Utilisation and Storage Imperial College London, London, United Kingdom, 2016.
35. Landau, L. D.; Lifshitz, E. M., *Fluid Mechanics: Landau and Lifshitz: Course of Theoretical Physics, Volume 6*. Elsevier: 2013; Vol. 6.
36. Cadogan, S. P.; Mistry, B.; Wong, Y.; Maitland, G. C.; Trusler, J. P. M., Diffusion Coefficients of Carbon Dioxide in Eight Hydrocarbon Liquids at Temperatures between (298.15 and 423.15) K at Pressures up to 69 MPa. *J. Chem. Eng. Data* **2016,** *61* (11), 3922-3932.
37. Chandler, D., Rough hard sphere theory of the self-diffusion constant for molecular liquids. *The Journal of Chemical Physics* **1975,** *62* (4), 1358-1363.
38. Kravchenko, O.; Thachuk, M., Transport properties of the rough hard sphere fluid. *The Journal of Chemical Physics* **2012,** *136* (4), 044520.
39. Chapman, S.; Cowling, T. G., *The Mathematical Theory of Nonuniform Gases: An Account of the Kinetic Theory of Viscosity, Thermal Conduction and Diffusion in Gases*. Cambridge University Press: Cambridge, 1970.
40. Enskog, S.; Chapman, S.; Cowling, T. G., *The Mathematical Theory of Non-Uniform Gases*. Cambridge University Press: Cambridge, 1939.
41. Silva, C. M.; Liu, H., Modelling of Transport Properties of Hard Sphere Fluids and Related Systems, and its Applications. In *Theory and Simulation of Hard-Sphere Fluids and Related Systems*, Mulero, Á., Ed. Springer Berlin Heidelberg: Berlin, Heidelberg, 2008; pp 383-492.

42. S. F. Y. Li; R. D. Trengove; Wakeham, W. A.; Zalaf, M., The Transport Coefficients of Polyatomic Liquids. *Int. J. Thermophys.* **1986,** *7*, 273-284.
43. S. F. Y. Li; Maitland, G. C.; Wakeham, W. A., The Thermal Conductivity of Liquid Hydrocarbons. *High Temp. High Press.* **1985,** *17*, 241-251.
44. Assael, M. J.; Dymond, J. H.; Tselekidou, V., Correlation of high-pressure thermal conductivity, viscosity, and diffusion coefficients for n-alkanes. *Int. J. Thermophys.* **1990,** *11* (5), 863-873.
45. Dysthe, D. K.; Fuchs, A. H.; Rousseau, B.; Durandeau, M., Fluid transport properties by equilibrium molecular dynamics. II. Multicomponent systems. *The Journal of Chemical Physics* **1999,** *110* (8), 4060-4067.
46. Dysthe, D. K.; Fuchs, A. H.; Rousseau, B., Prediction of Fluid Mixture Transport Properties by Molecular Dynamics. *Int. J. Thermophys.* **1998,** *19* (2), 437-448.
47. Feng, H.; Gao, W.; Sun, Z.; Lei, B.; Li, G.; Chen, L., Molecular Dynamics Simulation of Diffusion and Structure of Some n-Alkanes in near Critical and Supercritical Carbon Dioxide at Infinite Dilution. *J. Phys. Chem.* **2013,** *117* (41), 12525-12534.
48. Moultos, O. A.; Tsimpanogiannis, I. N.; Panagiotopoulos, A. Z.; Trusler, J. P. M.; Economou, I. G., Atomistic Molecular Dynamics Simulations of Carbon Dioxide Diffusivity in n-Hexane, n-Decane, n-Hexadecane, Cyclohexane, and Squalane. *J. Phys. Chem.* **2016,** *120* (50), 12890-12900.
49. Higashi, H.; Iwai, Y.; Arai, Y., Calculation of Self-Diffusion and Tracer Diffusion Coefficients near the Critical Point of Carbon Dioxide Using Molecular Dynamics Simulation. *Ind. Eng. Chem. Res.* **2000,** *39* (12), 4567-4570.
50. Iwai, Y.; Higashi, H.; Uchida, H.; Arai, Y., Molecular dynamics simulation of diffusion coefficients of naphthalene and 2-naphthol in supercritical carbon dioxide. *Fluid Phase Equilib.* **1997,** *127* (1), 251-261.
51. Moultos, O. A.; Tsimpanogiannis, I. N.; Panagiotopoulos, A. Z.; Economou, I. G., Atomistic Molecular Dynamics Simulations of CO2 Diffusivity in H2O for a Wide Range of Temperatures and Pressures. *J. Phys. Chem.* **2014,** *118* (20), 5532-5541.
52. Zabala, D.; Nieto-Draghi, C.; de Hemptinne, J. C.; López de Ramos, A. L., Diffusion Coefficients in CO2/n-Alkane Binary Liquid Mixtures by Molecular Simulation. *J. Phys. Chem.* **2008,** *112* (51), 16610-16618.
53. Higashi, H.; Iwai, Y.; Uchida, H.; Arai, Y., Diffusion coefficients of aromatic compounds in supercritical carbon dioxide using molecular dynamics simulation. *J. Supercrit. Fluids* **1998,** *13* (1-3), 93-97.
54. Wakeham, W. A., *Measurement of the Transport Properties of Fluids*. Blackwell Science: 1991.
55. Aris, R., On the Dispersion of a Solute in a Fluid Flowing Through a Tube. *Proc. Roy. Soc. Lond.* **1956,** *A285*, 67.
56. Taylor, G. I., Dispersion of soluble matter in solvent flowing slowly through a tube. *Proc. R. Soc. Lond.* **1953,** *A219*, 186-203.
57. Alizadeh, A.; Nieto de Castro, C. A.; Wakeham, W. A., The theory of the Taylor dispersion technique for liquid diffusivity measurements. *Int. J. Thermophys.* **1980,** *1* (3), 243-284.
58. Chen, H. C.; Chen, S. H., Tracer Diffusion of Crown Ethers in n-Decane and n-Tetradecane: An Improved Correlation for Binary Systems Involving Normal Alkanes. *Ind. Eng. Chem. Fundam.* **1985,** *24* (2), 187-192.
59. Chen, H. C.; Chen, S. H., Corresponding-States Correlation of Tracer Diffusion in Liquids. *Ind. Eng. Chem. Fundam.* **1985,** *24* (2), 183-187.
60. Chen, H.-C.; Chen, S.-H., Taylor dispersion measurement of the diffusivities of polymethylenes in dilute solutions. *Chem. Eng. Sci.* **1985,** *40* (3), 521-526.
61. Matthews, M. A.; Rodden, J. B.; Akgerman, A., High-temperature diffusion of hydrogen, carbon monoxide, and carbon dioxide in liquid n-heptane, n-dodecane, and n-hexadecane. *J. Chem. Eng. Data* **1987,** *32* (3), 319-322.
62. Cadogan, S. P.; Maitland, G. C.; Trusler, J. P. M., Diffusion Coefficients of CO_2 and N_2 in Water at Temperatures between 298.15 K and 423.15 K at Pressures up to 45 MPa. *J. Chem. Eng. Data* **2014,** *59* (2), 519-525.
63. Matthews, M. A.; Akgerman, A., Diffusion coefficients for binary alkane mixtures to 573 K and 3.5 MPa. *AIChE J.* **1987,** *33* (6), 881-885.

64. Chen, S. H.; Davis, H. T.; Evans, D. F., Tracer diffusion in polyatomic liquids. II. *J. Chem. Phys.* **1981,** *75* (3), 1422-1426.
65. Nunge, R. J.; Lin, T. S.; Gill, W. N., Laminar dispersion in curved tubes and channels. *J. Fluid Mech.* **1972,** *51* (2), 363-383.
66. Secuianu, C.; Maitland, G. C.; Trusler, J. P. M.; Wakeham, W. A., Mutual Diffusion Coefficients of Aqueous KCl at High Pressures Measured by the Taylor Dispersion Method. *J. Chem. Eng. Data* **2011,** *56* (12), 4840-4848.
67. Dymond, J. H., Transport Properties of Dense Fluids. In *Sixth Symposium on Thermophysical Properties, The American Society of Mechanical Engineers*, Liley, P. E., Ed. Atlanta, Georgia, U.S.A, 1973; pp 143-157.
68. Dymond, J. H., Interpretation of Transport Coefficientts on Basis of Van der Waals Model. I. Dense Fluids. *Physica* **1974,** *75*, 100-114.
69. Assael, M. J.; Dymond, J. H.; Patterson, P. M., Correlation and prediction of dense fluid transport coefficients. V. Aromatic hydrocarbons. *Int. J. Thermophys.* **1992,** *13* (5), 895-905.
70. Assael, M. J.; Dymond, J. H.; Papadaki, M.; Patterson, P. M., Correlation and prediction of dense fluid transport coefficients. I. n-alkanes. *Int. J. Thermophys.* **1992,** *13* (2), 269-281.
71. Assael, M. J.; Dymond, J. H.; Papadaki, M.; Patterson, P. M., Correlation and prediction of dense fluid transport coefficients: II. Simple molecular fluids. *Fluid Phase Equilib.* **1992,** *75*, 245-255.
72. Assael, M. J.; Dymond, J. H.; Patterson, P. M., Correlation and prediction of dense fluid transport coefficients. IV. A note on diffusion. *Int. J. Thermophys.* **1992,** *13* (4), 729-733.
73. Assael, M. J.; Dymond, J. H.; Papadaki, M.; Patterson, P. M., Correlation and prediction of dense fluid transport coefficients. III. n-alkane mixtures. *Int. J. Thermophys.* **1992,** *13* (4), 659-669.
74. Bleazard, J. G.; Teja, A. S., Extension of the Rough Hard-Sphere Theory for Transport Properties to Polar Liquids. *Ind. Eng. Chem. Res.* **1996,** *35* (7), 2453-2459.
75. Erkey, C.; Gadalla, H.; Akgerman, A., Application of rough hard sphere theory to diffusion in supercritical fluidst. *The Journal of Supercritical Fluids* **1990,** *3* (4), 180-185.
76. Matthews, M. A.; Akgerman, A., Hard-sphere theory for correlation of tracer diffusion of gases and liquids in alkanes. *The Journal of Chemical Physics* **1987,** *87* (4), 2285-2291.
77. Easteal, A. J.; Woolf, L. A., Tracer diffusion in hard-sphere liquids from molecular dynamics simulations. *Chem. Phys. Lett.* **1990,** *167* (4), 329-333.
78. Easteal, A. J.; Woolf, L. A.; Jolly, D. L., Self-diffusion in a dense hard-sphere fluid: A molecular dynamics simulation. *Physica A: Statistical Mechanics and its Applications* **1983,** *121* (1), 286-292.
79. Alder, B. J.; Gass, D. M.; Wainwright, T. E., Studies in Molecular Dynamics. VIII. The Transport Coefficients for a Hard-Sphere Fluid. *The Journal of Chemical Physics* **1970,** *53* (10), 3813-3826.
80. Assael, M. J.; Dymond, J. H.; Polimatidou, S. K., Correlation and prediction of dense fluid transport coefficients. VII. Refrigerants. *Int. J. Thermophys.* **1995,** *16* (3), 761-772.
81. Assael, M. J.; Dymond, J. H.; Polimatidou, S. K., Correlation and prediction of dense fluid transport coefficients. VI.n-alcohols. *Int. J. Thermophys.* **1994,** *15* (2), 189-201.
82. Grushka, E.; Kikta, E., Chromatographic Broadening Technique of Liquid Diffusivity Measureemnts. *J. Phys. Chem.* **1975,** *79* (20), 2199-2200.
83. Pratt, K. C.; Wakeham, W. A., Chromatographic Technique of Diffusivity Measurement. *J. Phys. Chem.* **1975,** *79* (20), 2198-2199.
84. Pratt, K. C.; Wakeham, W. A.; Ubbelohde, A. R. J. P., The mutual diffusion coefficient of ethanol-water mixtures: determination by a rapid, new method. *Proceedings of the Royal Society of London. A. Mathematical and Physical Sciences* **1974,** *336* (1606), 393-406.
85. Grushka, E.; Kikta, E. J., Extension of Chromatographic broadening Method of Measuring Diffusion Coefficients to Liquid-System. 1. Diffusion Coefficients of Some Alkylbenzenes in Chloroform. *J. Phys. Chem.* **1974,** *78* (22), 2297-2301.
86. Sarraute, S.; Costa Gomes, M. F.; Pádua, A. A. H., Diffusion Coefficients of 1-Alkyl-3-methylimidazolium Ionic Liquids in Water, Methanol, and Acetonitrile at Infinite Dilution. *J. Chem. Eng. Data* **2009,** *54* (9), 2389-2394.

87. Atwood, J. G.; Goldstein, J., Measurements of diffusion coefficients in liquids at atmospheric and elevated pressure by the chromatographic broadening technique. *J. Phys. Chem.* **1984,** *88* (9), 1875-1885.
88. Weinheimer, R. M.; Evans, D. F.; Cussler, E. L., Diffusion in surfactant solutions. *J. Colloid Interf. Sci.* **1981,** *80* (2), 357-368.
89. Funazukuri, T.; Nishimoto, N.; Wakao, N., Binary Diffusion Coefficients of Organic Compounds in Hexane, Dodecane, and Cyclohexane at 303.2-333.2 K and 16.0 MPa. *J. Chem. Eng. Data* **1994,** *39* (4), 911-915.
90. Funazukuri, T.; Kong, C. Y.; Kagei, S., Binary diffusion coefficients in supercritical fluids: Recent progress in measurements and correlations for binary diffusion coefficients. *The Journal of Supercritical Fluids* **2006,** *38* (2), 201-210.
91. Karaiskakis, G.; Gavril, D., Determination of diffusion coefficients by gas chromatography. *J. Chromatogr. A* **2004,** *1037* (1), 147-189.
92. Suárez, J. J.; Medina, I.; Bueno, J. L., Diffusion coefficients in supercritical fluids: available data and graphical correlations. *Fluid Phase Equilib.* **1998,** *153* (1), 167-212.
93. Silva, C. M.; Macedo, E. A., Diffusion Coefficients of Ethers in Supercritical Carbon Dioxide. *Ind. Eng. Chem. Res.* **1998,** *37* (4), 1490-1498.
94. Catchpole, O. J.; King, M. B., Measurement and Correlation of Binary Diffusion Coefficients in Near Critical Fluids. *Ind. Eng. Chem. Res.* **1994,** *33* (7), 1828-1837.
95. Bruno, T. J., Measurement of diffusion in fluid systems - Applications to the supercritical fluid region. *J. Thermophys Heat Transfer* **1994,** *8* (2), 329-333.
96. Levelt Sengers, J. M. H.; Deiters, U. K.; Klask, U.; Swidersky, P.; Schneider, G. M., Application of the Taylor dispersion method in supercritical fluids. *Int. J. Thermophys.* **1993,** *14* (4), 893-922.
97. Liu, H.; Silva, C. M.; Macedo, E. A., Unified approach to the self-diffusion coefficients of dense fluids over wide ranges of temperature and pressure—hard-sphere, square-well, Lennard–Jones and real substances. *Chem. Eng. Sci.* **1998,** *53* (13), 2403-2422.
98. Noel, J. M.; Erkey, C.; Bukur, D. B.; Akgerman, A., Infinite Dilution Mutual Diffusion Coefficients of 1-Octene and 1-Tetradecene in Near Critical Ethane and Propane. *J. Chem. Eng. Data* **1994,** *39* (4), 920-921.
99. Erkey, C.; Akgerman, A., Chromatography theory: Application to supercritical fluid extraction. *AIChE J.* **1990,** *36* (11), 1715-1721.
100. Akgerman, A.; Erkey, C.; Orejuela, M., Limiting diffusion coefficients of heavy molecular weight organic contaminants in supercritical carbon dioxide. *Ind. Eng. Chem. Res.* **1996,** *35* (3), 911-917.
101. Eaton, A. P.; Akgerman, A., Infinite-dilution diffusion coefficients in supercritical fluids. *Ind. Eng. Chem. Res.* **1997,** *36* (3), 923-931.
102. Callendar, R.; Leaist, D. G., Diffusion Coefficients for Binary, Ternary, and Polydisperse Solutions from Peak-Width Analysis of Taylor Dispersion Profiles. *J. Solution Chem.* **2006,** *35* (3), 353-379.
103. Leaist, D. G., Ternary diffusion coefficients of 18-crown-6 ether–KCl–water by direct least-squares analysis of Taylor dispersion measurements. *J. Chem. Soc., Faraday Trans.* **1991,** *87* (4), 597-601.
104. Castillo, R.; Garza, C., Temperature dependence of the mutual diffusion coefficients in aqueous solutions of alkali metal chlorides. *Int. J. Thermophys.* **1993,** *14* (6), 1145-1152.
105. Leaist, D. G., Tracer ionic diffusion coefficients from liquid chromatography. *Electrochim. Acta* **1991,** *36* (2), 309-313.
106. Tominaga, T.; Matsumoto, S.; Koshiba, T.; Yamamoto, Y., Tracer diffusion of the tris(1,10-phenanthroline)iron(II) cation in aqueous salt solutions. Effect of hydrophobic interactions. *Journal of the Chemical Society, Faraday Transactions 1: Physical Chemistry in Condensed Phases* **1988,** *84* (12), 4261-4266.
107. Vinograd, J. R.; McBain, J. W., Diffusion of Electrolytes and of the Ions in their Mixtures. *J. Am. Chem. Soc.* **1941,** *63* (7), 2008-2015.
108. Rysselberghe, P. V., Interpretation of Diffusion Data for Some Strong Electrolytes. *J. Am. Chem. Soc.* **1938,** *60* (10), 2326-2331.
109. Hartley, G. S.; Runnicles, D. F.; Donnan, F. G., The porous diaphragm method of measuring diffusion velocity, and the velocity of diffusion of potassium chloride in water.

Proceedings of the Royal Society of London. Series A. Mathematical and Physical Sciences **1938,** *168* (934), 401-419.
110. Gordon, A. R., The Diffusion Constant of an Electrolyte, and Its Relation to Concentration. *The Journal of Chemical Physics* **1937,** *5* (7), 522-526.
111. McBain, J. W.; Dawson, C. R., The diffusion of potassium chloride in aqueous solution. *Proceedings of the Royal Society of London. Series A - Mathematical and Physical Sciences* **1935,** *148* (863), 32-39.
112. McBain, J. W.; Liu, T. H., Diffusion of Electrolytes, non-Electrolytes and Colloidal Electrolytes. *J. Am. Chem. Soc.* **1931,** *53* (1), 59-74.
113. Clack, B. W., On the study of diffusion in liquids by an optical method. *Proceedings of the Physical Society of London* **1923,** *36* (1), 313-335.
114. Newman, J.; Chapman, T. W., Restricted diffusion in binary solutions. *AIChE J.* **1973,** *19* (2), 343-348.
115. Agar, J. N.; Lobo, V. M. M., Measurement of diffusion coefficients of electrolytes by a modified open-ended capillary method. *Journal of the Chemical Society, Faraday Transactions 1: Physical Chemistry in Condensed Phases* **1975,** *71* (0), 1659-1666.
116. Tanaka, K., Effect of electrolytes on the self-diffusion coefficient of water. *Journal of the Chemical Society, Faraday Transactions 1: Physical Chemistry in Condensed Phases* **1976,** *72* (0), 1121-1123.
117. Rard, J. A.; Miller, D. G., Mutual diffusion coefficients of barium chloride-water and potassium chloride-water at 25 .degree. from Rayleigh interferometry. *J. Chem. Eng. Data* **1980,** *25* (3), 211-215.
118. Chang, Y. C.; Myerson, A. S., The diffusivity of potassium chloride and sodium chloride in concentrated, saturated, and supersaturated aqueous solutions. *AIChE J.* **1985,** *31* (6), 890-894.
119. Myerson, A. S.; Chang, Y. C., Diffusional separation in ternary systems. *AIChE J.* **1986,** *32* (10), 1747-1749.
120. Pinto, N. G.; Graham, E. E., Multicomponent diffusion in concentrated electrolyte solutions: Effect of solvation. *AIChE J.* **1987,** *33* (3), 436-443.
121. Leaist, D. G.; Hao, L., Gravitational stability of Taylor dispersion profiles. Revised diffusion coefficients for barium chloride-potassium chloride-water. *J. Phys. Chem.* **1993,** *97* (7), 1464-1469.
122. Lobo, V. M. M., Mutual diffusion coefficients in aqueous electrolyte solutions (Technical Report). *Pure Appl. Chem.* **1993,** *65* (12), 2613.
123. Selim, M. S.; Al-Naafa, M. A.; Jones, M. C., Brownian diffusion of hard spheres at finite concentrations. *AIChE J.* **1993,** *39* (1), 3-16.
124. Al-Naafa, M. A.; Selim, M. S., Measurement of diffusion coefficients by Taylor's method of hydrodynamic stability. *AIChE J.* **1994,** *40* (8), 1412-1417.
125. Lobo, V. M. M.; Ribeiro, A. C. F.; Andrade, S. G. C. S., Computation of the Diffusion Coefficients in Aqueous Electrolyte Solutions from Onsager-Fuoss and Pikal Theories. *Ber. Bunsen-Ges. Phys. Chem.* **1995,** *99* (5), 713-720.
126. Müller, K. J.; Hertz, H. G., A Parameter as an Indicator for Water−Water Association in Solutions of Strong Electrolytes. *J. Phys. Chem.* **1996,** *100* (4), 1256-1265.
127. Bernard, O.; Cartailler, T.; Turq, P.; Bium, L., Mutual diffusion coefficients in electrolyte solutions. *J. Mol. Liq.* **1997,** *73-74*, 403-411.
128. Leaist, D. G.; Lu, R., Diffusion coefficients measured by Taylor dispersion in a Fourier ring Aqueous lanthanum chloride at 25 °C. *J. Chem. Soc., Faraday Trans.* **1997,** *93* (9), 1755-1761.
129. Lobo, V. M. M.; Ribeiro, A. C. F.; Verissimo, L. M. P., Diffusion coefficients in aqueous solutions of potassium chloride at high and low concentrations. *J. Mol. Liq.* **1998,** *78* (1), 139-149.
130. Ribeiro, A. C. F.; Lobo, V. M. M.; Leaist, D. G.; Natividade, J. J. S.; Veríssimo, L. P.; Barros, M. C. F.; Cabral, A. M. T. D. P. V., Binary Diffusion Coefficients for Aqueous Solutions of Lactic Acid. *J. Solution Chem.* **2005,** *34* (9), 1009-1016.
131. Woolf, L. A.; Tilley, J. F., Revised values of integral diffusion coefficients of potassium chloride solutions for the calibration of diaphragm cells. *J. Phys. Chem.* **1967,** *71* (6), 1962-1963.

132. Miller, D. G., Application of Irreversible Thermodynamics to Electrolyte Solutions. I. Determination of Ionic Transport Coefficients lij for Isothermal Vector Transport Processes in Binary Electrolyte Systems1,2. *J. Phys. Chem.* **1966,** *70* (8), 2639-2659.
133. McCall, D. W.; Douglass, D. C., The Effect of Ions on the Self-Diffusion of Water. I. Concentration Dependence. *J. Phys. Chem.* **1965,** *69* (6), 2001-2011.
134. Firth, J. G.; Tyrrell, H. J. V., 381. Diffusion coefficients for aqueous silver nitrate solutions at 25°, 35°, and 45° from diaphragm-cell measurements. *Journal of the Chemical Society (Resumed)* **1962,** (0), 2042-2047.
135. Woolf, L. A.; Miller, D. G.; Gosting, L. J., Isothermal Diffusion Measurements on the System H_2O-Glycine-KCl at 25; Tests of the Onsager Reciprocal Relation. *J. Am. Chem. Soc.* **1962,** *84* (3), 317-331.
136. Longsworth, L. G., The Temperature Dependence of the Soret Coefficient of Aqueous Potassium Chloride. *J. Phys. Chem.* **1957,** *61* (11), 1557-1562.
137. Mills, R.; Adamson, A. W., The Measurement of Self-diffusion in Electrolyte Solutions1,2. *J. Am. Chem. Soc.* **1955,** *77* (13), 3454-3458.
138. Rulfs, C. L., Polarographic Diffusion Coefficients. *J. Am. Chem. Soc.* **1954,** *76* (8), 2071-2074.
139. Stokes, R. H., Integral Diffusion Coefficients of Potassium Chloride Solutions for Calibration of Diaphragm Cells. *J. Am. Chem. Soc.* **1951,** *73* (7), 3527-3528.
140. Harned, H. S., Solutions of Electrolytes. *Annu. Rev. Phys. Chem.* **1951,** *2* (1), 37-50.
141. Stokes, R. H., The Diffusion Coefficients of Eight Uni-univalent Electrolytes in Aqueous Solution at 25°. *J. Am. Chem. Soc.* **1950,** *72* (5), 2243-2247.
142. Stokes, R. H., An Improved Diaphragm-cell for Diffusion Studies, and Some Tests of the Method. *J. Am. Chem. Soc.* **1950,** *72* (2), 763-767.
143. Gosting, L. J., A Study of the Diffusion of Potassium Chloride in Water at 25° with the Gouy Interference Method. *J. Am. Chem. Soc.* **1950,** *72* (10), 4418-4422.
144. Harned, H. S.; Blake, C. A., The Diffusion Coefficient of Potassium Chloride in Water at 4°. *J. Am. Chem. Soc.* **1950,** *72* (5), 2265-2266.
145. Harned, H. S.; Nuttall, R. L., The Diffusion Coefficient of Potassium Chloride in Aqueous Solution at 25. *Ann. N. Y. Acad. Sci.* **1949,** *51* (4), 781-788.
146. Harned, H. S.; Nuttall, R. L., The Differential Diffusion Coefficient of Potassium Chloride in Aqueous Solutions. *J. Am. Chem. Soc.* **1949,** *71* (4), 1460-1463.
147. Harned, H. S.; Nuttall, R. L., The Diffusion Coefficient of Potassium Chloride in Dilute Aqueous Solution. *J. Am. Chem. Soc.* **1947,** *69* (4), 736-740.
148. Gordon, A. R., The Diaphragm Cell Method of Measuring Diffusion. *Ann. N. Y. Acad. Sci.* **1945,** *46* (5), 285-308.
149. Harned, H. S.; French, D. M., A Conductance Method for the Determination of the Diffusion Coefficients of Electrolytes. *Ann. N. Y. Acad. Sci.* **1945,** *46* (5), 267-284.
150. Erkey, C.; Akgerman, A., Translational-rotational coupling parameters for mutual diffusion in N-octane. *AIChE J.* **1989,** *35* (3), 443-448.
151. Chen, S. H.; Davis, H. T.; Evans, D. F., Tracer diffusion in polyatomic liquids. III. *J. Chem. Phys.* **1982,** *77* (5), 2540-2544.
152. Snijder, E. D.; te Riele, M. J. M.; Versteeg, G. F.; van Swaaij, W. P. M., Diffusion Coefficients of CO, CO_2, N_2O, and N_2 in Ethanol and Toluene. *J. Chem. Eng. Data* **1995,** *40* (1), 37-39.
153. Ferrell, R. T.; Himmelblau, D. M., Diffusion coefficients of nitrogen and oxygen in water. *J. Chem. Eng. Data* **1967,** *12* (1), 111-115.
154. Frank, M. J. W.; Kuipers, J. A. M.; van Swaaij, W. P. M., Diffusion Coefficients and Viscosities of CO_2 + H_2O, CO_{-2} + CH_3OH, NH_3 + H_2O, and NH_3 + CH_3OH Liquid Mixtures. *J. Chem. Eng. Data* **1996,** *41* (2), 297-302.
155. Han, P.; Bartels, D. M., Temperature Dependence of Oxygen Diffusion in H_2O and D_2O. *J. Phys. Chem.* **1996,** *100* (13), 5597-5602.
156. Hamborg, E. S.; Derks, P. W. J.; Kersten, S. R. A.; Niederer, J. P. M.; Versteeg, G. F., Diffusion Coefficients of N_2O in Aqueous Piperazine Solutions Using the Taylor Dispersion Technique from (293 to 333) K and (0.3 to 1.4) mol·dm−3. *J. Chem. Eng. Data* **2008,** *53* (7), 1462-1466.
157. Mrazovac, S. M.; Milan, P. R.; Vojinovic-Miloradov, M. B.; Tosic, B. S., Dynamic model of methane–water diffusion. *Appl. Math. Model.* **2012,** *36* (9), 3985-3991.

158. Leplat, P., GEOCHEMICAL PROSPECTING FOR PETROLEUM. In *Advances in Organic Geochemistry*, Hobson, G. D.; Speers, G. C., Eds. Pergamon: 1970; p 181.
159. Witherspoon, P. A.; Saraf, D. N., Diffusion of Methane, Ethane, Propane, and n-Butane in Water from 25 to 43°. *J. Phys. Chem.* **1965,** *69* (11), 3752-3755.
160. Chen, Y.-A.; Chu, C.-K.; Chen, Y.-P.; Chu, L.-S.; Lin, S.-T.; Chen, L.-J., Measurements of diffusion coefficient of methane in water/brine under high pressure. *Terr. Atmos. Ocean Sci.* **2018,** *29*, 577-587.
161. Jähne, B.; Heinz, G.; Dietrich, W., Measurement of the diffusion coefficients of sparingly soluble gases in water. *J. Geophys. Res. [Oceans]* **1987,** *92* (C10), 10767-10776.
162. Pratt, K. C.; Slater, D. H.; Wakeham, W. A., A rapid method for the determination of diffusion coefficients of gases in liquids. *Chem. Eng. Sci.* **1973,** *28* (10), 1901-1903.
163. Maharajh, D. M.; Walkley, J., The Temperature Dependence of the Diffusion Coefficients of Ar, CO2, CH4, CH3Cl, CH3Br, and CHCl2F in Water. *Can. J. Chem.* **1973,** *51* (6), 944-952.
164. Guo, H.; Chen, Y.; Lu, W.; Li, L.; Wang, M., In situ Raman spectroscopic study of diffusion coefficients of methane in liquid water under high pressure and wide temperatures. *Fluid Phase Equilib.* **2013,** *360*, 274-278.
165. Lu, W. J.; Chou, I. M.; Burruss, R. C.; Yang, M. Z., In situ Study of Mass Transfer in Aqueous Solutions under High Pressures via Raman Spectroscopy: A New Method for the Determination of Diffusion Coefficients of Methane in Water near Hydrate Formation Conditions. *Appl. Spectrosc.* **2006,** *60* (2), 122-129.
166. Gubbins, K. E.; Bhatia, K. K.; Walker Jr., R. D., Diffusion of gases in electrolytic solutions. *AIChE J.* **1966,** *12* (3), 548-552.
167. Guzmán, J.; Garrido, L., Determination of Carbon Dioxide Transport Coefficients in Liquids and Polymers by NMR Spectroscopy. *J. Phys. Chem.* **2012,** *116* (20), 6050-6058.
168. Takeuchi, H.; Fujine, M.; Sato, T.; Onda, K., Simulatneous Determination of Diffusion Coefficients and Solubility of Gas in Liquid by a Diaphragm Cell. *J. Chem. Eng. Jpn.* **1975,** *8* (3), 252-253.
169. Luthjens, L. H.; de Leng, H. C.; Warman, J. M.; Hummel, A., Diffusion coefficients of gaseous scavengers in organic liquids used in radiation chemistry. *International Journal of Radiation Applications and Instrumentation. Part C. Radiation Physics and Chemistry* **1990,** *36* (6), 779-784.
170. Teng, Y.; Liu, Y.; Song, Y.; Jiang, L.; Zhao, Y.; Zhou, X.; Zheng, H.; Chen, J., A Study on CO2 Diffusion Coefficient in n-decane Saturated Porous Media by MRI. *Energy Procedia* **2014,** *61*, 603-606.
171. Nikkhou, F.; Keshavarz, P.; Ayatollahi, S.; Jahromi, I. R.; Zolghadr, A., Evaluation of interfacial mass transfer coefficient as a function of temperature and pressure in carbon dioxide/normal alkane systems. *Heat Mass Transfer.* **2015,** *51* (4), 477-485.
172. Du, D.; Zheng, L.; Ma, K.; Wang, F.; Sun, Z.; Li, Y., Determination of diffusion coefficient of a miscible CO2/n-hexadecane system with Dynamic Pendant Drop Volume Analysis (DPDVA) technique. *Int. J. Heat Mass Transfer* **2019,** *139*, 982-989.
173. Hao, M.; Song, Y.; Su, B.; Zhao, Y., Diffusion of CO2 in n-hexadecane determined from NMR relaxometry measurements. *Phys. Lett. A* **2015,** *379* (18), 1197-1201.
174. Davies, G. A.; Ponter, A. B.; Craine, K., The diffusion of carbon dioxide in organic liquids. *The Canadian Journal of Chemical Engineering* **1967,** *45* (6), 372-376.
175. Hayduk, W.; Cheng, S. C., Review of relation between diffusivity and solvent viscosity in dilute liquid solutions. *Chem. Eng. Sci.* **1971,** *26* (5), 635-646.
176. Pacheco-Roman, F. J.; Hejazi, S. H.; Maini, B. B., Estimation of Low-Temperature Mass-Transfer Properties of Methane and Carbon Dioxide in n-Decane, Hexadecane, and Bitumen Using the Pressure-Decay Technique. *Energy Fuel.* **2016,** *30* (7), 5232-5239.
177. Rezk, M. G.; Foroozesh, J., Determination of mass transfer parameters and swelling factor of CO2-oil systems at high pressures. *Int. J. Heat Mass Transfer* **2018,** *126*, 380-390.
178. Yang, D.; Gu, Y., Determination of Diffusion Coefficients and Interface Mass-Transfer Coefficients of the Crude Oil−CO2 System by Analysis of the Dynamic and Equilibrium Interfacial Tensions. *Ind. Eng. Chem. Res.* **2008,** *47* (15), 5447-5455.
179. Guo, P.; Wang, Z.; Shen, P.; Du, J., Molecular Diffusion Coefficients of the Multicomponent Gas−Crude Oil Systems under High Temperature and Pressure. *Ind. Eng. Chem. Res.* **2009,** *48* (19), 9023-9027.

180. Helbæk, M.; Hafskjold, B.; Dysthe, D. K.; Sørland, G. H., Self-Diffusion Coefficients of Methane or Ethane Mixtures with Hydrocarbons at High Pressure by NMR. *J. Chem. Eng. Data* **1996,** *41* (3), 598-603.
181. Colgate, S. O.; House, V. E.; Thieu, V.; Zachery, K.; Hornick, J.; Shalosky, J., High-pressure cylindrical acoustic resonance diffusion measurements of methane in liquid hydrocarbons. *Int. J. Thermophys.* **1995,** *16* (3), 655-662.
182. Killie, S.; Hafskjold, B.; Borgen, O.; Ratkje, S. K.; Hovde, E., High-pressure diffusion measurements by Mach-Zehnder interferometry. *AIChE J.* **1991,** *37* (1), 142-146.
183. Dysthe, D. K.; Hafskjold, B.; Breer, J.; Cejka, D., Interferometric Technique for Measuring Interdiffusion at High Pressures. *J. Phys. Chem.* **1995,** *99* (28), 11230-11238.
184. Jamialahmadi, M.; Emadi, M.; Müller-Steinhagen, H., Diffusion coefficients of methane in liquid hydrocarbons at high pressure and temperature. *J. Pet. Sci. Eng.* **2006,** *53* (1), 47-60.
185. Yang, C.; Gu, Y., Diffusion coefficients and oil swelling factors of carbon dioxide, methane, ethane, propane, and their mixtures in heavy oil. *Fluid Phase Equilib.* **2006,** *243* (1), 64-73.
186. Svrcek, W. Y., Gas Solubility, Viscosity and Density Measurements for Athabasca Bitumen. *J. Can. Pet. Technol.* **1982,** *21* (4), 38.
187. Mehrotra, A. K., Viscosity, density and gas solubility data for oil sand bitumens. Part III: Wabasca bitumen saturated with N2, CO, CO2 and C2H6. *AOSTRA J. Res.* **1985,** *2.2*, 93.
188. Tharanivasan, A. K.; Yang, C.; Gu, Y., Measurements of Molecular Diffusion Coefficients of Carbon Dioxide, Methane, and Propane in Heavy Oil under Reservoir Conditions. *Energy Fuel.* **2006,** *20* (6), 2509-2517.
189. Cussler, E. L., *Diffusion Mass Transfer in Fluid Systems*. 3rd ed. ed.; Cambridge, New York: Cambridge University Press, 2009 3rd ed.
190. Wilhelm, E.; Battino, R.; Carpenter, R. L., Binary gaseous diffusion coefficients. II. Methane and carbon tetrafluoride with cyclohexane, methylcyclohexane, benzene, and toluene at 1 atm at 10-70.deg. *J. Chem. Eng. Data* **1974,** *19* (3), 245-247.
191. Park, T.; Rettich, T. R.; Battino, R.; Wilhelm, E., Binary gaseous diffusion coefficients. 5. Cyclooctane and trans-1,2-dimethylcyclohexane with helium, argon, and methane, and sulfur hexafluoride at 1 atm and 313-343 K. *J. Chem. Eng. Data* **1987,** *32* (2), 191-193.
192. Denoyelle, L.; Bardon, C., Influence of diffusion on enhanced oil recovery by CO_2 injection. In *In: International symposium on CO2 enhanced oil recovery*, Budapest, Hungary, 1983.
193. Sigmund, P. M., Prediction of Molecular Diffusion At Reservoir Conditions. Part 1-Measurement And Prediction of Binary Dense Gas Diffusion Coefficients. *J. Can. Pet. Tech.* **1976,** *15* (02), 11.
194. da Silva, F. V.; Belery, P., Molecular Diffusion in Naturally Fractured Reservoirs: A Decisive Recovery Mechanism. In *SPE Annual Technical Conference and Exhibition*, Society of Petroleum Engineers: San Antonio, Texas, 1989; p 14.
195. Cadogan, S. P. Diffusion of CO_2 in Fluids Relevant to Carbon Capture, Utilisation and Storage. Imperial College London, London, UK, 2015.
196. Liu, X.; Schnell, S. K.; Simon, J.-M.; Bedeaux, D.; Kjelstrup, S.; Bardow, A.; Vlugt, T. J. H., Fick Diffusion Coefficients of Liquid Mixtures Directly Obtained From Equilibrium Molecular Dynamics. *J. Phys. Chem.* **2011,** *115* (44), 12921-12929.
197. Krishna, R.; van Baten, J. M., The Darken Relation for Multicomponent Diffusion in Liquid Mixtures of Linear Alkanes: An Investigation Using Molecular Dynamics (MD) Simulations. *Ind. Eng. Chem. Res.* **2005,** *44* (17), 6939-6947.
198. Li, S.; Falconer, J. L.; Noble, R. D.; Krishna, R., Modeling Permeation of CO2/CH4, CO2/N2, and N2/CH4 Mixtures Across SAPO-34 Membrane with the Maxwell−Stefan Equations. *Ind. Eng. Chem. Res.* **2007,** *46* (12), 3904-3911.
199. Li, S.; Falconer, J. L.; Noble, R. D.; Krishna, R., Interpreting Unary, Binary, and Ternary Mixture Permeation Across a SAPO-34 Membrane with Loading-Dependent Maxwell−Stefan Diffusivities. *The Journal of Physical Chemistry C* **2007,** *111* (13), 5075-5082.
200. Krishna, R.; van Baten, J. M., Using molecular simulations for screening of zeolites for separation of CO2/CH4 mixtures. *Chem. Eng. J.* **2007,** *133* (1), 121-131.

201. Krishna, R.; van Baten, J. M., Linking the loading dependence of the Maxwell–Stefan diffusivity of linear alkanes in zeolites with the thermodynamic correction factor. *Chem. Phys. Lett.* **2006,** *420* (4), 545-549.
202. Krishna, R.; van Baten, J. M.; García-Pérez, E.; Calero, S., Diffusion of CH4 and CO2 in MFI, CHA and DDR zeolites. *Chem. Phys. Lett.* **2006,** *429* (1), 219-224.
203. Krishna, R.; van Baten, J. M., Diffusion of Alkane Mixtures in Zeolites: Validating the Maxwell−Stefan Formulation Using MD Simulations. *J. Phys. Chem.* **2005,** *109* (13), 6386-6396.
204. Chempath, S.; Krishna, R.; Snurr, R. Q., Nonequilibrium Molecular Dynamics Simulations of Diffusion of Binary Mixtures Containing Short n-Alkanes in Faujasite. *J. Phys. Chem.* **2004,** *108* (35), 13481-13491.
205. dos Santos, T. J. P.; Abreu, C. R. A.; Horta, B. A. C.; Tavares, F. W., Self-diffusion coefficients of methane/n-hexane mixtures at high pressures: An evaluation of the finite-size effect and a comparison of force fields. *The Journal of Supercritical Fluids* **2020,** *155*, 104639.
206. PFITZNER, J., Poiseuille and his law. *Anaesthesia* **1976,** *31* (2), 273-275.
207. Cadogan, S. P.; Hallett, J. P.; Maitland, G. C.; Trusler, J. P. M., Diffusion Coefficients of Carbon Dioxide in Brines Measured Using 13C Pulsed-Field Gradient Nuclear Magnetic Resonance. *J. Chem. Eng. Data* **2015,** *60* (1), 181-184.
208. Alizadeh, A. A.; Wakeham, W. A., Mutual diffusion coefficients for binary mixtures of normal alkanes. *Int. J. Thermophys.* **1982,** *3* (4), 307-323.
209. Aljeshi, Y. A.; Taib, M. B. M.; Trusler, J. P. M., Modelling the Diffusion Coefficients of Dilute Gaseous Solutes in Hydrocarbon Liquids. *Int. J. Thermophys.* **2021,** *42*.
210. Taib, M. B. M.; Trusler, J. P. M., Diffusion Coefficients of Methane in Methylbenzene and Heptane at Temperatures between 323 K and 398 K at Pressures up to 65 MPa. *Int. J. Thermophys.* **2020,** *41* (8), 119.
211. Taib, M. B. M.; Trusler, J. P. M., Correction to: Diffusion Coefficients of Methane in Methylbenzene and Heptane at Temperatures between 323 K and 398 K at Pressures up to 65 MPa. *Int. J. Thermophys.* **2020,** *41* (11), 154.
212. Lu, W.; Guo, H.; Chou, I. M.; Burruss, R. C.; Li, L., Determination of diffusion coefficients of carbon dioxide in water between 268 and 473K in a high-pressure capillary optical cell with in situ Raman spectroscopic measurements. *Geochim. Cosmochim. Acta* **2013,** *115*, 183-204.
213. Sell, A.; Fadaei, H.; Kim, M.; Sinton, D., Measurement of CO2 Diffusivity for Carbon Sequestration: A Microfluidic Approach for Reservoir-Specific Analysis. *Environ. Sci. Technol.* **2013,** *47* (1), 71-78.
214. Riazi, M. R., A new method for experimental measurement of diffusion coefficients in reservoir fluids. *J. Pet. Sci. Eng.* **1996,** *14* (3), 235-250.
215. Sigmund, P. M., Prediction of Molecular Diffusion At Reservoir Conditions. Part II - Estimating the Effects Of Molecular Diffusion And Convective Mixing In Multicomponent Systems. *J. Can. Pet. Tech.* **1976,** *15* (03).
216. Reamer, H. H.; Duffy, C. H.; Sage, B. H., Methane–n-Pentane–Methane in Liquid Phase. *Industrial & Engineering Chemistry* **1956,** *48* (2), 282-284.
217. Reamer, H. H.; Opfell, J. B.; Sage, B. H., Diffusion Coefficients in Hydrocarbon Systems Methane-Decane-Methane in Liquid Phase - Methane-Decane-Methane in Liquid Phase. *Industrial & Engineering Chemistry* **1956,** *48* (2), 275-282.
218. Hayduk, W.; Buckley, W. D., Effect of molecular size and shape on diffusivity in dilute liquid solutions. *Chem. Eng. Sci.* **1972,** *27* (11), 1997-2003.
219. Lemmon, E. W.; Bell, I. H.; Huber, M. L.; McLinden, M. O. *NIST Standard Reference Database 23: Reference Fluid Thermodynamic and Transport Properties-REFPROP, Version 10.0*, National Institute of Standards and Technology: Gaitherburg, 2018.
220. Avgeri, S.; Assael, M. J.; Huber, M. L.; Perkins, R. A., Reference Correlation of the Viscosity of Toluene from the Triple Point to 675 K and up to 500 MPa. *J. Phys. Chem. Ref. Data* **2015,** *44* (3), 033101.
221. Michailidou, E. K.; Assael, M. J.; Huber, M. L.; Abdulagatov, I. M.; Perkins, R. A., Reference Correlation of the Viscosity of n-Heptane from the Triple Point to 600 K and up to 248 MPa. *J. Phys. Chem. Ref. Data* **2014,** *43* (2), 023103.
222. Tenji, D.; Thol, M.; Lemmon, E. W.; Span, R., Fundamental Equation of State for n-Heptane. *to be submitted to Int. J. Thermophys.* **2018**.

223. Antoniadis, K. D.; Assael, M. J.; Wakeham, W. A., Transport Properties of Fluids. In *Encyclopedia of Life Support Systems (EOLSS), Developed under the Auspices of the UNESCO*, Eolss Publishers: Paris, France, 2013.
224. Audonnet, F.; Pádua, A. A. H., Viscosity and density of mixtures of methane and n-decane from 298 to 393 K and up to 75 MPa. *Fluid Phase Equilib.* **2004,** *216* (2), 235-244.
225. Kim, M.-H.; Pettersen, J.; Bullard, C. W., Fundamental process and system design issues in CO2 vapor compression systems. *Prog. Energy Combust. Sci.* **2004,** *30* (2), 119-174.
226. Hernandez; , J. C.; Vesovic, V.; Carter, J. N.; Lopez, E. In *Sensitivity of Reservoir Simulations to Uncertainties in Viscosity*, SPE/DOE Improved Oil Recovery Symposium, 2002.
227. Francke, H.; Thorade, M., Density and viscosity of brine: An overview from a process engineers perspective. *Chem. Erde Geochem.* **2010,** *70*, 23-32.
228. Fitch, B., Viscometers: A Practical Guide. *Machinery Lubrication* 2013.
229. Houari, A., Determining the viscosity of liquids using an extended falling ball method. *Physics Education* **2011,** *46* (6), 688-691.
230. Swindells, J.; Coe, J.; Godfrey, T., Absolute viscosity of water at 20 °C. *J. Research Natl. Bur. Standards* **1952,** *Vol: 48*.
231. Wakeham, W.; Assael, M.; Marmur, A.; Coninck, J.; Blake, T.; Theron, S.; Zussman, E., Material Properties: Measurement and Data. In *Springer Handbook of Experimental Fluid Mechanics*, Tropea, C.; Yarin, A. L.; Foss, J. F., Eds. Springer Berlin Heidelberg: Berlin, Heidelberg, 2007; pp 85-177.
232. Kashefi, K.; Chapoy, A.; Bell, K.; Tohidi, B., Viscosity of binary and multicomponent hydrocarbon fluids at high pressure and high temperature conditions: Measurements and predictions. *J. Pet. Sci. Eng.* **2013,** *112*, 153-160.
233. Maitland, G. C.; Smith, E. B., Viscosities of binary gas mixtures at high temperatures. *Journal of the Chemical Society, Faraday Transactions 1: Physical Chemistry in Condensed Phases* **1974,** *70* (0), 1191-1211.
234. Guevara, F. A.; McInteer, B. B.; Wageman, W. E., High-Temperature Viscosity Ratios for Hydrogen, Helium, Argon, and Nitrogen. *The Physics of Fluids* **1969,** *12* (12), 2493-2505.
235. Trappeniers, N. J.; Botzen, A.; Van Den Berg, H. R.; Van Oosten, J., The viscosity of neon between 25°C and 75°C at pressures up to 1800 atmospheres. Corresponding states for the viscosity of the noble gases up to high densities. *Physica* **1964,** *30* (5), 985-996.
236. Nagashima, A.; Tanishita, I., Viscosity Measurement of Water and Steam at High Temperatures and High Pressures. *Bulletin of JSME* **1969,** *12* (54), 1467-1478.
237. Rivkin, S. L.; Levin, A. Y.; Izrailevskii, L. B.; Kharistonov, K. G., Experimental investigation of the viscosity of heavy water at temperatures of 200–375 °C and pressures up to 500 Bar. *Thermal Engineering* **1972,** *19*, 130-134, English translation of Teploenergetika.
238. Ejima, T.; Shimakage, K.; Sato, Y.; Okuda, H.; Kumada, N.; Ishigaki, A., Viscosity Measurement of Alkali Chlorides with Capillary Viscometer. *Nippon Kagaku Kaishi* **1982,** *1982* (6), 961-968.
239. Isdale, J. D. Viscosity of simple liquids including measurement and prediction at elevated pressure. University of Strathclyde, Strathclyde, 1976.
240. Irving, J. B. Viscosity Measurements at Pressures Up to 14 000 Bar Using an Automatic Falling Cylinder Viscometer. University of Glasgow, Glasgow, 1980.
241. Glen, N. F. Viscosity coefficient measurement at elevated pressure. University of Glasgow, Glasgow, 1983.
242. Dymond, J. H.; Awan, M. A.; Glen, N. F.; Isdale, J. D., Transport properties of nonelectrolyte liquid mixtures. VIII. Viscosity coefficients for toluene and for three mixtures of toluene + hexane from 25 to 100°C at pressures up to 500 MPa. *Int. J. Thermophys.* **1991,** *12* (2), 275-287.
243. Hubbard, R.; Brown, G., Rolling Ball Viscometer. *Industrial & Engineering Chemistry Analytical Edition* **1943,** *15* (3), 212-218.
244. Lewis, H. W., Calibration of Rolling Ball Viscometer. *Anal. Chem.* **1953,** *25* (3), 507-508.
245. Sage, B. H., Measurement of viscosities of liquids saturated with gases at high pressures. *Industrial & Engineering Chemistry Analytical Edition* **1933,** *5 (4)*, 261-263.
246. Nishibata, K.; Izuchi, M., A rolling ball viscometer for high pressure use. *Physica B+C* **1986,** *139-140*, 903-906.

247. Walters, K., *Rheometry*. Chapman and Hall: London, United Kingdom, 1975.
248. Cheng, D. C. H., The effect of secondary flow on the viscosity measurement using the cone-and-plate viscometer. *Chem. Eng. Sci.* **1968,** *23* (8), 895-899.
249. Caudwell, D. R.; Trusler, J. P. M.; Vesovic, V.; Wakeham, W. A., Viscosity and Density of Five Hydrocarbon Liquids at Pressures up to 200 MPa and Temperatures up to 473 K. *J. Chem. Eng. Data* **2009,** *54* (2), 359-366.
250. Mohammed, M. Viscosity and Density of Asymmetric Hydrocarbon Mixtures. Imperial College London, 2016.
251. Liu, Z.; Trusler, J. P. M.; Bi, Q., Viscosities of Liquid Cyclohexane and Decane at Temperatures between (303 and 598) K and Pressures up to 4 MPa Measured in a Dual-Capillary Viscometer. *J. Chem. Eng. Data* **2015,** *60* (8), 2363-2370.
252. Malta, J. Á. M. S. C.; Calabrese, C.; Nguyen, T.-B.; Trusler, J. P. M.; Vesovic, V., Measurements and modelling of the viscosity of six synthetic crude oil mixtures. *Fluid Phase Equilib.* **2020,** *505*, 112343.
253. McBride-Wright, M. Viscosity and density of aqueous fluids with dissolved CO2. Imperial College London, London, United Kingdom, 2014.
254. Caudwell, D. R. Viscosity of dense fluid mixtures. Imperial College London, 2004.
255. Caudwell, D. R.; Trusler, J. P. M.; Vesovic, V.; Wakeham, W. A., The viscosity and density of n-Dodecane and n-Octadecane at pressures up to 200 MPa and temperatures up to 473 K. *Int. J. Thermophys.* **2004,** *25* (5), 1339-1352.
256. Caudwell, D.; Goodwin, A. R. H.; Trusler, J. P. M., A robust vibrating wire viscometer for reservoir fluids: results for toluene and n-decane. *J. Pet. Sci. Eng.* **2004,** *44* (3), 333-340.
257. Assael, M. J.; Papadaki, M.; Dix, M.; Richardson, S. M.; Wakeham, W. A., An absolute vibrating-wire viscometer for liquids at high pressures. *Int. J. Thermophys.* **1991,** *12* (2), 231-244.
258. Assael, M. J.; Oliveira, C. P.; Papadaki, M.; Wakeham, W. A., Vibrating-wire viscometers for liquids at high pressures. *Int. J. Thermophys.* **1992,** *13* (4), 593-615.
259. Peleties, F.; Trusler, M., Viscosity of Liquid Di-isodecyl Phthalate at Temperatures Between (274 and 373) K and at Pressures up to 140 MPa. *J. Chem. Eng. Data* **2011,** *56*.
260. Allal, A.; Moha-ouchane, M.; Boned, C., A New Free Volume Model for Dynamic Viscosity and Density of Dense Fluids Versus Pressure and Temperature. *Phys. Chem. Liq.* **2001,** *39* (1), 1-30.
261. Llovell, F.; Marcos, R. M.; Vega, L. F., Free-Volume Theory Coupled with Soft-SAFT for Viscosity Calculations: Comparison with Molecular Simulation and Experimental Data. *J. Phys. Chem. B* **2013,** *117* (27), 8159-8171.
262. Allal, A.; Boned, C.; Baylaucq, A., Free-volume viscosity model for fluids in the dense and gaseous states. *Physical Review E* **2001,** *64* (1), 011203.
263. Llovell, F.; Marcos, R. M.; Vega, L. F., Transport Properties of Mixtures by the Soft-SAFT plus Free-Volume Theory: Application to Mixtures of n-Alkanes and Hydrofluorocarbons. *J. Phys. Chem. B* **2013,** *117* (17), 5195-5205.
264. Llovell, F.; Vilaseca, O.; Jung, N.; Vega, L. F., Water+1-alkanol systems: Modeling the phase, interface and viscosity properties. *Fluid Phase Equilib.* **2013,** *360*, 367-378.
265. Quinones-Cisneros, S. E.; Deiters, U. K., Generalization of the friction theory for viscosity modeling. *J. Phys. Chem. B* **2006,** *110* (25), 12820-12834.
266. Quiñones Cisneros, S.; K. Zéberg-Mikkelsen, C.; Fernández, J.; Garcia, J., *General friction theory viscosity model for the PC-SAFT equation of state*. 2006; Vol. 52, p 1600-1610.
267. Quiñones-Cisneros, S. E.; Zéberg-Mikkelsen, C. K.; Stenby, E. H., Friction theory prediction of crude oil viscosity at reservoir conditions based on dead oil properties. *Fluid Phase Equilib.* **2003,** *212* (1), 233-243.
268. Quinones-Cisneros, S. E.; Zeberg-Mikkelsen, C. K.; Stenby, E. H., The friction theory (f-theory) for viscosity modeling. *Fluid Phase Equilib.* **2000,** *169* (2), 249-276.
269. Tan, S. P.; Adidharma, H.; Towler, B. F.; Radosz, M., Friction Theory Coupled with Statistical Associating Fluid Theory for Estimating the Viscosity of n-Alkane Mixtures. *Ind. Eng. Chem. Res.* **2006,** *45* (6), 2116-2122.
270. Liu, H. T.; Yang, F. F.; Zhang, K.; Duan, Y. Y.; Yang, Z., Residual Entropy Scaling Model for the Viscosity of Noble Gases. *Kung Cheng Je Wu Li Hsueh Pao/Journal of Engineering Thermophysics* **2021,** *42* (1), 1-8.

271. Mairhofer, J., A residual entropy scaling approach for viscosity based on the GERG-2008 equation of state. *Ind. Eng. Chem. Res.* **2021,** *60* (6), 2652-2662.
272. Taib, M. B. M.; Trusler, J. P. M., Residual entropy model for predicting the viscosities of dense fluid mixtures. *The Journal of Chemical Physics* **2020,** *152* (16), 164104.
273. Lötgering-Lin, O.; Gross, J., Group Contribution Method for Viscosities Based on Entropy Scaling Using the Perturbed-Chain Polar Statistical Associating Fluid Theory. *Ind. Eng. Chem. Res.* **2015,** *54* (32), 7942-7952.
274. Galliero, G.; Boned, C.; Fernández, J., Scaling of the viscosity of the Lennard-Jones chain fluid model, argon, and some normal alkanes. *J. Chem. Phys.* **2011,** *134* (6), 064505.
275. Dehlouz, A.; Privat, R.; Galliero, G.; Bonnissel, M.; Jaubert, J. N., Revisiting the Entropy-Scaling Concept for Shear-Viscosity Estimation from Cubic and SAFT Equations of State: Application to Pure Fluids in Gas, Liquid and Supercritical States. *Ind. Eng. Chem. Res.* **2021,** *60* (34), 12719-12739.
276. Abramson, E. H., Viscosity of carbon dioxide measured to a pressure of 8 GPa and temperature of 673 K. *Physical Review E* **2009,** *80* (2), 021201.
277. Fouad, W. A., Thermal Conductivity of Pure Fluids and Multicomponent Mixtures Using Residual Entropy Scaling with PC-SAFT - Application to Refrigerant Blends. *J. Chem. Eng. Data* **2020,** *65* (12), 5688-5697.
278. Bell, I. H.; Hellmann, R.; Harvey, A. H., Zero-Density Limit of the Residual Entropy Scaling of Transport Properties. *J. Chem. Eng. Data* **2020,** *65* (3), 1038-1050.
279. Vaz, R. V.; Magalhães, A. L.; Fernandes, D. L. A.; Silva, C. M., Universal correlation of self-diffusion coefficients of model and real fluids based on residual entropy scaling law. *Chem. Eng. Sci.* **2012,** *79*, 153-162.
280. Bell, I. H.; Laesecke, A., Viscosity of refrigerants and other working fluids from residual entropy scaling. In *16th International Refrigeration and Air Conditioning Conference* 2016.
281. Novak Lawrence, T., Fluid Viscosity-Residual Entropy Correlation. *Int. J. Chem. React. Eng.* **2011,** *9* (1).
282. Bell, I. H., Probing the link between residual entropy and viscosity of molecular fluids and model potentials. *Proc. Nat. Acad. Sci. U.S.A.* **2019,** *116* (10), 4070-4079.
283. Ciotta, F.; Trusler, J. P. M.; Vesovic, V., Extended hard-sphere model for the viscosity of dense fluids. *Fluid Phase Equilib.* **2014,** *363*, 239-247.
284. de Wijn, A. S.; Vesovic, V.; Jackson, G.; Trusler, J. P. M., A kinetic theory description of the viscosity of dense fluids consisting of chain molecules. *J. Chem. Phys.* **2008,** *128*, 204901.
285. Sun, T.; Teja, A. S., Correlation and Prediction of the Viscosity and Thermal Conductivity of Dense Fluids. *J. Chem. Eng. Data* **2009,** *54* (9), 2527-2531.
286. Assael, M. J.; Dymond, J. H.; Papadaki, M.; Patterson, P. M., Correlation and prediction of dense fluid transport coefficients. *Fluid Phase Equilibria* **1992,** *75*, 245-255.
287. Bannerman, M. N.; Lue, L., Transport properties of highly asymmetric hard-sphere mixtures. *The Journal of Chemical Physics* **2009,** *130* (16), 164507.
288. Jacek, P., Hard-sphere kinetic models for inert and reactive mixtures. *Journal of Physics: Condensed Matter* **2016,** *28* (41), 414022.
289. Pisarev, V.; Kondratyuk, N., Prediction of viscosity-density dependence of liquid methane+n-butane+n-pentane mixtures using the molecular dynamics method and empirical correlations. *Fluid Phase Equilib.* **2019,** *501*.
290. Wijn, A. S. d.; Riesco, N.; Jackson, G.; Trusler, J. P. M.; Vesovic, V., Viscosity of liquid mixtures: The Vesovic-Wakeham method for chain molecules. *J. Chem. Phys.* **2012,** *136* (7), 074514.
291. Riesco, N.; Vesovic, V., Extended hard-sphere model for predicting the viscosity of long-chain n-alkanes. *Fluid Phase Equilib.* **2016,** *425*, 385-392.
292. Cowling, S. C. a. T. G., The Mathematical Theory of Non-uniform Gases: An Account Of The Kinetic Theory Of Viscosity, Thermal Conduction And Diffusion In Gases. *Cambridge University Press, Cambridge, U.K.* **1970**.
293. Neufeld, P. D.; Janzen, A. R.; Aziz, R. A., Empirical Equations to Calculate 16 of the Transport Collision Integrals Ω(l, s)* for the Lennard-Jones (12–6) Potential. *J. Chem. Phys.* **1972,** *57* (3), 1100-1102.

294. Monnery, W. D.; Svrcek, W. Y.; Mehrotra, A. K., Viscosity: A critical review of practical predictive and correlative methods. *The Canadian Journal of Chemical Engineering* **1995,** *73* (1), 3-40.
295. Poling, B. E.; Reid, R. C.; Prausnitz, J. M., *The properties of gases and liquids*. United States, 1987.
296. Yaws, C. L., *Thermophysical properties of chemical and hydrocarbons*. 1st ed.; William Andrew Inc. : Norwich, NY, 2008.
297. Wilke, C. R., A Viscosity Equation for Gas Mixtures. *The Journal of Chemical Physics* **1950,** *18* (4), 517-519.
298. L. Zipperer; F. Herning, Beitrag zur Berechnung der Zähigkeit technischer Gasgemische aus den Zähigkeitswerten der Einzelbestandteile. *Das Gas- und Wasserfach* **1936,** *4:49ff*.
299. van Velzen, D.; Cardozo, R. L.; Langenkamp, H., A Liquid Viscosity-Temperature-Chemical Constitution Relation for Organic Compounds. *Industrial & Engineering Chemistry Fundamentals* **1972,** *11* (1), 20-25.
300. Baled, H. O.; Gamwo, I. K.; Enick, R. M.; McHugh, M. A., Viscosity models for pure hydrocarbons at extreme conditions: A review and comparative study. *Fuel* **2018,** *218*, 89-111.
301. Lohrenz, J.; Bray, B. G.; Clark, C. R., Calculating Viscosities of Reservoir Fluids From Their Compositions. *J. Pet. Technol.* **1964,** *16* (10), 1171-1176.
302. Przedziecki, J. W.; Sridhar, T., Prediction of liquid viscosities. *AIChE J.* **1985,** *31* (2), 333-335.
303. Stephan, K.; Lucas, K., *Viscosity of dense fluids*. 1st edition ed.; Plenum Press: New York, 1979.
304. Alder, B. J.; Gass, D. M.; Wainwright, T. E., Studies in molecular dynamics. VIII. The transport coefficients for a hard-sphere fluid. *The Journal of Chemical Physics* **1970,** *53* (10), 3813-3826.
305. Hansen, J.-P.; McDonald, I. R., Chapter 5 - Perturbation Theory. In *Theory of Simple Liquids (Third Edition)*, Academic Press: Burlington, 2006; pp 109-146.
306. Ciotta, F. Viscosity of asymmetric liquid mixtures under extreme conditions. Imperial College London, London, 2010.
307. Vesovic, V.; Wakeham, W. A., The prediction of the viscosity of dense gas mixtures. *Int. J. Thermophys.* **1989,** *10* (1), 125-132.
308. Vesovic, V.; Wakeham, W. A., Prediction of the viscosity of fluid mixtures over wide ranges of temperature and pressure. *Chem. Eng. Sci.* **1989,** *44* (10), 2181-2189.
309. Davis, H. T.; Rice, S. A.; Sengers, J. V., On the Kinetic Theory of Dense Fluids. IX. The Fluid of Rigid Spheres with a Square-Well Attraction. *The Journal of Chemical Physics* **1961,** *35* (6), 2210-2233.
310. McLaughlin, I. L.; Davis, H. T., Kinetic Theory of Dense Fluid Mixtures. I. Square-Well Model. *The Journal of Chemical Physics* **1966,** *45* (6), 2020-2031.
311. Galliéro, G.; Boned, C.; Baylaucq, A., Molecular Dynamics Study of the Lennard−Jones Fluid Viscosity: Application to Real Fluids. *Ind. Eng. Chem. Res.* **2005,** *44* (17), 6963-6972.
312. Galliero, G.; Nieto-Draghi, C.; Boned, C.; Avalos, J. B.; Mackie, A. D.; Baylaucq, A.; Montel, F., Molecular Dynamics Simulation of Acid Gas Mixtures: A Comparison between Several Approximations. *Ind. Eng. Chem. Res.* **2007,** *46* (15), 5238-5244.
313. Ely, J. F.; Hanley, H. J. M., Prediction of transport properties. 1. Viscosity of fluids and mixtures. *Industrial & Engineering Chemistry Fundamentals* **1981,** *20* (4), 323-332.
314. Pedersen, K. S.; Fredenslund, A.; Christensen, P. L.; Thomassen, P., Viscosity of crude oils. *Chem. Eng. Sci.* **1984,** *39* (6), 1011-1016.
315. Christensen, P. L.; Fredenslund, A. A., A corresponding states model for the thermal conductivity of gases and liquids. *Chem. Eng. Sci.* **1980,** *35* (4), 871-875.
316. Teja, A. S.; Rice, P., Generalized corresponding states method for the viscosities of liquid mixtures. *Industrial & Engineering Chemistry Fundamentals* **1981,** *20* (1), 77-81.
317. Aasberg-Petersen, K.; Knudsen, K.; Fredenslund, A., Prediction of viscosities of hydrocarbon mixtures. *Fluid Phase Equilib.* **1991,** *70* (2), 293-308.
318. Hirschfelder, J. O.; Curtiss, C. F.; Bird, R. B., *Molecular theory of gases and liquids*. 1964.

319. Eyring, H., The Activated Complex in Chemical Reactions. *The Journal of Chemical Physics* **1935,** *3* (2), 107-115.
320. Burgess, W. A.; Tapriyal, D.; Gamwo, I. K.; Morreale, B. D.; McHugh, M. A.; Enick, R. M., Viscosity Models Based on the Free Volume and Frictional Theories for Systems at Pressures to 276 MPa and Temperatures to 533 K. *Ind. Eng. Chem. Res.* **2012,** *51* (51), 16721-16733.
321. Llovell, F.; Marcos, R. M.; Vega, L. F., Transport Properties of Mixtures by the Soft-SAFT + Free-Volume Theory: Application to Mixtures of n-Alkanes and Hydrofluorocarbons. *J. Phys. Chem. B* **2013,** *117*, 5195.
322. Llovell, F.; Marcos, R. M.; Vega, L. F., Free-Volume Theory Coupled with Soft-SAFT for Viscosity Calculations: Comparison with Molecular Simulation and Experimental Data. *J. Phys. Chem. B* **2013,** *117*, 8159.
323. Rosenfeld, Y., Relation between the transport coefficients and the internal entropy of simple systems. *Phys. Rev. A* **1977,** *15* (6), 2545-2549.
324. Dyre, J. C., Perspective: Excess-entropy scaling. *J. Chem. Phys.* **2018,** *149* (21), 210901.
325. Dzugutov, M., A universal scaling law for atomic diffusion in condensed matter. *Nature* **1996,** *381*, 137.
326. Chopra, R.; Truskett, T. M.; Errington, J. R., On the Use of Excess Entropy Scaling to Describe the Dynamic Properties of Water. *J. Phys. Chem. B* **2010,** *114* (32), 10558-10566.
327. Chopra, R.; Truskett, T. M.; Errington, J. R., Excess entropy scaling of dynamic quantities for fluids of dumbbell-shaped particles. *J. Chem. Phys.* **2010,** *133* (10), 104506.
328. Chopra, R.; Truskett, T. M.; Errington, J. R., On the Use of Excess Entropy Scaling To Describe Single-Molecule and Collective Dynamic Properties of Hydrocarbon Isomer Fluids. *J. Phys. Chem. B* **2010,** *114* (49), 16487-16493.
329. Goel, T.; Patra, C. N.; Mukherjee, T.; Chakravarty, C., Excess entropy scaling of transport properties of Lennard-Jones chains. *J. Chem. Phys.* **2008,** *129* (16), 164904.
330. Lötgering-Lin, O.; Gross, J., Group Contribution Method for Viscosities Based on Entropy Scaling Using the Perturbed-Chain Polar Statistical Associating Fluid Theory. *Ind. Eng. Chem. Res.* **2015,** *54* (32), 7942-7952.
331. Hopp, M.; Mele, J.; Gross, J., Self-Diffusion Coefficients from Entropy Scaling Using the PCP-SAFT Equation of State. *Ind. Eng. Chem. Res.* **2018,** *57* (38), 12942-12950.
332. Hopp, M.; Gross, J., Thermal Conductivity of Real Substances from Excess Entropy Scaling Using PCP-SAFT. *Ind. Eng. Chem. Res.* **2017,** *56* (15), 4527-4538.
333. Hopp, M.; Gross, J., Thermal Conductivity from Entropy Scaling: A Group-Contribution Method. *Ind. Eng. Chem. Res.* **2019,** *58* (44), 20441-20449.
334. Hopp, M.; Mele, J.; Hellmann, R.; Gross, J., Thermal Conductivity via Entropy Scaling: An Approach That Captures the Effect of Intramolecular Degrees of Freedom. *Ind. Eng. Chem. Res.* **2019,** *58* (39), 18432-18438.
335. Lötgering-Lin, O.; Fischer, M.; Hopp, M.; Gross, J., Pure Substance and Mixture Viscosities Based on Entropy Scaling and an Analytic Equation of State. *Ind. Eng. Chem. Res.* **2018,** *57* (11), 4095-4114.
336. Fouad, W. A.; Vega, L. F., On the anomalous composition dependence of viscosity and surface tension in refrigerant blends. *J. Mol. Liq.* **2018,** *268*, 190-200.
337. Fouad, W. A.; Vega, L. F., Transport properties of HFC and HFO based refrigerants using an excess entropy scaling approach. *J. Supercrit. Fluids* **2018,** *131*, 106-116.
338. Rokni, H. B.; Moore, J. D.; Gupta, A.; Mhugh, M. A.; Gavaises, M., Entropy scaling based viscosity predictions for hydrocarbon mixtures and diesel fuels up to extreme conditions. *Fuel* **2019,** *241*, 1203-1213.
339. Novak, L. T., Predicting Natural Gas Viscosity with a Mixture Viscosity Model for the Entire Fluid Region. *Ind. Eng. Chem. Res.* **2013,** *52* (45), 16014-16018.
340. Delage-Santacreu, S.; Galliero, G.; Hoang, H.; Bazile, J.-P.; Boned, C.; Fernandez, J., Thermodynamic scaling of the shear viscosity of Mie n-6 fluids and their binary mixtures. *J. Chem. Phys.* **2015,** *142* (17), 174501.
341. Davani, E.; Falcone, G.; Teodoriu, C.; McCain, W. D., Jr., HPHT viscosities measurements of mixtures of methane/nitrogen and methane/carbon dioxide. *Journal of Natural Gas Science and Engineering* **2013,** *12*, 43-55.

342. Locke, C. R.; Stanwix, P. L.; Hughes, T. J.; Johns, M. L.; Goodwin, A. R. H.; Marsh, K. N.; Galliero, G.; May, E. F., Viscosity of {xCO(2) + (1-x)CH4} with x=0.5174 for temperatures between (229 and 348) K and pressures between (1 and 32) MPa. *J. Chem. Thermodyn.* **2015,** *87*, 162-167.
343. Kestin, J.; Ro, S. T., The Viscosity of Nine Binary and Two Ternary Mixtures of Gases at Low Density. *Ber. Bunsen-Ges. Phys. Chem.* **1974,** *78* (1), 20-24.
344. Kestin, J.; Yata, J., Viscosity and Diffusion Coefficient of Six Binary Mixtures. *The Journal of Chemical Physics* **1968,** *49* (11), 4780-4791.
345. Jackson, W. M., Viscosities Of The Binary Gas Mixtures, Methane-Carbon Dioxide And Ethylent-Argon. *J. Phys. Chem.* **1956,** *60* (6), 789-791.
346. Diller, D. E., Measurements of the viscosity of compressed gaseous and liquid methane + ethane mixtures. *J. Chem. Eng. Data* **1984,** *29* (2), 215-221.
347. Abe, Y.; Kestin, J.; Khalifa, H. E.; Wakeham, W. A., The Viscosity and Diffusion Coefficients of the Mixtures of Light Hydrocarbons with Other Polyatomic Gases. *Ber. Bunsen-Ges. Phys. Chem.* **1979,** *83* (3), 271-276.
348. Abe, Y.; Kestin, J.; Khalifa, H. E.; Wakeham, W. A., Viscosity and diffusion coefficients of mixtures of four light-hydrocarbon gases. *Physica A* **1978,** *93* (1-2), 155-170.
349. Diller, D. E.; Van Poolen, L. J.; Dos Santos, F. V., Measurements of the viscosities of compressed fluid and liquid carbon dioxide + ethane mixtures. *J. Chem. Eng. Data* **1988,** *33* (4), 460-464.
350. Humberg, K.; Richter, M.; Trusler, J. P. M.; Span, R., Measurements and modelling of the viscosity of (methane + ethane) mixtures at temperatures from (253.15 to 473.15)K with pressures up to 2 MPa. *J. Chem. Thermodyn.* **2020,** *147*, 106104.
351. Giddings, J. G.; Kao, J. T. F.; Kobayashi, R., Development of a High-Pressure Capillary-Tube Viscometer and Its Application to Methane, Propane, and Their Mixtures in the Gaseous and Liquid Regions. *The Journal of Chemical Physics* **1966,** *45* (2), 578-586.
352. Huang, E. T. S.; Swift, G. W.; Kurata, F., Viscosities and densities of methane-propane mixtures at low temperatures and high pressures. *AIChE J.* **1967,** *13* (5), 846-850.
353. Gozalpour, F.; Danesh, A.; Todd, A. C.; Tohidi, B., Viscosity, density, interfacial tension and compositional data for near critical mixtures of methane plus butane and methane plus decane systems at 310.95 K. *Fluid Phase Equilib.* **2005,** *233* (2), 144-150.
354. Czubinski, F. F.; Al Ghafri, S. Z. S.; Hughes, T. J.; Stanwix, P. L.; May, E. F., Viscosity of a xCH(4) + (1-x)C3H8 mixture with x=0.8888 at temperatures between (203 and 424) K and pressures between (2 and 31) MPa. *Fuel* **2018,** *225*, 563-572.
355. Stanwix, P. L.; Locke, C. R.; Hughes, T. J.; Johns, M. L.; Goodwin, A. R. H.; Marsh, K. N.; May, E. F., Viscosity of {xCH(4) + (1-x)C3H8} with x=0.949 for Temperatures between (200 and 423) K and Pressures between (10 and 31) MPa. *J. Chem. Eng. Data* **2015,** *60* (1), 118-123.
356. Locke, C. R.; Stanwix, P. L.; Hughes, T. J.; Kisselev, A.; Goodwin, A. R. H.; Marsh, K. N.; May, E. F., Improved Methods for Gas Mixture Viscometry Using a Vibrating Wire Clamped at Both Ends. *J. Chem. Eng. Data* **2014,** *59* (5), 1619-1628.
357. Carmichael, L. T.; Berry, V. M.; Sage, B. H., Viscosity of a mixture of methane and butane. *J. Chem. Eng. Data* **1967,** *12* (1), 44-47.
358. Dolan, J. P.; Ellington, R. T.; Lee, A. L., Viscosity of Methane-n-Butane Mixtures. *J. Chem. Eng. Data* **1964,** *9* (4), 484-487.
359. Locke, C. R.; Fang, D.; Stanwix, P. L.; Hughes, T. J.; Xiao, G.; Johns, M. L.; Goodwin, A. R. H.; Marsh, K. N.; May, E. F., Viscosity and Dew Point Measurements of {xCH(4) + (1-x)C4H10} for x=0.9484 with a Vibrating-Wire Viscometer. *J. Chem. Eng. Data* **2015,** *60* (12), 3688-3695.
360. Diaz Pena, M.; Cheda, J. A. R., Viscosity of Alkane Mixtures. *An. Quim.* **1975,** *71*, 257-261.
361. Bagzis, L. D. Viscosity of Saturated Hydrocarbon Mixtures. MSc. Thesis, Oklahoma State University, 1969.
362. Kian, K.; Scurto, A. M., Viscosity of compressed CO2-saturated n-alkanes: CO2/n-hexane, CO2/n-decane, and CO2/n-tetradecane. *The Journal of Supercritical Fluids* **2018,** *133*, 411-420.

363. Rabe, D. Experimental Determination of Dynamic Viscosity and Density of Binary Liquid Mixtures of n-Heptane with CO2, CH4, C2H6, C3H8 and of Toluene with CH4 and C3H8. TU Berlin, Berlin, 1981
364. Volkov, O. I. K. V. S., Viscosity of Solutions of Methane in n-Octane and n-Decane on the Fluid-Vapour Equilibrium Line. *Ukr. khim. Zh. Russ.* **1974,** (40), 88-90.
365. Barrufet, M. A.; Salem, S. K. E.-S.; Tantawy, M.; Iglesias-Silva, G. A., Liquid Viscosities of Carbon Dioxide + Hydrocarbons from 310 K to 403 K. *J. Chem. Eng. Data* **1996,** *41* (3), 436-439.
366. Cullick, A. S.; Mathis, M. L., Densities and viscosities of mixtures of carbon dioxide and n-decane from 310 to 403 K and 7 to 30 MPa. *J. Chem. Eng. Data* **1984,** *29* (4), 393-396.
367. Lee, A. L.; Eakin, B. E., Viscosity of Methane-n-Decane Mixtures. *J. Chem. Eng. Data* **1966,** *11* (3), 281-287.
368. Kariznovi, M.; Nourozieh, H.; Abedi, J., Phase composition and saturated liquid properties in binary and ternary systems containing carbon dioxide, n-decane, and n-tetradecane. *J. Chem. Thermodyn.* **2013,** *57*, 189-196.
369. Dauge, P.; Baylaucq, A.; Marlin, L.; Boned, C., Development of an isobaric transfer viscometer operating up to 140 MPa. Application to a methane plus decane system. *J. Chem. Eng. Data* **2001,** *46* (4), 823-830.
370. Nourozieh, H.; Kariznovi, M.; Abedi, J., Measurement and correlation of saturated liquid properties and gas solubility for decane, tetradecane and their binary mixtures saturated with carbon dioxide. *Fluid Phase Equilib.* **2013,** *337*, 246-254.
371. Canet, X.; Baylaucq, A.; Boned, C., High-pressure (up to 140 MPa) dynamic viscosity of the methane plus decane system. *Int. J. Thermophys.* **2002,** *23* (6), 1469-1486.
372. Peleties, F. Advanced Fluid Property Measurement for Oilfield Applications. Imperial College London, London, 2007.
373. Daridon, J.-L.; Cassiède, M.; Paillol, J. H.; Pauly, J., Viscosity measurements of liquids under pressure by using the quartz crystal resonators. *Rev. Sci. Instrum.* **2011,** *82* (9), 095114.
374. Knapstad, B.; Skjølsvik, P. A.; Øye, H. A., Viscosity of the n-Decane—Methane System in the Liquid Phase. *Ber. Bunsen-Ges. Phys. Chem.* **1990,** *94* (10), 1156-1165.
375. Nourozieh, H.; Kariznovi, M.; Abedi, J., Vapor–liquid equilibrium measurement and thermodynamic modeling of binary systems (methane+n-tetradecane). *Fluid Phase Equilib.* **2012,** *318*, 96-101.
376. Kariznovi, M.; Nourozieh, H.; Abedi, J., Measurement and equation of state prediction of vapor–liquid equilibrium and physical properties for the system methane+n-octadecane. *Fluid Phase Equilib.* **2012,** *314*, 102-106.
377. Ciotta, F.; Maitland, G.; Smietana, M.; Trusler, J. P. M.; Vesovic, V., Viscosity and Density of Carbon Dioxide + 2,6,10,15,19,23-Hexamethyltetracosane (Squalane). *J. Chem. Eng. Data* **2010,** *55* (9), 4126-4126.
378. Tomida, D.; Kumagai, A.; Yokoyama, C., Viscosity Measurements and Correlation of the Squalane + CO2 Mixture. *Int. J. Thermophys.* **2007,** *28* (1), 133-145.
379. Binti Mohd Taib, M.; Trusler, J. P. M., Viscosity and Density of 1,3-Dimethylbenzene + Carbon Dioxide at Temperatures from 298 to 423 K and at Pressures up to 100 MPa. *J. Chem. Eng. Data* **2020,** *65* (4), 2186-2193.
380. Baylaucq, A.; Boned, C.; Canet, X.; Zéberg-Mikkelsen, C.; Quiñones Cisneros, S.; Zhou, H., Dynamic Viscosity Modeling of Methane + n-Decane and Methane + Toluene Mixtures : Comparative Study of Some Representative Models. *Pet. Sci. Technol.* **2005,** *23*, 143-157.
381. Baylaucq, A.; Boned, C.; Canet, X.; Zéberg-Mikkelsen, C. K., High-Pressure (up to 140 MPa) Dynamic Viscosity of the Methane and Toluene System: Measurements and Comparative Study of Some Representative Models. *Int. J. Thermophys.* **2003,** *24* (3), 621-638.
382. Thol, M.; Richter, M., Dynamic Viscosity of Binary Fluid Mixtures: A Review Focusing on Asymmetric Mixtures. *Int. J. Thermophys.* **2021,** *42* (11), 37.
383. Hu, R.; Crawshaw, J. P.; Trusler, J. P. M.; Boek, E. S., Rheology and Phase Behavior of Carbon Dioxide and Crude Oil Mixtures. *Energy Fuel.* **2017,** *31* (6), 5776-5784.
384. Zhou, Y.; Wu, J. T.; Lemmon, E. W., Thermodynamic Properties of o-Xylene, m-Xylene, p-Xylene, and Ethylbenzene. *J. Phys. Chem. Ref. Data* **2012,** *41* (2), 26.

385. Harris, K. R.; Bair, S., Temperature and Pressure Dependence of the Viscosity of Diisodecyl Phthalate at Temperatures between (0 and 100) °C and at Pressures to 1 GPa. *J. Chem. Eng. Data* **2007,** *52* (1), 272-278.
386. Caetano, F. J. P.; Fareleira, J. M. N. A.; Oliveira, C. M. B. P.; Wakeham, W. A., New Measurements of the Viscosity of Diisodecyl Phthalate Using a Vibrating Wire Technique. *J. Chem. Eng. Data* **2005,** *50* (6), 1875-1878.
387. Caetano, F. J. P.; Fareleira, J. M. N. A.; Oliveira, C. M. B. P.; Wakeham, W. A., Viscosity of di-isodecylphthalate: A potential standard of moderate viscosity. *Int. J. Thermophys.* **2004,** *25* (5), 1311-1322.
388. Caetano, F. J. P.; Fareleira, J. M. N. A.; Fernandes, A. C.; Oliveira, C. M. B. P.; Serro, A. P.; Simões de Almeida, I. M.; Wakeham, W. A., Diisodecylphthalate (DIDP)—a potential standard of moderate viscosity: Surface tension measurements and water content effect on viscosity. *Fluid Phase Equilib.* **2006,** *245* (1), 1-5.
389. Caetano, F. J. P.; Fareleira, J. M. N. A.; Fröba, A. P.; Harris, K. R.; Leipertz, A.; Oliveira, C. M. B. P.; Trusler, J. P. M.; Wakeham, W. A., An Industrial Reference Fluid for Moderately High Viscosity. *J. Chem. Eng. Data* **2008,** *53* (9), 2003-2011.
390. Peleties, F.; Segovia, J. J.; Trusler, J. P. M.; Vega-Maza, D., Thermodynamic properties and equation of state of liquid di-isodecyl phthalate at temperature between (273 and 423)K and at pressures up to 140MPa. *J. Chem. Thermodyn.* **2010,** *42* (5), 631-639.
391. Peleties, F.; Martin Trusler, J. P.; Goodwin, A. R. H.; Maitland, G. C., Circulating pump for high-pressure and high-temperature applications. *Rev. Sci. Instrum.* **2005,** *76* (10), 3.
392. Xu, X. C.; Jaubert, J. N.; Privat, R.; Arpentinier, P., Prediction of Thermodynamic Properties of Alkyne-Containing Mixtures with the E-PPR78 Model. *Ind. Eng. Chem. Res.* **2017,** *56* (28), 8143-8157.
393. Assael, M. J.; Papadaki, M.; Wakeham, W. A., Measurements of the viscosity of benzene, toluene, and m-Xylene at pressure up to 80 MPa. *Int. J. Thermophys.* **1991,** *12* (3), 449-457.
394. Et-Tahir, A.; Boned, C.; Lagourette, B.; Xans, P., Determination of the viscosity of various hydrocarbons and mixtures of hydrocarbons versus temperature and pressure. *Int. J. Thermophys.* **1995,** *16* (6), 1309-1334.
395. Kashiwagi, H.; Makita, T., Viscosity of twelve hydrocarbon liquids in the temperature range 298–348 K at pressures up to 110 MPa. *Int. J. Thermophys.* **1982,** *3* (4), 289-305.
396. Meng, X. Y.; Gu, X. Y.; Wu, J. T.; Vesovic, V., Viscosity measurements of ortho-Xylene, meta-Xylene, para-Xylene and ethylbenzene. *J. Chem. Thermodyn.* **2016,** *95*, 116-123.
397. Yang, T. Y.; Xia, S. Q.; Song, S.; Fu, X. X.; Ma, P. S., Densities and viscosities of N-formylmorpholine (NFM) plus p-Xylene, plus o-Xylene, plus m-Xylene at different temperatures and atmospheric pressure. *J. Chem. Eng. Data* **2007,** *52* (5), 2062-2066.
398. Lemmon, E. W.; Bell, I. H.; Huber, M. L.; McLinden, M. O., NIST Standard Reference Database 23: Reference Fluid Thermodynamics and Transport properties-REFPROP, Version 10.0, National Institute of Standard and Technology. **2018**.
399. Cao, F. L.; Meng, X. Y.; Wu, J. T.; Vesovic, V., Reference Correlation of the Viscosity of meta-Xylene from 273 to 673 K and up to 200 MPa. *J. Phys. Chem. Ref. Data* **2016,** *45* (1), 12.
400. Calabrese, C. Viscosity and Density of Reservoir Fluids with Dissolved CO2. Imperial College of London, London, 2017.
401. Span, R.; Wagner, W., Equations of state for technical applications. II. Results for nonpolar fluids. *Int. J. Thermophys.* **2003,** *24* (1), 41-109.
402. Michailidou, E. K.; Assael, M. J.; Huber, M. L.; Perkins, R. A., Reference Correlation of the Viscosity of n-Hexane from the Triple Point to 600 K and up to 100 MPa. *J. Phys. Chem. Ref. Data* **2013,** *42* (3), 033104.
403. Span, R.; Wagner, W., A new equation of state for carbon dioxide covering the fluid region from the triple-point temperature to 1100 K at pressures up to 800 MPa. *J. Phys. Chem. Ref. Data* **1996,** *25* (6), 1509-1596.
404. Span, R.; Lemmon, E. W.; Jacobsen, R. T.; Wagner, W.; Yokozeki, A., A Reference Equation of State for the Thermodynamic Properties of Nitrogen for Temperatures from 63.151 to 1000 K and Pressures to 2200 MPa. *J. Phys. Chem. Ref. Data* **2000,** *29* (6), 1361-1433.
405. Lemmon, E. W.; Jacobsen, R. T., Viscosity and Thermal Conductivity Equations for Nitrogen, Oxygen, Argon, and Air. *Int. J. Thermophys.* **2004,** *25* (1), 21-69.

406. Wagner, W.; Pruss, A., The IAPWS Formulation 1995 for the Thermodynamic Properties of Ordinary Water Substance for General and Scientific Use. *J. Phys. Chem. Ref. Data* **2002,** *31* (2), 387-535.
407. Ciotta, F.; Trusler, J. P. M., Improved Understanding of Vibrating-Wire Viscometer−Densimeters. *J. Chem. Eng. Data* **2010,** *55* (6), 2195-2201.
408. Huber, M. L.; Laesecke, A.; Xiang, H. W., Viscosity correlations for minor constituent fluids in natural gas: n-Octane, n-Nonane and n-Decane. *Fluid Phase Equilib.* **2004,** *224* (2), 263-270.
409. Wong, C. K.; Qiu, F. *Experimental Measurement of viscosity of the binary mixture of m-Xylene and CO2*; Report, Imperial College London London, UK, 2017.
410. Comunas, M. J. P.; Baylaucq, A.; Boned, C.; Fernandez, J., High-pressure measurements of the viscosity and density of two polyethers and two dialkyl carbonates. *Int. J. Thermophys.* **2001,** *22* (3), 749-768.
411. Dymond, J. H.; Malhotra, R., THE TAIT EQUATION - 100 YEARS ON. *Int. J. Thermophys.* **1988,** *9* (6), 941-951.
412. Fesard, A. *Viscosity and Density of liquid Diisodecyl-phthalate with dissolved CO2 at Temperatures between 313 and 373K and Pressures up to 800 bar*; Report, Imperial College London: London, UK, 2018.
413. Laesecke, A.; Muzny, C. D., Reference Correlation for the Viscosity of Carbon Dioxide. *J. Phys. Chem. Ref. Data* **2017,** *46* (1), 013107.
414. Rosenfeld, Y., A quasi-universal scaling law for atomic transport in simple fluids. *J. Phys.: Condens. Matter* **1999,** *11* (28), 5415.
415. Hoover, W. G., *Molecular dynamics*. Springer: 1986; Vol. 258.
416. Gnan, N.; Schrøder, T. B.; Pedersen, U. R.; Bailey, N. P.; Dyre, J. C., Pressure-energy correlations in liquids. IV. “Isomorphs” in liquid phase diagrams. *The Journal of Chemical Physics* **2009,** *131* (23), 234504.
417. Huber, M. L. *Models for Viscosity. Thermal Conductivity, and Surface Tension of Selected Pure Fluids as Implemented in REFPROP v10.0*; 2018.
418. Novak, L., Self-Diffusion Coefficient and Viscosity in Fluids. *Int. J. Chem. React. Eng.* **2011,** *9* (1).
419. Novak, L. T., Predictive Corresponding-States Viscosity Model for the Entire Fluid Region: n-Alkanes. *Ind. Eng. Chem. Res.* **2013,** *52* (20), 6841-6847.
420. Bell, I. H.; Messerly, R.; Thol, M.; Costigliola, L.; Dyre, J. C., Modified Entropy Scaling of the Transport Properties of the Lennard-Jones Fluid. *J. Phys. Chem.* **2019,** *123* (29), 6345-6363.
421. Lemmon, E. W. A generalized model for the prediction of the thermodynamic properties of mixtures including vapor-liquid equilibrium. University of Idaho, 1996.
422. Kunz, O.; Klimeck, R.; Wagner, W.; Jaeschke, M., *The GERG-2004 wide range equation of state for natural gases and other mixtures GERG TM15 2007*. VDI-Verl.: Düsseldorf, 2007.
423. Kunz, O.; Wagner, W., The GERG-2008 Wide-Range Equation of State for Natural Gases and Other Mixtures: An Expansion of GERG-2004. *J. Chem. Eng. Data* **2012,** *57* (11), 3032-3091.
424. Knez, Ž.; Škerget, M.; Ilič, L.; Lütge, C., Vapor–liquid equilibrium of binary CO2–organic solvent systems (ethanol, tetrahydrofuran, ortho-xylene, meta-xylene, para-xylene). *The Journal of Supercritical Fluids* **2008,** *43* (3), 383-389.
425. Walther, D.; Platzer, B.; Maurer, G., High-pressure (vapour + liquid) equilibria of (carbon dioxide + methylbenzene or 1,2-dimethylbenzene or 1,3-dimethylbenzene or 1,4-dimethylbenzene) at temperatures between 313 K and 393 K and pressures up to 17.3 MPa. *J. Chem. Thermodyn.* **1992,** *24* (4), 387-399.
426. Vera, J. H.; Orbey, H., Binary vapor-liquid equilibria of carbon dioxide with 2-methyl-1-pentene, 1-hexene, 1-heptene, and m-xylene at 303.15, 323.15, and 343.15 K. *J. Chem. Eng. Data* **1984,** *29* (3), 269-272.
427. Sebastian, H. M.; Simnick, J. J.; Lin, H.-M.; Chao, K.-C., Gas-liquid equilibrium in mixtures of carbon dioxide + toluene and carbon dioxide + m-xylene. *J. Chem. Eng. Data* **1980,** *25* (3), 246-248.

428. Mohamed, R. S.; Holder, G. D., High pressure phase behavior in systems containing CO2 and heavier compounds with similar vapor pressures. *Fluid Phase Equilib.* **1987,** *32* (3), 295-317.
429. Ng, H. J.; Huang, S. S. S.; Robinson, D. B., Equilibrium phase properties of selected m-xylene binary systems. m-Xylene-methane and m-xylene carbon dioxide. *J. Chem. Eng. Data* **1982,** *27* (2), 119-122.
430. Byrne, J. E.; Battino, R.; Wilhelm, E., The solubility of gases in liquids 8. Solubility of He, Ne, Ar, Kr, CO2, CH4, CF4, and SF6 in o-, m-, and p-xylene at 283 to 313 K. *J. Chem. Thermodyn.* **1975,** *7* (6), 515-522.
431. Galliero, G.; Boned, C., Thermal conductivity of the Lennard-Jones chain fluid model. *Physical Review E* **2009,** *80* (6), 061202.
432. Gerek, Z. N.; Elliott, J. R., Self-Diffusivity Estimation by Molecular Dynamics. *Ind. Eng. Chem. Res.* **2010,** *49* (7), 3411-3423.
433. Johnson, M. E.; Head-Gordon, T., Assessing thermodynamic-dynamic relationships for waterlike liquids. *J. Chem. Phys.* **2009,** *130* (21), 214510.
434. Agarwal, M.; Singh, M.; Sharma, R.; Parvez Alam, M.; Chakravarty, C., Relationship between Structure, Entropy, and Diffusivity in Water and Water-Like Liquids. *J. Phys. Chem.* **2010,** *114* (20), 6995-7001.
435. Zmpitas, J.; Gross, J., Modified Stokes-Einstein Equation for Molecular Self-Diffusion Based on Entropy Scaling. *Ind. Eng. Chem. Res.* **2021,** *60* (11), 4453-4459.
436. Bell, I. H., Entropy Scaling of Viscosity - II: Predictive Scheme for Normal Alkanes. *J. Chem. Eng. Data* **2020,** *65* (11), 5606-5616.
437. Bell, I. H., Entropy Scaling of Viscosity - I: A Case Study of Propane. *J. Chem. Eng. Data* **2020,** *65* (6), 3203-3215.
438. Yang, X.; Xiao, X.; May, E. F.; Bell, I. H., Entropy Scaling of Viscosity—III: Application to Refrigerants and Their Mixtures. *J. Chem. Eng. Data* **2021,** *66* (3), 1385-1398.
439. Mairhofer, J., A Residual Entropy Scaling Approach for Viscosity Based on the GERG-2008 Equation of State. *Ind. Eng. Chem. Res.* **2021,** *60* (6), 2652-2662.
440. Bell, I. H., Entropy Scaling of Viscosity—I: A Case Study of Propane. *J. Chem. Eng. Data* **2020,** *65* (6), 3203-3215.
441. Hopp, M.; Gross, J., Thermal Conductivity of Real Substances from Excess Entropy Scaling Using PCP-SAFT. *Ind. Eng. Chem. Res.* **2017,** *56* (15), 4527-4538.
442. Yang, X.; Kim, D.; May, E. F.; Bell, I. H., Entropy Scaling of Thermal Conductivity: Application to Refrigerants and Their Mixtures. *Ind. Eng. Chem. Res.* **2021**.
443. Bell, I. H., Entropy Scaling of Viscosity—II: Predictive Scheme for Normal Alkanes. *J. Chem. Eng. Data* **2020,** *65* (11), 5606-5616.
444. Fenghour, A.; Wakeham, W. A.; Vesovic, V., The Viscosity of Carbon Dioxide. *J. Phys. Chem. Ref. Data* **1998,** *27* (1), 31-44.
445. Iwasaki, H.; Takahashi, M., Viscosity of carbon dioxide and ethane. *J. Chem. Phys.* **1981,** *74* (3), 1930-1943.
446. Badalyan, A. G.; Rodchenko, S. I., Viscosity of n-Octane. *IzV. Vyssh. Uchebn. ZaVed. Neft I Gaz* **1986,** *29*, 61-64.
447. Assael, M. J.; Dymond, J. H.; Papadaki, M., VISCOSITY COEFFICIENTS OF BINARY N-HEPTANE+N-ALKANE MIXTURES. *Fluid Phase Equilib.* **1992,** *75*, 287-297.
448. Carmichael, L. T.; Berry, V. M.; Sage, B. H., Viscosity of hydrocarbons. n-decane. *J. Chem. Eng. Data* **1969,** *14* (1), 27-31.
449. Yang, Z.; Bi, Q.; Feng, S., Viscosity Measurement of Endothermic Fuels at Temperatures from 303 K to 673 K and Pressures up to 5.00 MPa. *J. Chem. Eng. Data* **2016,** *61* (10), 3472-3480.
450. Stephan, K.; Heckenberger, T., Thermal Conductivity and Viscosity data of Fluid Mixtures. *Ber. Bunsen-Ges. Phys. Chem.* **1990,** *94* (10), 1170-1171.
451. Galliéro, G.; Boned, C.; Baylaucq, A.; Montel, F., Influence of the mass ratio on viscosity in Lennard–Jones mixtures: The one-fluid model revisited using nonequilibrium molecular dynamics. *Fluid Phase Equilib.* **2005,** *234* (1-2), 56-63.
452. Hu, R.; Crawshaw, J. P.; Trusler, J. P. M.; Boek, E. S., Rheology of Diluted Heavy Crude Oil Saturated with Carbon Dioxide. *Energy Fuel.* **2015,** *29* (5), 2785-2789.

507. Ciotta, F.; Maitland, G.; Smietana, M.; Trusler, J. P. M.; Vesovic, V., Viscosity and Density of Carbon Dioxide+2,6,10,15,19,23-Hexamethyltetracosane (Squalane). *J. Chem. Eng. Data* **2009,** *54* (9), 2436-2443.
508. Hu, R.; Crawshaw, J. P.; Trusler, J. P. M.; Boek, E. S., Rheology and Phase Behavior of Carbon Dioxide and Crude Oil Mixtures. *Energy Fuel.* **2017,** *31* (6), 5776-5784.
509. Zhou, Y.; Wu, J. T.; Lemmon, E. W., Thermodynamic Properties of o-Xylene, m-Xylene, p-Xylene, and Ethylbenzene. *J. Phys. Chem. Ref. Data* **2012,** *41* (2), 26.
510. Yang, X.; Xiao, X.; May, E. F.; Bell, I. H., Entropy Scaling of Viscosity—III: Application to Refrigerants and Their Mixtures. *J. Chem. Eng. Data* **2021,** *66* (3), 1385-1398.
511. Rokni, H. B.; Moore, J. D.; Gupta, A.; Mhugh, M. A.; Gavaises, M., Entropy scaling based viscosity predictions for hydrocarbon mixtures and diesel fuels up to extreme conditions. *Fuel* **2019,** *241*, 1203-1213.
512. Galliéro, G.; Boned, C.; Baylaucq, A.; Montel, F., Influence of the mass ratio on viscosity in Lennard–Jones mixtures: The one-fluid model revisited using nonequilibrium molecular dynamics. *Fluid Phase Equilib.* **2005,** *234* (1-2), 56-63.

Appendices

Appendix 4A: Experimental Results for Diffusion Coefficient of CH_4 in Methylbenzene

Diffusion coefficient D_{12} of methane at infinite dilution in methylbenzene at various temperatures T and pressure p, together with standard deviations σ_D [a]

p/MPa	T/K	D_{12} (10^{-9} $m^2 \cdot s^{-1}$)	10^2 (σ_D/D_{12})
1.00	323.18	7.02	0.5
1.12	348.18	9.14	0.4
1.07	373.15	11.08	0.3
1.03	398.17	13.46	0.2
10.79	323.16	6.67	0.2
9.99	348.14	8.70	1.5
10.93	373.15	10.81	1.0
9.10	398.13	13.38	0.2
38.41	323.16	5.48	1.6
31.52	348.15	7.59	0.3
31.37	373.15	9.43	0.3
31.56	398.25	11.38	0.1
51.56	323.15	4.89	0.4
53.24	348.21	6.33	0.2
52.77	373.21	7.95	0.2
51.30	398.26	9.76	0.7
67.21	323.19	4.42	0.3
62.56	348.19	6.06	0.4
64.32	373.22	7.29	0.5
64.68	398.26	8.73	0.2

[a] Standard uncertainties are $u(T) = 0.02$ K, $u(p) = 0.05$ MPa, $u(D_{12}) = 0.023 D_{12}$

Appendix 4B: Experimental Results for Diffusion Coefficient of CH_4 in Heptane

Diffusion coefficient D_{12} of methane at infinite dilution in heptane at various temperatures T and pressure p, together with standard deviations σ_D [a]

p/MPa	T/K	D_{12} (10^{-9} $m^2 \cdot s^{-1}$)	10^2 (σ_D/D_{12})
1.03	323.18	8.92	0.2
1.02	348.19	10.52	0.5
1.02	373.22	13.41	0.4
1.08	398.29	16.77	0.3
9.87	323.18	7.95	0.6
10.87	348.21	10.17	0.4
9.85	373.22	12.37	0.7
9.91	398.25	14.88	0.5
25.86	323.18	6.93	0.6
23.75	348.18	9.30	0.5
23.56	373.23	11.60	0.3
25.90	398.29	13.89	0.3
52.54	323.19	5.35	0.3
49.50	348.19	7.18	0.6
50.87	373.23	9.64	0.2
48.91	398.25	11.53	0.2
62.11	323.18	5.11	0.5
62.99	373.23	8.49	0.3
62.65	398.25	10.25	0.2

[a] Standard uncertainties are $u(T) = 0.02$ K, $u(p) = 0.05$ MPa, $u(D_{12}) = 0.023D_{12}$

Appendix 4C: Fitting Parameters for Correlation of Diffusion Coefficient

Parameter for D_0 and b from Equation 2 for diffusion coefficient of methane in methylbenzene and heptane at various temperatures T, together with absolute average relative deviations Δ_{AAD} and maximum absolute relative deviations Δ_{MAD} for the diffusion coefficients

T/K	D_0 (10^{-9} $m^2.s^{-1}$)	b (MPa^{-1})	Δ_{AAD}	Δ_{MAD}
		Methylbenzene		
323.17	7.15	7.19 x 10^{-3}	0.8%	1.2%
343.26	9.32	6.98 x 10^{-3}	1.0%	1.6%
373.18	11.49	6.93 x 10^{-3}	1.5%	3.0%
398.21	13.93	7.02 x 10^{-3}	1.7%	2.9%
		Heptane		
323.18	8.82	9.17 x 10^{-3}	1.6%	2.2%
348.20	10.91	8.11 x 10^{-3}	2.4%	3.2%
355.23	13.48	7.04 x 10^{-3}	1.5%	2.2%
398.27	16.58	7.57 x 10^{-3}	1.5%	2.2%

Appendix 4D: Fitting Parameters for Correlation of Diffusion Coefficient

Parameters for Equation 4.3 and 4.4 for D_0 and b, together with absolute average relative deviations Δ_{AAD} and maximum absolute relative deviations Δ_{MAD} for the diffusion coefficients

	Methylbenzene	Heptane
d_0 ($m^2.s^{-1}$)	-2.206 x 10^{-8}	-2.479 x 10^{-8}
d_1 ($m^2.s^{-1}$)	9.010 x 10^{-11}	1.032 x 10^{-10}
b_0 (MPa^{-1})	2.967 x 10^{1}	9.860 x 10^{1}
b_1 (MPa^{-1})	-1.248 x 10^{-1}	-4.817 x 10^{-1}
b_2 (MPa^{-1})	1.705 x 10^{-4}	6.352x 10^{-4}
Δ_{AAD}	1.4%	3.7%
Δ_{MAD}	3.7%	5.6%

Appendix 4E: Fitting Parameters for the Hydrodynamic Radius of Methane

Parameters for Equation 4.9 for the hydrodynamic radius a of methane, together with absolute average relative deviations Δ_{AAD} and maximum absolute relative deviations Δ_{MAD} for the diffusion coefficients

	Methylbenzene	Heptane
a_0 (nm)	0.2797	0.3034
a_1 (nm)	-0.0537	-0.0582
Δ_{AAD}	3.4%	3.5%
Δ_{MAD}	9.4%	6.2%

Appendix 8A: Experimental Viscosity η and Density ρ of (1 – x) m-xylene + x CO_2 at x = 0.191.[a]

p/MPa	η/(μPa·s)	ρ/(kg·m^{-3})	p/MPa	η/(μPa·s)	ρ/(kg·m^{-3})
	T = 298.34 K			T = 372.86 K	
4.112	532.80	876.38	9.827	279.25	814.91
13.157	567.29	883.28	21.257	313.18	823.98
24.997	620.13	891.72	35.172	346.13	837.59
50.047	733.69	907.14	52.252	382.68	851.63
75.022	850.54	920.63	77.297	443.44	870.97
8.577	546.39	879.76	89.842	474.59	877.35
	T = 322.41 K			T = 423.49 K	
18.727	462.22	866.28	9.287	203.45	760.88
25.132	486.01	871.31	16.717	216.71	772.66
50.022	572.98	888.69	30.377	241.76	791.36
77.637	663.50	906.81	49.982	282.74	812.41
94.212	750.41	919.83	75.062	324.17	834.28
9.397	428.98	857.15			

[a] Expanded uncertainties are $U(T)$ = 0.20 K, $U(p)$ = 0.04 MPa, $U(x)$ = 0.0011 , $U(\rho)$ = 0.002ρ and $U(\eta)$ = 0.02η with a coverage factor k of 2**.**

Appendix 8B: Experimental Viscosity η and Density ρ of (1 – x) m-xylene + x CO_2 at x = 0.377.[a]

p/MPa	η/(μPa·s)	ρ/(kg·m^{-3})	p/MPa	η/(μPa·s)	ρ/(kg·m^{-3})
	T = 298.13 K			T = 372.66 K	
4.01	425.29	885.53	8.02	228.64	808.50
8.03	440.28	890.92	10.02	234.04	811.66
15.03	465.51	895.42	12.09	239.28	815.07
30.05	517.43	907.49	18.02	252.72	822.64
50.08	590.79	921.42	33.34	282.12	841.84
	T = 323.01 K		49.87	317.57	857.99
6.04	339.46	860.60	64.88	349.42	870.80
9.98	358.21	864.64		T = 423.67 K	
25.06	394.48	879.99	12.02	170.85	757.99
40.03	432.73	895.12	15.22	175.37	764.81
	T = 348.58 K		20.02	182.65	774.01
11.01	283.79	839.45	50.71	238.86	816.22
20.29	306.08	850.12	75.25	275.84	840.90
34.74	342.61	865.41	94.77	306.84	857.00
50.49	382.32	878.52			

[a] Expanded uncertainties are $U(T)$ = 0.20 K, $U(p)$ = 0.04 MPa, $U(x)$ = 0.0016, $U(\rho)$ = 0.002ρ and $U(\eta)$ = 0.02η with a coverage factor k of 2.

Appendix 8C: Experimental Viscosity η and Density ρ of (1 – x) m-xylene + x CO_2 at x = 0.464.[a]

p/MPa	η/(μPa·s)	ρ/(kg·m^{-3})	p/MPa	η/(μPa·s)	ρ/(kg·m^{-3})
	T = 298.15 K			T =373.17 K	
17.55	391.44	911.967	18.36	214.67	824.093
22.32	403.70	916.457	25.04	224.31	834.721
35.45	443.32	928.001	50.12	272.64	866.644
50.56	489.86	939.978	74.26	315.90	890.133
73.48	553.06	956.138	94.69	347.02	906.818
	T = 323.17 K			T = 423.79 K	
16.84	310.63	881.832	28.86	171.78	782.493
25.45	327.79	891.616	50.23	205.85	817.959
50.23	387.73	915.033	74.85	241.71	847.840
72.88	442.90	932.902	94.46	268.15	867.004
81.31	463.60	938.973			
	T =348.31 K				
15.63	249.44	850.466			
25.29	267.55	863.739			
50.05	319.57	890.518			
74.35	367.60	911.802			
93.31	410.12	925.751			

[a] Expanded uncertainties are $U(T)$ = 0.20 K, $U(p)$ = 0.04 MPa, $U(x)$ = 0.0021, $U(\rho)$ = 0.002ρ and $U(\eta)$ = 0.02η with a coverage factor k of 2.

Appendix 8D: Experimental Viscosity η and Density ρ of (1 – x) m-xylene + x CO_2 at x = 0.616.[a]

p/MPa	η/(μPa·s)	ρ/(kg·m^{-3})	p/MPa	η/(μPa·s)	ρ/(kg·m^{-3})
	T = 298.17 K			T = 348.46 K	
8.48	294.03	907.30	16.92	202.85	849.31
12.72	306.41	912.55	25.11	219.89	863.00
24.50	338.02	925.92	50.43	266.49	895.90
49.89	393.45	950.59	74.01	305.28	919.47
73.51	457.47	969.01	98.30	348.27	939.63
	T = 323.34 K			T = 372.97 K	
15.70	247.32	882.39	14.99	165.68	808.65
25.07	263.89	895.54	25.77	184.34	831.49
49.70	318.69	922.92	52.89	230.35	872.33
72.92	365.08	943.61	75.30	262.92	896.84
90.98	400.00	957.61	94.92	294.43	914.70
				T = 423.92 K	
			34.61	146.87	784.40
			52.87	172.39	818.41
			75.74	205.84	849.69
			95.69	225.06	871.94

[a] Expanded uncertainties are $U(T)$ = 0.20 K, $U(p)$ = 0.04 MPa, $U(x)$ = 0.0032, $U(\rho)$ = 0.002ρ and $U(\eta)$ = 0.02η with a coverage factor k of 2.

Appendix 8E: Experimental Viscosity η and Density ρ of (1 – x) m-xylene + x CO_2 at x = 0.652.[a]

p/MPa	η/(μPa·s)	ρ/(kg·m^{-3})	p/MPa	η/(μPa·s)	ρ/(kg·m^{-3})
	T = 298.38 K			T = 348.35 K	
15.94	285.68	918.96	16.11	185.22	843.95
25.04	309.52	929.86	25.05	200.62	861.81
49.78	364.89	955.68	49.90	243.63	897.77
74.86	427.85	976.20	73.78	287.36	923.48
95.82	474.75	991.39	95.03	317.07	942.55
	T = 323.04 K				
14.98	228.81	881.12			
25.09	248.23	896.54			
49.87	295.08	927.06			
75.54	341.97	951.47			
90.87	372.70	963.98			

[a] Expanded uncertainties are $U(T)$ = 0.20 K, $U(p)$ = 0.04 MPa, $U(x)$ = 0.0024, $U(\rho)$ = 0.002ρ and $U(\eta)$ = 0.02η with a coverage factor k of 2.

Appendix 9A: Experimental Viscosity η and Density ρ of (1 – x) DIDP + x CO_2 at x = 0.207.[a]

P	η	ρ	P	η	ρ
MPa	**mPa·s**	**kg·m^{-3}**	**MPa**	**μPa·s**	**kg·m^{-3}**
	T = 313.02 K			T =342.64 K	
24.28	43.996	961.29	7.08	11.33	929.76
	T = 372.22 K		19.85	13.899	943.06
19.93	6.103	924.02	39.60	18.845	954.71
37.45	7.795	939.42	59.63	25.763	965.62
40.08	8.084	941.27	72.25	31.005	971.71
60.01	10.327	954.77	79.61	34.543	975.13
79.43	13.259	966.32			

[a] Expanded uncertainties are $U(T)$ = 0.20 K, $U(p)$ = 0.04 MPa, $U(x)$ = 0.0024, $U(\rho)$ = 0.002ρ and $U(\eta)$ = 0.02η with a coverage factor k of 2.

Appendix 9B: Experimental Viscosity η and Density ρ of (1 – x) DIDP + x CO_2 at x = 0.411.[a]

P	η	ρ	P	η	ρ
MPa	**μPa·s**	**kg·m^{-3}**	**MPa**	**μPa·s**	**kg·m^{-3}**
	T = 298.25 K			T =342.64 K	
48.61	127.6	988.33	17.33	10.3	941.30
	T = 313.01 K		31.88	12.8	950.60
19.95	31.8	963.25	40.14	14.5	955.42
37.82	45.6	976.64	59.97	19.4	966.35
40.02	47.1	974.37	79.97	25.4	976.26
59.84	67.3	984.26		T = 372.22 K	
79.76	95.0	993.24	24.58	5.4	927.07
			39.90	6.6	937.47
			59.85	8.4	949.44
			79.98	10.7	960.26

[a] Expanded uncertainties are $U(T)$ = 0.20 K, $U(p)$ = 0.04 MPa, $U(x)$ = 0.0024, $U(\rho)$ = 0.002ρ and $U(\eta)$ = 0.02η with a coverage factor k of 2.

Appendix 9C: Experimental Viscosity η and Density ρ of (1 – x) DIDP + x CO_2 at x = 0.610.[a]

P	η	ρ	P	η	ρ
MPa	**mPa·s**	**kg·m^{-3}**	**MPa**	**μPa·s**	**kg·m^{-3}**
	T = 313.00 K			T =342.62 K	
19.50	14.46	964.69	20.01	5.94	943.19
39.87	19.58	977.18	41.07	7.86	957.31
51.64	23.28	983.33	52.03	8.98	964.12
63.00	28.19	989.42	60.05	9.94	968.85
79.50	36.12	997.44	79.76	12.58	979.34
	T = 372.22 K				
31.30	3.63	931.25			
39.95	4.01	937.57			
59.86	5.01	950.68			
79.67	6.39	962.21			
20.02	3.25	922.10			

Appendix 9C: Experimental Viscosity η and Density ρ of (1 – x) DIDP + x CO_2 at x = 0.810.[a]

P	η	ρ	P	η	ρ
MPa	**mPa·s**	**kg·m^{-3}**	**MPa**	**μPa·s**	**kg·m^{-3}**
	T = 313.00 K			T =342.64 K	
31.59	3.102	977.41	19.79	1.549	938.19
39.93	3.353	984.46	40.97	1.825	958.81
59.80	4.069	998.55	59.75	2.218	974.22
68.09	4.633	1004.82	72.21	2.538	983.18
79.91	5.097	1012.32	80.03	2.671	988.37
	T = 372.36 K				
19.83	1.043	909.03			
40.04	1.072	933.04			
59.97	1.258	951.72			
71.40	1.572	960.69			
80.00	1.585	967.16			